

Wash-off and sediment transport experiments in a full-scale urban drainage physical model

Presented by **Juan Naves**

Doctoral Thesis

2019

Civil Engineering Ph.D. Program

Supervisors: **Jose Anta**

Jerónimo Puertas



UNIVERSIDADE DA CORUÑA



UNIVERSIDADE DA CORUÑA

Los abajo firmantes hacen constar que son los directores de la Tesis Doctoral titulada **“Wash-off and sediment transport experiments in a full-scale urban drainage physical model”** realizada por **Juan Naves García-Rendueles**, cuya firma también se incluye, en el marco del Programa de Doctorado en Ingeniería Civil de la Universidade da Coruña, dando consentimiento para su presentación y posterior defensa.

The undersigned hereby certifies that they are supervisors of the Doctoral Thesis entitled **“Wash-off and sediment transport experiments in a full-scale urban drainage physical model”** developed by **Juan Naves García-Rendueles**, whose signature is also included, in the framework of the Civil Engineering Ph.D. Program at the University of A Coruña, consenting to its presentation and subsequent defense.

Directores:

Jose Anta Álvarez

Jerónimo Puertas Agudo

Doctorando:

Juan Naves García-Rendueles

Agradecimientos

En primer lugar, quiero agradecer a Jose Anta y Jerónimo Puertas la oportunidad de trabajar con ellos y realizar esta tesis doctoral. Ha sido un verdadero placer tenerlos como directores de tesis, siempre disponibles, guiándome y ayudándome en todo lo que he necesitado. Gracias por todo vuestro tiempo, dedicación y esfuerzo invertidos en esta tesis. Mención especial también para Joaquín Suárez, por apoyarme y ayudarme en todo lo que he necesitado.

Mi agradecimiento al Ministerio de Ciencia, Innovación y Universidades por la ayuda para contratos predoctorales de Formación de Profesores Universitarios (FPU14/01778) de la que he sido beneficiario durante estos cuatro últimos años. Además, esta beca me ha permitido iniciarme en la docencia y disfrutar de una estancia en el Swiss Federal Institute of Aquatic Science and Technology (EAWAG) de Suiza (EST17/00715). Una parte de la investigación ha sido financiada adicionalmente por el Ministerio de Ciencia, Innovación y Universidades en el ámbito de los proyectos POREDRAIN (RTI2018-094217-B-C33) y SEDUNIT (CGL2015-69094-R)

Durante mi estancia, tuve el placer de estar bajo la supervisión de Jörg Rieckermann, a quién agradezco sinceramente todo el tiempo y ayuda que me ha dedicado. También me gustaría agradecerles a él y a todo su departamento la gran acogida y el trato recibido, que hicieron de mi estancia una gran experiencia tanto profesional como personal.

Durante los numerosos ensayos de laboratorio he contado con la ayuda de muchas personas cuya contribución ha sido imprescindible para llevarlos a cabo con éxito. Gracias al personal del CITEEC (Miguel, Gonzalo, Jose, Dani, Esteban, Paula) por su colaboración en todas las fases de los ensayos, llegamos a instalar hasta 1400 goteros uno a uno. Agradecer también a Montse por su ayuda con los cientos de muestras analizadas en unos meses intensos. Muchas gracias a Manu y a Esteban por su apoyo durante los ensayos, su disposición a mojarse desinteresadamente y todo lo que hemos pasado juntos. Gracias también a todos los demás compañeros con los que he tenido la suerte de compartir habitáculos todos estos años por generar un ambiente espectacular que hace todo mucho más llevadero.

Por último, quiero dedicar esta tesis a Sara y a mi familia.

Contents

Contents	i
List of figures	iii
List of tables	xi
Abstract	1
Resumen	1
Resumo	2
Chapter 1: Introduction, results and conclusions	3
1 General outlook.....	5
2 State of the art.....	6
2.1 Sediment build-up	7
2.2 Sediment wash-off.....	8
2.3 Gully pots sediment accumulation and resuspension.....	12
2.4 In-sewer sediment accumulation, erosion, and transport	13
3 Motivation for the current thesis	14
4 Objectives.....	16
5 Main results	17
6 General conclusions.....	31
7 Future research	33
Chapter 2: Preliminary wash-off tests	35
1 Introduction.....	37
2 Material and methods	38
2.1 Experimental setup.....	38
2.2 Experimental procedure	40
3 Results and discussion	43
3.1 Initial surface sediment load tests.....	43
3.2 Sediment distribution method tests.....	44
3.3 Distance from the curb tests	45
3.4 Curb accumulation tests.....	46
4 Conclusions.....	47
Chapter 3: Development of a new rainfall simulator	49
1 Introduction.....	51
2 Material and methods	52
2.1 Rainfall simulator description.....	52
2.2 Calibration procedure.....	53
2.3 Rain properties of calibrated rainfall simulator	55
3 Results and discussion	56
3.1 Natural rain properties	56
3.2 Calibration results.....	57
3.3 Rain properties of the developed rainfall simulator	58
4 Conclusions.....	59
Chapter 4: Overland flow velocities characterization	61
1 Introduction.....	63
2 Materials and methods	66
2.1 Physical model description	66
2.2 Surface model topography	67
2.3 Numerical model	68
2.4 Determination of overland flow velocity fields	69
2.5 Determination of flow discharges	73

3	Results and discussion	74
3.1	Elevation data and model discretization	74
3.2	Application of the 2D shallow water model	75
3.3	Application of LSPIV to determine overland flow velocities	78
4	Conclusions.....	83
Chapter 5: Hydraulic, wash-off and sediment transport experiments.....		85
1	Introduction.....	87
2	Physical model description.....	89
2.1	Rainfall simulator.....	89
2.2	Model surface.....	90
2.3	Drainage system	90
3	Hydraulic experiments.....	91
3.1	Surface and pipe depths.....	91
3.2	Flow discharge.....	92
3.3	Surface velocities.....	94
3.4	Experimental procedure.....	96
4	Wash-off and sediment transport experiments.....	97
4.1	Sediment initial conditions.....	98
4.2	TSS measurement.....	99
4.3	Particle size distributions.....	101
4.4	Mass balance	101
4.5	Experimental procedure.....	103
5	Data availability	104
5.1	Hydraulic, wash-off and sediment transport experiments data	104
5.2	PIV analysis data.....	104
5.3	SfM topography data.....	104
6	Conclusions.....	104
Chapter 6: Analysis of a physical-based urban wash-off model.....		107
1	Introduction.....	109
2	Materials and methods	111
2.1	Numerical model	111
2.2	Laboratory experiments	114
2.3	Global sensitivity analysis.....	116
2.4	Local sensitivity analysis	118
2.5	Variables and parameters ranges.....	119
2.6	Implementation.....	121
2.7	Assessment of model predictions	122
3	Results	122
3.1	Model and ranges performance.....	122
3.2	Global sensitivity analysis.....	123
3.3	Local sensitivity analysis	127
4	Discussion	131
4.1	Interpretation of the sensitivity analysis results	131
4.2	Transferability to field studies.....	132
4.3	General perspectives for modelling urban wash-off.....	134
5	Conclusions.....	134
References.....		137
Appendix A: Resumen extendido de la tesis.....		157
Appendix B: List of publications from thesis outcomes.....		175
Appendix C: List of publication related with thesis topic.....		177

List of figures

Chapter 1

- Figure 1.1.** Sediment mobilization through urban catchments with separating sewer system. Pollutants are accumulated in catchment surfaces in dry weather periods and can be washed off and transported through gully pots to the sewer system.6
- Figure 1.2.** Accumulated solids load with respect the elapsed time since last cleaning by sweeping or rain (Sartor and Boyd, 1972).....7
- Figure 1.3.** Exponential wash-off equation performance for different surface roughness and particle sizes (Sartor and Boyd, 1972).....9
- Figure 1.4.** Suspended solids transport scheme in an urban wash-off physically-based 1D approach (Deletic *et al.* 1997). The model considers detachment of particles by rain and runoff shear and assumes no deposition. Once into suspension, solids are transported by overland flow, which is divided into a shallow flow perpendicular to the curb and a gutter flow modeled as a triangular channel longitudinally to the curb.10
- Figure 1.5.** Conceptual scheme of the mobilization of sediment in Hairsine-Rose wash-off formulation applied to an urban catchment. Taken from Hong *et al.* (2016a).....11
- Figure 1.6.** Urban drainage physical model general view taken from Fraga (2015).15
- Figure 1.7.** General view of the urban drainage physical model with the nozzles-based rainfall simulator and rain intensity map generated.....17
- Figure 1.8.** Initial sediment distributions and loads tested in the preliminary tests.18
- Figure 1.9.** TSS pollutographs and discharges (a) and mass percentage final distributions (b) for a sediment load of 20 g/m, spread homogeneously over a 5-meter-long and 1-meter-wide surface, attached or separated 1 or 2 m from the curb. Values in parentheses indicate the mass error balance.....19
- Figure 1.10.** General image of the new rainfall simulator (a). Detail of drippers circuits above the horizontal mesh (b).20
- Figure 1.11.** Rain intensity maps and raindrop size and velocity distribution for the three rain intensities that is possible to generate. The solid curve represent the experimental relation between diameter and terminal velocity (Gunn and Kinzer 1949).....21
- Figure 1.12.** Experimental setup scheme for the recording of runoff videos used in the PIV analysis with fluorescent particles. The resulted steady velocity distribution generated by the lowest rainfall intensity is also plotted.22
- Figure 1.13.** Elevation maps measured by (a) traditional point survey and (b) SfM photogrammetric technique. The velocity distributions resulted in the marked area from the

implementation of the topographies in a 2D shallow water model was plotted next to each elevation map.....**23**

Figure 1.14. Surface and in-pipe depth, flow discharge and surface velocities measuring points in hydraulic experiments (a). Flow discharge at the pipe system outlet (b) and surface (c) and in-pipe (d) water depths for the highest rain intensity.....**24**

Figure 1.15. Particle size distribution of the five sediment classes used (a). Mean diameter and gradation coefficients are also indicated in the plot. Sediment initial distribution over the model surface (b).**25**

Figure 1.16. Measuring points and variables for the wash-off and sediment transport experiments.....**25**

Figure 1.17. Total suspended solids (TSS) results in both gully pots and in the pipe system outlet for the five different grain sizes (D1-D5) and rain intensities of 80, 50 and 30 mm/h.**26**

Figure 1.18. Mass balances results for the five different grain sizes (D1-D5) and rain intensities of 80, 50 and 30 mm/h.**27**

Figure 1.19. TSS experimental results and five best-fitted TSS simulations for the experiments with rain intensities of 50 (up) and 80 mm/h (down) and sediment classes D2 and D3, respectively. The parameter sets of the five best-fitted predictions are also included.**28**

Figure 1.20. SRC and EFAST first order and total effect sensitivity indices of the Hairsine-Rose parameters for the total washed off mass in gully pot 1 and for each of the laboratory experiments considered (colors for rain intensities and x-position for sediment classes)...**29**

Figure 1.21. Sensitivity results for the Elementary Effects method for the 30 mm/h and sediment class D1 test. Plots show the sensitivity to the total washed off mass through gully pot 2. The ranking of the three most influential input factors is shown in the upper-left corner of the plot.**30**

Chapter 2

Figure 2.1. Geometry (a) and photograph of the experimental setup (b).**39**

Figure 2.2. Rain intensity map over street surface (a) and scheme of sewer outlet tanks (b).**39**

Figure 2.3. Individual turbidity (FNU) and TSS (mg/L) regressions.**41**

Figure 2.4. Distribution of the initial dust deposited over roadway surface in performed experiments. Two photographs from initial load and curb accumulation test are also included.**42**

- Figure 2.5.** Samples and turbidity signal derived TSS pollutographs and discharges at the sewer outlet (a) and mass percentage final distributions (b) for sediment loads of 4, 16 and 32 g/m² over a 4 m² surface in a 0.5 m grid. Values in parentheses indicate the mass errors balance (ϵ_M).44
- Figure 2.6.** Samples and turbidity signal derived TSS pollutographs and discharges (a) and mass percentage final distributions (b) placing a sediment load of 16 g/m² over a 4 m² surface on a 0.5 m grid, a 0.25 m grid or spreading homogenously. Values in parentheses indicate the mass errors balance (ϵ_M).45
- Figure 2.7.** Samples and turbidity signal derived TSS pollutographs and discharges (a) and mass percentage final distributions (b) for a sediment load of 20 g/m, spread homogeneously over a 5-meter-long and 1-meter-wide surface, attached or 1 or 2 m separated from the curb. Values in parentheses indicate the mass error balance (ϵ_M).45
- Figure 2.8.** Samples and turbidity signal derived TSS pollutographs and discharges (left) and mass percentage final distributions (right) for a sediment load of 20 g/m, spreaded homogeneously over a 5-m-long and 3, 1 or 0.5-m-wide surface and placed with a stepped distribution. Values in parentheses indicate the mass error balance (ϵ_M).46

Chapter 3

- Figure 3.1.** General image of the rainfall simulator in its final configuration above the urban drainage physical model. Disdrometer and vessels for measuring rain intensity are also shown in the image (image a). Detail of both types of drippers inserted in the circuits above the horizontal mesh (image b).53
- Figure 3.2.** Vessels disposed over the model surface to measure rain intensity and uniformity for different mesh types and distances to drippers during calibration.55
- Figure 3.3.** Relation of raindrop mean diameter and velocity with respect to the rain intensity measured by disdrometer.56
- Figure 3.4.** Raindrop size and velocity distribution of natural rainfalls with intensities ranging from 25 to 35 mm/h. The mean of the number of raindrops registered by disdrometer classified in sizes and velocities is compared with experimental relation between diameter and terminal velocity (Gunn and Kinzer 1949), which is represented by the solid curve.56
- Figure 3.5.** Rain intensity map of the physical model surface, which has an approximate area of 36 m², for the three intensities that the rainfall simulator is able to generate. Plots include the mean rainfall intensity measured and the Christiansen's uniformity coefficient (UC) resulted.58
- Figure 3.6.** Number of raindrops, classified according their diameter and velocity, obtained by disdrometer in an interval of 10 s and for the three rain intensities that is possible to generate. The solid curve represent the experimental relation between diameter and terminal velocity Gunn and Kinzer (1949).59

Chapter 4

Figure 4.1. (a) Physical model scheme and (b) general image of the facility.....66

Figure 4.2. (a) Texturized image projection over the street surface used for the application of SfM and (b) 3D dense point reconstruction of the model.68

Figure 4.3. Layout of the experimental configuration for overland runoff velocity measurements in the physical model.69

Figure 4.4. Image processing and LSPIV data analysis methodology.....71

Figure 4.5. Topographies of the physical model obtained from (a) traditional point survey and (b) SfM photogrammetric technique. Longitudinal and transversal cross section plotted in Figure 4.6 and Figure 4.13 are marked in the maps.....74

Figure 4.6. Comparison of the longitudinal ($x = 0.75$ m and $x = 0.10$ m) and transversal ($y = 3.75$ m) profiles extracted from the model domain generated from traditional point data and SfM topographies.75

Figure 4.7. Experimental and numerical flow results in both gully pots and for the three rainfall intensities studied. The variance in the measured experimental flow discharge (grey) and the LSPIV measure interval (purple) are shown.....76

Figure 4.8. Numerical depth-averaged velocity vectors using the traditional data point topography for 30, 50 and 80 mm/h rainfall intensity.....77

Figure 4.9. Numerical depth-averaged velocity vectors using the SfM topography for 30, 50 and 80 mm/h rainfall intensity.....77

Figure 4.10. Experimental surface velocity fields for the three studied rainfalls using LSPIV.79

Figure 4.11. Comparison of the experimental and numerical x-component (up) and y-component (down) velocities using the experimental data obtained from the LSPIV technique and the numerical results, with the traditional point data topography (left) and the SfM topography (right), respectively. The three different rainfall intensities of 30 mm/h, 50 mm/h and 80 mm/h are represented in blue, yellow and black.....80

Figure 4.12. Density comparison (histograms) for x-component (a) y-component (b) and module (c) of experimental and numerical velocities.....81

Figure 4.13. Numerical and experimental depth-averaged velocity sections comparison ($X = 0.75$ m, $X = 0.10$ m and $Y = 3.75$ m) for the three rainfall intensities studied.....82

Chapter 5

Figure 5.1. Street section physical model scheme.....89

Figure 5.2. General image of the rainfall simulator with the experimental setup for the measurement of rain intensity maps. Results for the intermediate rainfall are also plotted.	90
Figure 5.3. Surface and in-pipe depth, flow discharge and surface velocities measuring points in hydraulic experiments.	91
Figure 5.4. Distance sensors installed on the street surface (a) and on pipes (b) to measure water depths. Data registered for the highest rain intensity is also shown.	92
Figure 5.5. Setup for the measurement of gully pot discharges from the water level over a v-notch in an underground deposit. The result obtained in gully pot 2 for the rain intensity of 50 mm/h is also shown in the plot as an example.	93
Figure 5.6. Pipe system outlet setup for the measurement of flow discharges, turbidity and suspended solids transport. The flow discharge registered in for the rain intensity of 50 mm/h is also plotted.	93
Figure 5.7. Flow discharge data processing from the raw recorded signal to the flow result at the pipe system outlet for the intermediate rain intensity.	94
Figure 5.8. Experimental setup scheme for the recording of runoff videos used in the PIV analysis with fluorescent particles. The resulted steady velocity distribution generated by the lowest rainfall intensity is also plotted.	95
Figure 5.9. Measuring points in wash-off and sediment transport experiments.	98
Figure 5.10. Initial distribution of sediment over the model surface for the wash-off and sediment transport tests.	99
Figure 5.11. Particle size distribution of the five sediment classes used. Mean diameter and gradation coefficients ($\sigma_g = \sqrt{(D_{84}/D_{16})}$) are also indicated in the plot.	99
Figure 5.12. Total suspended solids (TSS) results in both gully pots and in the pipe system outlet for the five different grain sizes (D1-D5) and rain intensities of 80, 50 and 30 mm/h.	100
Figure 5.13. PSD and TSS samples measuring points at the entrance of gully pots (a) and at the pipe system outlet (b).	101
Figure 5.13. Mass balances results for the five different grain sizes (D1-D5) and rain intensities of 80, 50 and 30 mm/h.	102

Chapter 6

Figure 6.1. Physical model scheme and initial distribution of the sediment.	114
Figure 6.2. Total suspended solids (TSS) and experimental flow results in both gully pots for the four different grain sizes (D1-D4) and rain intensities of 80, 50 and 30 mm/h. It can be seen that the complete pollutographs of the experiments have been a satisfactory measure	

here, through analyzing the manual grab samples for all the diameters and rain intensities.116

Figure 6.3. TSS experimental results and five best-fitted TSS simulations for the experiments with rain intensities of 50 (up) and 80 mm/h (down) and sediment classes D2 and D3, respectively. It can be see that predictions agree well with experimental results. The contours of all the simulations performed in the global SA are also included (dashed lines), and illustrate the sensitivity of the model output to the plausible values of H-R parameters.123

Figure 6.4. Standardized Regression Coefficients (SRC) of the Hairsine-Rose parameters for the total washed off mass (row 1) and the TSS maximum value (row 2) in each gully pot (columns) and for each laboratory experiment (colours for the rain intensities and x-position for the sediment classes). The degree of transparency represents the R^2 value. The plots show that the critical mass is the most important H-R parameter and that there is a strong relation between the grain size of the sediment and the relative importance of rain-driven and flow-driven detachment parameters.124

Figure 6.5. EFAST first order and total effect sensitivity indices of the Hairsine-Rose parameters for the total washed off mass (row 1) and the TSS maximum value (row 2) in each gully pot (columns) and for each of the laboratory experiments (colors for rain intensities and x-position for sediment classes). It can be seen that the critical mass is the most important H-R parameter. $\alpha 0$, $h0$ and F occupy a secondary level of influence with respect to the total washed mass, but only F in the case of the TSS peak results.....126

Figure 6.6. Sensitivity results for the Elementary Effects method. Plots show the sensitivity to the total washed off mass through gully pot 2 for each of the three rainfall intensities and four grain sizes considered in the experiments. The ranking of the three most influential input factors is shown in the upper-left corner of each case. In general, Ms_0 , D_{50} and Ms_{cr} are the factors with the most influence on the result for all the laboratory experiments.128

Figure 6.7. Sensitivity results for the Elementary Effects method. Plots show the sensitivity to the TSS maximum value in gully pot 2 in all cases. The ranking of the three most influential input factors is shown in the upper-left corner of each case. In general, Ms_0 , D_{50} , Ms_{cr} and F are the factors with the most influence on results.130

Appendix A

Figura A.1. Esquema general del modelo físico de drenaje urbano y mapa de intensidades de lluvia generado por el simulador de lluvia basado en difusores a presión que se utilizó en los ensayos preliminares.160

Figura A.2. Cargas iniciales y distribuciones de sedimentos utilizadas en los ensayos preliminares.....161

Figura A.3. Concentraciones de SST y caudales (a) y balances de masas al final de los ensayos (b) para una carga de sedimentos de 20 g/m, distribuido uniformemente en un área de 5 m

x 1 m, pegada a la cuneta o separada 1 o 2 m de la misma. El error en el cierre de los balances de masas se indica para cada caso ensayado.....162

Figura A.4. Imagen general del nuevo simulador de lluvia basado en goteros (a) y detalle de los circuitos de goteros sobre la malla horizontal para romper y distribuir las gotas de lluvia generadas.163

Figura A.5. Mapa de intensidades de lluvia y distribuciones de tamaños y velocidades de gota para las tres lluvias que el simulador es capaz de generar. La curva negra representa la relación experimental entre el diámetro y la velocidad terminal de las gotas.....164

Figura A.6. Configuración experimental para la grabación de los vídeos usados para la medida de velocidades superficiales a través de la técnica PIV. Se incluyen además las velocidades medias obtenidas en régimen permanente para la lluvia con la intensidad más baja.165

Figura A.7. Mapas de elevaciones obtenidos mediante medidas manuales puntuales (primera fila) y mediante la técnica fotogramétrica SfM (segunda fila). En la segunda columna se muestran las distribuciones de velocidades obtenidas con cada una de las topografías utilizando un modelo 2D de aguas someras y considerando la menor intensidad de lluvia.166

Figura A.8. Puntos de medida de calados superficiales y en tubería, caudales y velocidades en los ensayos hidráulicos realizados (a). También se incluye el caudal registrado a la salida de la red de tuberías (b), y los calados medidos en el punto S11 de la superficie (c) y en el punto S4 de la red de tuberías (d) para la lluvia de mayor intensidad.167

Figura A.9. Granulometrías de las cinco clases de sedimentos utilizadas incluyendo su tamaño medio y su coeficiente de gradación (izquierda). Distribución inicial de sedimentos sobre la superficie del modelo (derecha).....168

Figura A.10. Puntos de medida y variables consideradas en los ensayos de lavado y transporte de sedimentos.168

Figura A.11. Sólidos en suspensión totales (SST) en las arquetas y en el punto de vertido para las 5 clases de sedimento diferentes (D1-D5) y las tres intensidades de lluvia.169

Figura A.12. Balances de masas para las cinco clases de sedimento (D1-D5) e intensidades de lluvia de 80, 50 y 30 mm/h.170

Figura A.13. Resultados experimentales de SST en la entrada de los imbornales y las cinco mejores predicciones para los ensayos con intensidades de lluvia de 50 (arriba) y 80 mm/h (abajo) y clases de sedimento D2 y D3 respectivamente. Se incluye además los valores de los parámetros de la formulación de Hairsine-Rose para los 5 mejores ajustes.....171

Figura A.14. Coeficientes de sensibilidad global de la masa total lavada por el imbornal 1, obtenidos mediante los métodos SRC y EFAST, respecto a los parámetros de la formulación de Hairsine-Rose y para cada uno de los casos experimentales considerados (colores para las intensidades de lluvia y posición para la clase de sedimentos utilizada).172

Figura A.15. Resultados del análisis de sensibilidad local para la masa total lavada por el imbornal 2 para el caso de 30 mm/h y clase de sedimento D1, usando el método de Elementary Effects y considerando todas las variables de entrada del modelo.**173**

List of tables

Chapter 3

Table 3.1. Configurations of the tests performed during rainfall simulator calibration.....**54**

Table 3.2. Results of the tests performed during the rainfall simulator calibration.**57**

Chapter 5

Table 5.1. Hydraulic tests configurations.....**96**

Table 5.2. Configuration of PIV experiments.**97**

Table 5.3. Wash-off and sediment transport tests ID and configurations.....**103**

Chapter 6

Table 6.1. Sediment granulometries considered (D1-D4) and total washed off mass for the twelve laboratory experiments.**115**

Table 6.2. Parameters and ranges of variation used in the global sensitivity analysis.....**119**

Table 6.3. Input factor ranges for the local sensitivity analysis.**120**

Table 6.4. Ranges of Hairsine-Rose parameters for the local sensitivity analysis.**120**

Abstract

The continuous growth of cities and the consequent increase in impermeable surfaces make runoff management essential for the sustainable urban development. However, the high variability of pollutant build-up and wash-off processes in urban catchments complicates the development of modelling tools to design and manage palliative measures aimed at reducing environmental impacts of stormwater pollution.

In this thesis, an extensive experimental campaign analyzing sediment wash-off, gully pot trapping and in-pipe sediment transport was carried out in a physical rainfall simulator model. In the tests, the different variables involved in these processes were accurately measured under laboratory-controlled conditions. The use of a full-scale urban drainage physical model, the development of a novel rainfall simulator, and the precise definition of hydraulic variables allow the transferability of the results to real field catchments, and render the provided data optimal for the development and validation of more accurate models and formulations. The results obtained have been used to evaluate and analyze a physically-based urban wash-off model, which has recently been proposed as an alternative for adequately modelling the complex physical phenomena in question.

Resumen

El continuo crecimiento de las ciudades y el consecuente aumento de las superficies impermeables hacen que la gestión de las aguas pluviales sea esencial para un desarrollo urbano sostenible. Sin embargo, la variabilidad asociada a los procesos de acumulación y lavado de contaminantes en cuencas urbanas complica el desarrollo de modelos para el diseño y gestión de medidas paliativas que reduzcan el impacto ambiental producido por la escorrentía urbana.

En esta tesis se ha llevado a cabo una extensa campaña experimental en la que las variables involucradas en los procesos de lavado y transporte de sedimentos, incluyendo flujos a través de imbornales y tuberías, fueron medidas con precisión y en condiciones controladas de laboratorio. La utilización de un modelo físico de drenaje urbano a escala real, el desarrollo de un novedoso simulador de lluvia y la definición precisa de las variables hidráulicas permiten la transferibilidad de los resultados a cuencas reales y hacen que los datos proporcionados sean óptimos para el desarrollo y validación de formulaciones y modelos más precisos. Los resultados han servido además para evaluar y analizar un modelo de lavado basado en procesos físicos, que se ha planteado recientemente como alternativa para modelizar adecuadamente los complejos fenómenos físicos involucrados.

Resumo

O continuo crecemento das cidades e o consecuente aumento das superficies impermeables fan que a xestión das augas pluviais sexa esencial para un desenvolvemento urbano sustentable. Con todo, a variabilidade asociada aos procesos de acumulación e lavado de contaminantes en concas urbanas complica o desenvolvemento de modelos para o deseño e xestión de medidas paliativas que reduzan o impacto ambiental producido pola escorrentía urbana.

Nesta tese levouse a cabo unha extensa campaña experimental na que as variables involucradas nos procesos de lavado e transporte de sedimentos, incluíndo fluxos a través de sumidoiros e tubaxes, foron medidas con precisión e en condicións controladas de laboratorio. A utilización dun modelo físico de drenaxe urbana a escala real, o desenvolvemento dun novo simulador de choiva e a definición precisa das variables hidráulicas permiten a transferibilidade dos resultados a concas reais e fan que os datos proporcionados sexan óptimos para o desenvolvemento e validación de formulacións e modelos máis precisos. Os resultados serviron ademais para avaliar e analizar un modelo de lavado baseado en procesos físicos, que se expuxo recentemente como alternativa para modelizar adecuadamente os complexos fenómenos físicos involucrados.

Chapter 1

Introduction, results and conclusions

1 General outlook

The percentage of the global population living in cities and towns is increasing significantly, and urban areas are expected to continue to grow over the coming decades (UN 2018). The sustainable development of cities, with the maintenance of healthy living conditions and the minimization of impacts on the urban environment, is thus a current challenge of science and engineering in the field of urban water systems. In terms of urban stormwater, the increase in impervious areas as a consequence of urban expansion modifies the natural hydrology of catchments and leads to higher runoff volumes and flow discharges. In addition, there is an increase in the total load and peak concentrations of pollutants that are accumulated in urban surfaces during dry weather, which can be washed off in rain events and transported by runoff into drainage systems and eventually to aquatic media (Anta *et al.* 2006, Zafra *et al.* 2017). The impact of these pollutants in receiving environments represents one of the most significant environmental issues in urban areas (Butler *et al.* 2018). In addition, this issue is being exacerbated by the impacts of climate change, which is leading to longer dry weather intervals and more extreme rainfall events, increasing potential wash-off and drainage systems overflows (Semadeni-Davies *et al.* 2008). A thorough understanding of pollutant wash-off processes is therefore essential in order to design mitigation measures and thus to foster the sustainable development of urban areas.

In this context, pollutants such as heavy metals and Polycyclic Aromatic Hydrocarbons (PAH) have been found to be closely related to the finest fractions of suspended particles in runoff (Sartor and Boyd 1972, Akan and Houghtalen 2003, Herngren *et al.* 2005a, Zafra *et al.* 2011). Accordingly, total suspended solids (TSS) concentrations are being used as indicators in the study of pollutant wash-off (Rossi *et al.* 2009, Sikorska *et al.* 2015) and might even be a good proxy for other emerging pollutants such as microplastics (Dris *et al.* 2015, Dehghani *et al.* 2017). TSS build-up, wash-off and transport modelling is thus an important tool for the development of management and treatment techniques to minimize environmental impacts of these contaminants. However, the accuracy of the empirical build-up and wash-off equations implemented in commercial urban drainage models is still quite limited (Schellart *et al.* 2010, Gorgoglione *et al.* 2019) and TSS mobilization in urban environments is currently an area of cutting-edge research. New promising trends, such as physically-based approaches, are being developed to improve the understanding of wash-off phenomena and to overcome limitations when modelling this process. Finally, an understanding of sediment transport by runoff through gully pots and sewers is also necessary in order to give an integral response to the mobilization of pollutants in urban areas (Bertrand-Krajewski 1993).

2 State of the art

The process of the mobilization of sediments in urban areas starts with the accumulation or build-up of particles in impervious surfaces such as roads, sidewalks or roofs. These particles come from human activities, traffic, and surrounding land uses, and can be washed off during rain events. Sediments are transported by the stormwater runoff to sewer systems through gully pots, in which they can be deposited and then eroded, depending on particles and flow characteristics. Finally, in combined sewers, sediments are transported by sewers to treatment plants or, where the event exceeds the capacity of the system or there is a lack of mitigation measures, to the receiving water bodies through Combined Sewer Overflows (CSO). In the case of separate sewer systems, stormwater runoff is often conducted to water bodies without treatment. As an alternative, Sustainable Urban Drainage Systems (SUDS) have become a more commonly seen solution for the management and treatment of stormwater (Woods-Ballard *et al.* 2007).

Figure 1.1 shows the pollutant mobilization processes through a street section with a separated sewer system. These processes, which are characterized by a large variability (Wijesiri 2016), are still difficult to predict using current approaches and are one of the most challenging issues in urban hydrology. The remainder of this section focuses on the state of the art concerning four main processes: i) sediment build-up, ii) wash-off, iii) gully pots sediment accumulation and resuspension, and iv) in-sewer sediment accumulation, erosion and transport.

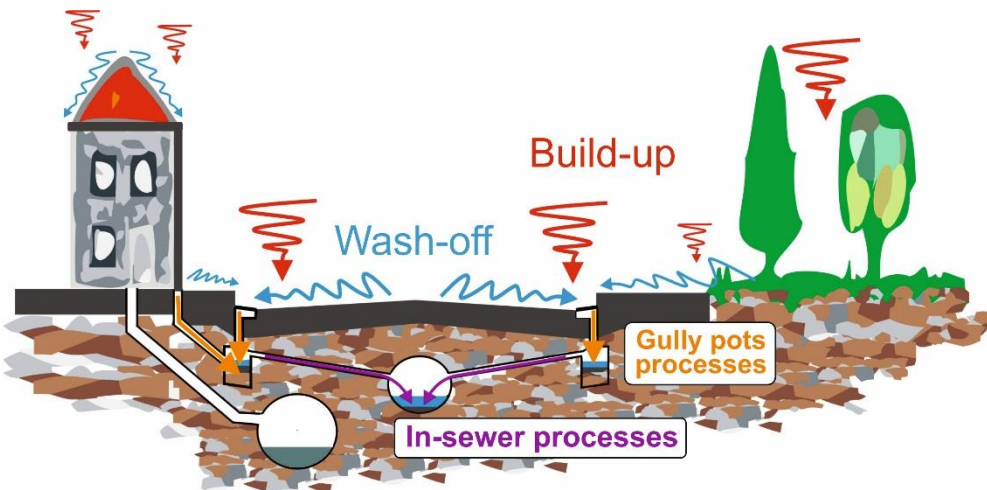


Figure 1.1. Sediment mobilization through urban catchments with separating sewer system. Pollutants are accumulated in catchment surfaces in dry weather periods and can be washed off and transported through gully pots to the sewer system.

2.1 Sediment build-up

Build-up is the pollutant accumulation process that takes place over the surfaces of urban catchments during dry weather. APWA (1969) carried out the first study analyzing the accumulation of pollutants in Chicago and suggested that build-up was a lineal phenomenon depending on the time elapsed since the last cleaning by rain or sweeping. Then, Sartor and Boyd (1972), in one of the most significant studies in urban runoff pollution, proposed the following exponential build-up equation from an extensive field campaign:

$$B = a(1 - e^{-bt}) \quad (1)$$

where B is the built up mass, t the antecedent dry days, and a and b the maximum accumulation and the accumulation rate parameters, which depend on the land uses (Figure 1.2). The novelty of this equation (Eq. 1) is that it presents the accumulation of sediments as a finite process, increasing the accumulation to a certain value of equilibrium.

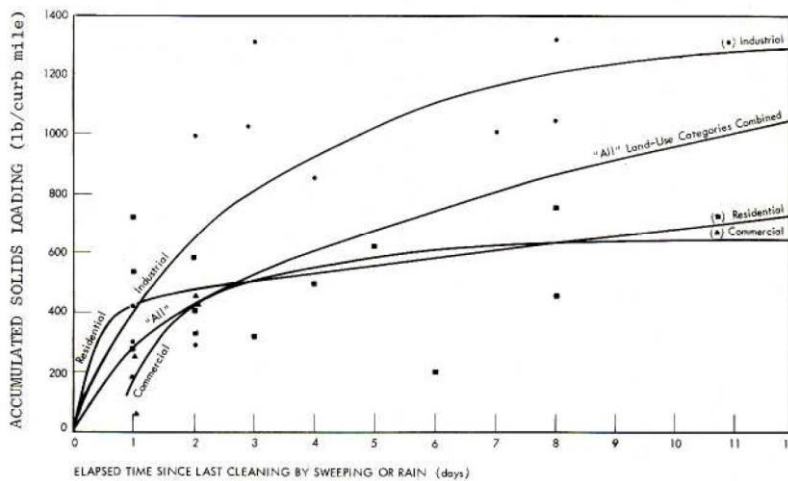


Figure 1.2. Accumulated solids load with respect to the elapsed time since last cleaning by sweeping or rain (Sartor and Boyd, 1972).

Using the same parameters as in the exponential equation, Roesner (1982) proposed an asymptotic approach (Eq. 2) to model the rapid accumulation that developed during the first days and the trend of the build-up curve to an equilibrium value. Ball *et al.* (1998) obtained a good performance using both the previous asymptotic approach and a power equation (Eq. 3) to model the temporal variation in the build-up measured in a road gutter and its proximities. These equations can be written as:

$$B = \frac{at}{b+t} \quad (2)$$

$$B = a \cdot t^b \quad (3)$$

where B is the built up mass, t the antecedent dry days, and a and b the curve fitting parameters.

The approaches presented have been used extensively to model build-up in different studies (e.g. Charbeneau and Barret 1998, Soonthornnonda and Christensen 2008, Chow *et al.* 2013, Morgan *et al.* 2017) but without coming to a consensus solution, given that the accumulation process is highly dependent on the study site. This is because the rate of accumulation and the redistribution of particles is not uniform and depend on different variables characterized by high variability such as wind, rainfall, catchment characteristics, surrounding land uses, traffic conditions, and other natural and anthropogenic activities (Deletic *et al.* 2005, Vaze and Chiew 2002, Hengren *et al.* 2005a). Wijesiri *et al.* (2015b, 2016) have recently assessed the variability presented in pollutant build-up process in urban catchments, concluding that a main source of uncertainty that reduces the reliability of build-up models is the different behavior of coarse and fine particles during accumulation period. Following this insight, and considering further natural and human activities as variables, Wei *et al.* (2019) increased the performance of the original power build-up model to 17%.

The previously mentioned studies are based on field sampling programs where particles are collected from reduced measurement areas in roads or streets. Sartor and Boyd (1972) measurements showed that the concentration of particles is not homogeneously distributed over surfaces and that it decreases with the distance to the curbs, with more than 80% of the total load being found in the first 0.5 m. In addition, Deletic and Orr (2005) observed the same trend and found that sediments collected next to curbs presented coarser grain sizes (around 400 μm) than in middle positions (55 μm). Hence, another source of uncertainty in modelling build-up is the representativeness of field data. To avoid this issue, the available mass over the catchment surface before a rain event can be obtained by inferring it from sewer section runoff monitoring and wash-off models (Sutherland *et al.* 1998, Sandoval *et al.* 2018). However, this method must be used with care, given that results are affected by the uncertainties and variability in build-up, wash-off, and sewer sediment transport parameters. In addition, only a fraction of the available pollutant is washed during a rain event (Egodawatta 2007) and the susceptibility to be washed is greater in finer particles (Zafra 2008), so the results obtained in this way are also unrepresentative of the total accumulated load. Finally, as reported in the following section (Sect. 2.2), results from modelling wash-off process are still rather uncertain.

2.2 Sediment wash-off

The wash-off process involves particle mobilization and transport over the catchment surface during rain events. The most widely used approach for modelling urban wash-off is the exponential equation developed by Sartor and Boyd (1972), which is implemented, sometimes with slight modifications, in several urban drainage models, such as SWMM

(Rossman, 2015). This empirical equation (Eq. 4) was developed from field measurements using a portable rainfall simulator in a real street. It computes the amount of material removed (W) at a given time from the beginning of the event (t) from the initial load of sediment available (W_0), the rainfall intensity (r), and a proportionality constant (k) dependent on street surface characteristics.

$$W = W_0(1 - e^{-krt}) \quad (4)$$

Although, as noted in Figure 1.3, the results in Sartor and Boyd (1972) showed that total washed off mass depends on particle size distribution and surface roughness, the exponential approach was usually accepted as a way of modelling wash-off without considering this variability in the definition of model parameters. In addition, despite this lumped formulation being widely accepted by users, the predictive results obtained are currently rather uncertain (Schellart *et al.* 2010, Gorgoglione *et al.* 2019) when we look at intra-event variability, and hence they are not particularly useful for engineering risk assessment or design. This is mainly due to the fact that these lumped equations are only roughly approximate with respect to the complexity of physical phenomena, considering as key variables the initial load of sediment available and the rain intensity, but neglecting spatial and temporal heterogeneities (Wang *et al.* 2011). For example, among other things, they rarely consider rainfall heterogeneities, complex geometries in urban catchments (e.g. curbs, gully pots), spatial distributions of sediments, or variability in sediment characteristics.

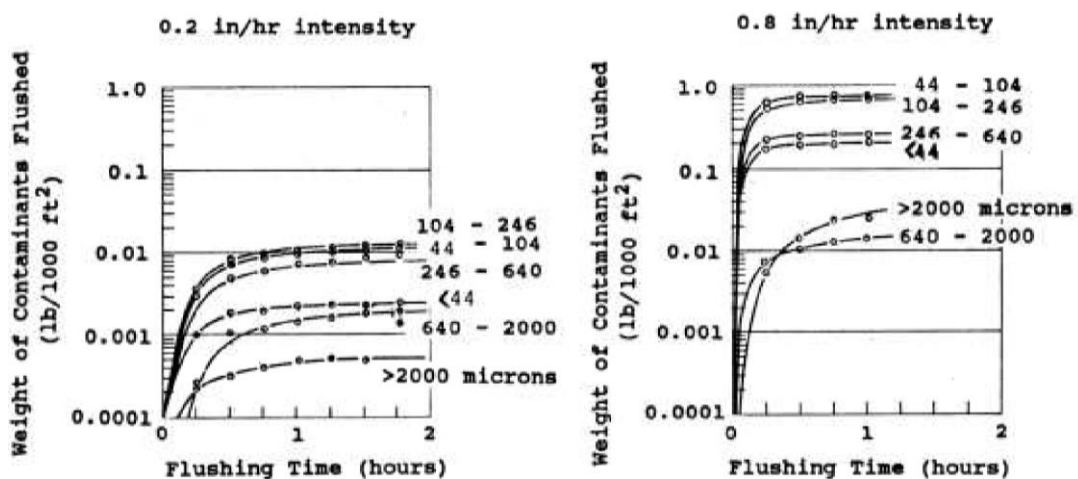


Figure 1.3. Exponential wash-off equation performance for different surface roughness and particle sizes (Sartor and Boyd, 1972).

Since Sartor and Boyd (1972), some studies have tried to improve empirical equations in order to deal with accuracy problems. Egodawatta *et al.* (2007) noted that only a fraction of the sediments available in street surfaces are washed off during rain events. In order to

consider this insight, they included a new parameter (Eq. 5), called the capacity factor (C_F). Then, taking as a basis Eq. 5, Muthusamy *et al.* (2018) carried out a laboratory-scale experimental study in a 1 m² bituminous rainfall simulator with different surface slopes and showed that the capacity factor (C_F) is also significantly dependent on the surface slope.

$$W = W_0 C_F (1 - e^{-krt}) \quad (5)$$

These improvements helped to give physical meaning to parameters and showed that surface wash-off is dependent on a number of important variables, hence increasing knowledge of the process. However, the equations proposed still do not consider certain other important variables, such as the sediment characteristics or the heterogeneities of urban catchments, and the increase in the number of parameters makes model calibration more difficult due to the interactions between the variables involved. In addition, these approaches are developed using studies performed in reduced and homogeneous areas, and their transferability to medium- and large-scales is not trivial given the complex flows that appear in the surroundings of street elements like gully pots or curbs. For these reasons, the improvements in the accuracy of results of empirical equations are limited.

Alternative physically-based approaches have been proposed to overcome these limitations, and consider the physical processes involved in surface wash-off such as the detachment of surface particles by raindrops impact or runoff shear, their transport by overland flow, and their deposition. Deletic *et al.* (1997) developed a 1D model taking into account spatial distribution of solids over the street surface separating longitudinal curb flow and perpendicular roadway and sidewalk flow during computation (Figure 1.4). This approach assumes no deposition and considers the entrainment of particles into suspension by rainfall and runoff shear. The results obtained showed a good agreement of the results in their application to two different urban catchments of around 250 m² when the rainfall- and flow-driven detachment was calculated separately, showing the possibilities for models of this kind.

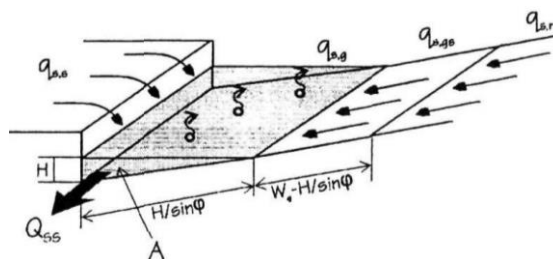


Figure 1.4. Suspended solids transport scheme in an urban wash-off physically-based 1D approach (Deletic *et al.* 1997). The model considers the detachment of particles by rain and runoff shear and assumes no deposition. Once into suspension, solids are transported by overland flow, which is divided into a shallow flow perpendicular to the curb and a gutter flow modeled as a triangular channel longitudinally to the curb.

Meanwhile, Shaw *et al.* (2006, 2009) assumed that particles are suspended due to raindrop impacts and are then transported by flow until their deposition. This assumption worked well in a 0.105 m wide test channel using a rainfall generator and 500–590 μm particles. In contrast to this approach, Massoudieh *et al.* (2008) modeled the detachment of particles as a function of flow velocity by a power expression. All these studies showed the potential of physically-based models for modelling TSS wash-off in urban areas considering spatial distribution of sediments and modelling the different processes involved using a 1D approach.

The use of 2D models is a step towards the increased accuracy of wash-off models in real catchments, allowing for the reproduction of heterogeneities of urban catchments and complex surface overland flows in a better way. The physically-based wash-off formulation developed in Hairsine and Rose (1992a, 1992b) was used, coupled with a 2D shallow water model, in Hong *et al.* (2016a, 2016b, 2019) in order to calibrate the TSS mobilization on a road catchment of 2661 m^2 for different rain events. In this approach, pollutant mobilization is computed by performing a mass exchange in each of the elements of the catchment mesh for each time step using the following equation:

$$\frac{\partial hC}{\partial t} + \frac{\partial q_x C}{\partial x} + \frac{\partial q_y C}{\partial y} = e_r + r_r - d \quad (6)$$

Here, q_x and q_y are the two components of the specific discharge in a surface flow and h is water depth, and the depth average concentration of sediment (C) in the water column can be increased by the detachability of particles due to rain (e_r) or runoff shear (r_r). It is then transported suspended in the water flow until its deposition (d). Figure 1.5 shows a scheme of the modelled processes.

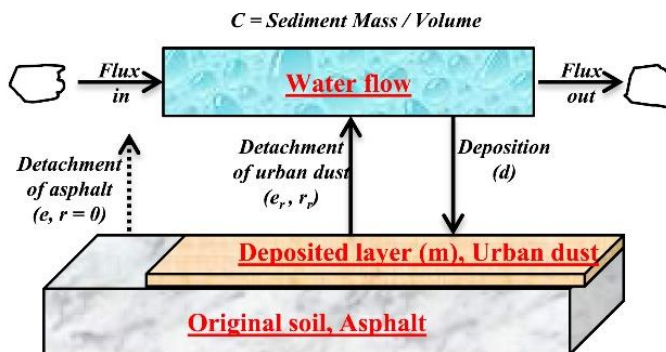


Figure 1.5. Conceptual scheme of the mobilization of sediment in Hairsine-Rose’s wash-off formulation applied to an urban catchment. Taken from Hong *et al.* (2016a).

Rain-driven detachability is assumed to depend on rain intensity and considers the availability of particles on the surface and the protection against raindrop impacts by the

water layer. Likewise, flow-driven detachability computes the transfer of solids due to the effect of the runoff stream power and depends on a critical threshold, from which a fraction of the stream power excess produces the entrainment of particles. Finally, the deposition rate depends on the settling velocity, which is affected by the size and density of particles. The variations in surface sediment mass (m) is thus obtained as:

$$\frac{\partial m}{\partial t} = d - (e_r + r_r) \quad (7)$$

The good agreement between model outputs and field-measured pollutographs, together with a detailed representation of wash-off processes, makes this approach an optimal tool for improving our understanding of the physical phenomena, and encourages further research. However, these kinds of physically-based models face the same problem as empirical models: the variability of build-up and wash-off processes makes the accurate definition of the model input variables difficult (Pitt *et al.* 2004). The associated uncertainties hinder the individual contribution of each factor in the results, complicating the development of such models. Therefore, realistic experiments in laboratory controlled condition are an opportunity to increase our understanding of wash-off processes from an accurate definition of input variables. In these conditions, physical-based wash-off models can be analyzed to identify the variables that govern the phenomena, and thus to simplify these models appropriately to ensure their transferability to real field applications.

2.3 Gully pots sediment accumulation and resuspension

Gully pots are placed at the entrance of sewer systems to retain part of the coarser suspended particles transported by runoff, protecting downstream sewer elements from wear and deposition and decreasing the pollutant contribution of runoff. Gully pots are thus important elements in the wash-off process of pollutants (Butler *et al.* 1995, Butler and Karunaratne 1995). Two processes can occur in gully pots during rain events: i) under normal operating conditions, part of the particles transported by runoff tend to be deposited, avoiding their entrance into the sewer system, and ii) in the most energetic events or when the sand trap capacity of the gully pots is exceeded, existing deposits can be eroded and resuspended into the sewer system. In the latter case, blockage of the gully pot may be produced, with the subsequent flood risk (Ten Veldhuis *et al.* 2011, Rodriguez *et al.* 2012). Therefore, modelling sediment transport through gully pots is an important tool in urban stormwater management as a means of preventively maintaining gully pots so that they keep their retaining efficiency and thus possible blockages are avoided (Ackers *et al.* 1996).

Accordingly, several studies and prediction models have been developed to simulate sediment transport through gully pots. In a laboratory study, the earlier studies of Lager *et al.* (1977) found that coarser particles were retained less than finer ones and that the trap efficiency of gully pots decreased for higher water discharges. Grottker (1990) confirmed

these insights by performing additional laboratory tests and proposed an empirical equation for modelling gully pot efficiency depending on inflow rate and particle size. This equation does not consider the accumulated sediment bed, which had been found as a main variable in Fletcher and Pratt (1981). Butler and Karunaratne (1995) proposed a simple model, one which only considers the sedimentation of particles, using laboratory experimental results. This model was completed with erosion processes and validated in Butler and Memon (1999), and is still being developed, as seen in Ciccarello *et al.* (2012) where analytical and experimental studies were performed using different settling velocities formulations and particle sizes.

A continuous pollutant wash-off model, which also considers both erosion and sedimentation of particles in the gully pot sand trap, was developed by Deletic *et al.* (2000). In this study, long-term simulations also demonstrated the importance of gully pots in retaining significant fine sediment particles. Memon and Butler (2002) also performed long term simulations of pollutant wash-off, resulting in gully pots efficiencies of up to 40% in the suspended solids load. The main problem of the presented models is the need for accurate data in order to calibrate the different parameters due to the high variability of the process and the importance of the geometry of the gully pots in terms of their efficiency. Considering this variability, alternative statistical models (Rodríguez *et al.* 2012, Post *et al.* 2016) have recently been developed by means of extensive long term field data with preventive management purposes against blockages.

The main general conclusions to be drawn from the studies cited in this section are that sedimentation and erosion processes developed in gully pots are highly relevant in modelling the entry of sediments in sewer system. Therefore, approaches to gully pots should continue to be improved in order to be included in urban drainage models and thus to achieve reliable sediment transport results in sewer networks.

2.4 In-sewer sediment accumulation, erosion, and transport

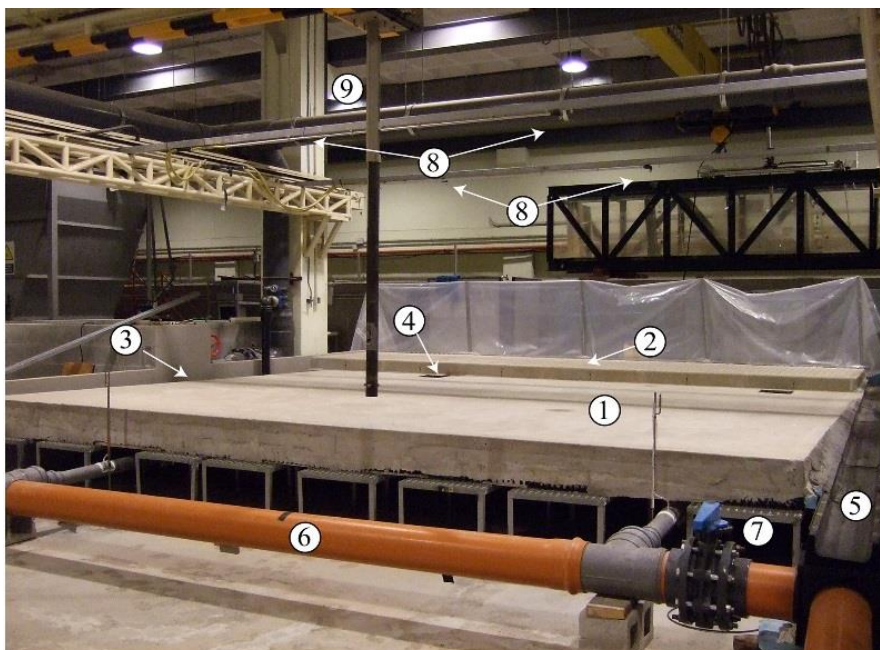
As with previous processes, sediment accumulation, erosion, and transport in sewers is a complex phenomenon to model due to the high variability of the variables involved such as flow shear stress and sediment characteristics. Once stormwater is introduced into the sewer system, transported sediments can be deposited in sewer inverts depending on flow conditions and geometry. This decreases the hydraulic capacity of sewer system by reducing the cross section and increasing the bed roughness (Ackers *et al.* 1996). Sediment deposits may also be eroded in extreme events, increasing pollutant concentration in stormwater (Tait *et al.* 2003), and hence are an important environmental issue for receiving water bodies. Therefore, modelling in-sewer sediment transport is an important tool for the design of new infrastructures and management strategies, and to optimize the significant associated costs here.

Three processes must be considered in order to understand in-sewer sediment transport: i) deposition of sediments, ii) erosion of deposited sediments, and iii) transport of particles by flow (Butler *et al.* 2003, 2018). Regarding sediment transport, this can be divided into bed load transport, in which particles are moved through sliding, rolling or by saltation, and suspended transport, in which particles are moved and remain in the flow. Sediment transport formulations traditionally used in urban drainage models (e.g. Ackers-White or Meyer-Peter and Muller formula) are usually taken from river sand transport formulations. The transferability of their predictions to urban drainage is not trivial due to the changes in problem conditions such as finer and partly cohesive particles, the presence of pipe walls, and unsteady flow (Bertrand-Krajewski 2006). Laboratory and field studies are thus required to validate formulations and to analyze possible modifications as a means of adapting the equations to sewer flows (e.g. Skipworth *et al.* 1999, De Sutter *et al.* 2003). These studies achieved good performance for stormwater systems, but their implementation in combined sewers is still difficult since they do not consider cohesiveness in bedload particles, which decreases the detachment and transport of bedload particles (Rushforth *et al.* 2003, Banasiak and Verhoeven 2008).

3 Motivation for the current thesis

A recurring problem in the development and testing of existing and new urban wash-off formulations is that the uncertainties in the definition of input variables can be propagated through the model, leading to unreliable results. The variability of build-up phenomena makes it difficult to accurately measure important variables such as the sediment characteristics or initial load without affecting the initial conditions of rain events. This is even more notable in the case of physically-based models, where the definition of additional input variables, such as rainfall properties or spatial sediment distribution, and the need for calibration data to precisely represent runoff flows, can be further sources of error. Experimental laboratory studies using simulated rainfall are an optimal tool to address this problem, providing accurately measured data in controlled conditions in order to analyze and develop more reliable wash-off models. However, studies carried out to date are limited to very small and simplified catchments and the definition of hydraulic variables is not common. For instance, both Egodawatta *et al.* (2007) and Muthusamy *et al.* (2018) achieved meaningful results in the understanding of wash-off process using rainfall simulators in uniform 3 m² field and 1 m² laboratory catchments, respectively, without measuring overland flow characteristics. This makes the transferability of the developed equations to catchment-scale applications difficult, in which complex overland flows are developed next to curbs or in the vicinity of gully pots.

In this context, a very suitable facility was available to study wash-off process under controlled laboratory conditions at the Hydraulic Laboratory of the Center for Technological Innovation in Construction and Civil Engineering (CITEEC), University of A Coruña (UDC). This facility was designed and operated by the Water and Environmental Engineering Research Team (GEAMA) of the UDC, and was used previously by the author's research group to develop and calibrate an urban dual drainage 2D/1D hydrodynamic model (Fraga 2015), and was also the topic of the author's bachelor thesis (Naves 2012). Figure 1.6 includes a general image of the facility, which consists of a 1:1 scale street section of 36 m² including a rainfall simulator, an impervious surface formed by a sidewalk and a roadway, and a drainage system that drains generated runoff through two gully pots and a pipe network to a common outlet. This facility allows for the proper analysis of the mobilization of sediments in realistic and complex surface flows, the performance of gully pots and in-pipe sediment accumulation, erosion, and transport process, ensuring a high level of transferability of the results to field sites, while retaining the ability for accurate measurement of the variables involved.



1- Roadway 3- Runoff basin 5- Outflow channel 7- Valve 2 9- Positioner
 2- Pavement 4- Manhole 6- Pipe 3 8- Diffusers

Figure 1.6. Urban drainage physical model, general view, from Fraga (2015).

An extensive and accurate wash-off and sediment transport experimental data base, carried out in this facility, is an important step forward in the field of pollutant wash-off, providing the scientific community with the necessary information in order to develop, calibrate or

validate new and existing formulations. As mentioned above, the accurate measurement of input variables is especially valuable in the case of novel physically-based urban wash-off models. This allows for assessing the performance of models and parameters without considering disturbances caused by uncertainties, making it possible to simplify and develop new deterministic wash-off models for a better applicability in real field catchments.

4 Objectives

In view of the importance of pollutant wash-off phenomena in urban environments and the need for reliable and accurate data to develop and evaluate existing and new wash-off formulations, the main objective of this thesis is to carry out an extensive experimental campaign, where variables involved in wash-off process can be accurately measured in laboratory controlled conditions, to be used as a basis for the analysis and assessment of physically-based wash-off and sediment transport models. To this end, the following partial objectives were established:

- Development of an experimental methodology to accurately measure TSS mobilization through the different parts of the physical model. In this way it is expected that the most important variables on which to focus our efforts will be determined.
- Revision of the existing rainfall simulator, and the consideration of updating it, for more realistic rain generation in order to ensure the transferability of experimental results. This objective includes the accurate measurements of rain properties.
- Hydraulic characterization of experiments. This is especially important since runoff flow is the basis for wash-off processes such as the detachment of particles due to the flow shear stress and their suspended transportation.
- Conducting the extensive experimental campaign accurately by monitoring TSS mobilization through the different elements of the model and varying rain intensity and sediment grain sizes. The results obtained will be published in open data repositories for the greatest possible dissemination.
- Finally, the application of experimental wash-off results for the assessment, through a sensitivity analysis, of the performance of a physically-based wash-off model. In this way, the usefulness of the data obtained can also be demonstrated.

5 Main results

This thesis comprises 6 chapters. Following the current introduction (Chapter 1), the remaining chapters are organized in such a way that each one can be considered as an individual study, including its own and specific state of the art, methodology, results, and conclusions. The current section summarizes the main contents and results of the thesis and provides coherence and unity to the different studies therein, explaining how the objectives set out in the project are addressed. As stated in Section 3 (motivation for the current thesis), the background of this thesis is the study presented in Fraga (2015), in which the present author collaborated during his bachelor thesis (Naves 2012). It included the development and validation of an urban drainage 2D/1D hydrodynamic model using hydraulic experiments performed in a full-scale urban drainage physical model. This facility has shown its usefulness to represent and analyze the complex flows that are developed in urban catchments, also considering gully pot and pipe system flow interactions. Therefore, the urban drainage physical model has been used to carry out the wash-off and sediment transport experiments objective of this doctoral thesis.

First, preliminary wash-off tests are presented in Chapter 2. This study analyzed the mobilization of total TSS for different initial spatial distributions and sediment loads placed over the roadway surface of the physical model. The objectives of these tests were to develop a methodology to accurately measure TSS mobilization, identifying the main variables affecting sediment wash-off and sediment transport processes, and checking the feasibility of wash-off experiments. The rainfall simulator used in Fraga (2015), which consists of four nozzles covering the entire model surface, was used to generate a rainfall with a duration of 5 minutes and a mean rain intensity of 101 mm/h. Figure 1.7 shows a scheme of the physical model and the rain intensity map produced by the nozzle-based simulator used in preliminary tests.

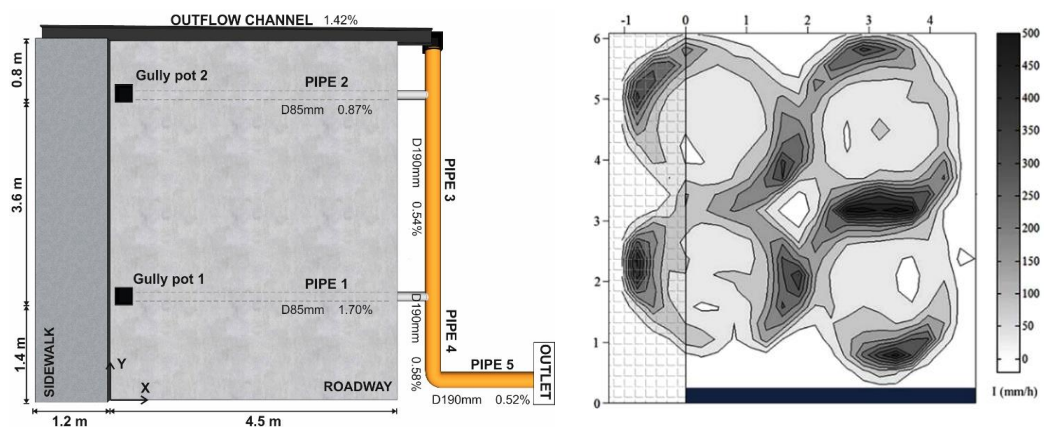


Figure 1.7. General scheme of the urban drainage physical model and the rain intensity map generated by the nozzles-based rainfall simulator used in preliminary tests.

At the sewer network outlet, flow discharges were registered and TSS pollutographs were obtained by manual grab samples and turbidity records. At the end of each test, a mass balance was performed between the initial load of sediments and the masses that remained in the different parts of the physical model (surface, gully pots, pipes, model outlet), checking the reliability of the performed experiments and allowing for the analysis of the mobilization of sediments through the model. Eleven experiments were configured to assess the influence of the initial load, spatial distribution method, distance from gully pot, and distribution area dimensions in the TSS wash-off process. The initial configuration of the tests are included in Figure 1.8.

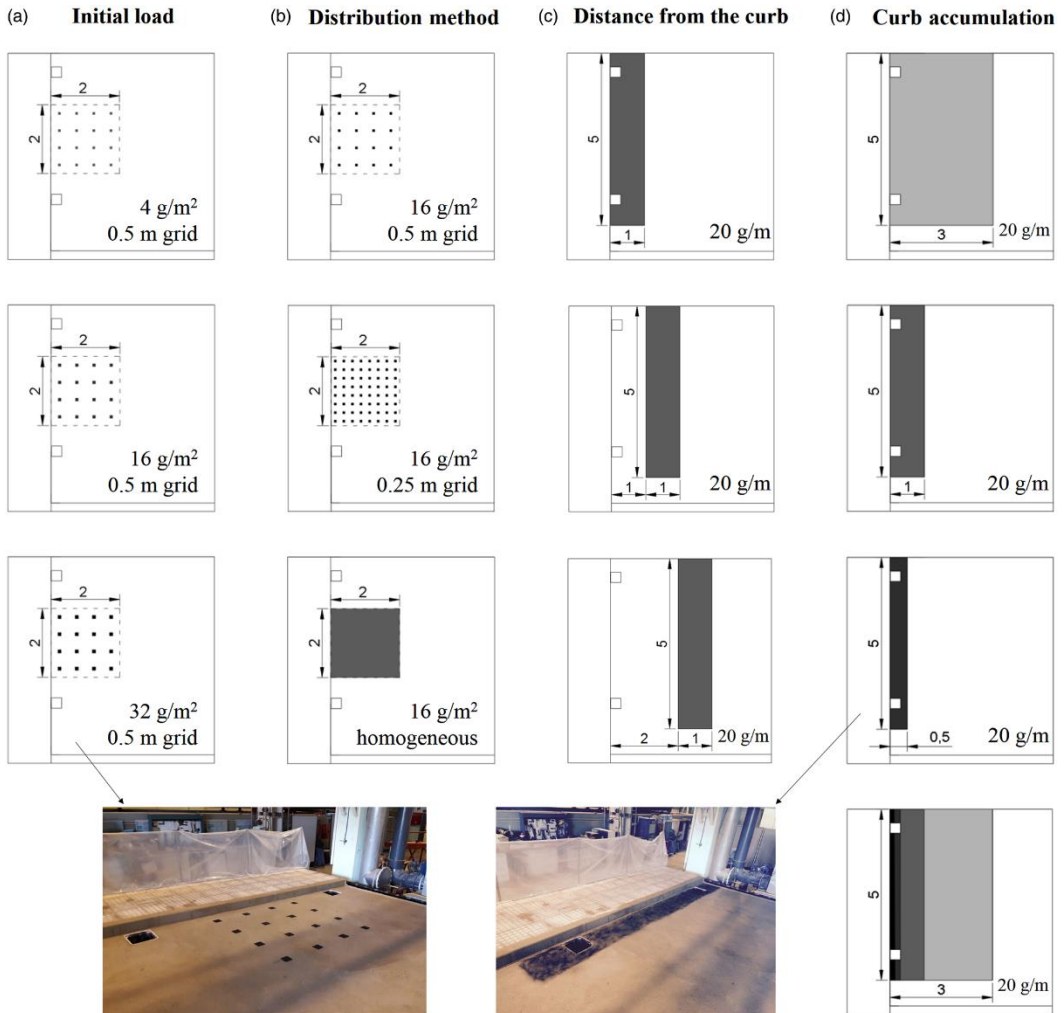


Figure 1.8. Initial sediment distributions and loads tested in the preliminary tests.

The results here showed that sediment initial load and distribution cannot completely explain pollutant wash-off processes because other variables, such as the spatial rainfall distribution and the runoff characteristics, also affect the outlet pollutographs and system mass balances. This was concluded from the results of the experiments where the sediment load is distributed at different distances from the model curb (Figure 1.9). While the TSS pollutograph peak showed, as expected, a slight decrease and delay when the sediment load was moved away at 1 m from the curb, it was more than halved in the case of placing sediments at 2 m from the curb. As can be inferred from Figure 1.7, high intensities produced at around 1.5 m from the curb affect the mobilization of sediment placed at greater distances. These preliminary results addressed the first partial objective raised in Section 4 showing the capability of the procedure to accurately measure sediment wash-off, revealing the high influence of the simulated rainfall and the need for a precise definition of overland runoff to understand wash-off processes.

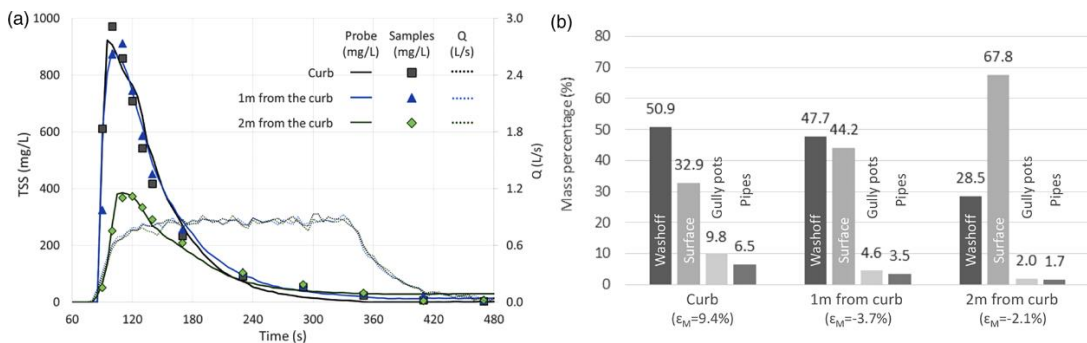


Figure 1.9. TSS pollutographs and discharges (a) and mass percentage final distributions (b) for a sediment load of 20 g/m, spread homogeneously over a 5-meter-long and 1-meter-wide surface, attached or separated 1 or 2 m from the curb. Values in parentheses indicate the mass error balance (ϵ_M).

The needs observed in the preliminary results were addressed in Chapter 3 and Chapter 4 in order to develop more realistic and useful wash-off and sediment transport experiments. First, in view of the rain properties of the previous rainfall simulator (Figure 1.7) and their high influence in TSS mobilization, Chapter 3 includes the development of a new large-scale rainfall simulator. This simulator consists of two pressure-compensating dripper grids above a horizontal mesh, which disperses and breaks generated raindrops to increase rainfall spatial uniformity and produce drop size distribution similar to natural rain. The most appropriate characteristics of the mesh and its distance to dripper grids have been calibrated by considering natural rain measurements and using a laser Parsivel 2 disdrometer and rain gauges to measure drop size and velocity distributions and rain uniformity, respectively. The

final configuration of the rainfall simulator and the experimental measuring equipment used are shown in Figure 1.10.

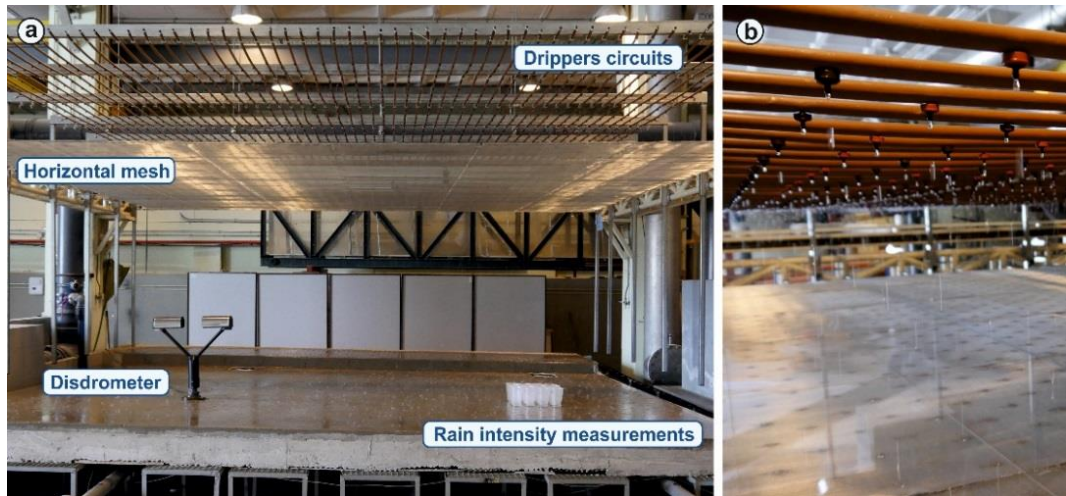


Figure 1.10. General image of the new rainfall simulator (a). Detail of dripper circuits above the horizontal mesh (b).

Once the rainfall simulator was calibrated, the properties of the generated rain were measured. The new rainfall simulator can generate three different rain intensities (mean rain intensities of 32.9, 54.9 and 79 mm/h) with Christiansen's Uniformity Coefficients (C_u) of 81, 89 and 91%, respectively, with a mean drop size of 0.95 mm and a drop impact velocity over 85% of terminal velocity for the mean drop size. Figure 1.11 shows the rain intensity map and the raindrop size and velocity distributions for the three rain intensities. Rain intensity and drop size distribution can be easily modified by changing design parameters. This flexibility, together with the almost uniform rain and the suitable raindrop sizes generated, makes the new rainfall simulator an optimal tool for wash-off studies, ensuring the transferability of the results obtained to real field applications as raised in the objectives of the current thesis.

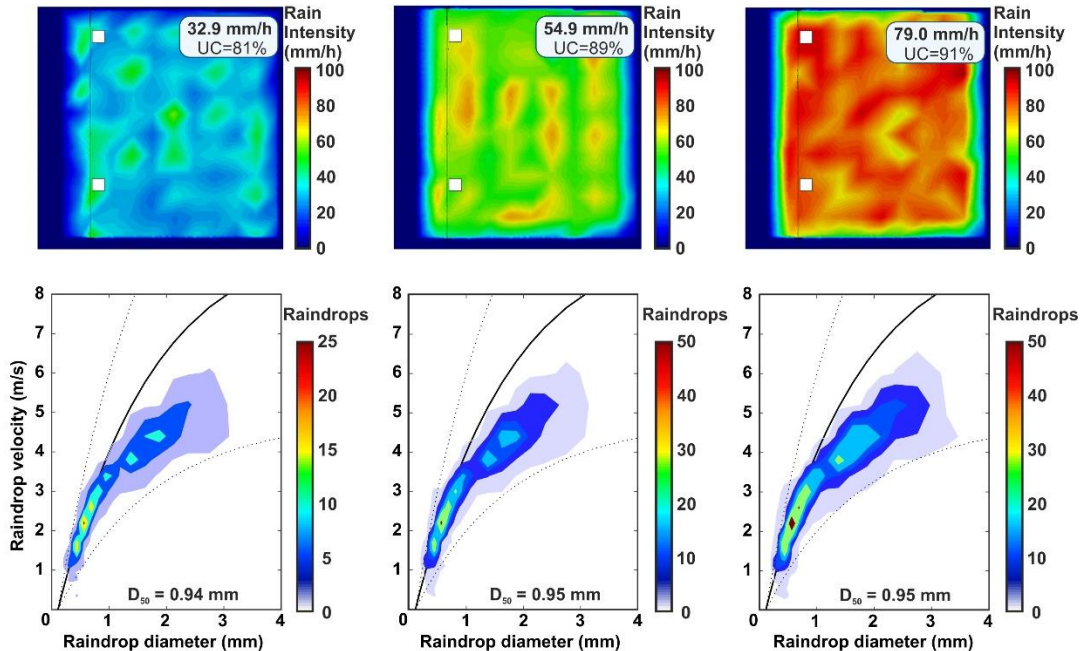


Figure 1.11. Rain intensity maps and raindrop size and velocity distribution for the three rain intensities that can be generated. The solid curves represent the experimental relation between diameter and terminal velocity (Gunn and Kinzer 1949).

Using the newly developed rainfall simulator, Chapter 4 addresses the need for an accurate representation of the overland runoff for a better understanding of the surface wash-off process. The importance of a hydraulic characterization of the experiments lies in the fact that suspended particles are transported by flow until their deposition, and that runoff shear may also contribute to the detachment of particles. In this context, a modification of the Large Scale Particle Image Velocimetry (LSPIV) visualization technique, using fluorescent particles and UV illumination, was developed to measure surface velocities with overland water depths in the order of a few millimeters and the presence of raindrops. Results obtained showed the existence of main drainage channels in surface runoff due to surface irregularities, which condition the mobilization of particles over the model surface. Figure 1.12 includes the experimental setup used to record videos for the PIV analysis and the velocity distribution results for the lowest rain intensity, in which drainage channels can be observed.

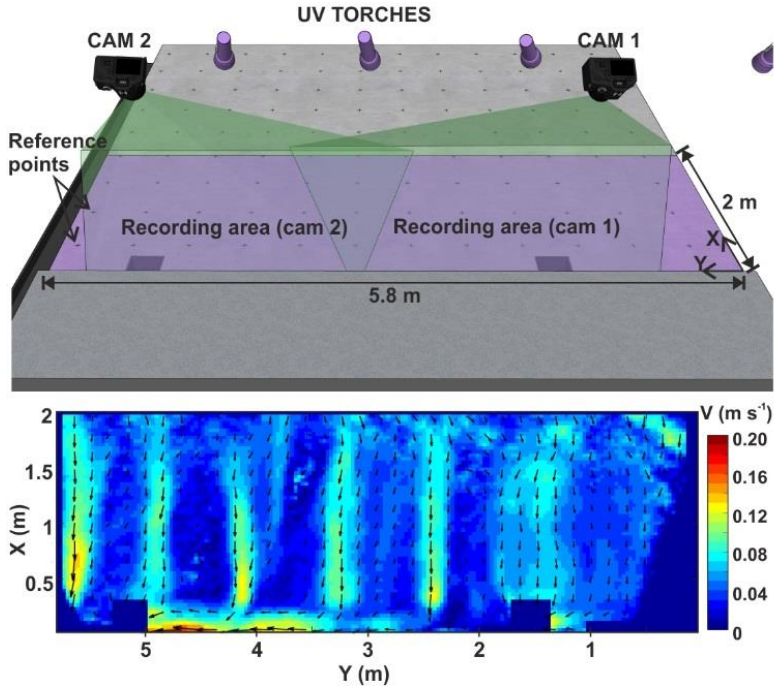


Figure 1.12. Experimental setup scheme for recording runoff videos used in the PIV analysis with fluorescent particles. The resulting steady velocity distribution generated by the lowest rainfall intensity is also plotted.

The low water depths developed make an accurate elevation map necessary to achieve a suitable representation of surface flow. Accordingly, the Structure from Motion (SfM) photogrammetric technique was used to obtain a high-resolution topography to model surface flow using a 2D shallow water model. The 2D model was calibrated using the flow discharges measured at the entrance of the two existing gully pots, and the results were compared with those obtained using traditional data point measured topography with a resolution of 0.5 m. Very similar results were found, using the same calibrated parameters, when comparing the flow discharge results at the gully pots. However, the velocity distributions obtained showed significant differences, especially in the shallowest flow areas, where only the high-definition topography was able to represent the main drainage channels of a few millimeters' depth found using the LSPIV technique. Figure 1.13 shows the elevation maps measured and the surface velocity results obtained using the 2D shallow water model for each topography, which were calibrated with the flow discharge at the gully pots. This study, included in Chapter 4, highlights the importance of detailed elevation map modelling of surface flow in shallow water conditions and the need for surface velocity calibration data to achieve useful and accurate results. In addition, the modified LSPIV technique was presented as a suitable non-intrusive tool for the experimental measurement

of surface velocities with the presence of raindrops. Finally, photogrammetry was positively assessed to obtain physical model elevations for hydraulic modelling purposes.

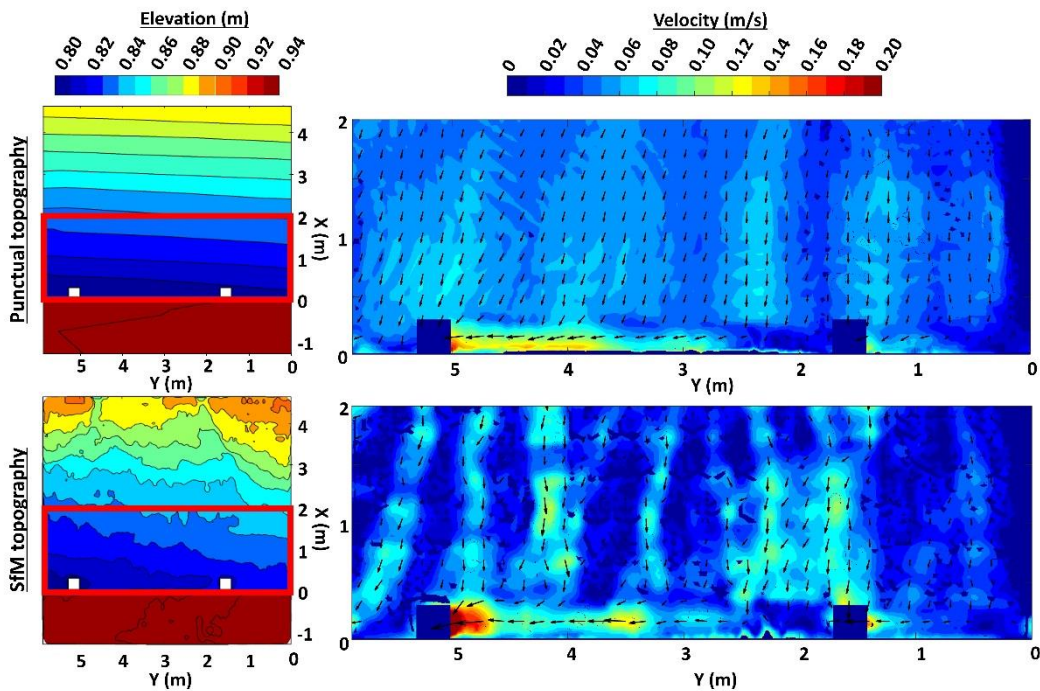


Figure 1.13. Elevation maps measured by traditional point survey (first row) and the SfM photogrammetric technique (second row). The velocity distributions results from the implementation of the topographies in a 2D shallow water model, in the area attached to the curb and for the lowest rain intensity, were plotted next to each elevation map.

After this, the detailed hydraulic characterization of the experiments was completed with the measurement of surface and in-pipe water depths and the registration of discharges at the entrance of the gully pots and at the pipe system outlet. A series of six experiments were performed looking at the measuring points presented in Figure 1.14 and using the three rain intensities that the rainfall simulator is able to generate. Figure 1.14 also includes examples of the water discharges and depths registered during the experiments for the highest rain intensity. The methodology used and the raw and processed data collected during these experiments are described in detail in Chapter 5. In addition, that chapter explains the use of an unseeded LSPIV technique as an additional method to measure overland flow velocities by analyzing the movement of bubbles and water reflections, which may be an alternative to fluorescent particles as a means of measuring very shallow flows in field applications, where the use of fluorescent particles and UV illumination is not trivial.

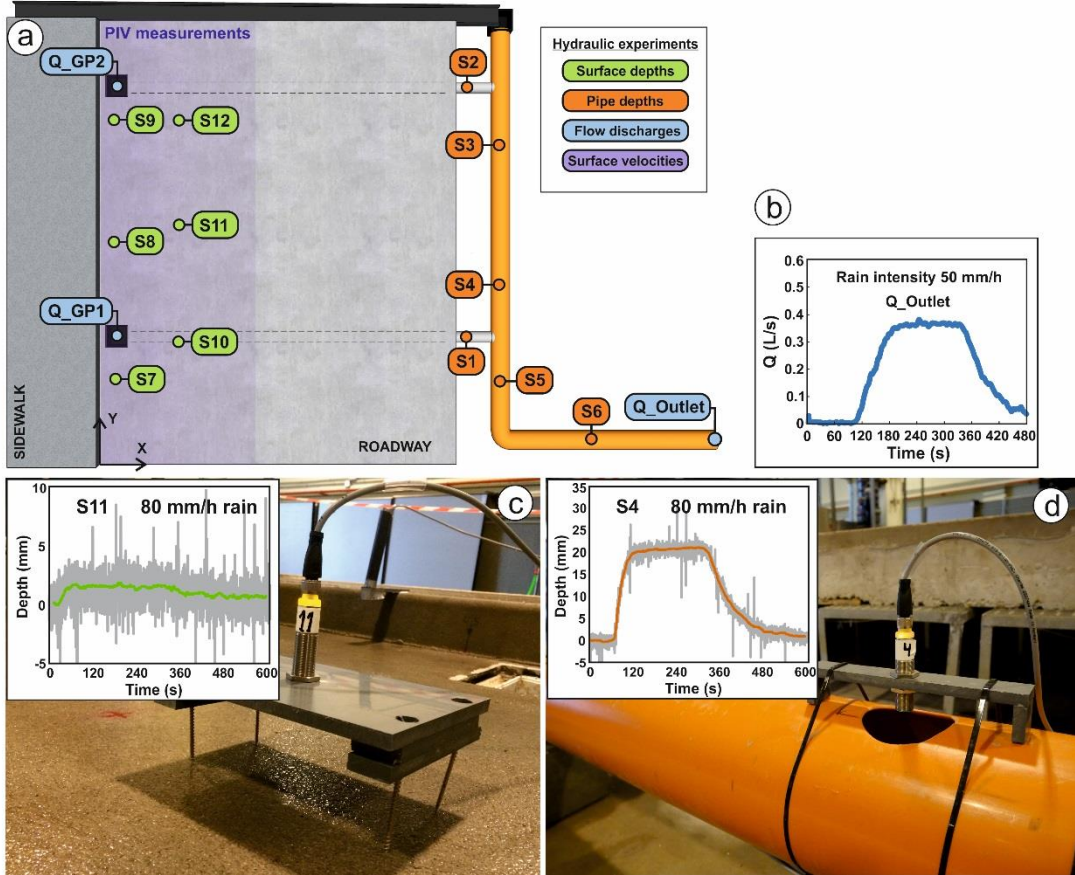


Figure 1.14. Surface and in-pipe depth, flow discharge, and surface velocity measuring points in hydraulic experiments (a). Flow discharge at the pipe system outlet (b), and surface (c) and in-pipe (d) water depths for the highest rain intensity.

Once the hydraulics of the experiments was precisely determined, an extensive experimental campaign was performed accurately measuring TSS mobilization through the urban drainage physical model from given, accurately known initial sediment conditions. The three different rain intensities (30, 50 and 80 mm/h) and five sediment granulometries (d_{50} ranging from 30 to 275 microns) were tested in 23 wash-off and sediment transport experiments, which are also presented in Chapter 5. Figure 1.15a plots sediment classes granulometries that were placed over the surface in a realistic way (Figure 1.15b) as initial sediment conditions of each test.

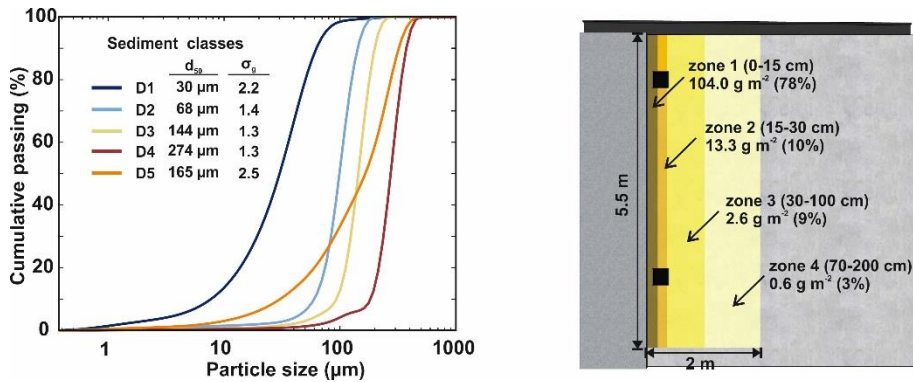


Figure 1.15. Particle size distribution of the five sediment classes used (left). Mean diameter and gradation coefficients ($\sigma_g = \sqrt{D_{84}/D_{16}}$) are also indicated in the plot. Sediment initial distribution over the model surface (right).

In these experiments, simulated rainfall was generated for 5 minutes, and TSS and Particle Size Distribution (PSD) samples at the entrance of the gully pots and at the pipe system outlet were collected to analyze the mobilization of the different fractions of particles through the model. PSD samples are especially interesting for the continuous granulometry (sediment class D5 in Figure 1.15) to analyze the different behavior of particles depending on their grain size in the same test. In addition, online turbidity records were registered at the pipe system outlet to obtain on-line TSS concentrations following the methodology developed in the preliminary tests. The variables considered in these experiments and the measuring points are presented in Figure 1.16.

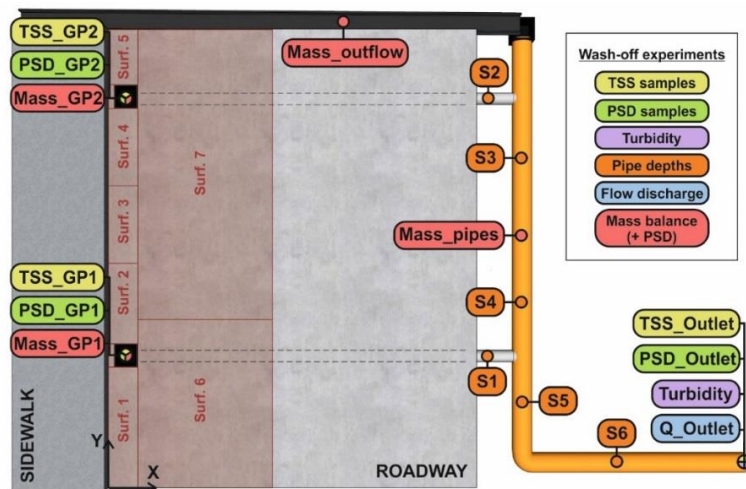


Figure 1.16. Measuring points and variables for the wash-off and sediment transport experiments.

The results of measuring TSS mobilization during the experiments for the five sediment classes and the three rain intensities at the entrance of the gully pots and at the pipe system outlet are shown in Figure 1.17. Particle sizes are presented in these results as the key variable in the wash-off process. The finest sediment (sediment class D1 with a mean diameter of 30 μm) produced the highest concentration at the gully pots and at the pipe system outlet with a large difference with respect to other particle sizes. In addition, the TSS concentrations measured for the continuous granulometry D5 ($d_{50}=165 \mu\text{m}$), both at the gully pots and at the pipe system outlet, were between those obtained for sediments D2 ($d_{50}=68 \mu\text{m}$) and D3 ($d_{50}=144 \mu\text{m}$). Therefore, we can see that considering the mean particle size as representative can lead to erroneous estimates in modelling wash-off.

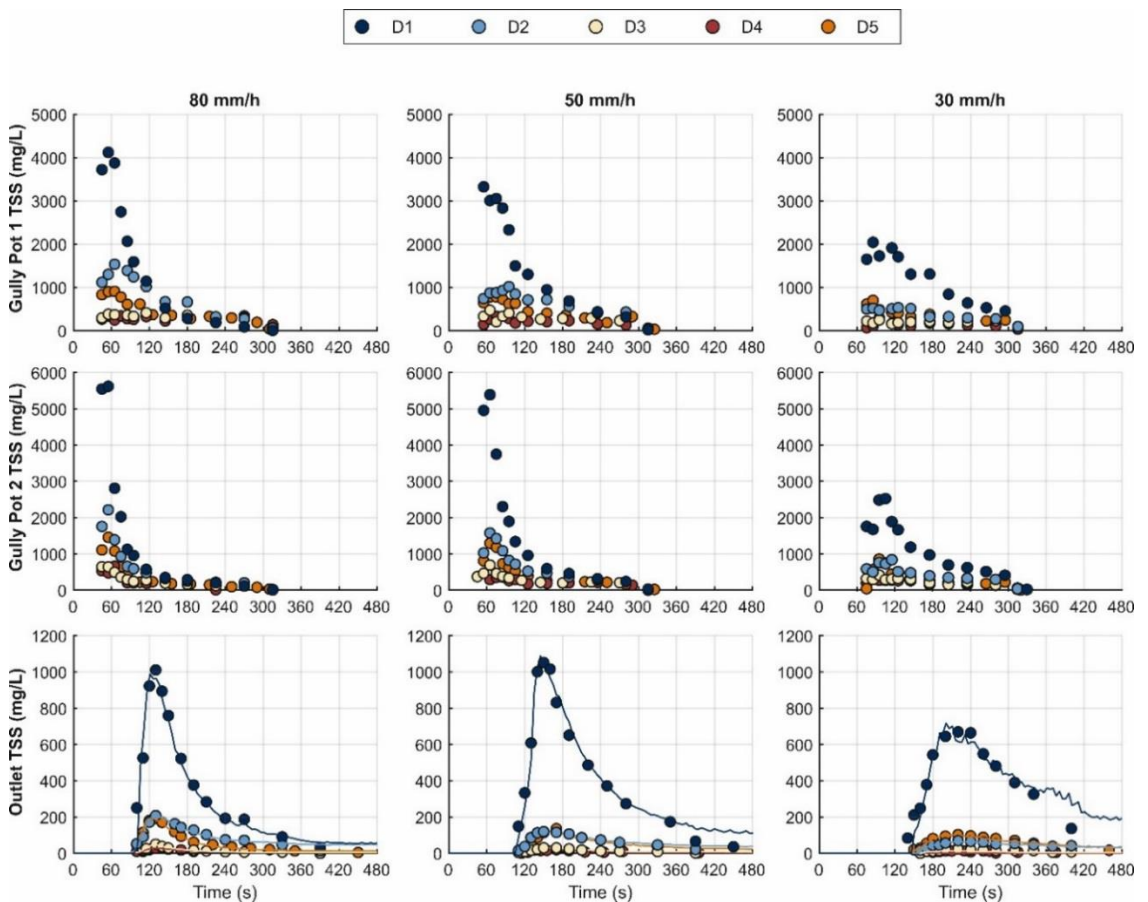


Figure 1.17. Total suspended solids (TSS) results in both gully pots and the pipe system outlet for the five different grain sizes (D1-D5) and rain intensities of 80, 50 and 30 mm/h.

At the end of each experiment, a sediment mass balance was performed, following the methodology developed in preliminary wash-off experiments, to assess the final distribution

of sediment in the different parts of the physical model and to ensure the reliability of the experimental results. The sediment masses obtained from each part of the model are presented in Figure 1.18 for the different rain intensities and sediment granulometries tested. The errors in the mass balances between the initial surface sediment mass and the masses collected at the end of the experiments plus the sediment washed from the physical model during the experiment were below 5%. This result is very satisfactory in consideration of the phenomena under study and to ensure the reliability of the experimental results. The PSD of mass balance samples were also measured using a laser coulter particle size analyzer in order to analyze the deposition of the different grain sizes at the end of the experiments.

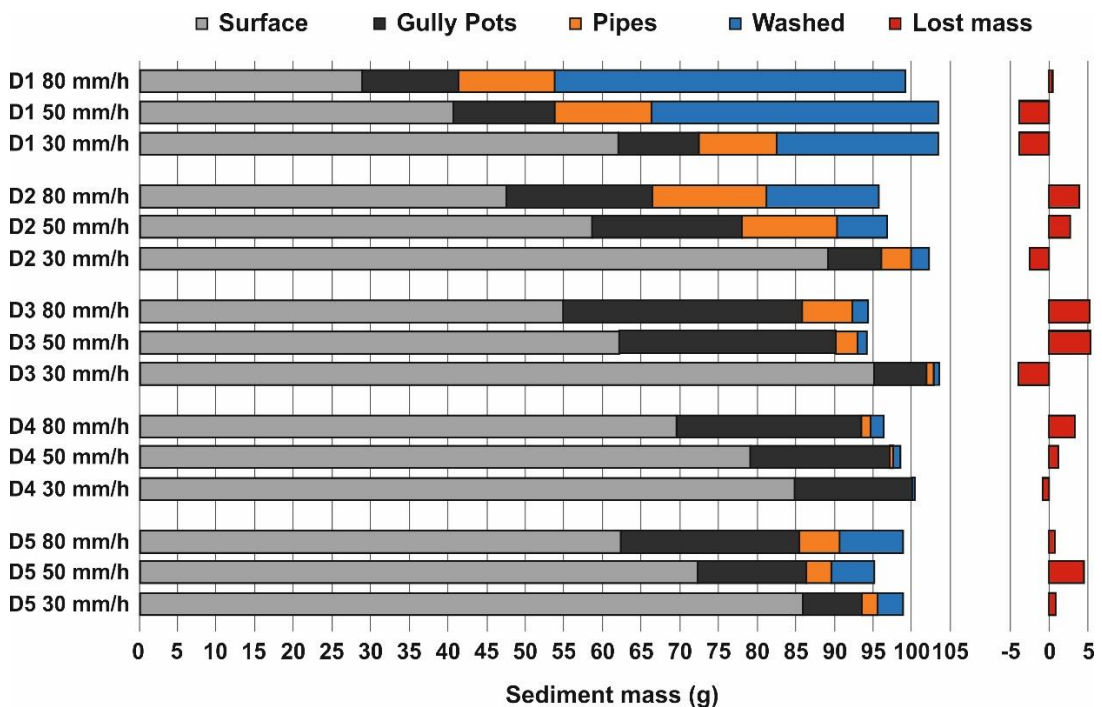


Figure 1.18. Mass balances results for the five different grain sizes (D1-D5) and rain intensities of 80, 50 and 30 mm/h.

The raw and processed data obtained in this thesis from hydraulic, wash-off, and sediment transport experiments were published in the Zenodo data repository within the scope of the WASHREET project (<https://zenodo.org/communities/washtreet>) and are openly available for other authors to use. A main data package (Naves *et al.* 2019c) contains the data related to the hydraulic, wash-off, and sediment transport experiments described in this doctoral thesis. These data address the lack of accurate measured data for modelling pollutant wash-off processes and can be used to develop, calibrate and validate urban drainage models, including wash-off and sediment transport processes in the different components of the

drainage system (surface, gully pots, in-pipe) without considering uncertainties in the input variables. Two additional packages (Naves *et al.* 2019d, Naves *et al.* 2019e) are provided to include detailed raw and processed data regarding the PIV analysis and the SfM photogrammetric technique, respectively. These datasets can be used to assess and optimize seeded and unseeded PIV techniques and in the study of the novel application of photogrammetric techniques for hydraulic modelling purposes, respectively.

The final chapter of this thesis (Chapter 6) presents the application of the TSS concentration results at the gully pots to assess and analyze a physically-based urban wash-off model, which uses the Hairsine-Rose formulation coupled with Iber, a 2D shallow water model developed by the author’s research group. Figure 1.19 includes the model predictions obtained in the analysis for the experiments with rain intensities of 50 and 80 mm/h and sediment classes D2 and D3, respectively. The study has shown that the flexibility of the model allowed for the replication of the laboratory results from accurately measured initial conditions by tuning the six H-R model parameters. However, different sets of parameters showed similar TSS results, indicating that this flexibility also leads to identifiability problems when calibrating the model.

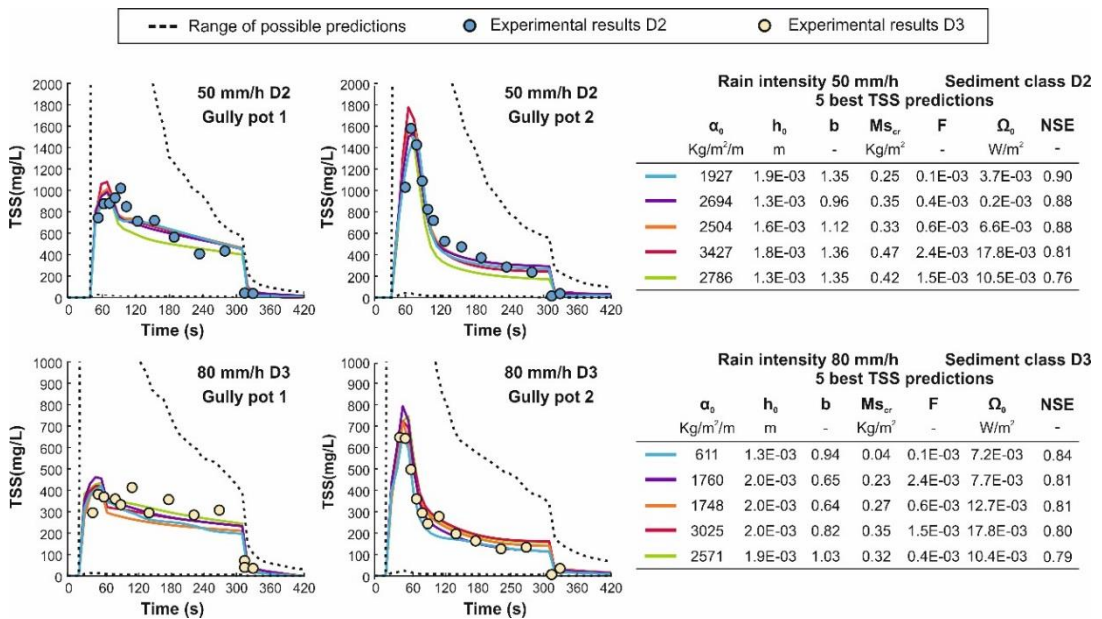


Figure 1.19. TSS experimental results and five best-fitted simulations for the experiments with rain intensities of 50 (up) and 80 mm/h (down) and sediment classes D2 and D3, respectively. The parameter sets of the five best-fitted predictions are also included.

In this context, the study contributes to the understanding of physically-based urban wash-off models through an in-depth sensitivity analysis in order to provide the information

necessary to choose the most important parameters and to simplify the model in order to deal with identifiability. The accurate measurement of the input variables and the precise definition of hydraulics have made it possible to separate the individual contribution of the parameters of the Hairsine-Rose sediment transport model and to analyze their influence in the total washed off mass and the TSS peak at both gully pots. Figure 1.20 shows the sensitivity of the washed off mass in gully pot 1, obtained using both the Standardized Regression Coefficients method and the Extended Fourier Amplitude Test, to the Hairsine-Rose parameters for the 12 tests considered in this study. The analysis showed that both the total washed off mass and the TSS peak concentration were highly sensitive to the critical mass ($M_{s_{cr}}$), as this parameter considers the reduction in the detachment of particles due to a lack of sediment on the impervious surfaces. In addition, rain- (α_0 , h_0) and flow-driven (F) detachment parameters were presented as key for smaller (mean grain sizes of 30 and 68 μm) and larger (144 and 274 μm) sediment particles, respectively, with b and Ω_0 being almost negligible. The differences between the total (bars with dark colors) and first order effect indices (bars with light colors) in Figure 1.20b show the variance of the results due to interactions between parameters. It has been found that interactions play an important role in the results, especially in the TSS peak concentration and in the larger diameters (sediment classes 3 and 4) for the total washed off mass. This has highlighted the need for sensitivity results to simplify the model before calibration.

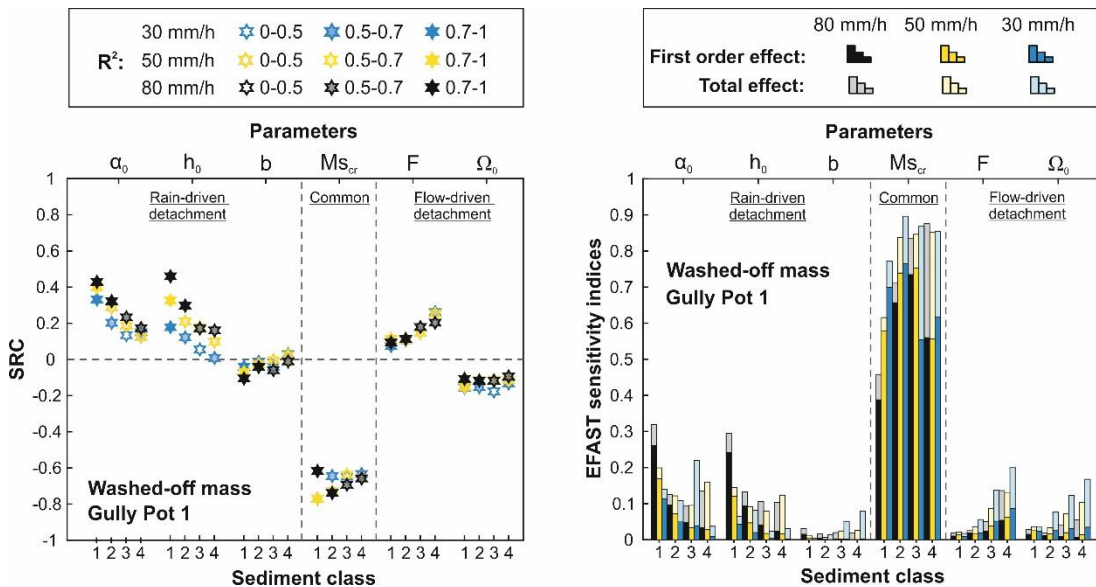


Figure 1.20. SRC and EFAST first order and total effect sensitivity indices of the Hairsine-Rose parameters for the total washed off mass in gully pot 1 and for each of the laboratory experiments considered (colors for rain intensities and x-position for sediment classes).

The relative importance of hydraulics, initial sediment conditions, and model parameters in model outputs has been also investigated to ensure the transferability of the results to real field studies, where it is not possible to define the model input variables with the same degree of accuracy as in the laboratory physical model. Figure 1.21 includes the local sensitivity results for the rain intensity of 30 mm/h and sediment class D1 test. The initial load of sediment and the mean grain size were seen to be the most important variables, thus underlining the need for very accurate measurements in order to avoid the variability associated with the build-up process affecting the results of the model. This need for accurate input variables, together with the high computational cost of the model, limit current applications to real-world catchments. However, model speedup and improvements in analysis efficiency are being developed nowadays and more laboratory and field studies should be performed to increase the understanding of input variables and model parameters. The results obtained are promising and merit further investigation in order to work on treatment and management techniques to minimize the impact of urban surface contaminants on urban environment.

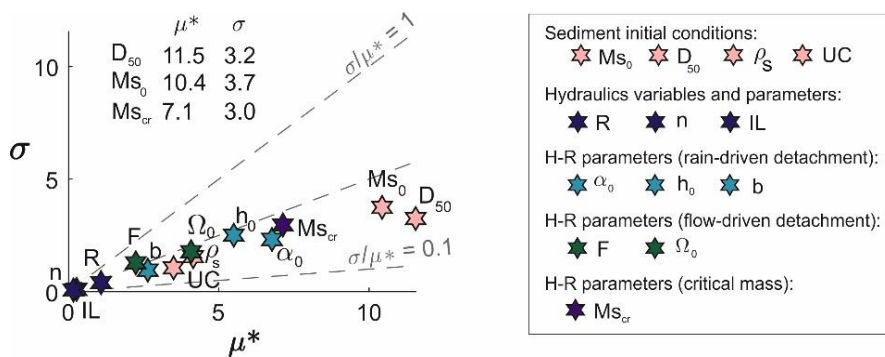


Figure 1.21. Sensitivity results for the Elementary Effects method for the 30 mm/h and sediment class D1 test. Plots show the sensitivity to the total washed off mass through gully pot 2. The ranking of the three most influential input factors is shown in the upper-left corner of the plot.

Finally, two papers including part of the work presented in this thesis have been included in Appendix B. After this, Appendix C lists additional publications in the field of urban drainage in which the author has collaborated during his doctoral work. These studies concern an experimental and numerical analysis of the flow performance of egg-shaped sewer pipes, and two studies performed in a real wastewater facility where the accumulation, erosion, and in-sewer sediment transport were investigated. These additional studies have contributed significantly to the author's training and experience, and show the high variability associated with sediment transport processes in real field applications.

6 General conclusions

In this thesis, an extensive experimental dataset has been obtained by analyzing the wash-off and sediment transport processes through an urban drainage physical model. This dataset addresses the lack of accurate data to be used in developing more reliable urban wash-off and sediment transport models. The presented experiments are performed in a 1:1 scale physical model, considering complex surface flows developed next to curbs or in gully pot surroundings and using a realistic rainfall simulator, ensuring thus a high transferability of the results to field applications. Moreover, in addition to the accurate measurement of the variables involved in TSS mobilization, hydraulic calibration data is also provided to precisely represent overland flow, which is key in the detachment and transport of sediment particles. These data have made it possible to analyze the performance of a physically-based urban wash-off approach, and have also demonstrated its usefulness. In this research, then, the following main conclusions have been drawn:

- In preliminary tests, an experimental methodology has been developed to accurately measure the wash-off and sediment transport processes. The procedure includes a final mass balance that made it possible to ensure and quantify the reliability of the experimental results in each test, resulting in mass balance maximum errors of around 9.4%, which are considered satisfactory considering the phenomena under study. Results showed that sediment initial load and distribution cannot completely explain pollutant wash-off processes because other variables, such as the uniformity of the rain, greatly affect the outlet pollutographs and system mass balances. A precise definition of overland flow has also been found essential to understand processes involved in wash-off phenomena.
- Accordingly, a new drop-forming rainfall simulator was developed to replace the one used in the preliminary tests, in order to ensure the transferability and comparability of experimental results with field studies. The new rainfall simulator is able to generate three different rainfalls with mean rain intensities of 32.9, 54.9 and 79 mm/h and an almost uniform distribution (Christiansen's Uniformity Coefficients of 81, 89 and 91% respectively). In addition, a mean drop size of 0.95 mm and a drop impact velocity of over 85% of terminal velocity for the mean drop size were obtained by calibrating the simulator against natural rain measurements. This results in the new rainfall simulation design being an optimal tool for wash-off studies.
- The velocity distribution of overland flow has been precisely measured in shallow water conditions of a few millimeters' depth by a modified LSPIV technique, which uses fluorescent particles as tracers to avoid raindrop interferences. Experimental results showed the presence of some main drainage channels perpendicular to the curb of the physical model due to irregularities in the model surface. An accurate

representation of the overland flow was achieved using a 2D shallow water model with a high-definition elevation map obtained using photogrammetric techniques. This study highlighted the need for detailed topography to accurately represent surface flow in very shallow water conditions and to assess positively the visualization techniques used for hydraulic modelling purposes.

- An experimental dataset concerning hydraulic, wash-off, and sediment transport experiments has been obtained using the three different rain intensities that the proposed new rainfall simulator is able to generate and five sediment classes with different granulometries (d_{50} ranging from 30 to 275 μm). The measurement of TSS, particle size distributions, and flow discharges at the entrance of the gully pots and at the sewer system outlet presented the sediment granulometry as key variables for wash-off and sediment transport processes and reported that considering mean grain size as representative can lead to erroneous estimates modelling pollutant wash-off. The mobilization of sediments through the physical model depending on the sediment granulometry and the rain intensity was also analyzed by performing mass balances, which were also used to indicate the reliability of the experiments. Results showed that, even using the finest sediment and the highest rain intensity, only a fraction of the sediment is washed completely from the physical model. The errors found when performing the mass balances were below the 5% of the initial sediment mass, which is very satisfactory and demonstrate the accurate measurement of wash-off processes. Finally, the open access publication of the data makes our work replicable and provides essential data for testing and developing existing and new wash-off and sediment transport formulations.
- The accurately measured input variables and the precise representation of surface flow have made it possible to perform an in-depth sensitivity analysis of a physically-based urban wash-off model, which uses the Hairsine-Rose formulation coupled with a 2D shallow water model, without considering the usual field uncertainties that may hide the individual contribution of each input factor in the results. Model results showed that it was possible to successfully reproduce laboratory experiments by tuning the wash-off model parameters, but suggested a complex calibration process due to identifiability problems. The analysis presented provided the necessary information to properly simplify the model in order to address this issue, and proposed a reduction from 6 to 3 model parameters to properly model the individual contribution of the rain-driven and flow-driven detachment of particles. The study also reported the high influence in the TSS results of the sediment initial conditions, which confirmed the need for accurate input data to properly analyze and develop the model. The promising results obtained, and the insights that are being seen nowadays in model speedup and improvements in

analysis efficiency, make the model analyzed an effective tool to increase the understanding of the process involved in pollutant wash-off in urban catchments.

The research overall has sought to increase our understanding of pollutant wash-off and sediment transport processes, as a means of developing more reliable urban drainage models in order to improve management and treatment techniques for sustainable development of urban areas. The results obtained are a step towards this objective, providing significant data for scientific community in order to develop, calibrate, or validate existing and new formulations, and contribute to the identification of processes and variables that govern pollutant wash-off phenomena.

7 Future research

The experimental results used to analyze the performance of the physically-based wash-off model involved the overland flow representation and the TSS measurements collected at the entrance of gully pots for the four sediment classes with uniform granulometry. Therefore, only a part of the provided results was used, and useful data remains for analysis and further use. For instance, TSS samples and flow discharges at the pipe system outlet, together with gully pots results, are suitable and accurate information of inflow and outflow TSS concentrations, which is optimal for the analysis of in-pipe sediment transport processes and for the development of dual drainage models.

Moreover, a continuous and realistic granulometry was also used in the experiments with additional measurements of the temporal variations of particle size distribution in gully pots and pipe system outlet discharges. The results allow for the analysis of multiclass approaches, which are a solution to the unrepresentativeness of mean diameter and density in real field applications for modelling TSS mobilization. These models have an associated increase in complexity due to the consideration of several grain sizes, and their feasibility and performance should be assessed.

Mass balance measurements are also notable results and can increase our knowledge of pollutant wash-off processes. The sediment masses that are deposited in the model at the end of the experiments, as well as their granulometries, indicate the fraction of particles that pass through the different parts of the model depending on the initial sediment grain size and the rainfall intensity, showing, for example, that for the lower intensities only the finer fractions reach the pipe system outlet. This information may also be used in gully pots performance analysis and models.

Other interesting measurements that were not analyzed in depth in this thesis include the use of bubbles and water reflections in surface flow as tracers for the measurement of overland velocity distributions through the LSPIV technique. Fluorescent particles and UV

illumination have demonstrated their usefulness as a non-intrusive method to measure very shallow flows with the presence of raindrops. However, the assessment of a reliable, unseeded LSPIV method is an interesting tool to simplify the measurement methodology, especially for field campaign purposes.

Regarding the use of the data for the analysis and development of physically-based models, a sensitivity analysis was performed in this thesis as the first step toward a rigorous systems analysis. It has allowed us to assess the performance of the model and to identify the most important parameters, and has provided information as a means of simplifying the model to address identifiability problems. Taking this outcome into account, the experimental data also provide an opportunity to properly calibrate the model and to compare the results to the predictions of usual empirical formulations, quantifying the differences and analyzing model errors.

Another important task to address is the transferability of the knowledge obtained in laboratory controlled conditions to real field applications, which was discussed at length in chapter 6 (Section 4.2). The difficulties of measuring accurately input variables, the neglect of spatial and temporal heterogeneities and the high computational cost of physically-based models limit current field applications. However, the progress made in the understanding of build-up processes, the increasing availability of accurate data, the representation of detailed physical processes by physically-based models, and improvements in model speedup and in analysis efficiency all serve to make the future of pollutant wash-off modelling a promising area of work, and encourage us to conduct more field and laboratory studies to increase our understanding of the phenomena. This future work should not be oriented towards developing more and more complex models accurately representing all the physical processes, but should move towards models capable of considering the spatial and temporal heterogeneities of urban catchments and the key processes involved. The identification of the main variables that govern pollutant wash-off would then be needed to be able to simplify models adequately, rendering them useful for practical applications, this towards better treatment and management techniques for minimizing the impact of urban surface contaminants, such as microplastics, heavy metals and PAH, on the environments of towns and cities.

Chapter 2

Preliminary wash-off tests

1 Introduction

The contemporary trend of fast urbanization and population migration to cities and towns has resulted in the development of more impervious surfaces such as urban areas, roads and parking lots. Some of the consequences of this trend are greater hydrograph runoff volumes and flow velocities and shorter concentration times. The result is an overall increase in pollution levels (Butler and Davies 2010). Pollutants such as sediments, nutrients, organic matter, heavy metals, hydrocarbons or pesticides are accumulated over impervious surfaces during dry days and washed into water bodies through surface runoff during rainfalls (Gastaldini *et al.* 2013). This causes significant environmental impacts and constitutes a great problem in urban areas, as it has been demonstrated in several studies (e.g. Anta *et al.* 2006, Zafra *et al.* 2008, Miguntanna *et al.* 2010). An understanding of pollutant wash-off and transport process in sewer systems is essential to estimate the mobilization of pollutants and to improve treatment techniques to minimize their impact on the environment.

Wind and rain characteristics, surrounding land uses, traffic conditions, catchment characteristics or street sweeping and other human activities are presented by different authors as key factors that affect pollution build-up and redistribution of particles (see among others Deletic *et al.* 1997, Vaze and Chiew 2002, Hengren 2005a). Therefore, total load distribution of sediment across the road is not uniform and is influenced by the existence of natural or artificial barriers like vegetation, footpaths or curbs as shown by Deletic and Orr (2005). As part of the given study, sediment collected from sampling sites with different distances from the curb were analysed showing that load and particle sizes decrease with distance from the curb, and two-thirds of these solids were presented within 0.5 m from the curb. Earlier studies (Sartor and Boyd 1972, Grottker 1987) reported the same phenomenon with a higher percentage of solids near the curb. As regards washed sediment sizes, a broad spread of data has been observed in previous quality runoff studies (Charters *et al.* 2015). In the work of Anta *et al.* (2006), a d₅₀ mean value of 38 µm was obtained and only 10% of solids were greater than 150 µm. These values are close to the overall average values reported by the work of Charters *et al.* (2015). Furthermore, studies such as developed by Chebbo and Gromaire (2004) reported that most of the pollutants are associated with the finest fraction of the sediments, which are the most difficult particles to eliminate by sedimentation techniques. Thus, in order to analyse wash-off and sediment transport processes, these finest fractions of the surface sediments are considered the most interesting ones.

Urban wash-off water quality models are usually based on empirical equations like the developed one by Sartor and Boyd (1972); such equations are implemented in most of the commercial codes like SWMM (Rossman 2015). Antecedent dry days and total runoff

volume are the main relevant variables for describing build-up and wash-off processes (Wang *et al.* 2011). Nevertheless, most of the approaches do not consider other aspects like the sediment characteristics, the definition of a threshold shear stress for particle movement or the influence of raindrops energy (Tomanovic and Maksimovic 1996), and the equations are often roughly approximate compared to the complexity of the physical phenomena (Bertrand-Krajewski 2006). In order to design and calibrate numerical models, several studies have been developed to characterize build-up and wash-off process in urban catchments of different sizes. For instance, Egodawatta *et al.* (2007) suggest that an isolated storm event has the capacity to wash only a fraction of pollutant and this fraction was related to rainfall intensity, the kinetic energy of rainfall and characteristics of the pollutants. In addition, different empirical approaches to build-up and wash-off processes were proposed by authors such as Wijesiri *et al.* (2015a), Chow *et al.* (2015) or Morgan *et al.* (2017).

The main objective of this work is to analyse how accumulation and dispersion of pollutants affect the wash-off process on a street section at the scale of 1:1. This facility has been used previously for hydraulic validation and calibration of the Water and Environmental Engineering Group (GEAMA) MODUS 2D-1D urban drainage model (Fraga *et al.* 2015a, 2015b).

2 Material and methods

2.1 Experimental setup

The laboratory installation consists of a full-scale street section built in the Hydraulic Laboratory of the Centre of Technological Innovation in Construction and Civil Engineering (CITEEC) at the University of A Coruña. The physical model geometry and overview of the installation are shown in Figure 2.1. The model consists of a concrete tile pavement and a concrete roadway linked to a sewer drainage network. Three gully pots, two of them at the roadway and a third one at the end of the lateral outflow channel with a rectangular cross section, collect the runoff to the sewer network which includes six circular pipes with two different diameters: 0.085 m (Pipe 1 and Pipe 2) and 0.19 m (Pipes 3, 4, 5 and 6). The surface has an average transversal slope of 2% to the 0.15 m high concrete curb and a 0.5% longitudinal slope to the outflow channel. The sewer network characteristics and a detailed bathymetry of the model can be consulted in Fraga *et al.* (2015a).

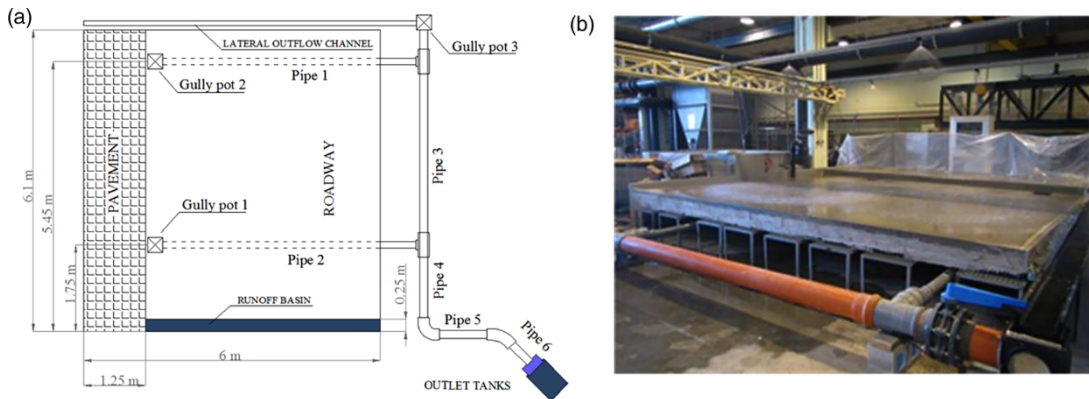


Figure 2.1. Geometry (a) and photograph of the experimental setup (b).

Four nozzles of Fulljet 3/4HH71WSQ (Spraying System Co., Wheaton, IL, USA) located 2 m above the surface generate the rainfall in the model. The kinetic energy of falling raindrops is a key variable in the wash-off process because it affects the degree to which pollutants are detached from the surface on impact. Therefore, nozzles have been selected taking into account raindrops' fall velocity (7.62 m/s) and mean size (0.0028 m), in order to reproduce faithfully real rain characteristics (Hudson 1963). The rain intensity distribution at the roadway and pavement surface was measured by the volume of water collected in a 0.25 m grid of test tubes during 3 min of rainfall. Rain intensity map (Figure 2.2a) shows that intensity is higher in two opposite areas for each diffuser and where they overlap. Average rainfall intensity (101.44 mm/h) corresponds to a high intensity of real rain.

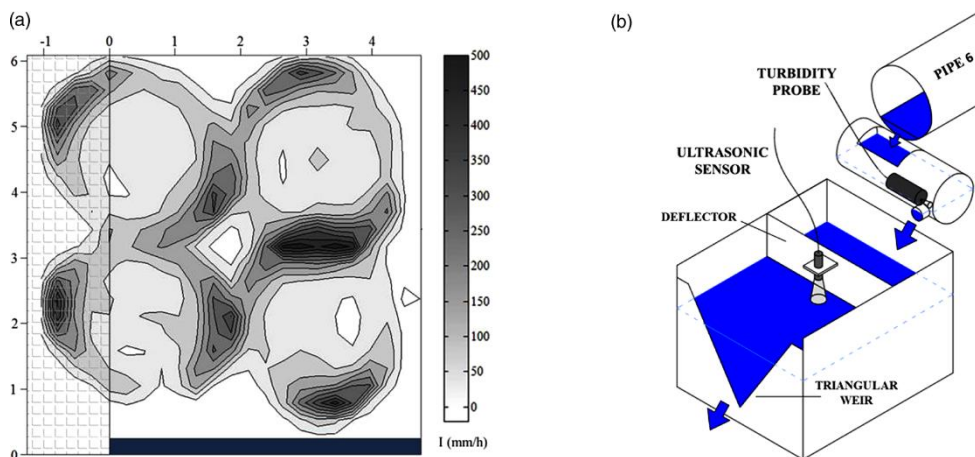


Figure 2.2. Rain intensity map over street surface (a) and scheme of sewer outlet tanks (b).

Two tanks located at the sewer network outlet were used to measure turbidity and discharge volume (Figure 2.2b). A turbidity probe (Solitax) was installed in the first tank,

which has a reduced volume (0.16 m diameter and 0.4 m length), allowing measuring the turbidity records with sufficient depth. The turbidity was measured with a 5-s frequency and a measurement accuracy of ± 0.01 FNU (Formazin Nephelometric Unit). This tank drains into a bigger reservoir ($0.5 \times 0.6 \text{ m}^2$) where discharge was measured by a triangular weir. In addition, discharge was redundantly measured by a flowmeter installed at the rainfall generation system. The error between both measurements was less than 2%.

An industrial dust with $d_{50} = 40 \text{ }\mu\text{m}$ and $200 \text{ }\mu\text{m}$ maximum size was chosen to simulate runoff pollution according to the results from Anta *et al.* (2006). It has a suitable grain size and it also has excellent properties for a total suspended solids (TSS) analysis. This dust is not cohesive, it does not form floccules and it does not dissolve, so the sediment transport is completely in suspension allowing a greater control over solid discharges and mass balances.

2.2 Experimental procedure

Different build-up configurations were placed over the roadway surface before the beginning of the experiments. Once the sediment deposits were distributed, a constant rain was simulated for 5 min. During each experiment, turbidity and flow discharge were monitored continuously at the sewer network outlet. As both parameters were measured at different reservoirs, time shifts have been noticed at the beginning and at the end of the hydrograph caused by the retained volume in the outlet tank (Figure 2.2b). In order to compensate these time shifts (20 s maximum), the hydrograph was routed in the outlet of the turbidity probe reservoir from the discharge measured with a triangular weir and a variation of the outlet tank volume. The total amount of sediment mass from the runoff was determined from the hydrograph and pollutograph integration.

In the course of each test, 12 manual grab samples were collected with 250 mL vessels at the turbidity probe tank outlet as part of the runoff characterization. The purpose of sampling was to correlate TSS concentrations with the turbidity probe signal. The first 6 samples were collected every 10 s after the beginning of the flow discharge in order to record the peak of the pollutograph accurately. The next 6 samples were collected every 60 s with the aim of having data from the whole pollutograph. TSS values were obtained from samples following the APHA (1995) method. By means of a linear regression, the turbidity probe signal was converted to TSS concentration values. As suggested by Torres and Bertrand-Krajewski (2008), an individual trend line was obtained for each test, resulting in determination coefficients (R^2) above 0.96 for all experiments (Figure 2.3). All manual grab samples volumes were added to the measured flow hydrograph.

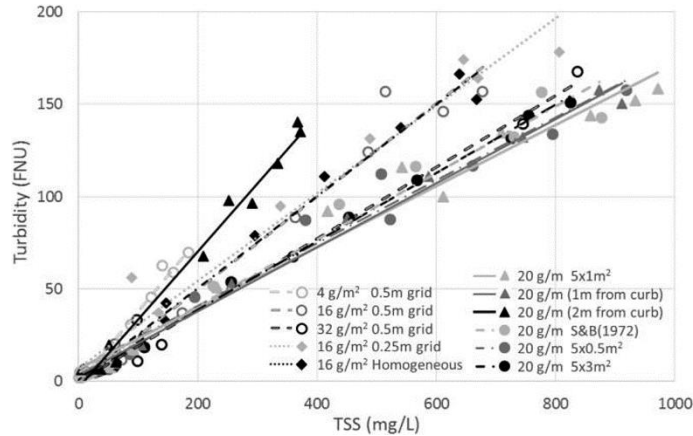


Figure 2.3. Individual turbidity (FNU) and TSS (mg/L) regressions.

At the end of each test, a percentage of the initial sediment load remained deposited over the pavement. In addition, some dust was retained inside gully pots and pipelines. These sediment fractions were recovered in order to calculate a sediment mass balance and assess the global accuracy of each test. Firstly, dust remained over the surface and inside gully pots it was collected with an industrial vacuum sweeper with a 98% sweeping efficiency. Some cement dust particles from the pavement surface were also collected in a small portion during this process. Sweeping blank experiments (without sediment loads over the surface) were performed to consider these particles in mass balances. Later, pipes 1, 2 and 3 were cleaned with a 1 L/s flow. TSS concentrations and flow discharge were measured in cleaning processes in order to calculate the mass associated with pipe sediment bed deposits.

Relative error in the mass balance of each test (ε_M) was obtained as the difference between the initial sediment load placed over the roadway surface (M_0) and the amount of mass recorded at the sewer outlet ($M_{outflow}$), the amount of mass recovered by the industrial sweeper at the pavement surface ($M_{surface}$) and gully pots (M_{gully}), and the sediments deposited in pipeline inverts (M_{pipes}) in accordance with Equation (1). In this equation the small fraction of cement dust particles (about a 2% of M_0) recovered by the vacuum sweeper has also been taken into account ($M_{cement\ dust}$).

$$\varepsilon_M = \frac{1}{M_0} [M_0 - (M_{outflow} + M_{surface} + M_{gully} + M_{pipe}) + M_{cement\ dust}] \quad (1)$$

Following this methodology, eleven experiments grouped into four sets of tests were performed. Figure 2.4 shows the sediment distribution and initial load for each test. The experiments were configured to assess the influence of the initial load, the spatial distribution method, the distance from the curb and the distribution area dimensions on the TSS wash-off.

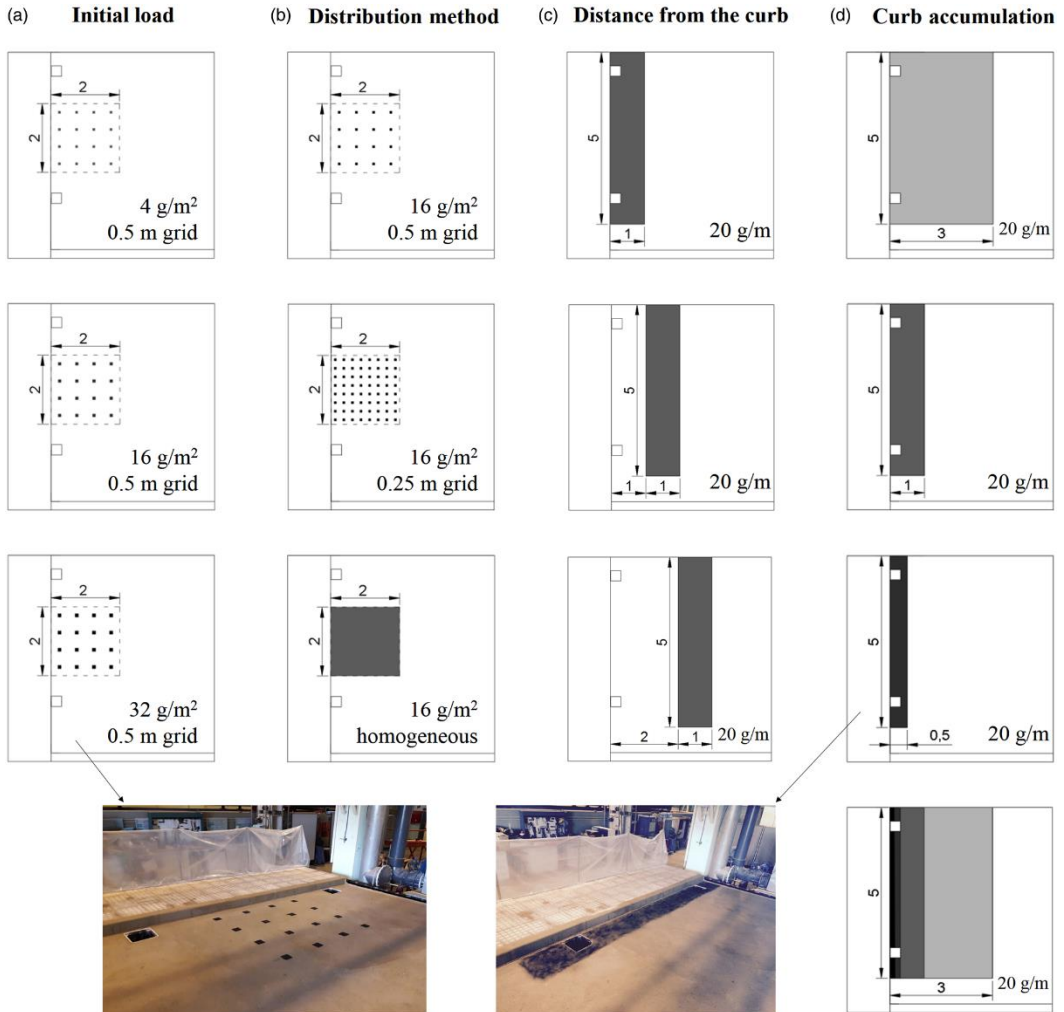


Figure 2.4. Distribution of the initial dust deposited over roadway surface in performed experiments. Two photographs from initial load and curb accumulation test are also included.

Initial surface sediment load tests: Several build-up studies, mentioned in the introduction section, were reviewed in order to select the most suitable initial load. Due to the wide range of variation of the initial sediment load, it became interesting to analyse how this parameter affects the mobilization of TSS. Therefore, in the first set of experiments called initial load tests (Figure 2.4a), three experiments with different pollutant loads of 4, 16 and 32 g/m² and the same distribution over the roadway surface were carried out. In all cases, dust was distributed in a 0.5 m grid on a total surface of 4 m². In these tests, sediment was deposited between the gully pots because runoff from this area is completely drained into gully pot 2 and sediment transport conditions are more controlled.

Sediment distribution method tests: Using a grid to distribute sediment in small rectangular piles (with an area of 0.0025 m^2) allows us to easily repeat and compare different tests, but this distribution method gets away from the way that pollutant appears over real roadways. This set of experiments was performed to study the influence of the sediment distribution, with the same initial sediment load (16 g/m^2) placed over the roadway (Figure 2.4b). In addition to the 0.5 m grid distribution of the first round of experiments, a 0.25 m grid and a homogeneous distribution were placed over a total surface of 4 m^2 .

Distance from the curb tests: In the third set of experiments, sediment was distributed along 5 m of the curb in 1-m-wide strips. For these tests, the strip was placed attached to the curb and 1 and 2 m away from it (Figure 2.4c). The purpose of these experiments was to compare the resulting pollutographs for different separations of the sediment strip from the gully pots.

Curb accumulation tests: Real roadway sediment accumulates near the curb (Grottker 1987, Deletic and Orr 2005). Therefore, in the last set of tests, a 20 g/m initial sediment load was attached along the curb with a 5-m-length strip with different widths for each experiment (Figure 2.4d). Firstly, dispersed load tests were performed with surface sediment widths of 0.5, 1 and 3 meters. In the last experiment, a more realistic distribution of the initial sediment load was placed following Sartor and Boyd (1972) measurements. This study concluded that 78% of the initial sediment load over a roadway surface was found within the first 0.15 m from the curb, then 10% and 9% over the next 0.15 and 0.70 m, respectively, and finally 3% over the rest of the surface up to the road median.

3 Results and discussion

3.1 Initial surface sediment load tests

Figure 2.5 shows the pollutographs and discharges measured during the initial load tests and mass balance results. A good agreement between turbidity derived pollutographs and manual samples was found. The TSS peak value measured increases in an approximately linear trend as the initial sediment load over roadway surface increases, without TSS peak temporal shift, so results can be extrapolated to other initial pollutant loads. Discharge remains constant in all cases because hydraulic experiment conditions do not vary throughout the configurations tested in this work.

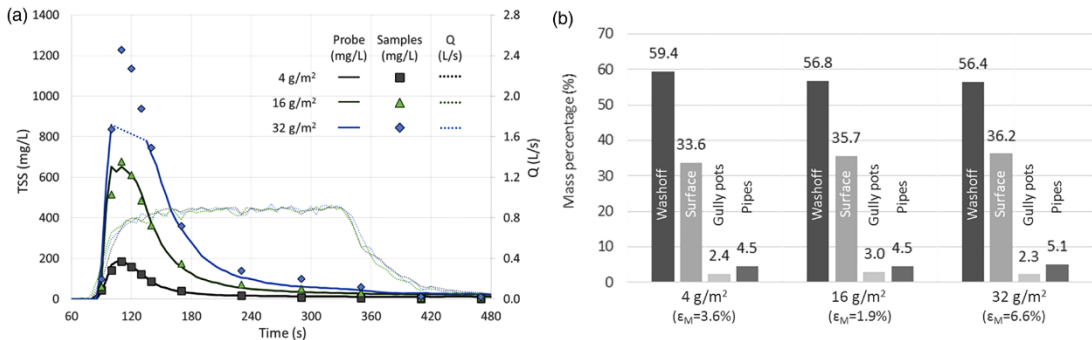


Figure 2.5. Samples and turbidity signal derived TSS pollutographs and discharges at the sewer outlet (a) and mass percentage final distributions (b) for sediment loads of 4, 16 and 32 g/m² over a 4 m² surface in a 0.5 m grid. Values in parentheses indicate the mass errors balance (ϵ_M).

In these experiments, $93\% \pm 1\%$ of sediment mass was washed off by rain or remained over the road surface. About $58\% \pm 2\%$ of mass was recorded at the sewer outlet and about $35\% \pm 2\%$ was collected over the surface after the end of each experiment. A non-negligible sediment mass was also deposited in the gully pots and pipes ($7\% \pm 1\%$ in mass). These sediment percentages were kept almost constant for all test conditions, therefore the percentage of sediment wash-off was unaffected by the initial sediment load over the roadway surface. Mass balance error (ϵ_M) was found below 7% for all experiments, which is reasonably low considering the scale of the system and the studied phenomenon. In the test with the highest TSS peak value, sediment mass at the system outlet was integrated from manual samples curve because the turbidity probe was out of range in these measurement conditions (roughly 800 mg/L, Figure 2.5a).

3.2 Sediment distribution method tests

Figure 2.6 shows the pollutographs and mass balances of the experiments with the same initial load (16 g/m²) and different surface distribution method. TSS peak concentrations are very similar in all these tests, with a slightly higher peak for the 0.25 m grid. Therefore, spreading sediment homogeneously does not introduce qualitative differences either in TSS pollutographs or in the mass distribution. This allowed the development of more realistic experiments with a homogenous distribution of the sediment load over the surface. The amount of mass collected in the runoff, surface, gully pots and pipes shows small variations between experiments, but the final distribution is similar to the previous tests. Consequently, mass balance is independent from the distribution method too. Again, small relative errors in the mass balances were determined in the tests (below 4% in these cases).

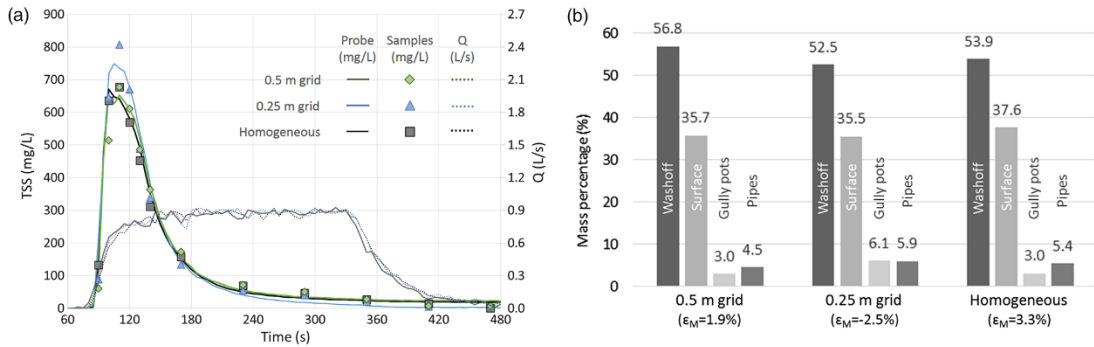


Figure 2.6. Samples and turbidity signal derived TSS pollutographs and discharges (a) and mass percentage final distributions (b) placing a sediment load of 16 g/m² over a 4 m² surface on a 0.5 m grid, a 0.25 m grid or spreading homogeneously. Values in parentheses indicate the mass errors balance (ϵ_M).

3.3 Distance from the curb tests

Results from the third set of experiments are shown in Figure 2.7. TSS concentration peaks at the sewer outlet were delayed and dumped as surface sediment transport path length was increased from the curb. When the surface load was placed near the curb, TSS peak was recorded after ~100 s from the beginning of the rainfall, meanwhile TSS peaks for tests with sediment area separated 1 and 2 m were collected at ~110 and ~120 s, respectively. Furthermore, smaller TSS concentrations were recorded for longer surface transport and, consequently, more sediments remained over the surface.

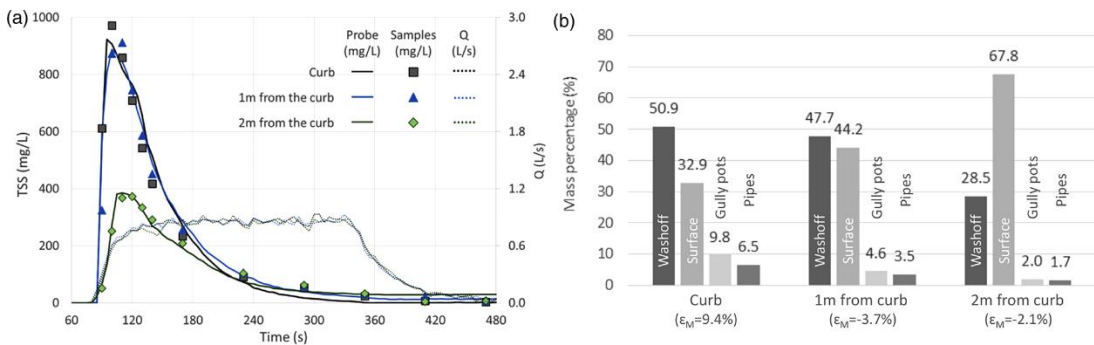


Figure 2.7. Samples and turbidity signal derived TSS pollutographs and discharges (a) and mass percentage final distributions (b) for a sediment load of 20 g/m², spread homogeneously over a 5-meter-long and 1-meter-wide surface, attached or 1 or 2 m separated from the curb. Values in parentheses indicate the mass error balance (ϵ_M).

For instance, in the test with sediment distributed 2 m from the curb, TSS peak concentrations at the sewer outlet were less than half compared with other experiments.

For this test, we have to notice the combined effect of the sediment transport path length with the spatial rainfall distribution. Thus, in the area situated between 1.6–2.0 m away from the curb the rain nozzles overlap each other and create a higher intensity rainfall zone (Figure 2.2a). High rain intensity areas hindered sediment transport from the pavement situated at a further distance from the curb and most of the sediment remain over the pavement. Previous experiments were not affected by this phenomenon because sediments were not placed upstream this high intensity area.

As stated previously, the sediment mass distribution over the surface, in gully pots and pipes is also affected by the position of the sediment strip in the street. When pollutants are far away from the curb, the amounts of sediments collected over the surface increases significantly (from ~30% to ~70% roughly); meanwhile, the mass recovered from gully pots, pipes and, especially, wash-off decreases. The maximum mass error balance was slightly increased in these tests ($\epsilon_M = 9.4\%$) probably due to the fact that the sediments were distributed over a larger area.

3.4 Curb accumulation tests

Finally, a more realistic sediment distribution was analysed in the curb accumulation tests. Figure 2.8a reveals that higher maximum TSS concentrations were recorded at the sewer outlet when the same amount of dust load of 20 g/m was distributed over a narrower wide strip. Thus, for a $5 \times 0.5 \text{ m}^2$, the TSS peak is 1,052 mg/L and, for a $5 \times 3 \text{ m}^2$, the peak is 824 mg/L. The recorded time to peak in these three tests is almost constant (about ~100 s from the beginning of the rainfall). Like, in the distance from the curb tests, as the amount of mass washed by the runoff decreases, more sediments remain over the surface and into gully pots and pipes (Figure 2.8b).

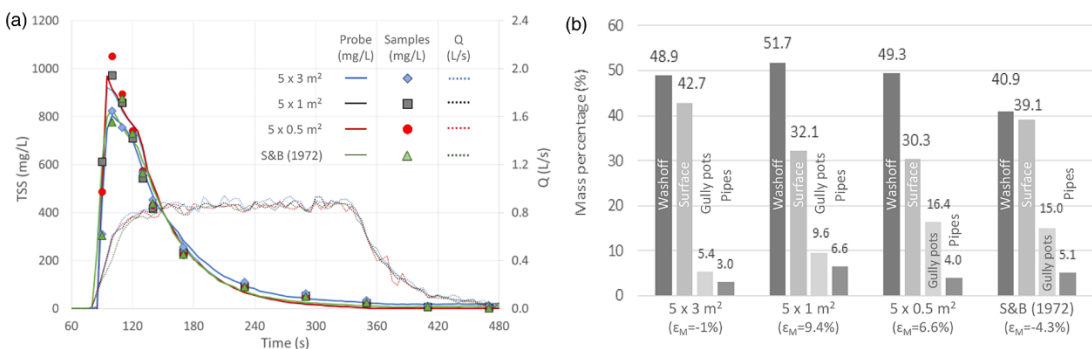


Figure 2.8. Samples and turbidity signal derived TSS pollutographs and discharges (left) and mass percentage final distributions (right) for a sediment load of 20 g/m, spreaded homogeneously over a 5-m-long and 3, 1 or 0.5-m-wide surface and placed with a stepped distribution. Values in parentheses indicate the mass error balance (ϵ_M).

The recorded pollutograph and mass balance for the Sartor and Boyd (1972) surface load distribution differ from the previous homogeneous strip load tests. Thus, the outlet pollutograph presents a smaller TSS peak (877 mg/L) and is recorded later (~110 s). In this case, a large percentage of the sediment load was distributed on a small area (0.15 m attached to the curb) where the highest water depths (~0.005 m) were recorded. These depths cause a decrease on sediment erodibility associated with the rain drops' kinematic energy, so a high sediment load is deposited near the curb at the end of the test. As the sediment is concentrated in a thinner strip, the wash-off efficiency of the curb over land flow may be reduced and more sediments could remain over the surface at the end of the experiment. From the mass balance point of view, the amount sediment collected from gully pots increased as more sediments were placed close to the curb. The effect of non-uniform rain explained in the previous section was also observed in the $5 \times 3 \text{ m}^2$ test, where one-third of the initial load was placed upstream of the high rain intensity area. The maximum error in the mass balance remained around 9.4%.

4 Conclusions

In this work, an experimental campaign was performed in a full-street physical model to assess some relevant aspects related with the wash-off and pipeline sediment transport processes in impervious urban areas. In the tests, the influence of the initial sediment load and its distribution over the street surface were analysed with a constant 5-minute rainfall. TSS pollutographs and flow discharges were recorded at the sewer outlet. After the rainfall, the sediment deposited over the street surface, gully pots and pipelines was measured in order to determine the mass distribution in different components of the system. Mass balances were performed to estimate the global test accuracy.

The first tests reveal that TSS peak value on pollutographs has an approximately linear relationship with initial sediment load over roadway surface, so results can be extrapolated to other surface load concentrations. In addition, it has been proven that the different methods of distributing the same amount of mass over the same total area do not produce qualitative differences either in the resulting pollutographs or in the mass distribution on the model. In the third and fourth sets of experiments, we observed that the maximum TSS values decrease as the surface sediment transport path length increases. Consequently, more sediments are deposited over the street surface. Nevertheless, these two parameters (surface sediment load and distribution) cannot explain completely pollutant wash-off processes because the spatial rainfall distribution or the runoff depth also affects the outlet pollutographs and system mass balances.

Finally, the obtained outcomes are part of a systematic database which is being developed at our laboratory facility. New tests considering different sediment grain sizes or rainfall intensities will be developed in future. The results obtained will allow the validation and calibration of sediment transport equations for surface wash-off, gully pot build-up and pipeline sediment transport in dual drainage models.

Chapter 3

Development of a new rainfall simulator

1 Introduction

Rainfall simulators are a recurring tool for laboratory and field studies in the area of urban drainage. The principal reason for this is that they open up the possibility of controlling the main variables that govern natural rainfall, being able to generate events with identical properties or varying certain relevant properties. Using a rainfall simulator with a suitable rain uniformity, and with distributions of drop sizes and velocities similar to real rain, is thus key for the reliability and transferability of the experimental results obtained. However, the difficulties in replicating natural rain lead to a wide range of designs, with no definitive solution having been identified (Kathiravelu *et al.* 2014). Rainfall simulator designs can be categorized into two main groups according to the way in which the raindrops are produced: i) pressurized nozzle simulators, and ii) drop-forming simulators. Both typologies present benefits and drawbacks that must be considered during the experimental design according to the objectives of the study. The variety of designs makes the measurement of rain properties such as uniformity, intensity, and raindrop size and velocity distribution essential to ensure the comparability of experimental results.

Pressurized nozzle simulators are commonly preferred for studies with simulated rainfall (Grismer 2011, Kathiravelu *et al.* 2014) due to their simple design and installation. Generated raindrops emerge from nozzles with a considerable initial velocity, so this typology produces satisfactory droplet velocity distributions at lower fall heights, reaching terminal drop velocities as in natural rain. The principal disadvantage is that nozzles require a relatively large orifice to generate a mean raindrop similar to real rain. This results in a high intensity storm if the nozzle sprays continuously (Isidoro *et al.* 2012). An oscillating bar (Aksoy *et al.* 2012, Hengren *et al.* 2005b, Egodawatta *et al.* 2007) or a solenoid-controlled simulator (Junior and Siqueira 2011) can be used to pause the spray and hence to reduce the rainfall intensity. However, Armstrong and Quinton (2009) examined the effect of intermittent rain in runoff sediment concentrations, concluding that results can be affected. When the spray stops, yields decrease over the street surface and the sediments are more exposed to the next period of high intensity rain, causing a greater detachment of soil particles. In addition, the overlapping of nozzles in medium- and large-scale studies significantly affects the spatial uniformity of rain intensity.

Drop-forming simulators have been seen to result in the better control of physical rain parameters than nozzle simulators, but have a more difficult design and assembly (Battany and Grismer 2000, Clarke and Walsh 2007). The uniformity of simulated rain benefits, because of the increase in the number of points where drops are generated. However, drops fall under the effect of gravity with a null initial velocity and they must fall a reasonable

distance in order to impact the surface at terminal velocity. For example, 1.5 mm drops require about 4 m of height of fall to achieve 95% of terminal velocity, as seen in Laws (1941).

This study focuses on the development of a rainfall simulator to study the wash-off and sediment transport processes in a 36 m² urban drainage physical model. Although the rainfall simulators used in urban drainage studies are based on nozzles (e.g. Al Ali *et al.* 2017, Al Mamoon *et al.* 2019), previous wash-off tests, in which four nozzles were used (Naves *et al.* 2017), have shown the importance of rainfall uniformity in the experimental results. Therefore, drop-forming was selected as the most suitable typology to improve the simulated rain and to achieve an appropriate spatial uniformity in this large-scale physical model. The description of the new rainfall simulator, its calibration, and the characteristics of the generated rainfall, are described in the remainder of this chapter.

2 Material and methods

2.1 Rainfall simulator description

The rainfall simulator that has been developed is located in the Hydraulic Laboratory of the Centre of Technological Innovation in Construction and Civil Engineering (CITEEC) at the University of A Coruña. It consists of two hose circuits placed above an urban drainage physical model with an approximate surface of 36 m². PCJ-CNL Netafim® drippers of 1.2 and 2 L/h are inserted in each circuit forming two grids of drippers with longitudinal and transversal separation of 0.20 m. Using this layout, the density of drippers in each circuit is 25 per m². Therefore, the simulator is able to generate rain intensities of 30 mm/h, 50 mm/h and, if both circuits are working at the same time, 80 mm/h. Pressure-compensating and anti-drain drippers have been chosen to avoid changes in flow rates due to pressure variations and to avoid water losses once the pressure is decreased below a certain value. The generated raindrops always fall on the same point of the model surface and have an approximate diameter of 4 mm, which is very high compared with natural rain. To fix this problem, a horizontal mesh is installed below the drippers circuits in order to break and distribute these uniform drops, improving rain uniformity and obtaining a heterogeneous drop size distribution. Figure 3.1 shows a general view of the rainfall simulator in its final configuration and a detail of the drippers inserted in the circuits.

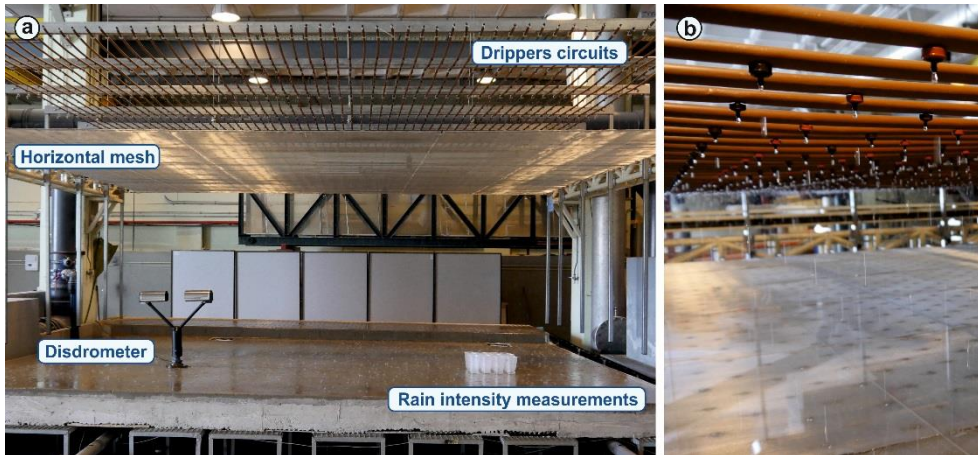


Figure 3.1. General image of the rainfall simulator in its final configuration above the urban drainage physical model. Disdrometer and vessels for measuring rain intensity are also shown (image a). Detail of both types of drippers inserted in the circuits above the horizontal mesh (image b).

2.2 Calibration procedure

Rain intensity, spatial uniformity, and kinetic energy of raindrops, which depends on their size and velocity, are the key rain variables that affect the wash-off process in the detachment of particles. Therefore, these variables were considered during the calibration process in a comparison with natural rain. First, the rainfall generator was installed and fixed as high as possible, approximately 2.6 m from the model surface, to allow bigger raindrops to achieve terminal velocity. Then, the calibration focused on establishing the optimal typology and position of the horizontal mesh that breaks and distributes generated raindrops. Rain intensity, spatial uniformity, and mean drop size and velocity were analyzed for nine different combinations of mesh size, material, and distance to drippers in order to simulate rainfall as similar as possible to natural rain. In these tests, rain intensity was set at the lowest rain intensity that it is possible to generate (30 mm/h), since it is expected to be the most demanding case in terms of rain uniformity. Then, configurations with better performance were also analyzed for the rain intensities of 50 and 80 mm/h. The configurations tested during the calibration process are summarized in Table 3.1.

Table 3.1. Configurations of the tests performed during rainfall simulator calibration.

Test	Mesh material	Mesh size (mm)	Drippers-mesh distance (m)	Rain intensity tested (mm/h)
1	Plastic	4.5	45	30
2	Plastic	4.5	70	30
3	Plastic	2	70	30
4	Plastic	1	45	30
5	Plastic	1	70	30
6	Metallic	2	45	30
7	Metallic	2	60	30
8	Metallic	2	70	30
9	Metallic	3	70	30
10	Metallic	2	70	50
11	Metallic	3	70	50
12	Metallic	2	70	80
13	Metallic	3	70	80

Rain intensity and uniformity were measured in each case using 16 vessels of 0.1 m in diameter as rain gauges, disposed together in a 4x4 grid covering a total surface area of 0.16 m² (Figure 3.2). Rain intensity was obtained from the water mass collected by each vessel in a 15 minute period of rain, and the result was then used to determine the Christiansen's Uniformity Coefficients (Christiansen 1942) as:

$$C_u = 100 \left(1 - \frac{\sum_{i=1}^n |\bar{x} - x_i|}{n\bar{x}} \right) \quad (1)$$

where x_i is the rain intensity in each vessel, \bar{x} their average, and n the total number of vessels.

A laser Parsivel 2 disdrometer (OTT, Kempten, Germany) was used during calibration (Figure 3.1a) to measure the mean diameter and velocity of raindrops. This equipment provides the number of raindrops that pass through a horizontal laser surface of approximately 54 cm² and classify them into 32 diameters and 32 velocity non-uniform ranges measuring the magnitude and the duration of signal attenuations (Tokay *et al.* 2014). Since the main objective of this chapter is the development of a rainfall simulator to generate rain as similar as possible to natural rain, the raindrop size and velocities distributions of local natural rain were also measured in February 2017 on the rooftop of the laboratory using the disdrometer with a sample frequency of 10 s. Data obtained was used as a reference in the comparison of the different configurations tested during the calibration of the simulator.



Figure 3.2. Vessels disposed over the model surface to measure rain intensity and uniformity for different mesh types and distances to drippers during calibration.

2.3 Rain properties of calibrated rainfall simulator

Once the rainfall simulator developed in this study had been calibrated, rain intensity, spatial uniformity, and raindrop size and velocity distribution were measured for the three rain intensities that it is able to generate. Similarly to the calibration methodology, rain intensity and uniformity were obtained from the water collected by 144 vessels placed over the full physical model surface in a 0.5 m x 0.5 m grid for a 5 minute period of rain (Figure 3.3). Finally, disdrometer measurements were used to register 10 s measurements of raindrop size and velocity distributions over 2 minutes.

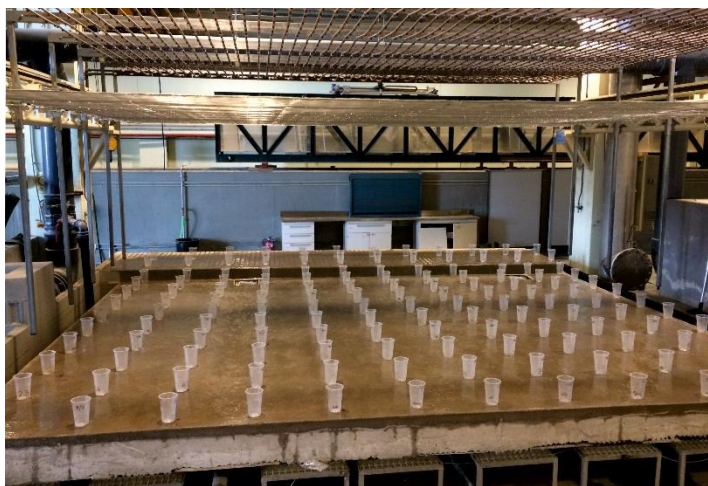


Figure 3.3. Vessels disposed over the entire model surface in a 0.5 m x 0.5 m grid to measure rain intensity and uniformity

3 Results and discussion

3.1 Natural rain properties recorded

Firstly, real rain properties registered by the disdrometer are presented as reference values to compare the different configurations tested in the calibration process. Plots in Figure 3.4 show the measured drop mean diameters and velocities according to their rain intensities. The results show that mean diameter and velocity remains almost constant for rain intensities over 20 mm/h, which is the case with the simulated rain, with approximate values of 1 mm and 3.4 m/s, respectively. In addition, the mean of 33 disdrometer measurements of natural rainfall with intensities ranging from 25 to 35 mm/h is shown in Figure 3.5. The plot represents the number of raindrops registered in 10 seconds classified into sizes and velocities and compared with the experimental relation between diameter and terminal velocity (Gunn and Kinzer 1949). These characteristics are established as objective values for the rainfall simulator under study.

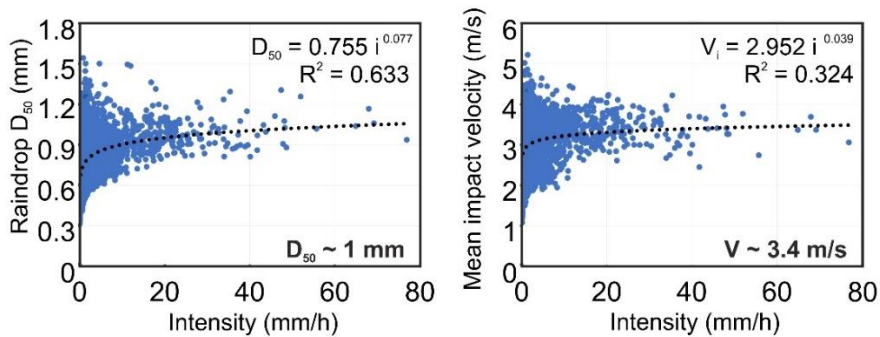


Figure 3.4. Relation of raindrop mean diameter and velocity with respect to the rain intensity measured by the disdrometer.

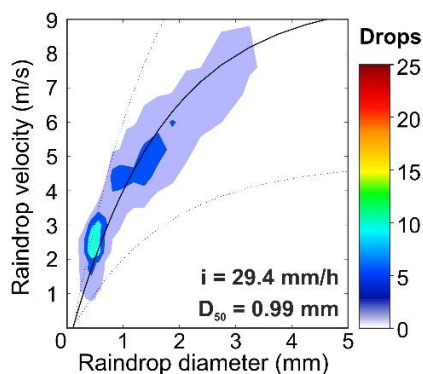


Figure 3.5. Raindrop size and velocity distribution of natural rainfalls with intensities ranging from 25 to 35 mm/h. The mean of the raindrops registered by the disdrometer classified in sizes and velocities is compared with experimental relation between diameter and terminal velocity (Gunn and Kinzer 1949), which is represented by the solid curve.

3.2 Calibration results

In this section the rain properties obtained for the different configurations tested during the calibration process are shown. Table 3.2 includes mean rain intensities, uniformity coefficients, mean raindrop diameters, and mean velocities measured for the test configurations reported in Table 3.1. In the first set of configurations using plastic meshes, it can be seen that larger mesh sizes (tests 1 and 2) produce uniformity coefficients of around 65% and mean raindrop sizes of around 0.85 mm, which is slightly lower than that observed in natural rain. In this case, the mesh size is similar to the diameter of the raindrops and a small area of distributions is observed when raindrops pass through the mesh and break. If the mesh size is reduced (tests 3-5), raindrops are distributed in a larger area and the uniformity coefficient is significantly increased, the mean diameter of the generated drops remaining almost constant. It can also be seen that increasing the mesh-drippers distance improves rain uniformity, since raindrops reach the mesh with a higher velocity distributing in a larger area. This also produces a slight decrease in the mean diameter and velocity registered. The weak point of these configurations is that the rain intensity measured decreases, perhaps due to the fact that the coarser mesh wires retain water easily.

Table 3.2. Results of the tests performed during the rainfall simulator calibration.

Test	Rain intensity (mm/h)	Uniformity coefficient (%)	Mean diameter (mm)	Mean velocity (m/s)
1	29.9	62.9	0.89	2.71
2	28.6	67.3	0.79	2.5
3	23.0	83.4	0.83	2.77
4	24.0	83.4	0.83	2.77
5	22.9	89.7	0.73	2.58
6	32.0	71.8	0.95	2.77
7	31.0	92.8	0.90	2.88
8	29.5	85.3	0.92	2.81
9	31.4	87.3	0.94	2.77
10	50.2	90.1	0.91	2.85
11	53.4	94	0.95	2.77
12	71.8	94.6	0.90	2.88
13	79.1	97.4	0.95	2.77

Using the metallic mesh with a 2 mm size (tests 6-8), the rain intensity is not reduced as in previous cases resulting in suitable rain intensities and mean raindrop sizes and velocities. These tests also illustrate the importance of ensuring that there is enough distance between the mesh and the dripper grids to allow raindrops to reach a higher velocity before the impact against the mesh, achieving a larger distribution and improving rain uniformity above 80%. Accordingly, the distance of 0.70 m was selected and the metallic 2 mm size mesh was

compared with a 3 mm size mesh for the three intensities that the simulator is able to generate (tests 9-13), in order to assess the possibility of increasing mean raindrop size to the reference value. Results show a slightly better behavior of the 3 mm size mesh regarding rain uniformity and mean drop size. Greater mesh sizes were not considered because, as seen in tests 1 and 2, the uniformity is significantly reduced for mesh sizes over 4 mm. Therefore, the metallic 3 mm size mesh installed 0.70 m below drippers was chosen as the optimal solution.

3.3 Rain properties of the developed rainfall simulator

Rain intensity, uniformity, and raindrop size and velocity distributions were measured with the configuration resulting from the calibration, and for the three rain intensities that it is possible to generate. Figure 3.6 shows the rain intensity maps and the uniformity coefficients with values over 81%, which means an almost uniform rain and a very significant improvement in the uniformity in comparison to the previous nozzle-based rainfall simulator and compared to most rainfall simulators in the literature.

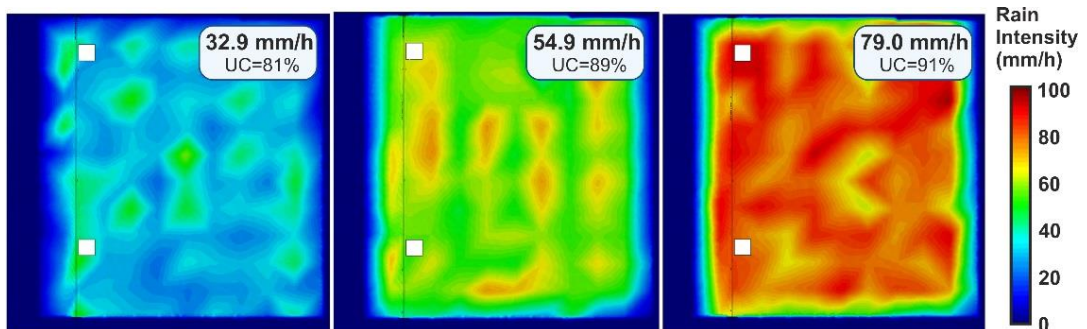


Figure 3.6. Rain intensity map of the physical model surface, which has an approximate area of 36 m^2 , for the three intensities that the rainfall simulator is able to generate. Plots include the mean rainfall intensity measured and the Christiansen's uniformity coefficient (UC) resulted.

The mean number of raindrops detected by the disdrometer in 10 s measurements over 2 minutes, classified in sizes and velocities for the three rain intensities, are presented in Figure 3.7. The mean raindrop sizes obtained, over 0.9 mm, and the heterogeneous distributions of sizes up to 3 mm are very close to those obtained in natural rain measurements (Figure 3.5). Regarding velocity distributions, bigger raindrops (around 2 mm) develop slightly lower velocities than the corresponding terminal velocity, which are represented by the solid curve in Figure 3.7. This can easily be fixed through a greater elevation of the simulator from the model surface, but this was not possible in our case due to laboratory limitations. However, the disdrometer data are registered at a height of 60 cm,

so raindrop velocities still increase before reaching the surface. The disdrometer measurement area was placed at the surface height outside the physical model, and it was estimated that 3 mm raindrops reach the model surface with more than 70% of the terminal velocity. This value is incremented to more than 80% in the case of the mean raindrop sizes obtained (around 0.9 mm).

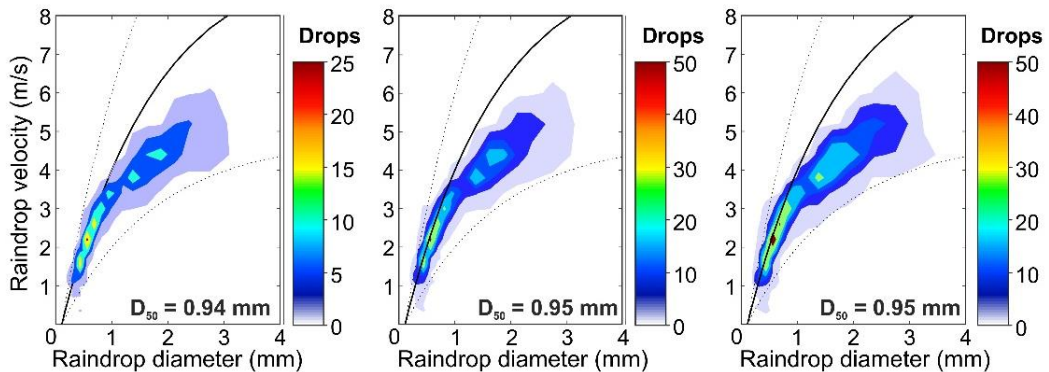


Figure 3.7. Number of raindrops, classified according their diameter and velocity, obtained by the disdrometer in an interval of 10 s and for the three rain intensities that it is possible to generate. The solid curves represent the experimental relation between diameter and terminal velocity (Gunn and Kinzer 1949).

4 Conclusions

In this study, a new drop-forming rainfall simulator was developed to be applied in wash-off and sediment transport studies in a street-scale laboratory physical model. To do this, the proposed rainfall simulator design, which consists of pressure-compensating dripper grids above a horizontal mesh that breaks and distributes raindrops was calibrated using natural rain as a reference. The mesh typology, mesh size and mesh-drippers distance that best fitted natural rain measurements were established, taking into account rain intensity, rain uniformity, and raindrop size and velocity distributions. Finally, the rain properties of the selected solution was measured for the three rain intensities that the rainfall simulator is able to generate. In view of the results obtained, the following three main conclusions were drawn:

- Modifying the density of drippers and their flow rate makes it possible to generate precisely a wide range of rainfalls with different intensities, keeping suitable uniformities and raindrop diameter distributions. This design has been presented as a suitable solution to simulate low rain intensities, which is a clear improvement over nozzles-based simulators that have to resort to intermittent rains.

- Very good spatial uniformity of rain intensities was obtained, both for high resolution measurements during calibration and for large-scale measurements during rain characterization of the final solution. The Christiansen's Uniformity Coefficients obtained, 81, 89 and 91% for the rain intensities of 30, 50 and 80 mm/h, respectively, showed almost uniform rainfalls, which confirms a good transferability of the experimental results that will be obtained when using the developed rainfall simulator.
- This rainfall simulator design allowed for controlling rain properties from the calibration of the mesh typology, mesh size, and mesh-drippers distance. The calibration performed in this study has achieved an accurate representation of raindrop size distribution using as a reference local natural rain measurements, and maintaining a good rain uniformity. Drippers must be placed as high as possible from the model surface for bigger raindrops to achieve terminal velocities.

Considering the difficulty of the challenge of simulating rain that is as real as possible, the results achieved here have been very satisfactory. The almost uniform rain uniformity and the suitable drop size and velocity distributions indicate that the rainfall simulator developed is optimal for wash-off and soil erosion experiments. In addition, the flexibility seen in controlling rain characteristics increases the value of the proposed design in that it is adaptable to a wide range of studies.

Chapter 4

Overland flow velocities characterization

1 Introduction

Physically-based urban drainage models are commonly used tools to predict urban floods or sewer system discharges (e.g. Chen *et al.* 2009, Leandro *et al.* 2009, Neal *et al.* 2009). The calibration of these models is often performed with data taken from the sewer network, principally flow discharges and water depths (e.g. Seyoum *et al.* 2011, Hong *et al.* 2016a). Nevertheless, there are significant processes related to overland flows, such as flood risk management (e.g. Martínez-Gomariz *et al.* 2016, Martínez Gomariz *et al.* 2017, Martínez-Gomariz *et al.* 2018) and the determination of the mobilization of the deposited pollutants over the street surface (e.g. Deletic *et al.* 1997, Egodawatta *et al.* 2007, Muthusamy *et al.* 2018). In these applications a good characterization of the surface flow is essential to achieve useful and accurate results. However, the difficulty in obtaining data on velocity fields and depths in overland flows makes the calibration of models a difficult task (Leitão *et al.* 2018).

In addition to the need for appropriate hydraulic calibration data, an accurate topography of the catchment is also required to simulate the urban runoff properly (De Almeida *et al.* 2018). Using inaccurate elevation maps for modelling the surface flow by means of a 2D shallow water model can lead to erroneous results regarding the determination of the extent of floods or flood risks (Hunter *et al.* 2008). Besides flood analysis, in the study of sediment wash-off during non-extreme rain events, the influence of the topography is also relevant in the model outputs. Thus, sediment transport capacity is influenced by the small overland flows depths, which may also hinder rainfall erosion capacity due to the impact of raindrops (Tomanovic and Maksimocik 1996). These both factors increase the sensitivity of the model's results to the topography, and at the same time make it more difficult to measure undisturbed water depths and overland flow velocities in order to calibrate the model. Furthermore, in studies of this type, such as the one developed by Hong *et al.* (2016a, b), an accurate spatial and temporal representation of the runoff is key to reducing the propagation of hydraulic uncertainties to the sediment transport equations, since the hydraulic variables are used as an input for the flow-driven erosion, the transport, and the eventual deposition of sediments (Hairsine and Rose 1992a, b).

The sensitivity to the model topography is greater in the case of small catchments or laboratory physical models, where a reduced area is considered (e.g. Wijesiri *et al.* 2015a, Naves *et al.* 2017, Muthusamy *et al.* 2018). In typical urban flooding studies with 2D shallow water models, the topography is usually derived from airborne LiDAR with a resolution of about 0.25 m to 1.00 m, with root mean square errors (RMSE) for elevations of about 5–15 cm (Hunter *et al.* 2008, Neal *et al.* 2009, Fraga *et al.* 2016). This spatial resolution may be insufficiently accurate for a physically based approach of sediment wash-off, in which the elements of the digital terrain models are in the order of a few centimeters or even millimeters. In such cases, a terrestrial laser topography or on-vehicle LiDAR (Hong *et al.*

2016a), combined with conventional topographic techniques, can provide high-resolution and precise elevation data, but this implies a significant economic cost.

In this regard, visualization techniques are presented as a possible low-cost alternative to traditional methodologies for obtaining high-resolution elevation grid data. The photogrammetric technique Structure from Motion (SfM), which is based on stereoscopic principles, allows the reconstruction of a 3D object by means of overlapping images. Traditional photogrammetric methods require the location and positioning of cameras, or the location of ground control points to create a 3D object reconstruction. In contrast, SfM method solves the geometry and the position and orientation automatically, using a highly redundant bundle adjustment based on matching features in multiple overlapping and offsetting of images (Westoby *et al.* 2012). This greatly simplifies the methodology and makes it more affordable for non-expert users. Although this technique is being used widely in river bathymetric applications (see for instance the review in Detert *et al.* 2017), in the field of urban drainage the applications are still quite limited. We can cite here only some previous studies developed by the current authors to determine the topography of sewer sediment deposits at the laboratory scale (Regueiro-Picallo *et al.* 2018).

As noted above, a non-adequate topography can lead to the erroneous modelling of spatial and temporal surface flow distributions. But even with a very accurate digital terrain model, measured data such as discharges, water depth, and flow velocities are required in order to calibrate and validate models, and thus to obtain useful results (Hunter *et al.* 2008). The measurement of shallow flows generated in urban catchment surfaces do not allow for the use of traditional methods, since these techniques interfere with the observed flow. Likewise, flow sensors used in pipe flows are often quite large and affect to the determination of the hydraulic variables.

The non-intrusive Particle Image Velocimetry (PIV) techniques are considered a suitable solution, and are commonly used in laboratory and field studies to obtain velocity-field datasets (Adrian 1991, Raffel *et al.* 2007). PIV determines the displacement of particles seeded in the flow using cross-correlation methods on two image frames with a known time step between them. Large-scale PIV (LSPIV), proposed by Fujita *et al.* (1998), uses particles or other traces on the surface of the water flow, which are supposed to follow the same velocity. This variant uses the surface of the flow as the measurable plane, so it is easier to apply to field and realistic studies since the area under study can be much larger and expensive equipment such as complex lasers or cameras are not needed. Therefore, LSPIV methods are generally applied to measure surface velocities rather than depth averaged velocities, and errors in the determination of depth-averaged flow velocities may become more significant at higher flow depths.

LSPIV is commonly used in river surveys (Le Coz *et al.* 2010, Muste *et al.* 2011) to determine river discharges. In order to transform surface velocities into depth-averaged velocities, and subsequently the discharge, a velocity index of 0.85 is typically used, although this correction factor is not appropriate for all measurement situations and depends on flow nature, flow regime (steady or un-steady) and bed roughness (Muste *et al.* 2011). Furthermore, the LSPIV technique has also been used for measuring shallow water flows in laboratory studies (Weitbrecht *et al.* 2002). For example, Kantoush *et al.* 2008, Novak *et al.* 2017 apply LSPIV to investigate the flow field using artificial particles in a rectangular shallow reservoir and in an open-channel flow, respectively. In the case of Arques *et al.* (2018), by synchronizing four cameras, it was possible to resolve a large measurement area of 4.8 m × 1.22 m with high resolution LSPIV.

In the field of urban drainage, some studies using LSPIV in high water level conditions during flood events have recently been published. Guillén *et al.* (2017) presented a new approach to the study of the vulnerability of vehicles and people, where the LSPIV method is used to obtain superficial velocities from a domestic video. Martins *et al.* (2018) performed an extensive comparison between experimentally measured and numerically modelled flows for different manhole grate configurations. For this purpose, a detailed characterization of the velocity fields around these elements was performed by means of LSPIV. Leitão *et al.* (2018) presented the use of surveillance camera footage as a low-maintenance and easy-to-install alternative to measure surface flow by means of this image velocimetry. However, in the case of very shallow depths in non-extreme rain events, only a very preliminary measurement of the velocity of a small area using artificial tracers was found (Branisavljević and Prodanović 2006). Because of its solid performance in the different studies cited above, LSPIV can be considered as a suitable technique for obtaining velocity-field datasets with low water levels in urban areas. Nevertheless, due to small water depths here, commonly lower than 1 cm, and the presence of raindrops, which impact on the water surface and interfere in the surface flow and the recorded images, the accurate measurement of the velocities is a highly challenging task.

This study aims to achieve an accurate representation of the overland runoff in a full-scale urban drainage physical model, to be used as the basis for an application of a physically-based sediment wash-off 2D shallow water model. Due to the low depths developed in the laboratory model and the size of the catchment, this study focuses firstly on measuring a high-resolution topographic data using a low-cost photogrammetric technique, allowing thus for the proper simulation of the surface flow with a 2D shallow water model. Then, a hydraulic experimental characterization of the runoff is measured under controlled laboratory conditions to calibrate and assess the numeric results obtained. The maximum depths of around 5–8 mm, and the presence of raindrops that interfere in the visualization of the surface flow, made it necessary to develop a modified LSPIV methodology using fluorescent particles. To the authors' knowledge, no previous urban drainage studies have

applied LSPIV during rainfall events. Therefore, the present study is novel in the following ways:

- The SfM technique is used to obtain a high-resolution and accurate elevation map of an urban drainage physical model of 36 m².
- Extreme-shallow surface flow is measured in the presence of raindrops with a modified LSPIV methodology, by means of fluorescent particles.
- The photogrammetric topography and a traditional topographic survey using a gridded system have been implemented in a 2D shallow water model in order to validate both digital terrain models with the measured LSPIV velocity fields.

2 Materials and methods

2.1 Physical model description

Experimental testing was undertaken in the Hydraulic Laboratory of the Centre of Technological Innovation in Construction and Civil Engineering (CITEEC) at the University of A Coruña. The installation consists of a full-scale street section with a rainfall simulator located 2.6 m over a 36 m² concrete street surface, divided into a tiled pavement and a roadway (Figure 4.1). The runoff generated by rain drains into a sewer drainage system by means of three gully pots, two of these located along the curb and a third one at the end of a lateral outflow channel. The gully pot grate was removed in the tests to allow sampling of water quality parameters in them in a series of wash-off experiments not shown here. The surface has an approximate transversal slope of 2% up to the 0.15 m high concrete curb and a 0.5% longitudinal slope up to the outflow channel. A more detailed description of the physical model can be found in Naves *et al.* (2017).

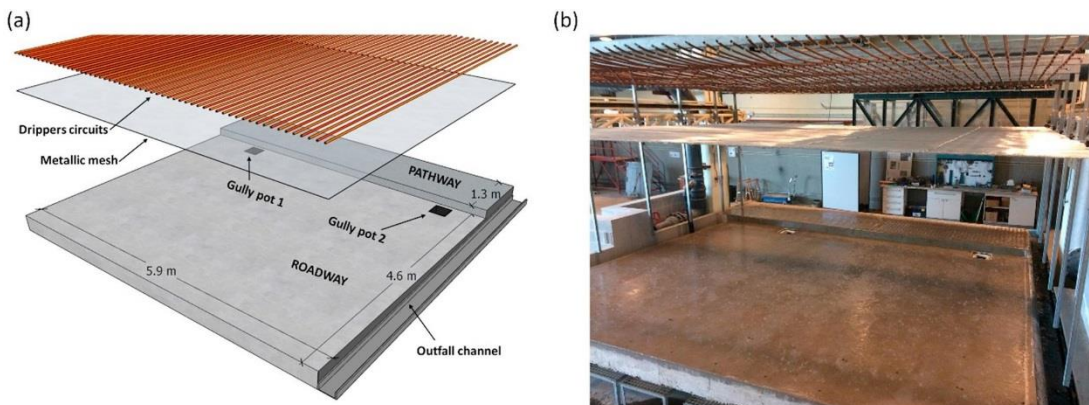


Figure 4.1. (a) Physical model scheme and (b) general image of the facility.

The rainfall simulator consists of two overlapped circuits of pipes with pressure-compensating irrigation drippers (PCJ-CNL, NetafimTM) inserted in a grid layout. The transversal and longitudinal distance between drippers in each circuit is 0.2 m (25 drippers per square meter) and the flow generated by one dripper is 1.2 and 2 L/h, respectively. This configuration makes it possible to simulate rainfall with a rain intensity of 30 mm/h, 50 mm/h and, if both circuits are used at the same time, 80 mm/h. A metallic welded wire mesh with 3 mm square openings, situated 0.6 m below the grids of drippers, breaks and distributes the generated raindrops to achieve a suitable uniformity and drop size distribution. The rain intensity distribution was measured from the volume collected in a 0.5 m × 0.5 m grid of vessels for 5 min. The obtained Christiansen Uniformity Coefficients (Christiansen 1942) values for 30 mm/h, 50 mm/h and 80 mm/h were 76%, 88% and 91%, respectively; hence, the rain can be considered almost uniform.

2.2 Surface model topography

2.2.1 Traditional point data survey

The 3D coordinates of a total of 144 points were determined over the whole surface of the physical model in a 0.5 m × 0.5 m grid. The x- and y-coordinates of each point of the grid were determined by triangulation from two reference points, while the z-coordinate was obtained by measuring the distance to a horizontal reference laser plane with a point gage tape. The error bounds of the measured horizontal coordinates were assumed to be approximately 1 cm for the horizontal coordinates, and about 1 mm for the vertical coordinates (Boiten 2003). The position of the points used for the topographic survey was drawn over the street surface with red crosses (see Figure 4.4). These marks were also used as reference points in the visualization techniques carried out in this study.

2.2.2 Structure from Motion survey

The SfM photogrammetric technique was applied to obtain a high-resolution elevations map of the physical model surface. The first step was to take a total of 64 images from different positions around the surface with a Lumix GH4 camera (focal length equal to 28 mm and image resolution 3264 × 2448 pixels). Then, the free license software VisualSFM (Wu *et al.* 2011, Wu 2013) was used to perform the 3D reconstruction of the physical model surface. This software uses triangulation to obtain the relative position of different features of the studied object which appear in several images at the same time. Therefore, it is necessary to ensure an overlap of the images of around 60% to increase the number of resulting points. In addition, enough contrast in the surface of the measured object is also needed in order to distinguish and correlate the common points between the images. In this particular case, the concrete surface is very homogeneous and it was not possible to apply directly the SfM

technique because the software cannot identify different features in the pictures. To avoid this problem, a colored and texturized image was projected over the surface of the model while the images were taken, and in this way a sufficiently dense point cloud was obtained (Figure 4.2).

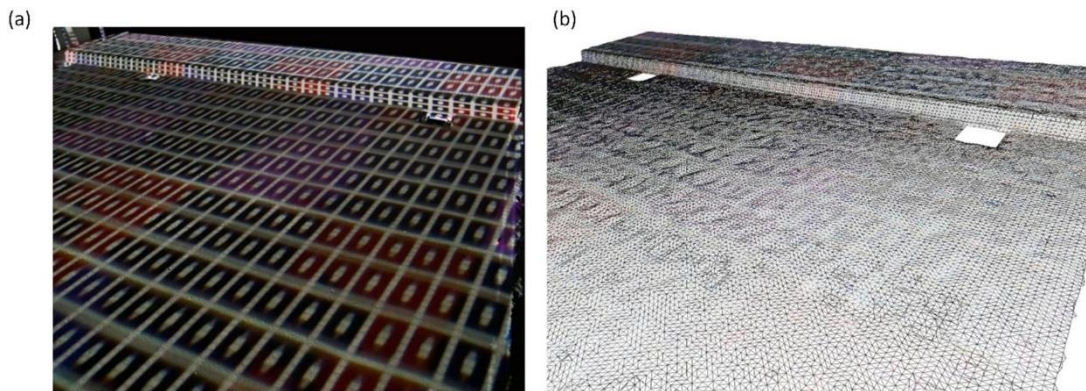


Figure 4.2. (a) Texturized image projection over the street surface used for the application of SfM and (b) 3D dense point reconstruction of the model.

A $\sim 976,000$ elements dense point cloud in a relative coordinate system was obtained by means of the SfM technique. A total number of 5 ground reference points, previously determined in the traditional data topographic survey, were used to scale and transform the point clouds to a coordinate system that was already known. This procedure was carried out with the open source software Meshlab (Cignoni *et al.* 2008). The RMSE resulting from the differences between the final coordinates and the calibration ground points was 2.2 mm. Finally, the Screened Poisson Surface Reconstruction in Meshlab (Kazhdan and Hoppe 2013) and a 40×60 elements two-dimensional median filter method was applied to the scaled and positioned point cloud in order to obtain a 5 mm squared despiked grid.

2.3 Numerical model

The Iber model (www.iberaula.es) was used to assess the effect of the different measured topographies in the overland flow velocity distribution and flow discharges into the model gully pots. The surface drainage model solves the 2D shallow-water equations, including rainfall and infiltration terms, with an explicit un-structured finite volume solver. The model has been validated in previous studies under overland flow conditions including rainfall-runoff transformation (Cea *et al.* 2010, Cea and Blade 2015). The surface runoff model Iber has also been implemented in the dual drainage model of the authors' research team, which has already been validated in field applications (Fraga *et al.* 2016) and in the same physical model presented in this study (Fraga *et al.* 2015a). A detailed and comprehensive description

of the numerical model and solver can be found in the previously cited studies. Following Fraga *et al.* (2015a), all the boundary conditions of the model were imposed as free critical depth discharge. In the present study, gully pots were not treated with any special stage-discharge curve, as the gully pots grates were removed.

2.4 Determination of overland flow velocity fields

The LSPIV technique was used to obtain the velocity field of the superficial flow within the first two meters of the pavement placed next to the curb of the physical model. This area presents the highest depths and velocities due to the transversal slope of the street model, and it is the most interesting part from an urban wash-off point of view since it is known that most of the sediments build up in the first 0.5 m (Sartor and Boyd 1972, Grottker 1987). LSPIV are based on the analysis of the frames obtained from a video recording of some type of tracer that is supposed to follow the velocities of the superficial flow, so the selection of a suitable tracer and the correct way of recording the video are essential before beginning the experiments.

2.4.1 Experimental setup

Two Lumix GH4 cameras were used to apply the LSPIV technique. Both cameras used a focal length of 28 mm and were set to record video frames of size 3840x2178 pixels and a frame rate of 25 Hz. The cameras were positioned 2.2 m above the side of the pathway. The camera configuration ensures the detection of small particles around 1 mm diameter and allows for the recording of an area large enough to capture the half length of the physical model curb (Figure 4.3).

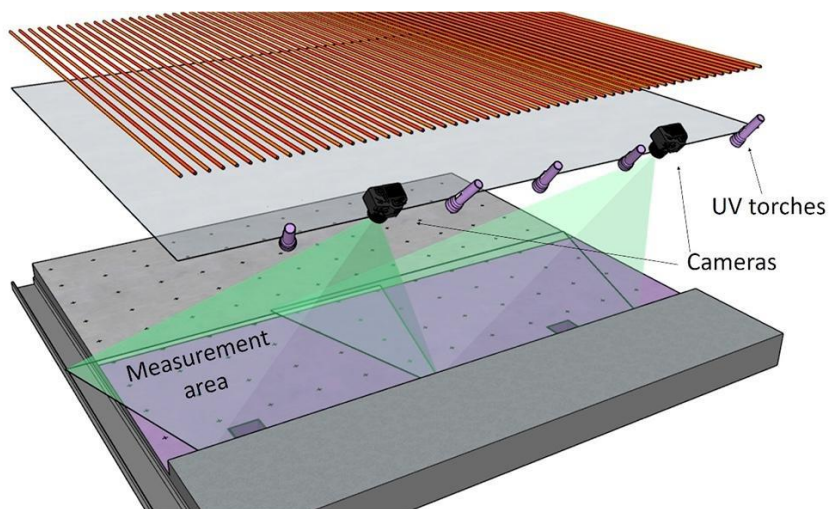


Figure 4.3. Layout of the experimental configuration for overland runoff velocity measurements in the physical model.

The conditions of the experiments must be taken into account in the selection of the particles used as a tracer. First, the particles have to be small and light enough to be transported by the flow considering the low depths developed in the surface of the physical model. The maximum depths for the maximum rain intensity are below 10 mm next to the curb and around 3 mm on the rest of the surface. Furthermore, the presence of raindrops between the cameras and the water surface and their impacts on it produces different image patterns that affect the accuracy of PIV algorithms, which are not able to distinguish between tracers and these other picture features. To deal with this problem, fluorescent ultraviolet (UV) particles and lamps were used to illuminate the physical model. Fluorescent particles have been used in the past in PIV applications to improve the quality of the acquired images, allowing measurements close to laser-reflective surfaces such as sediment beds or free surfaces (Pedocchi *et al.* 2008). In our study we produce inexpensive LSPIV particles by cutting an extruded 3D-printer fluorescent strand into pieces. These fluorescent particles (0.85 mm mean size) react with the shining UV light, so that in dark conditions it is possible to highlight the particles, distinguishing them from the rest of the disturbing features in the images, such as raindrops or water reflections. Therefore, five UV 100 LED torches (390 nm wavelength) were placed next to the cameras and pointing at the surface in order to illuminate homogeneously the measured surface during the experiments. In the Figure 4.3, a scheme of the experimental setup is shown.

2.4.2 Experimental procedure

For each of the three rain intensities that the rainfall simulator can generate, the measure of the superficial flow by means of the LSPIV technique began by turning off the ambient laboratory lights while the cameras were recording. Then, the UV torches were turned on and the rain started. Once steady conditions were reached, after approximately 150 s, particles were spread manually along the side of the roadway during the rest of the experiment, which has a total rainfall duration of 300 s. This allows the particles to be transported to the measurement area without causing disturbances in the flow or in the video, and we ensure the recording of at least one minute of a suitable particles flow in steady conditions at the measurement area.

2.4.3 Image processing and LSPIV data analysis

Once the experiment was finished, 1500 frames (60 s) were extracted from the video as recorded in steady flow conditions. The frames were processed with the procedure schematized in Figure 4.4, which consists of the following steps:

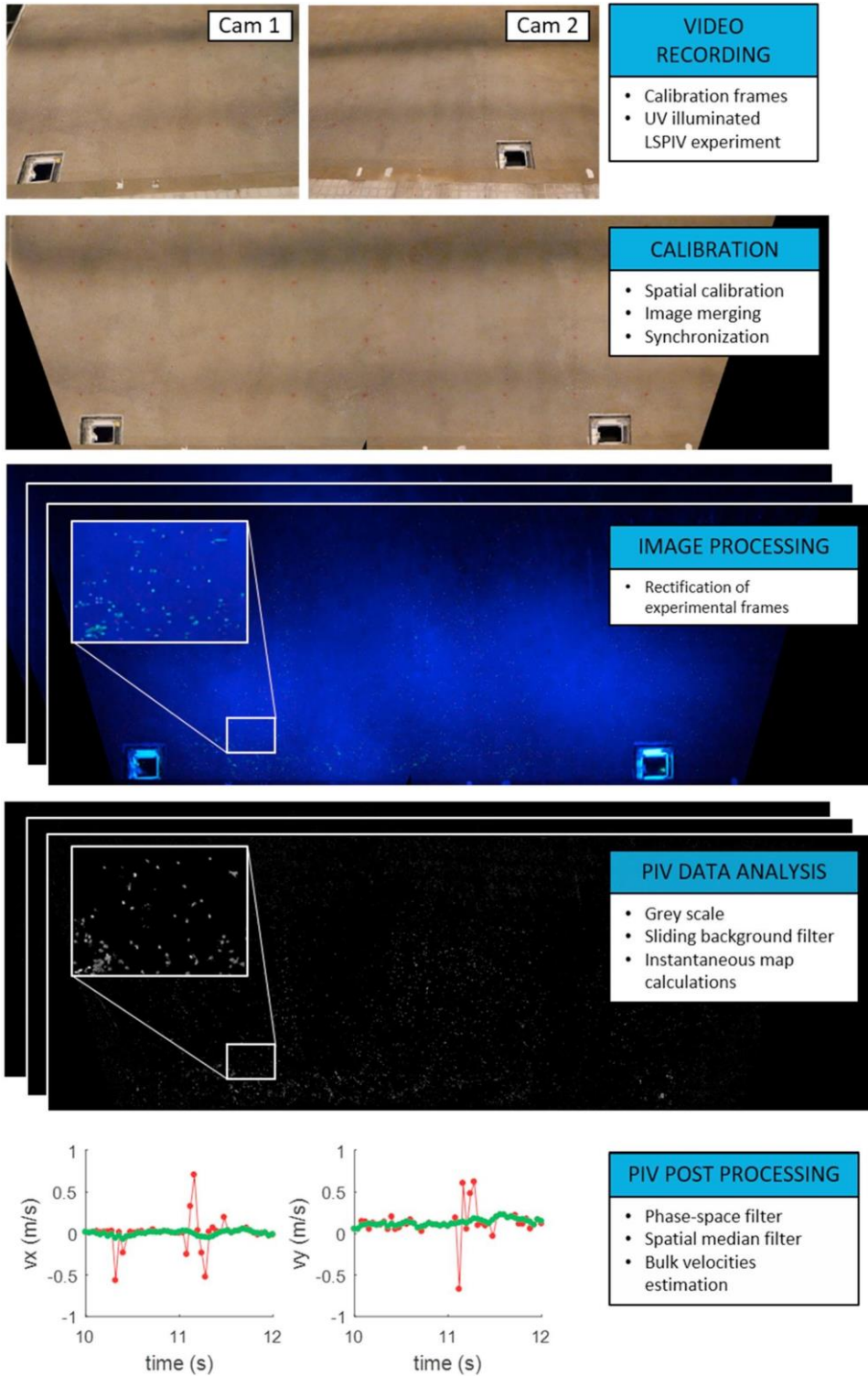


Figure 4.4. Image processing and LSPIV data analysis methodology.

Spatial calibration

The angle of view of the cameras and the lens distortion cause a deformation in the video frames recorded, so the extracted frames from the video sequences were dewarped to correct image perspective and to convert the image units from pixels to real world metrics. This procedure was performed using a spatial calibration of the images using the red cross marks drawn on the model surface during the gridded point data topographic survey. The point coordinates were used as a reference to transform the camera frames to an orthogonal Cartesian coordinate system. In each experiment and for each camera, the standard Matlab algorithm 'fitgeotrans' was applied to one frame recorded in normal light conditions. A total number of 28 and 24 reference points with known 2D coordinates were identified in the calibration frame of each camera. The software provided a rototranslation matrix to transform the frames recorded during the experiments. In these new scaled and orthoreferenced images obtained by applying the matrix, 1 pixel corresponds to 1 mm in real-world coordinates. Finally, the common referenced points between the cameras were used to crop and join the image. A similar procedure for image calibration was performed by Arques *et al.* (2018).

The final position of all the reference points in the calibrated image was compared with the known coordinates, obtaining a maximum error of about 2% in the total displacement between marks. This calibration procedure was applied for each experiment to avoid errors because of possible small movements or tilts of the cameras between experiments. The time synchronization between cameras was done through identifying the frame at the moment that the lights of the laboratory was turned off. The process is very fast and it is easy to identify the first frame recorded in dark conditions, so this method provided the maximum possible accuracy, which is equal to the time step between frames (0.04 s).

PIV data analysis

Before the application of the PIV cross-correlation algorithms to the recorded images, the rectified and merged images were converted to grey scale, and a moving sliding background with a 0.25 threshold filter was then applied. Thus, in each frame those pixels with 25% of similarity in the grey value with the same pixel from the previous frame were transformed to black. The application of the sliding background filter reduces the effect of background image features such as surface microtopography roughness or tracer particles that settled temporarily on the shallowest or dry flow regions. The velocity of these particles would be zero and the mean velocity estimation in the interrogation area is biased.

For the determination of the instantaneous velocity maps the open source PIV tool for Matlab 'PIVLab' (Thielicke and Stamhuis 2014) was used. An adaptive cross-correlation procedure was performed using squared interrogation areas of 128, 64 and 32 pixels,

resulting in a regular grid of velocity vectors of 3.2 cm and 0.04 s of resolution. To estimate the cross-correlation between frames an FFT approach was used, and in the final step a window deformation scheme was applied to increase PIV accuracy (Raffel *et al.* 2007).

PIV data post-processing and velocity calculation

Once the velocity fields were obtained, the possible outliers were detected with a temporal 2D filter using a phase-space thresholding method developed by Goring and Nikora (2002), taking into account both velocity components in each point throughout the duration of the experiment. The filter removes less than the 8% of the velocity vectors. Then, these outliers were replaced by means of a linear interpolation following Cea *et al.* (2007). In Figure 4.4 (lower part), a real example of the performance of the temporal 2D filter in a selected point in one experiment can be seen. Finally, in the Matlab toolbox 'pivmat' environment (Moisy 2017), a spatial median filter of 3x3 elements was performance to all the frames.

The obtained velocity fields correspond to the surface flow velocity. In order to obtain the mean depth-averaged velocity value, it is necessary to determine a velocity-index or flow velocity correction factor. In river surveys, the determination of the velocity-index is based on the application of the log-law velocity profile to the streamwise velocities (Le Coz *et al.* 2010). For the complex shallow flows developed in urban surfaces, this assumption may be questionable, and some authors use different velocity index values ranging roughly from 0.6 to 1 (e.g. Leitão *et al.* 2018, Martins *et al.* 2018). Nevertheless, due to the relatively shallow flow depths under consideration, errors arising from this assumption are not expected to be significant, since depth-averaged velocities are relatively small, and other uncertainties related to the methodology may be expected (for instance due to the trapping of seeding particles in the shallowest areas). Taking all these considerations into account, and from a practical point of view, the classical index velocity value of 0.85 was applied in this study.

2.5 Determination of flow discharges

In addition to the surface velocity field, the inflow discharges in the gully pots were measured for the 3 rainfall intensities in order to calibrate the 2D shallow water model. A triangular weir was installed in two underground tanks placed under the gully pots. In each tank an ultrasonic distance sensor (UB500-18GM75-I-V15, Pepperl and Fuchs) was installed in order to measure the flow discharge over the triangular weir. First, the spikes of the 10 Hz raw signal were removed using a moving median filter of 5 s, replacing the peaks that overcome the double of the deviation by the median of this range. Then, the flow in the gully pots was obtained by means of a depth-flow pre-calibration and a volume compensation performed because of the changes of depth in the reservoir when the flow is increasing or decreasing. This methodology was described in more detail in Naves *et al.* (2017).

3 Results and discussion

In this section, the surface models from the traditional topographic survey and SfM photogrammetric data are first presented (Section 3.1). Then, we describe how the 2D shallow water model was used to simulate the runoff for 30 mm/h, 50 mm/h and 80 mm/h rain intensities with both topographies (Section 3.2). The measured discharges in physical model gully pots were used to calibrate the numerical model, and the simulated velocity maps are then presented. Finally, the experimental velocities obtained using the LSPIV technique in the physical model are presented and compared with the numerical results (Section 3.3).

3.1 Elevation data and model discretization

The elevation maps of the physical model obtained from the data point and the SfM topographic surveys are shown in Figure 4.5. Both topographies consist of a regular gridded data at 50 cm spatial resolution and of an SfM topography at 5 mm spatial resolution. The comparison between these elevation maps is focused on the area along the first two meters next to the curb ($x = 0$ m to $x = 2$ m). The elevation of 40 points placed in this region was obtained from both topographies. The RMSE of the elevations was 2.9 mm, indicating a high correlation between the topographies. Therefore, the SfM technique allows us to obtain a similar accuracy with a larger spatial resolution.

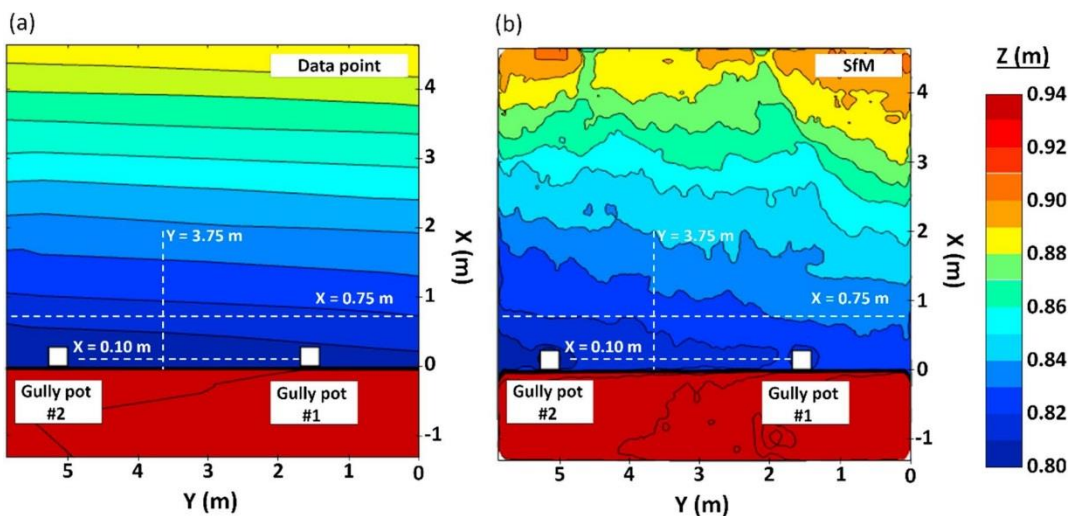


Figure 4.5. Topographies of the physical model obtained from (a) traditional point survey and (b) SfM photogrammetric technique. Longitudinal and transversal cross section plotted in Figure 4.6 and Figure 4.13 are marked in the maps.

The point data surface is smoother than the SfM surface, and as expected from the model description and building specifications, the transversal slope is higher and more uniform than the longitudinal slope. The SfM topography shows a more irregular contour line definition and the presence of small transversal valleys and crests, which serve as drainage channels orthogonal to the curb of the model. As will be shown below, these surface irregularities found between the traditional and SfM surveys affect the modelled runoff velocities, particularly in the case of low depths.

Both topographies were converted to a raster format decimated to a resolution of 5 cm. The model domain discretization was performed using a structured mesh made with triangular elements, with edge sizes ranging from 5 cm to 7 cm. The number of cells of the model is about 58,000 elements and was automatically generated from the raster files using the Iber software (Cea and Blade 2015). To highlight the differences in the domain discretization, Figure 4.6 shows a transversal profile at $y = 3.75$ m (upstream of gully pot 2) and two longitudinal profiles placed at $x = 0.75$ and $x = 0.10$ m, representing the surface morphology upstream and between the gully pots, respectively. The gridded data mesh presents a visible quantization error caused by the coarse 50 cm resolution of the original data points. The averaged slope of the profiles determined from the gridded point data and the SfM approach are similar, but the SfM longitudinal profiles show some depressions of few millimeters' depth at $y \sim 2.4$ m, $y \sim 3.3$ m, $x \sim 4$ m and $y \sim 4.8$ m, which act as drainage channels.

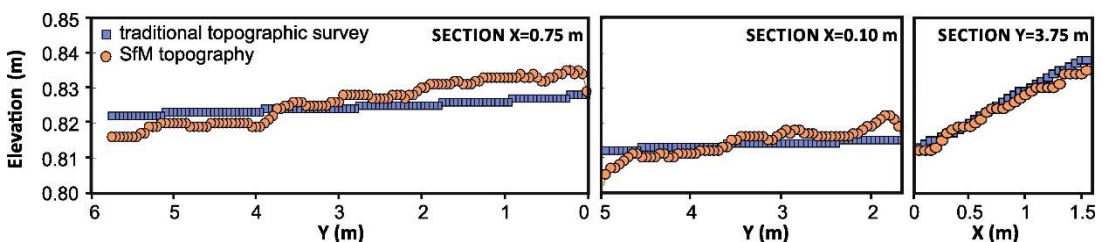


Figure 4.6. Comparison of the longitudinal ($x = 0.75$ m and $x = 0.10$ m) and transversal ($y = 3.75$ m) profiles extracted from the model domain generated from traditional point data and SfM topographies.

3.2 Application of the 2D shallow water model

The topographies presented in the previous section have been implemented in Iber 2D shallow water model to analyze their influence in modelling the runoff for the three rainfalls here, of 30, 50 and 80 mm/h and 5 min' duration. A common calibration dataset for all six cases (two topographies and three rain intensities) was defined in light of the discharges measured in the gully pots of the physical model. A non-formal calibration procedure was performed, changing the Manning coefficient and the initial losses of the concrete surface of the model. An initial loss of 0.6 mm was fixed to assure that modelled and measured

runoff volumes were similar. The Manning coefficient was set at 0.016. This value accounts for the extra bed roughness induced by the rainfall. Although the numerical model incorporates a variable-depth Manning formulation, slight improvements with variable roughness parametrization are achieved, this mainly in the recession and rising hydrographs limbs (Fraga *et al.* 2013), which are not compared with the LSPIV results, as will be shown below. From a practical point of view, a constant roughness parametrization produces results with a similar accuracy to the variable roughness-dependent formulations for the smooth surfaces (Cea *et al.* 2014).

A visual inspection of Figure 4.7 reveals a very good fit between the outputs of the numerical model with both topographies and the experimental results using the previous model's inputs. Therefore, if we look only at the discharges into the gully pots, the traditional measured topography has enough resolution to properly model the overland flows, while the SfM topography does not improve model accuracy.

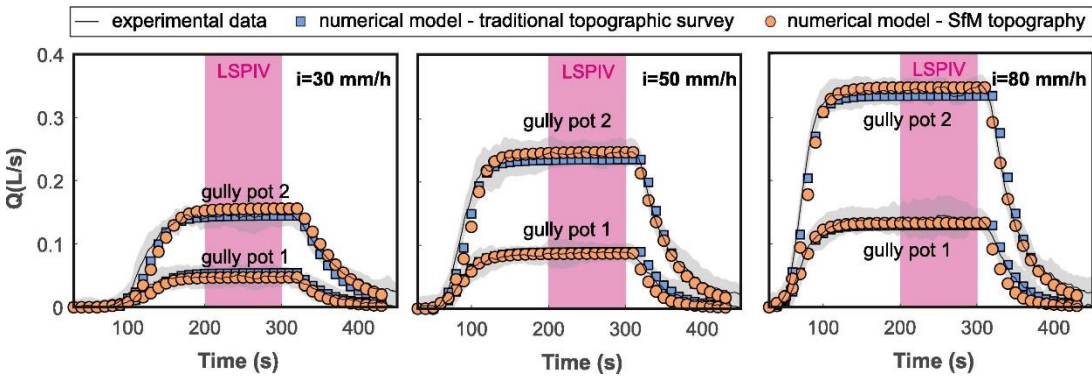


Figure 4.7. Experimental and numerical flow results in both gully pots and for the three rainfall intensities studied. The variance in the measured experimental flow discharge (grey) and the LSPIV measure interval (purple) are shown.

Figure 4.8 and Figure 4.9 present the depth-averaged velocity maps obtained for both topographies in steady conditions (e.g. after 200 s from the beginning of the rainfall). As numerical and experimental data do not match exactly, numerical data has been spatially interpolated. Therefore, to clarify the representation of the velocity vectors a spatial resolution of ~ 16 cm was selected for the graphics.

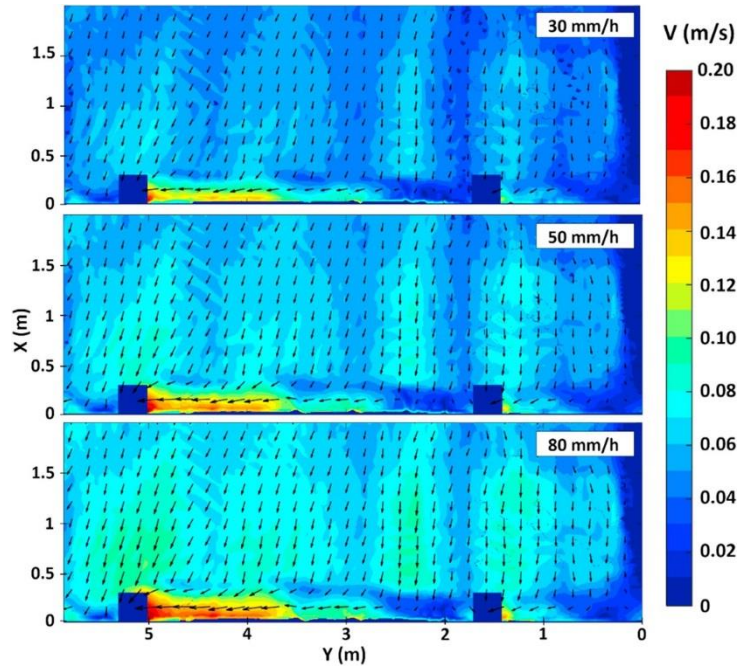


Figure 4.8. Numerical depth-averaged velocity vectors using the traditional data point topography for 30, 50 and 80 mm/h rainfall intensity.

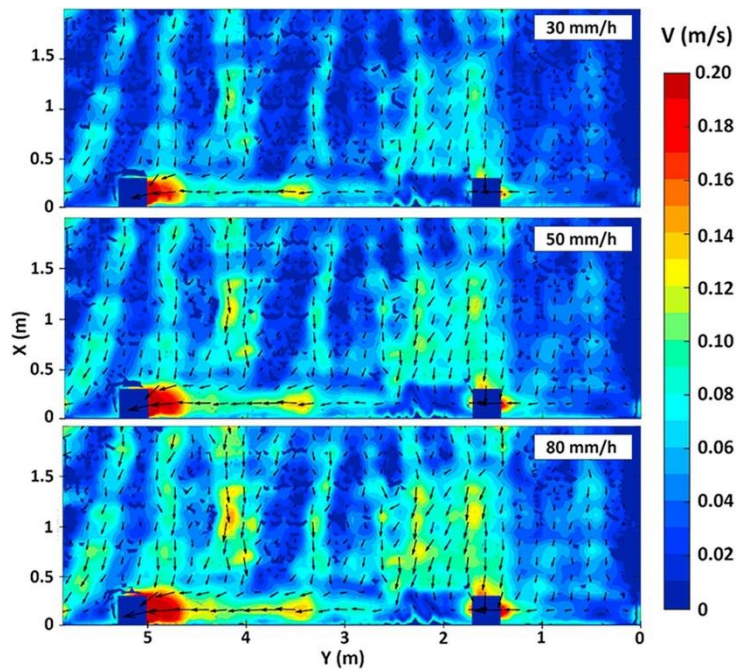


Figure 4.9. Numerical depth-averaged velocity vectors using the SfM topography for 30, 50 and 80 mm/h rainfall intensity.

Regarding the general flow patterns, in both model domains the runoff drains towards the two gully pots and the curb, due to the transversal and the longitudinal slope, but some preferential channel flows orthogonal to the curb direction appear when the SfM elevation map is used (Figure 4.9). Although these preferential channel flows could also be sensed by using the traditional measured topography, the higher resolution of the SfM technique results in far better defined drainage channels, where the velocities are roughly five times the velocities in the areas between them. Furthermore, the width and mean velocity of these transversal channels increased with rainfall intensity.

Another difference observed in the flow pattern determined using each topography is related to a velocity reduction of the curb channel flow at the junctions with the transversal drainage channels. This effect is more pronounced in SfM model domain at $y \sim 4$ m, where the more defined orthogonal junction between transversal and longitudinal overland flows produces a decrease in the average velocity of the curb flow. In addition to these differences, the overland flow obtained with the SfM model domain presents some areas with dry fronts due to the high sensitivity to the surface elevations variability in the shallowest depth conditions presented far away from the model curb.

Thus, considering the suitable performance of the gridded point data and SfM topographies for modelling gully pot discharges, it becomes necessary to asses with experimental velocity data which approach gives a better representation of the runoff flow patterns. This assessment will be performed using LSPIV data in the following section.

3.3 Application of LSPIV to determine overland flow velocities

As mentioned in the section on methodology, the surface velocities determined by applying the LSPIV technique with fluorescent particles were converted to depth-averaged velocities by applying a velocity index of 0.85. Figure 4.10 shows the vector field for the rainfall intensities of 30, 50 and 80 mm/h represented with the same spatial resolution as Figure 4.8 and Figure 4.9. The orthogonal channels to the curb which were found by using the SfM topography appear clearly in the experimental results. Furthermore, the decrease in the velocities in the junctions between the main transversal and the longitudinal flow channels noted in the previous section is also well registered by the experimental data. Regarding the velocities, it can be noted that the LSPIV and numerical results for SfM are of the same order of magnitude.

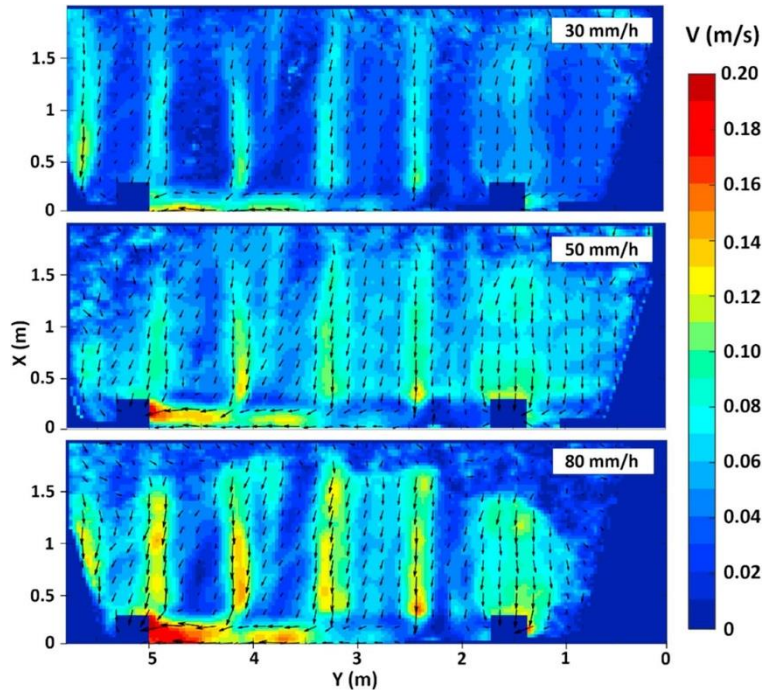


Figure 4.10. Experimental surface velocity fields for the three studied rainfalls using LSPIV.

From the results obtained in Figure 4.10, it can be seen that the LSPIV methodology developed in this study appears to be a suitable tool for measuring overland flow velocities over very shallow water depth conditions, in an area larger than 10 m^2 , and avoiding the presence of raindrop features in the recorded images using fluorescent particles. In addition, the importance of the UV illumination is noted in the furthest regions from the camera and torch positions, where the higher the rain intensity the less accurate are the measurements (e.g. $y < 1 \text{ m}$, $x > 1.6 \text{ m}$). This is caused by the interference of the raindrops with the light from the torches and the video recording, so a brighter UV illumination should be considered in the case of larger areas being measured.

The match between the experimental results and the velocity fields obtained using both topographies have been investigated in the comparison carried out for each velocity component in Figure 4.11. The comparison was limited to the area between gully pots and up to 1.5 m from the curb, this to avoid the area where the LSPIV measurements are less accurate due to irregular illumination. Firstly, a clearly different performance can be observed in the comparison of the LSPIV x-velocities with both numerical results. These x-velocities correspond to the flow transverse to the curb, where the drainage channels have been measured with the LSPIV technique. While the numerical results obtained using the traditional point data topography have an almost constant value, ranging from 0.05 to 0.08 m/s for the three rain intensities studied, the SfM topography results are distributed in

the range of variation of the experimental velocities (e.g. following the 1:1 slope relationship). This bias in the velocity distribution using the conventional topography is due to the fact that, with the lower resolution associated with this topography, the model is not able to reproduce the drainage channels and a homogeneous velocity results for all of this area. Regarding y-velocities, which correspond roughly to the curb flow, both implemented topographies showed similar results, with a slight increase of the dispersion in the case of those obtained using the SfM topography.

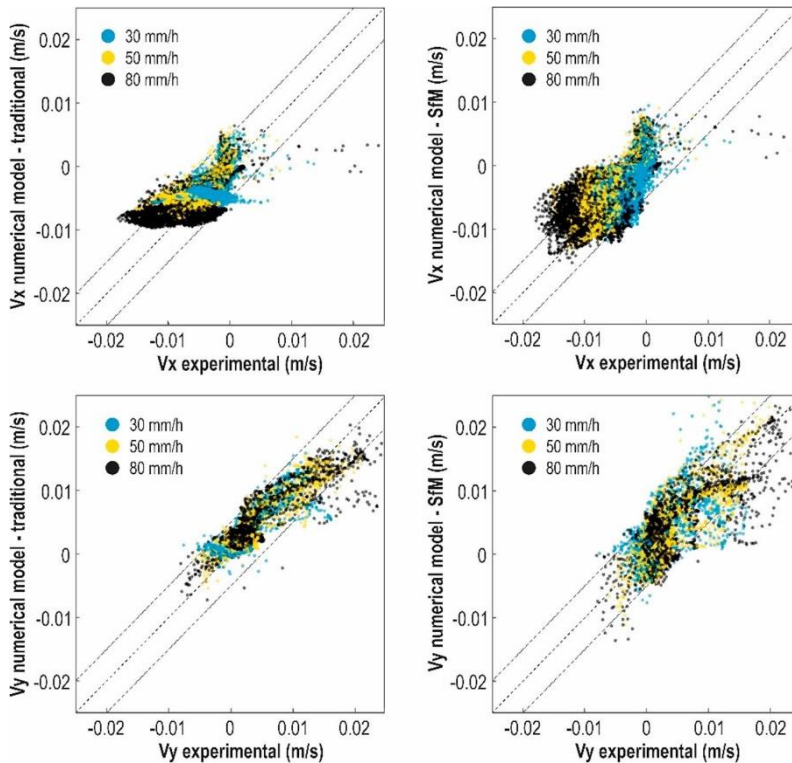


Figure 4.11. Comparison of the experimental and numerical x-component (up) and y-component (down) velocities using the experimental data obtained from the LSPIV technique and the numerical results, with the traditional point data topography (left) and the SfM topography (right), respectively. The three different rainfall intensities of 30 mm/h, 50 mm/h and 80 mm/h are represented in blue, yellow and black.

Figure 4.12 presents the results as a histogram for each velocity component of the experimental data and the empirical probability density function obtained with the point data and SfM topographies for the three different rainfall intensities. It can be seen that the distribution of the x-velocity component and mean velocities is better represented with the SfM numerical model. When comparing the velocity histograms (Figure 4.12a and c), we can

see that they have a similar shape, which points to a good relation between experimental and numerical results obtained with the SfM topography. The velocity distribution obtained with the traditional topographic survey model is concentrated in the range of 0.05–0.10 m/s due the inaccurate representation of the drainage channels placed in a transversal direction to the physical model curb. For the longitudinal velocity component (Figure 4.12b), both numerical probability density functions have a similar shape, although the calculated SfM presents a slightly larger dispersion than the gridded data values, as is shown in the lower part of Figure 4.11.

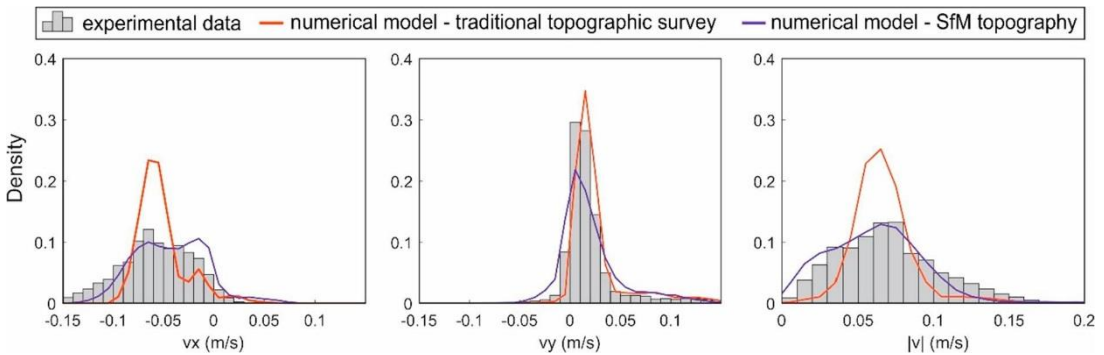


Figure 4.12. Density comparison (histograms) for x-component (a) y-component (b) and module (c) of experimental and numerical velocities.

In order to check and understand the different results obtained in the comparison of numerical and experimental data, depth-averaged (mean) velocity has been plotted in three sections of the model in Figure 4.13. The chosen sections are intended to represent the different types of flows over the physical model surface: first, a longitudinal section ($x = 0.75$ m) has been selected to compare the velocities distribution in the region of the drainage channels and to check how the higher resolution of the SfM topography allows us to represent channel velocity variation in the transversal flow; furthermore, an additional longitudinal section ($x = 0.10$ m) and a cross-section in $y = 3.75$ m have been used to assess the curb flow and investigate the higher dispersion shown in Figure 4.11, Figure 4.12 in the case of the SfM topography, despite its higher resolution. The uncertainty in the LSPIV experimental results has been included by plotting the standard deviation of the measured velocities in the recorded interval.

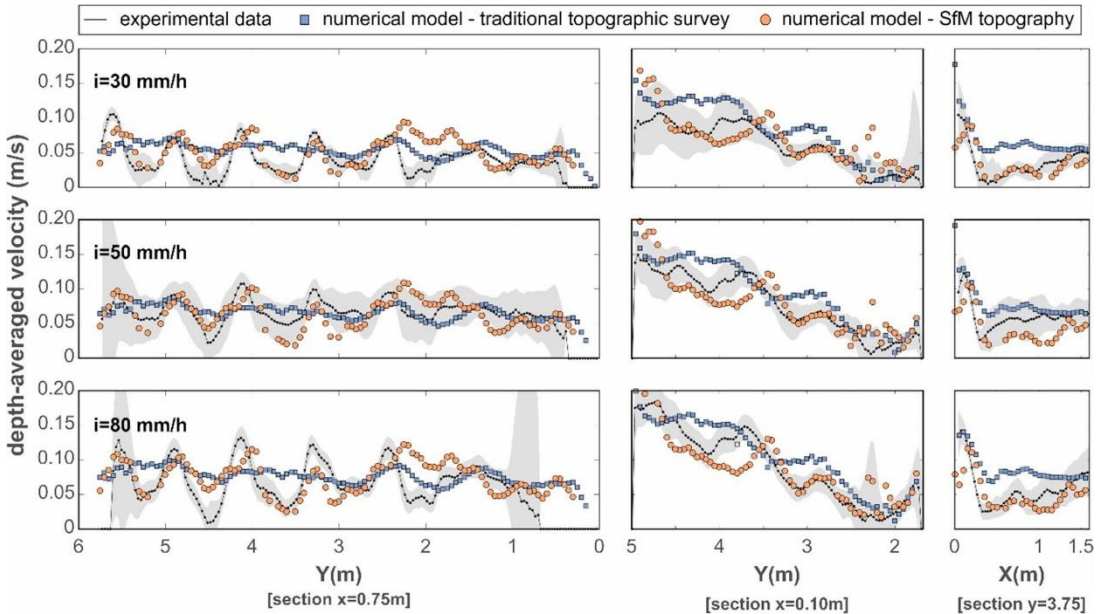


Figure 4.13. Numerical and experimental depth-averaged velocity sections comparison ($X = 0.75$ m, $X = 0.10$ m and $Y = 3.75$ m) for the three rainfall intensities studied.

Looking at the first section ($x = 0.75$ m) for all the rain intensities in Figure 4.13, it can be noted that the numeric results from the point data measured topography is not able to simulate the drainage channels and keep an almost constant velocity value over the cross-section, especially between $y \sim 5.5$ m and $y \sim 2$ m. However, the model with the SfM elevations shows a reasonable agreement with the experimental data and fits the peaks where the velocity increases in the drainage channels, with the exception to region ranging from $y \sim 1$ to $y \sim 2$ m. The standard deviation of the experimental velocity is about 0.01–0.02 m/s, except for the bounds of the visualization domain, where higher experimental errors are expected due to insufficient illumination.

In the case of the second section ($x = 0.10$ m), the influence of the topography in the numeric results is apparently lower due to the higher flow depth developed next to the curb. But although both numeric results simulate satisfactorily the increasing tendency of the curb flow velocity between the gully pots, the SfM model is able to follow the shape of the velocity changes produced in the junctions between the transversal channels with the curb flow, a slight variation of position being observed in the velocity peak around $y = 3.5$ m. Finally, the last transversal section shows a limitation of the SfM technique measuring the elevations of roughly the first centimeters next to the curb, in that we can see the reduction of the velocities around this area compared with the traditional topographic survey and the experimental results. These two discrepancies observed in the curb flow could explain the higher disparity presented by the y -velocities from the SfM topography with respect to the

experimental data observed and commented on in Figure 4.11. However, the photogrammetric technique provides a better fit in the rest of the section, confirming their better performance in modelling the runoff that has been shown above.

Overall, it can be concluded that the SfM model has a higher correlation with the experimental measurements. The results obtained with the SfM domain represent accurately the qualitative flow behavior, although some quantitative differences have been highlighted in the position of some of the peaks of the cross-sectional velocity profiles. These differences could be attributed to errors in the determination of the elevation maps or in the determination of the velocity fields. The errors related to the topography are more relevant in the areas with lower depths and close to the curb edge. The errors in the velocity determinations are mainly located in some specific areas of the model due to a poor local particle illumination, or related to the shallow water conditions tested in this study, commonly lower than 1 cm. In these conditions tracer particles can eventually settle, as they can be trapped by pavement surface irregularities, thus affecting the determined magnitude of the velocity vectors.

4 Conclusions

In this study, novel techniques such as SfM photogrammetry and a modified LSPIV were applied in order to obtain, using a 2D shallow water model, an accurate representation of the overland runoff generated by three different rain intensities, of 30, 50 and 80 mm/h, in an urban drainage physical model. Based on the results, the following conclusions can be drawn:

- The SfM photogrammetric technique provided a fast and effective way to obtain an elevation map that differed in a RMSE error of 2.9 mm from the traditional topographic survey coordinates of a regular rectangular grid of 0.5 m × 0.5 m, but with a spatial resolution 100 times higher.
- The modelled discharges into the gully pots obtained with a 2D shallow water model with gridded and with SfM topographies are almost identical. However, clear differences appear when the overland velocity fields are compared. The differences are due to the far higher spatial resolution of the SfM survey, revealing the existence of drainage channels of a few millimeters' depth placed orthogonally to the model curb. In these drainage channels the local velocities increased due to the small-scale irregularities of the surface.
- By means of fluorescent particles and UV illumination, LSPIV was presented as a very useful non-intrusive tool to accurately measure surface flow velocities in shallow

water conditions of few millimeters' depth with a high spatial resolution, including the longitudinal and transversal channel curb flow, in a medium-size area of around 10 m², and avoiding the presence of raindrops that might interfere in the measurements.

Thus, this study highlights not only the great value of the topographic modelling of surface flow in shallow water conditions and the importance of a detailed elevation map, but also the need for additional surface velocity calibration data as well as the register of hydraulic variables in the sewer network to achieve useful and accurate surface flow results. Furthermore, the findings of this study are intended to contribute to the development and improvement of new affordable techniques to measure these essential data and to be able to obtain a suitable surface flow representation to be used as the basis for wash-off and flood risk assessment studies in urban catchments.

Chapter 5

Hydraulic, wash-off and sediment transport experiments

1 Introduction

In urban environments, pollutants are accumulated during dry weather on roads, roofs and other impervious surfaces (Zafra *et al.* 2017). These pollutants are washed off in rain events and transported by stormwater runoff into drainage systems and eventually into aquatic media (Anta *et al.* 2006), representing one of the most significant environmental issues in urban areas (Egodawatta, 2007). In this context, concentrations of total suspended solids (TSS) are typically used as indicators in the study of the transport process of fine particles (Rossi *et al.* 2009, Sikorska *et al.* 2015), which have been found to be closely related to many pollutants, such as heavy metals and Polycyclic Aromatic Hydrocarbons (PAH) (Herngren *et al.* 2005a, Akan and Houghtalen 2003, Sartor and Boyd 1972) and might even be a good proxy for other emerging pollutants, such as microplastics (Dris *et al.* 2015, Dehghani *et al.* 2017). TSS wash-off and transport modelling is thus an important tool for the development of management and treatment techniques to minimize the environmental impact of these contaminants.

Several empirical equations and models have commonly been used in the literature to model urban wash-off (e.g. Sartor and Boyd 1972, Egodawatta *et al.* 2007, Leutnant *et al.* 2018, Muthusamy *et al.* 2018). However, the prediction accuracy of these lumped formulations is quite limited (Schellart *et al.* 2010). This due to i) difficulties in accurately measuring input variables such as the initial sediment load and characteristics, and ii) the fact that they do not consider spatial and sediment heterogeneities. Recently, physically-based wash-off models (Deletic *et al.* 1997, Shaw *et al.* 2006, Hong *et al.* 2016a, Naves *et al.* 2019b) have appeared as alternatives to empirical equations as a means of considering spatial heterogeneities in the distribution of sediments, and to model main wash-off processes such as the detachment of particles by raindrop impacts or runoff shear, particle transport and deposition. However, this leads to an increase in the input variables needed to accurately determine and make a precise representation of the surface flow needed. Gully pot modelling (Deletic *et al.* 2000, Post *et al.* 2016) and sewer transport modelling (Mannina *et al.* 2012, Hannouche *et al.* 2017), as well as interactions between surface and drainage systems (Djordjević *et al.* 2013, Fraga *et al.* 2015a, Rubinato *et al.* 2017, Martins *et al.* 2018), are also key in order to provide an integrated solution to runoff TSS mobilization.

Due to the variability and randomness of the sediment build-up process (Wijesiri *et al.* 2015b, Sandoval *et al.* 2018), field data uncertainties in the measurement of sediment input variables can be propagated through models and lead to unreliable results. In addition, variability and heterogeneity of rainfall and detailed geometries of urban catchments include additional uncertainties in wash-off modelling, which can lead to the incorrect evaluation of equations and models. In this regard, some authors have performed experimental studies over impervious surfaces where initial conditions are accurately determined (Shaw *et al.* 2006, Muthusamy *et al.* 2018) in order to assess new wash-off

formulations. However, the surfaces considered in these physical models are no larger than 1 m², and such models do not consider gully pots interactions or typical curb flows, so their application is limited to first approximations in simple urban catchments. In addition, laboratory experiments performed in physical models of gully pots (e.g. Butler *et al.* 1995, Ciccarello *et al.* 2011, Tang *et al.* 2016) and sewers (e.g. Ota and Perrusquia 2013, Safari *et al.* 2017) have also been seen as a potentially fruitful means of studying runoff quality in drainage systems. However, although some experiments in large-scale urban drainage facilities considering surface and drainage system flow are available in the literature (Moy de Vitry *et al.* 2017, Fraga *et al.* 2015a), data regarding TSS transport is quite limited. In addition, rainfall simulators are a useful tool for a better understanding of these processes of wash-off and sediment transport in urban areas, in which it has been seen that the uniformity and intensity of the generated rain is key (Naves *et al.* 2017).

In light of this, the current dataset provides a series of experiments in which variables involving sediment wash-off by rainfall and transport through gully pots and pipes were accurately measured under laboratory-controlled conditions. The experiments were performed in a full-scale street section physical model, including a 36 m² rainfall simulator and two gully pots that drain runoff into a drainage pipe system. First, we developed a novel rainfall simulator in order to generate realistic rainfall with suitable uniformities and drop size distributions. Then an accurate hydraulic characterization was performed, measuring flows and depths generated by a steady and uniform rainfall, additionally obtaining runoff velocity distributions and elevations using visualization techniques (Naves *et al.* 2019a). Finally, in a total of 23 experiments, concentrations of TSS at the entrance of gully pots and at the pipe system outlet were monitored to assess wash-off and sediment transport processes from accurately measured sediment initial conditions, using three different rainfall intensities and five sediment classes with different granulometries. The dataset is unique in that it is obtained on a 1:1 scale with realistic and very accurately measured initial conditions, and as such will allow other researchers to test models and hypotheses, thus improving our overall knowledge of urban wash-off and sediment transport. In addition, it provides videos of surface runoff and images of the physical model surface, and these are of use as a means of optimizing visualization techniques as a tool for obtaining calibration data for flood and urban drainage models.

The remainder of the chapter is structured as follows. The physical model used in the experiments is described in Sect. 2. The methodology followed in performing the hydraulic characterization of the experiments and the related data is set out in Sect. 3. Then, Sect. 4 presents details of the wash-off and sediment transport experiments methodology, plus the data here. Finally, details on the availability of the data, and the conclusions to be drawn from the study, are given in Sect. 5 and 6, respectively.

2 Physical model description

The laboratory facility (Figure 5.1) was built in the Hydraulic Laboratory of the Centre of Technological Innovation in Construction and Civil Engineering (CITEEC) at the University of A Coruña (Spain), and consists of a rainfall simulator over a 36 m² full-scale street section. Two gully pots and a lateral outflow channel drain the runoff generated by rainfall into a pipe network that transports runoff to a common outlet. The different parts that makes up the physical model are described in the following subsections.

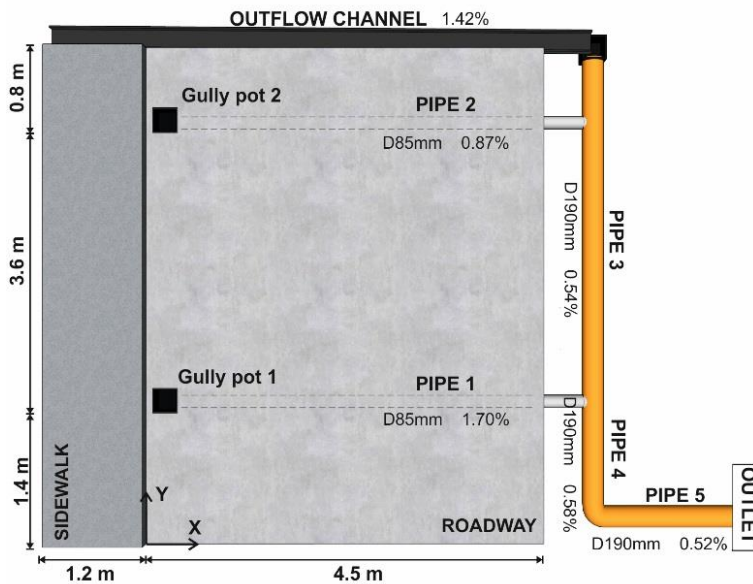


Figure 5.1. Street section physical model scheme.

2.1 Rainfall simulator

The rainfall simulator consists of 2,500 pressure-compensating irrigation drippers (PCJ-CNL, NetafimTM) disposed in a grid layout and inserted in two overlapped circuits of pipes, which are placed 2.6 m above the physical model surface. Drippers inserted in each circuit generate 1.2 and 2 L/h, respectively. Thus, given a distribution of 25 drippers per square meter in each circuit, the rainfall simulator is able to generate rainfall with a rain intensity of 30 or 50 mm/h. Both circuits can also be used at the same time generating a rain intensity of 80 mm h⁻¹. In addition, a metallic welded mesh with 3 mm square openings, located 0.6 m below the drippers, breaks and distributes drops to achieve realistic rainfall in terms of uniformity and raindrop size distribution. Rain intensity maps were measured for each rainfall from the volume collected in a 0.5 m x 0.5 m grid of vessels for 5 minutes, and are available in Naves

et al. (2019c). Figure 5.2 shows an image of the measuring process and the results for the intermediate rain intensity.

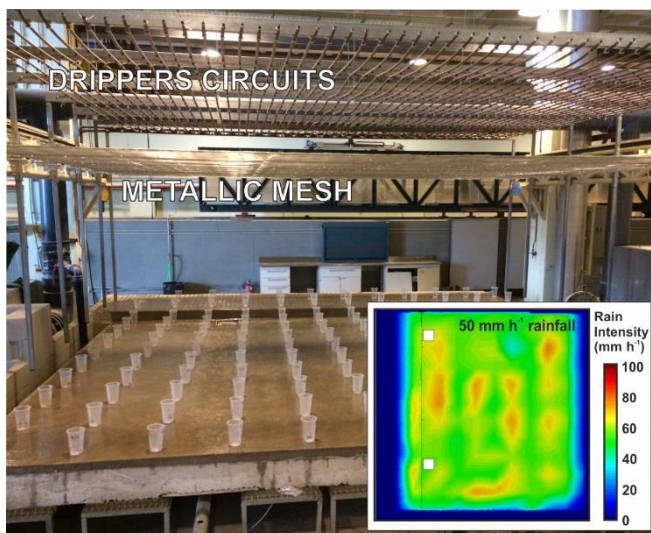


Figure 5.2. General image of the rainfall simulator with the experimental setup for the measurement of rain intensity maps. Results for the intermediate rainfall are also plotted.

2.2 Model surface

The street section surface model is formed by a tiled sidewalk separated by a 0.15 m high curb. Two elevation maps with different resolutions are provided, making it possible to implement the geometry in numerical models and to simulate runoff properly. First, a traditional topographic survey was carried out by measuring punctual distances from the surface to a reference laser plane with an accuracy of 0.5 mm and a resolution of 0.5 m x 0.5 m. In addition, the Structure from Motion (SfM) photogrammetric technique was used to obtain a 5 mm resolution elevation map. This technique provides a 3D reconstruction from the triangulation of different points that appear in several images of the analyzed objects. Raw images, the point cloud resulting from the SfM software, and the methodology and reference points used to obtain the final elevation map, are all available in Naves *et al.* (2019e), and can be used to assess, analyze and reproduce the implementation of this technique to hydraulic physical models.

2.3 Drainage system

The generated rainfall runoff drains into the pipe system through two gully pots located along the curb and a lateral outflow channel. Then, flow is transported from the gully pots and from the end of the outflow channel to a common pipe system outlet. All the geometric

details of the drainage system, such as gully pot dimensions, pipe diameters and slopes, are available in Naves *et al.* (2019c) for better replicability.

3 Hydraulic experiments

The accurate characterization of the superficial runoff and in-pipe flow play a key role in modelling wash-off and sediment transport. Therefore, the first set of experiments available consists of a detailed hydraulic characterization. In this regard, online measurements of surface and pipe depths and water flows in gully pots and at the pipe system outlet were registered for the three different rain intensities that the rainfall simulator was able to generate. In addition, two different particle image velocimetry (PIV) techniques were used to measure surface velocity distributions. The data on hydraulic experiments is described in the following subsections. Additionally, measuring points and sensor names are shown in Figure 5.3. Further details of location, sensors used, acquisition time and units for each result are also available in the dataset (Naves *et al.* 2019c).

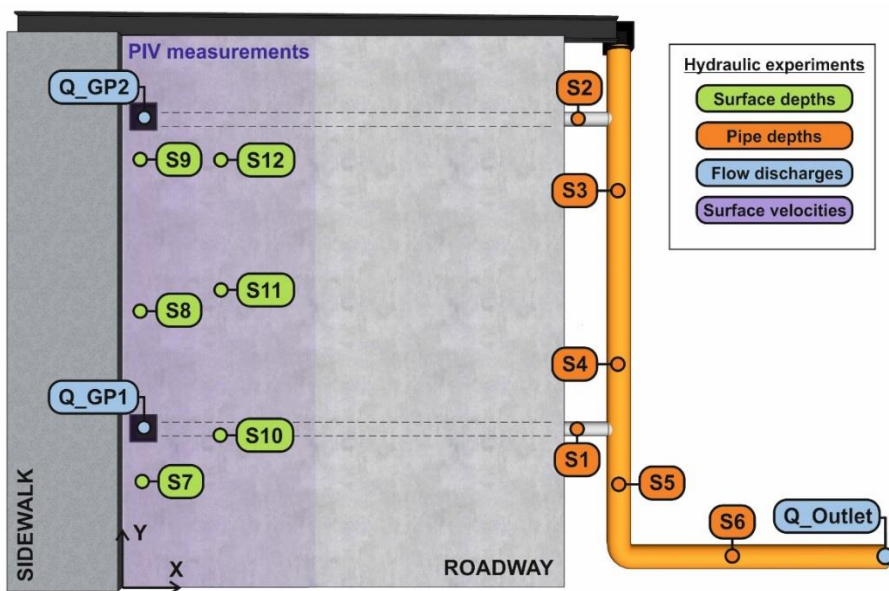


Figure 5.3. Surface and in-pipe depth, flow discharge and surface velocities measuring points in hydraulic experiments.

3.1 Surface and pipe depths

A total of 6 pipe depths (S1-S6) and 6 surface depths (S7-S12) were measured using ultrasonic distance sensors (UB500-18GM75-I-V15, Pepperl and Fuchs) with a sampling

frequency of 5 Hz. Prior to the experiments, sensors were pre-calibrated in order to convert the registered voltages to depths and discharges. To do this, signal-distance linear calibrations, with a determination coefficient (R^2) above 0.99, were obtained measuring five known distances from sensors to a reference plane. After this, the raw time series registered in the experiments were processed in the following way. First, a five seconds wide median filter was implemented to remove peak signals higher than twice the standard deviation. Then, a 20 seconds wide moving median was applied to smooth the signal. Finally, the pre-calibration was used to transform signals into distances and obtain depth results from the differences between the measurements during the experiment and the dry surface reference, which was measured for 60 seconds before the rain began. Figure 5.4 includes images of sensors installed on the street surface (left) and pipes (right), and some examples of depth results. Calibration data, raw signals, and processed results are available in Naves *et al.* (2019c) for other authors to use.

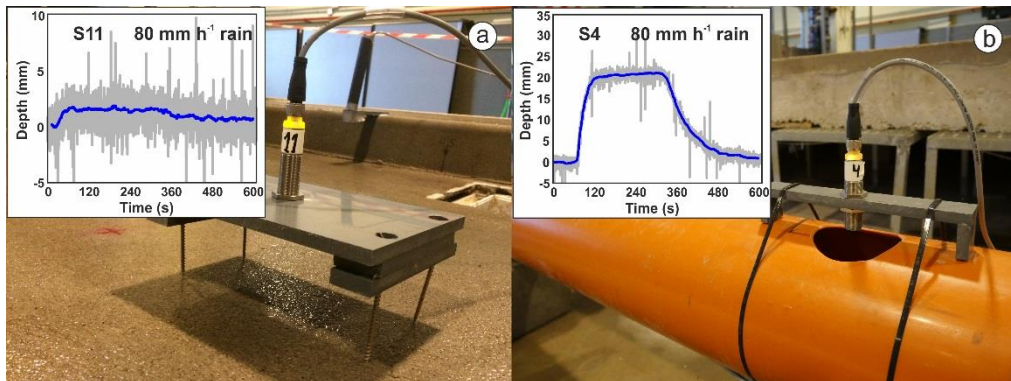


Figure 5.4. Distance sensors installed on the street surface (a) and on pipes (b) to measure water depths. Data registered for the highest rain intensity is also shown.

3.2 Flow discharge

Discharges in gully pots and at the pipe system outlet were measured using ultrasonic distance sensors (UB500-18GM75-I-V15, Pepperl and Fuchs) registering the level over a v-notch weir in three different deposits. The first deposit was 0.5 m x 0.6 m size and was installed at the pipe system outlet. The pipe outflow, after passing through a 0.4 m length and 0.16 m diameter deposit used in wash-off experiments (further details in Sect. 4.2), flowed into the deposit to obtain continuous measurements. Two additional deposits were installed below the gully pot in order to derive inflows as a way of measuring discharges following the same methodology. Figure 5.5 and Figure 5.6 show schemes of the configurations of the deposits and includes examples of the processed data available in Naves *et al.* (2019c).

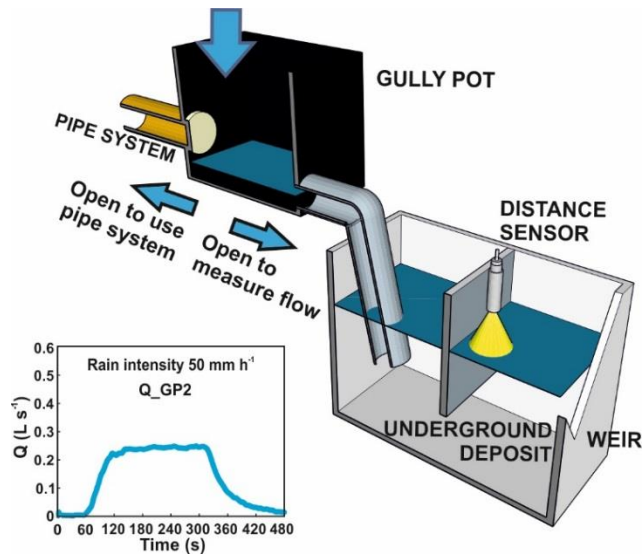


Figure 5.5. Setup for the measurement of gully pot discharges from the water level over a v-notch in an underground deposit. The result obtained in gully pot 2 for the rain intensity of 50 mm/h is also shown in the plot as an example.

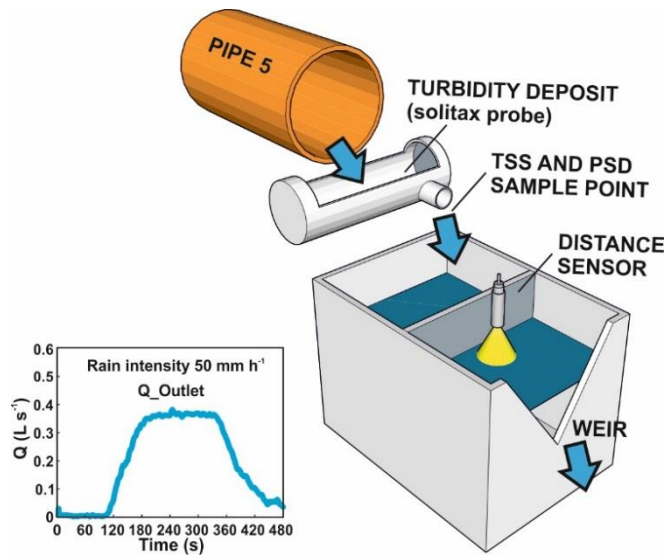


Figure 5.6. Pipe system outlet setup for the measurement of flow discharges, turbidity and suspended solids transport. The flow discharge registered in for the rain intensity of 50 mm/h is also plotted.

A signal-flow pre-calibration was performed for each sensor installed in these deposits. To do this, different known steady flows were introduced in the deposit to obtain a second-degree polynomial relation (obtaining R^2 over 0.99) in order to transform the signal recorded

into discharge. The signal processing starts by removing peaks higher than twice the standard deviation with a five seconds-wide median filter. Then, a five seconds-wide moving median was applied to the signal before obtaining flow time series using pre-calibration polynomial regression. However, these results corresponded to the deposit outflow, so it was necessary to consider the volume that was retained when the flow, and thus the water level in the deposits, varied. Signal-depth calibrations, as performed for surface and pipe depths, plus the area of the deposits, were thus used to take into account these variations of volume in time steps of 5 seconds, obtaining the water flow at the entrance of the deposits. Finally, flow time series were smoothed by a 20 seconds-wide moving median. Figure 5.7 shows the data processing procedure for the flow at the pipe system outlet generated by the intermediate rain intensity. Data regarding pre-calibrations and raw and processed signals are provided for each hydraulic experiment in Naves *et al.* (2019c).

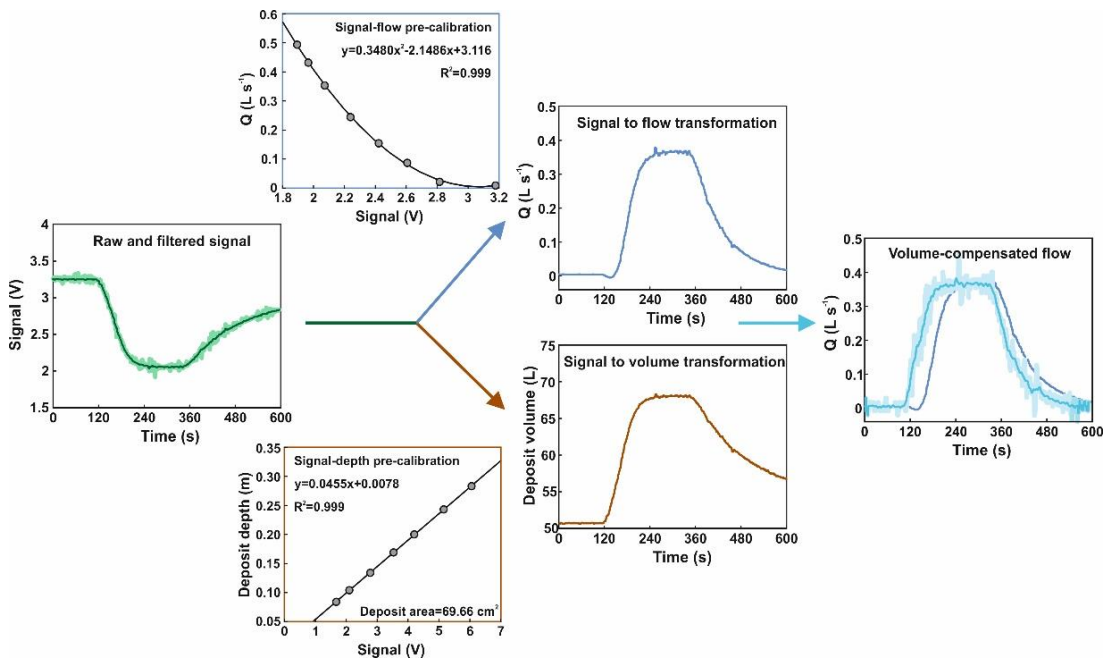


Figure 5.7. Flow discharge data processing from the raw recorded signal to the flow result at the pipe system outlet for the intermediate rain intensity.

3.3 Surface velocities

Surface flow velocities were measured using the PIV technique, which analyses the displacement between two consecutive frames of tracers that follow the studied flow. Frames were obtained from 4k and 25 fps videos recorded by two Lumix GH4 cameras (focal length 28 mm), which were installed above the sidewalk of the physical model, covering the first two meters of roadway from the curb. Two different tracers were used in the

experiments applying PIV: i) fluorescent particles illuminated by UV torches, and ii) water reflections and small bubbles generated by raindrop impacts. The analysis of the runoff velocities in steady conditions started by extracting 1,500 frames (60 s) from each camera recording. First, a spatial calibration was required to rectify the angle of the cameras and the lens distortion, and to join the images from each camera. Matlab algorithm 'fitgeotrans' was applied, identifying in each video reference points drawn in the model surface in order to transform video frames to an orthogonal reference system. Then, frames were converted to greyscale and a sliding background filter was applied, transforming to black those pixels with 25% or less relative difference in the grey value with the same pixel from the previous frame. The PIV tool for Matlab PIVLab (Thielicke and Stamhuis 2014) was used to obtain raw velocities from each pair of consecutive frames (using interrogation areas of 128, 64 and 32 pixels as settings). Finally, after a temporal 2D filter (Goring and Nikora 2002) and a spatial median filter of 3x3 elements using the Matlab toolbox 'pivmat' (Moisy 2017), the surface velocity distribution was obtained from the mean of all the results. For the videos recording water reflections and bubbles without particles, the same methodology was followed, but using a sliding background threshold of 10%.

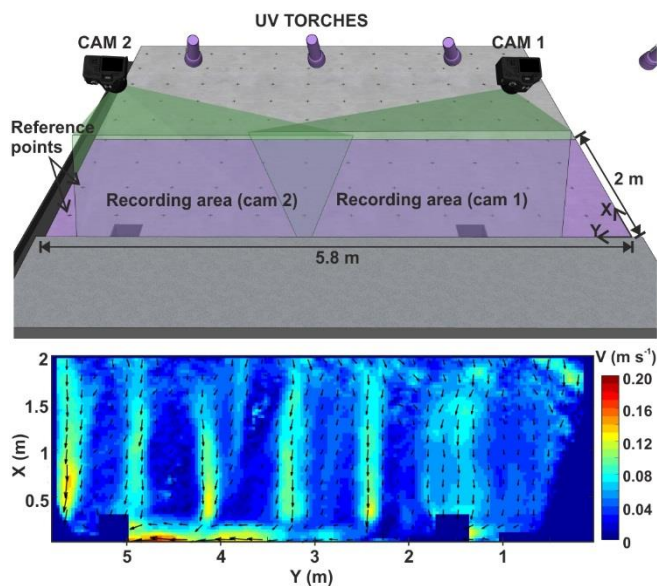


Figure 5.8. Experimental setup scheme for the recording of runoff videos used in the PIV analysis with fluorescent particles. The resulted steady velocity distribution generated by the lowest rainfall intensity is also plotted.

Figure 5.8 shows a scheme of the experimental setup and the steady results for the rain intensity of 30 mm/h obtained using fluorescent particles as tracers. Raw videos, frames processed for the PIV analysis, and velocity distribution results are all provided in Naves *et*

al. (2019d) for the use of other researchers. Further details of the fluorescent particles, the coordinates of reference point used, and the frames extracted from videos for the analysis can be also consulted.

3.4 Experimental procedure

Experiments consist of simulating a steady and homogeneous rainfall of 30, 50 or 80 mm/h intensity with a duration of 5 minutes. Online measurements of surface and pipe depths and gully pots and pipe system outlet discharges were registered from the beginning of the rain until 5 minutes after the rain stopped. As seen in Section 3.2, the measurement of discharge from gully pots requires closing their connection with the pipe system and deriving the gully pot inflow towards the underground deposit. This configuration prevented us from measuring total drained flow at the pipe system outlet, since the water that reached the outlet came uniquely from the outflow channel. Therefore, experiments for each rainfall were repeated with and without the connection between gully pots and the pipe system, in order to obtain discharges in the outlet and in both gully pots, respectively. Table 5.1 shows the six tests performed and their configuration.

Table 5.1. *Hydraulic tests configurations.*

ID	Rain intensity (mm/h)	Measuring point
HY01_30_GP	30	Gully pots
HY02_30_O	30	Outlet
HY03_50_GP	50	Gully pots
HY04_50_O	50	Outlet
HY05_80_GP	80	Gully pots
HY05_80_O	80	Outlet

Six more experiments (Table 5.2) were performed for the PIV analysis in order to record surface runoff with and without fluorescent particles for each rain intensity. These experiments started by spreading particles over the model surface. Cameras began recording and ambient lights were turned off. Then, UV torches were turned on and a steady and uniform rainfall was generated. As the particles were washed off by surface flow, it was necessary to add more particles on the roadway side during video recording. Steady runoff conditions were reached after approximately 150 seconds. For videos without particles, the same methodology was followed, but replacing the UV torches with conventional LED lamps. The first part of experiment 3 was not recorded, and an initial recording to extract a

calibration frame and a steady flow conditions video has been provided instead. Depths and discharges were not registered in this case.

Table 5.2. Configuration of PIV experiments.

Test ID	Rain intensity (mm/h)	Tracer	Illumination
1	30	Fluorescent particles	UV
2	50		
3	80		
4	30	Wave water reflections and air bubbles	LED lamps
5	50		
6	80		

4 Wash-off and sediment transport experiments

Once the hydraulics of the experiments was accurately determined, we focused on measuring wash-off and sediment transport processes from given accurately-known initial conditions. For this, TSS and Particle Size Distribution (PSD) samples at the entrance of the gully pots and at the pipe system outlet were collected for the three rain intensities and for five sediment classes, which have different granulometries, disposed realistically over the model surface. In addition, online turbidity records were registered at the pipe system outlet, and pipe depths and outlet discharge were measured following the methodology presented in Sections 3.1 and 3.2, respectively. At the end of each experiment, a mass balance was performed in order to assess the final distribution of sediment in the different parts of the physical model and to confirm the reliability of the experiments. The following subsections describe the data collected in these experiments, which is available in Naves *et al.* (2019c). Figure 5.9 shows measuring points and the identification names used.

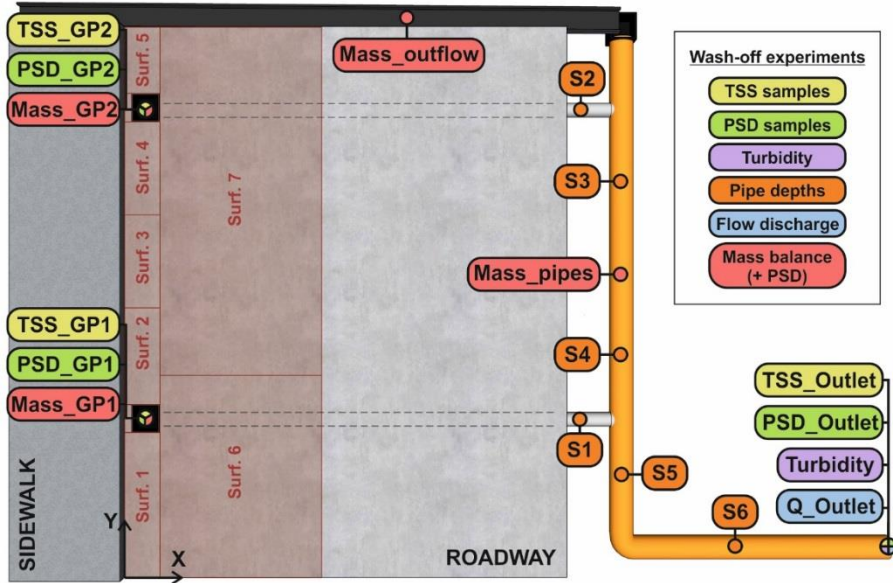


Figure 5.9. Measuring points in wash-off and sediment transport experiments.

4.1 Sediment initial conditions

The initial amount of sediment and its distribution was determined following Naves *et al.* (2017) and the references include therein. Therefore, a load of 20 g per meter of curb was disposed in a stepped distribution (Figure 5.10) along 5.5 m of curb, since sediments tend to be accumulated close to the curbs (Sartor and Boyd 1972, Grottker 1987, Deletic and Orr 2005). Considering that no sediment was distributed in the area of the gully pots, and that the gully pot and pipes were initially clean, the total initial mass used in each experiment was 99.44 g. The sediment used came from a roadway surface described in Fraga *et al.* (2016), and was sieved obtaining four uniform granulometries (classes D1-D4 in Figure 5.13) in order to analyze the effect of sediment grain size in the wash-off and sediment transport processes. A final sediment with a continuous granulometry (class D5 in Figure 5.11), formed from a combination of the previous granulometries, was used to study the effect of employing a more realistic multi-class sediment distribution. All classes of sediment granulometries, obtained accurately by a laser coulter particle size analyzer (Beckam-Coulter LS 13 320), are available in Naves *et al.* (2019c). A pycnometer was used to measure the density of the material for each sediment class, resulting in a common value of 2557 ± 16 kg/m³.

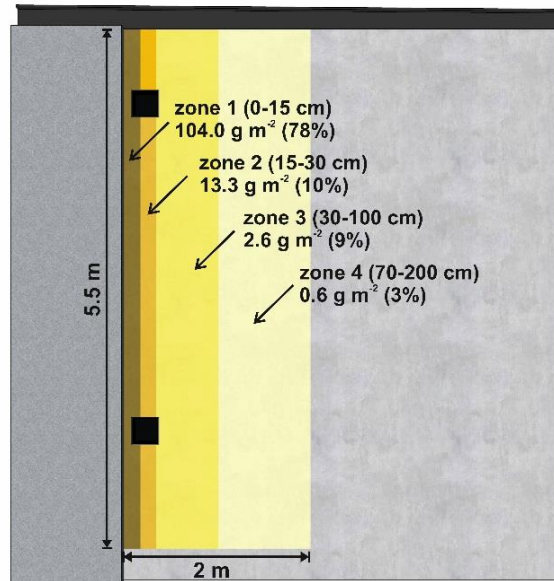


Figure 5.10. Initial distribution of sediment over the model surface for the wash-off and sediment transport tests.

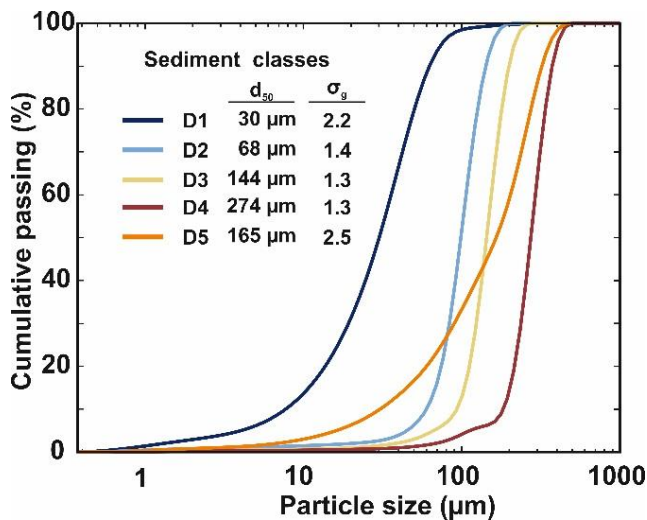


Figure 5.11. Particle size distribution of the five sediment classes used. Mean diameter and gradation coefficients ($\sigma_g = \sqrt{D_{84}/D_{16}}$) are also indicated in the plot.

4.2 TSS measurement

For each measuring point and experiment, the dataset in Naves *et al.* (2019c) provides the times at which manual samples were collected and the TSS concentrations resulting from filtering of the samples following the APHA (1995) standard methods. Samples were roughly

180 ml volume and were collected once a perimeter channel and a small deposit concentrated the flow at the entrance of the gully pots and at the pipe system outlet, respectively. The sample times were different for each rain intensity, since samples were taken from the moment that flow reached the measuring points until the physical model drained the water that remained after the rain stopped. In addition, the time between samples was shorter at the beginning of the experiment, this in order to detect the TSS peak. The results obtained measuring TSS mobilization during the experiments for the five sediment classes and the three rain intensities at the entrance of the gully pots and at the pipe system outlet are shown in Figure 5.12.

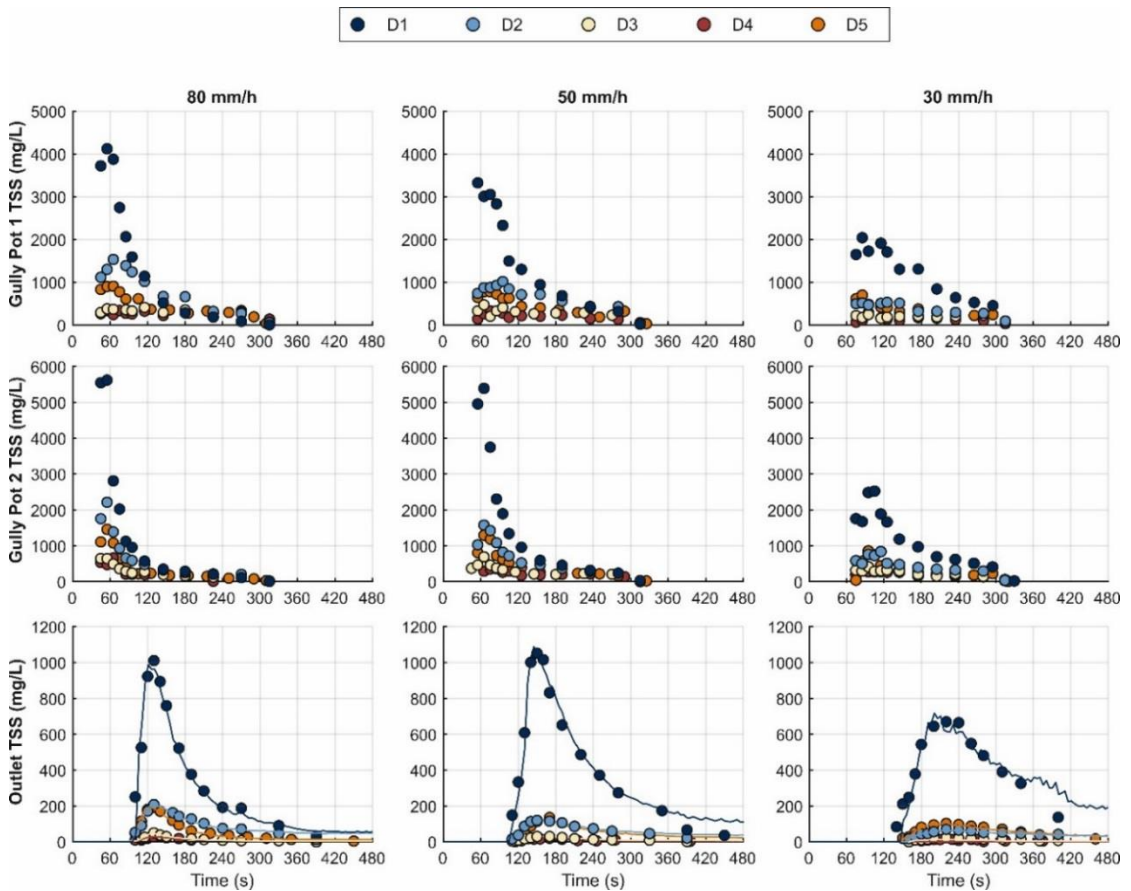


Figure 5.12. Total suspended solids (TSS) results in both gully pots and in the pipe system outlet for the five different grain sizes (D1-D5) and rain intensities of 80, 50 and 30 mm/h.

Particle sizes are presented in these results as key variable in wash-off process. The finest sediment (sediment class D1 with a mean diameter of 30 μm) produce the highest concentration at the gully pots and at the pipe system outlet with a big difference with

respect to the rest of particle sizes. In addition, the TSS concentrations measured for the continuous granulometry D5 ($d_{50}=165 \mu\text{m}$), both at gully pots and at pipes system outlet, were between those obtained for sediments D2 ($d_{50}=68 \mu\text{m}$) and D3 ($d_{50}=144 \mu\text{m}$). Therefore, considering the mean particle size as representative can lead to erroneous estimations modelling wash-off. In a lower level, rain intensity also affects significantly to the TSS mobilization as can be seen comparing the different columns in Figure 5.12.

4.3 Particle size distributions

Additional manual grab samples collected at the entrance of the gully pots and at the pipe system outlet were also analyzed with a laser coulter particle size analyzer to determine grain sizes that were being washed at each sample time. In the experiments with realistic and continuous granulometry (sediment class D5), a detailed characterization of the temporal variations of the PSD in gully pots and pipe system outlet were performed with a mean of eight PSD samples for each measuring point. The number of samples was lower for experiments with uniform granulometries (sediment classes D1-D4) since no significant temporal variations of the PSD were expected. PSD raw data and sample times are included in Naves *et al.* (2019c) for each measuring point. Figure 5.13 show images of these measuring points where the PSD and TSS samples are collected during the experiments.



Figure 5.13. PSD and TSS samples measuring points at the entrance of gully pots (a) and at the pipe system outlet (b).

4.4 Mass balance

The masses of sediment collected at the end of each experiment from surface, gully pots, and pipe system are also available in the dataset (Naves *et al.* 2019c). This makes it possible to perform mass balances following the methodology used in Naves *et al.* (2017) in order to analyze where the sediment is deposited depending on rain intensity and on sediment grain size. It may also be a useful indicator of the reliability of the results, in that it shows how much mass was controlled. Firstly, sediment masses that remained over the surface and

inside gully pots were collected with an industrial vacuum with a 98% sweeping efficiency. As can be seen in Figure 5.9, the surface was divided into 7 areas in order to analyze the final distribution of sediment over the street surface. Finally, pipes were cleaned using a pressure washer, and sediment deposited in pipes was collected with a 10 μm sieve at the pipe system outlet. To close mass balances adequately, it was necessary to take into account concrete particles, which were eroded from the model surface during the vacuuming process. To do this, eight blank experiments without sediments were performed following the same procedure to determine a mean concrete mass to subtract from the masses collected in the experiments. In this way, it was possible to consider exclusively the sediment mass in the mass balances. Blank masses collected are also available in Naves *et al.* (2019c). The PSD of mass balance samples were also measured using a laser coulter particle size analyzer (Beckam-Coulter LS I3 320) in order to analyze the deposition of the different grain sizes at the end of the experiments. The sediment masses obtained from each part of the model are presented in Figure 5.13 for the different rain intensities and sediment granulometries tested.

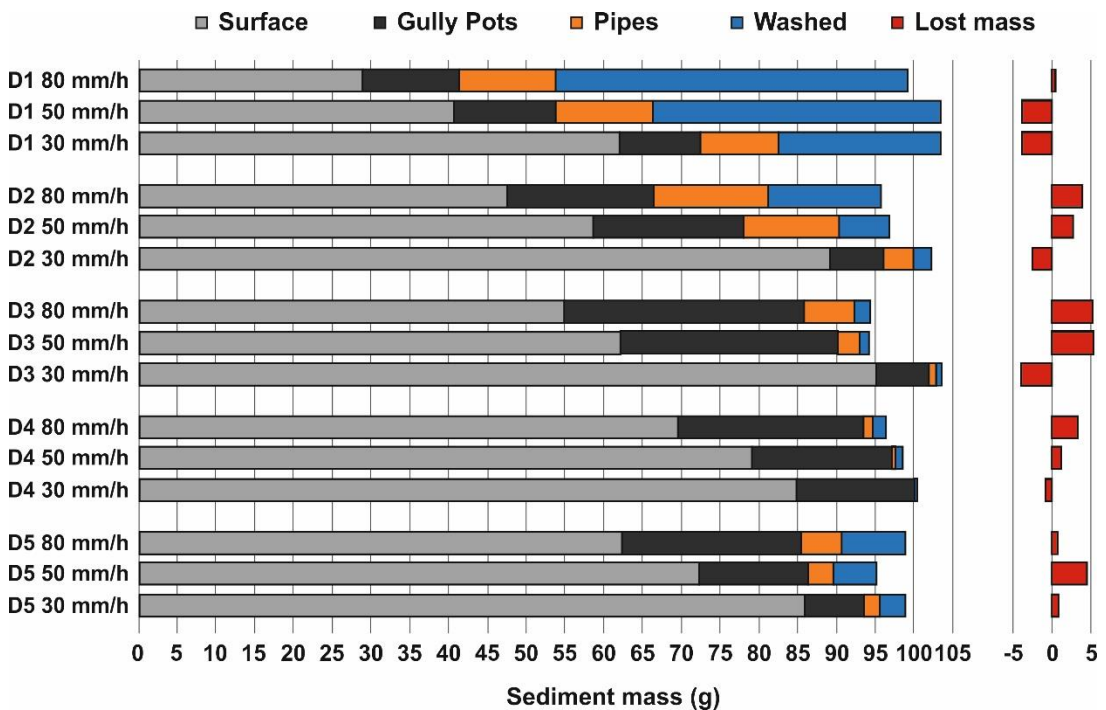


Figure 5.14. Mass balances results for the five different grain sizes (D1-D5) and rain intensities of 80, 50 and 30 mm/h.

The sediment mobilization depending on the sediment granulometry and the rain intensity can be analysed with the mass balance results. It can be seen that even using the finest

sediment and the highest rain intensity, only a fraction of the sediment is washed completely from the physical model and most part of the initial sediment mass remains in the physical model. It also can be noted that the continuous granulometry (sediment class D5) showed significant washed off masses even for the lower rain intensities, which correspond with the mobilization of the finest particles. The errors in the mass balances between the initial surface sediment mass and the masses collected at the end of the experiments plus the sediment washed from the physical model during the experiment were below 5%. This result is really satisfactory considering the studied phenomena and ensure the reliability of the experimental results, demonstrating the accurate measurement of wash-off and sediment transport processes.

4.5 Experimental procedure

Each test configuration combines a sediment class (D1-D5) and a homogeneous and steady rainfall (30, 50 or 80 mm/h) with a duration of 5 minutes. During the simulated event, manual grab samples in the three measurement points were collected and turbidity, pipe depths, and outlet discharge were registered up to 5 minutes after the rain stopped. Grab manual TSS and PSD samples at the entrance of the gully pots can interfere in the mass balance and in the TSS and PSD results at the pipe system outlet. Therefore, each experiment was repeated without manual samples at the gully pots, this to ensure reliability in pipe system outlet samples and final mass balances. However, some experiments with low rain intensity and larger sediment grain sizes were performed only once, since most of the sediment remained on surface or was deposited in gully pots, presenting negligible TSS concentrations at the pipe system outlet. Table 5.3 shows all the tests and their configurations, including those seven configurations not performed.

Table 5.3. Wash-off and sediment transport tests ID and configurations.

30 mm/h rain intensity			50 mm/h rain intensity			80 mm/h rain intensity		
Test ID	Sed. class	Measuring Point	Test ID	Sed. class	Measuring Point	Test ID	Sed. class	Measuring Point
ST01_30_D1_GP	D1	Gully pots	ST11_50_D1_GP	D1	Gully pots	ST21_80_D1_GP	D1	Gully pots
ST02_30_D1_O	D1	Outlet	ST12_50_D1_O	D1	Outlet	ST22_80_D1_O	D1	Outlet
ST03_30_D2_GP	D2	Gully pots	ST13_50_D2_GP	D2	Gully pots	ST23_80_D2_GP	D2	Gully pots
ST04_30_D2_O	D2	Not performed	ST14_50_D2_O	D2	Not performed	ST24_80_D2_O	D2	Outlet
ST05_30_D3_GP	D3	Gully pots	ST15_50_D3_GP	D3	Gully pots	ST25_80_D3_GP	D3	Gully pots
ST06_30_D3_O	D3	Not performed	ST16_50_D3_O	D3	Outlet	ST26_80_D3_O	D3	Outlet
ST07_30_D4_GP	D4	Gully pots	ST17_50_D4_GP	D4	Gully pots	ST27_80_D4_GP	D4	Gully pots
ST08_30_D4_O	D4	Not performed	ST18_50_D4_O	D4	Not performed	ST28_80_D4_O	D4	Not performed
ST09_30_D5_GP	D5	Gully pots	ST19_50_D5_GP	D5	Gully pots	ST29_80_D5_GP	D5	Gully pots
ST10_30_D5_O	D5	Outlet	ST20_50_D5_O	D5	Outlet	ST30_80_D5_O	D5	Outlet

5 Data availability

Three data packages are available in open access from the Zenodo data repository within the scope of the WASHTREET project, at the website <https://zenodo.org/communities/washtreet>. A main data package (Naves *et al.* 2019c) contains the data related with the hydraulic, wash-off, and sediment transport experiments described in this chapter. Two additional packages (Naves *et al.* 2019d, Naves *et al.* 2019e) are provided to include detailed raw and processed data regarding the PIV analysis and the SfM photogrammetric technique, respectively. A brief description of each data package is included below.

5.1 Hydraulic, wash-off and sediment transport experiments data

This main data package includes further details of the physical model, rain intensity maps, surface topographies, a description of the materials and methods used, and raw and processed data of hydraulic (except surface velocities data) and wash-off experiments. In addition, it provides a series of images and videos for a better understanding of the data. (<https://doi.org/10.5281/zenodo.3233918>)

5.2 PIV analysis data

The PIV data package provides, first, a detailed description of the methodology, data processing, and results. Raw 4K videos recorded with and without particles are also available for the three rain intensities. Second, it provides coordinates, calibration frames, and instructions to rectify video frames to an orthogonal reference system, plus the processed frames to perform the PIV analysis. Finally, the steady velocity distributions obtained from each video analysis are provided. (<https://doi.org/10.5281/zenodo.3239401>)

5.3 SfM topography data

The raw images used to apply the photogrammetric technique to the model surface are provided in this data package. In addition, descriptions of the methodology, the raw point cloud obtained from the SfM software, and the elevation map resulted, are also available. (<https://doi.org/10.5281/zenodo.3241337>)

6 Conclusions

Given the lack of data for the development of empirical and physically based urban wash-off models, plus the difficulty in conducting field studies accurately measuring key input

variables such as initial load of sediment, its spatial distribution, or the sediment characteristics, we have proposed here a series of experiments in which the different processes are accurately measured in laboratory-controlled conditions. Our experiments are unique in that they are performed in a full-scale physical model using a very realistic rainfall simulator. In addition, not only are the initial sediment conditions completely defined, but the hydraulic behavior of the experiments is also accurately determined, including depth and velocity measurements of very shallow flows. Finally, surface wash-off and in-pipe sediment transport is precisely measured by TSS and PSD samples and by analyzing the mobilization of sediments through performing mass balances at the end of the tests. The dataset introduced in this study, then, is useful in the following ways:

- Hydraulic and wash-off dual drainage modelling studies in urban catchments. Data can be used to develop, calibrate and validate urban drainage models, including wash-off and sediment transport processes in the different components of the drainage system (surface, gully pots, in-pipe) without considering uncertainties in the input variables. The use of different sediment classes also means that the analysis of single and multi-class sediment transport modelling is itself of interest. Finally, the data herein lead to our research being replicable, and thus allows other researchers to test their own models and hypotheses.
- Assessment and optimization of seeded and unseeded PIV techniques. The raw videos and data provided are of great use as a means of improving the understanding of the use of PIV analysis in urban environments, with very shallow flows and in the presence of raindrops.
- Study of the novel application of photogrammetric techniques for hydraulic modelling purposes. The raw images and raw point cloud results can be used to assess photogrammetric techniques in order for these to be used in further field and physical model applications.

Chapter 6

Analysis of a physical-based urban wash-off model

1 Introduction

The trend towards rapid urbanization and population migration to towns and cities has led to the development of more impervious surfaces, which themselves become a major contributor of pollutants in urban areas (Butler and Davies 2010). Urban runoff contains dissolved and suspended solids that have accumulated in streets, roofs and other surfaces, and are washed off during rain events (Zafra *et al.* 2008). Heavy metals and Polycyclic Aromatic Hydrocarbons (PAH) are traditionally considered to be the major causes of contamination in urban stormwater and have been found to be associated with fine particles (Hengren *et al.* 2005a, Akan and Houghtalen 2003, Sartor and Boyd 1972). In addition, recent studies (Dris *et al.* 2015, Dehghani *et al.* 2017, Vogelsang *et al.* 2019) have highlighted the significant presence of microplastics (sizes from 0.1 to 1000 μm) in urban catchments. Thus the transport process of these fine particles can be used to study stormwater quality during rain events, typically using the concentration of total suspended solids (TSS) as an indicator (Rossi *et al.* 2009, Sikorska *et al.* 2015).

A thorough understanding of the processes involved in the wash-off of suspended solids, then, is essential in estimating runoff pollution loads and concentrations, and in improving treatment and management techniques to minimize their impact on the environment (Anta *et al.* 2006). To that end, empirical wash-off equations (e.g. Sartor and Boyd 1972, Egodawatta *et al.* 2007, Leutnant *et al.* 2018, Muthusamy *et al.* 2018) have been developed and implemented in urban drainage models like SWMM (Rossman, 2015) over the last 40 years, but without significant advances in prediction accuracy (Schellart *et al.* 2010). These lumped formulations take as the main variables the initially available sediment load or the total runoff volume, and neglect spatial heterogeneities (Wang *et al.* 2011), which has the effect of only roughly approximating the complexity of the physical phenomena. Specifically, they do not take into account processes such as the detachment of soil particles due to raindrop impacts or runoff shear, the transport of these particles by the overland flow, or their deposition. Hence the predictive results obtained are rather uncertain, and they are not particularly useful for engineering risk assessment or design.

Given these limitations of the empirical lumped equations to adequately model a complex process such as urban wash-off, several physically-based models have arisen as alternatives. Deletic *et al.* (1997) considered the spatial distribution of the solid particles over the street surface and developed a new formulation, including the rainfall and the shear stress of the overland flow as main variables, to model the entrainment of the particles into suspension. In the wash-off model proposed in Shaw *et al.* (2006, 2009), the particles are suspended due to raindrop impacts on the flow, in which they are transported until their deposition. In the model introduced by Massoudieh *et al.* (2008), this particle detachment was assumed to be

a function of flow velocity. All these studies showed the potential for modelling the wash-off processes in impervious surfaces with physically-based formulations, but their 1D approximation limits their performance in real urban catchments. More recently, Hong *et al.* (2016a, b, 2019) evaluated and calibrated the urban wash-off process on a road catchment of 2661 m² using the physically-based Hairsine-Rose (H-R) formulation (Hairsine and Rose, 1992a, b) coupled with a 2D shallow water model. Their results show a promising level of agreement with respect to the field-measured pollutographs, suggesting that 2D physically-based wash-off models could be a feasible alternative to empirical wash-off equations for a better representation of the spatial and temporal heterogeneities in urban water quality studies.

However, several difficulties remain in the use of physical-based models to simulate urban wash-off: i) the high computational cost of these models currently limits their application to small urban catchments; ii) the H-R model was originally developed for, and is usually applied to, model erosion in rural catchments (Cea *et al.* 2016, Heng *et al.* 2011), so the lack of experience in urban catchments, and the large number of variables needed to model the physical processes, render the calibration of the model difficult; iii) due to the randomness and variability in the build-up process (Wijesiri *et al.* 2015a, Sandoval *et al.* 2018), uncertainty in accurately measuring some input variables, such as the initial load and the sediment distribution over the street surface and characteristics, can lead to unreliable model results in real-world studies.

Therefore, the aim of the present study is to contribute to the understanding of physically-based wash-off models in urban catchments by means of a rigorous sensitivity analysis, this on the basis of a series of specifically designed, full-scale laboratory experiments. In these, the physical properties, initial mass and spatial distribution of the deposited sediments in the urban surface were accurately measured under controlled laboratory conditions. This has allowed the assessment of the model sensitivity to the H-R model parameters through a global sensitivity analysis. Then, the uncertainties associated to all model inputs were considered in a local analysis to assess the relative importance in the water quality results of hydraulics, sediment inputs, and H-R model parameters. Hence, this study is novel regarding three specific aspects:

- The Hairsine-Rose wash-off model was applied coupled with a 2D shallow water model that is previously calibrated with experimental surface velocity and flow data to have the most realistic description of rainfall-runoff transformation.
- A series of tailored wash-off experiments were performed, where the wash-off process was accurately monitored under laboratory-controlled conditions. This experimental data is unique because they were obtained on a 1:1 scale including a realistic rainfall simulator of 36 m², using three rainfall intensities and four realistic

sediment distributions with different grain sizes. In addition, the data is openly available, which makes our research reproducible and enables others to test their own models and hypotheses.

- The results from our global and local sensitivity analyses provide the necessary information to choose the most important parameters and simplify the model to make it feasible to transfer the Hairsine-Rose erosion model to a broad field of scientific studies and practical applications in urban catchments.

The remainder of the chapter is structured as follows: the numerical model, the laboratory experiments, and the global and local sensitivity analysis methodology are described in Section 2; the results of the sensitivity analyses are set out in Section 3; Section 4 offers a discussion of the results; and finally, general conclusions of the study are presented in Section 5.

2 Materials and methods

The physically-based wash-off model and the different variables and parameters involved are introduced first, in Section 2.1. Then, Section 2.2 includes a description of the experimental facility and the methodology used in the laboratory experiments, which are used as a basis for the sensitivity analysis (SA). Section 2.3 and 2.4 describe the procedure and methods used to perform the global and the local SA. Finally, the ranges of the input factors considered, the implementation of the SA methods, and a preliminary assessment of model predictions, are set out in Sections 2.5, 2.6 and 2.7, respectively.

2.1 Numerical model

The physically-based urban wash-off model used in this study consists of a process-based H-R formulation coupled to a 2D shallow water model. The model was previously applied to soil erosion modelling in Cea *et al.* (2016). The only modification required for its application to urban environments was the definition of a non-erodible layer corresponding to the impervious surface.

2.1.1 Hydrodynamics

The model Iber (Bladé *et al.* 2014, García-Feal *et al.* 2018) was used as a basis for the implementation of the Hairsine-Rose sediment transport equations. This hydrodynamic model solves 2D unsteady depth-averaged shallow water equations using an explicit unstructured finite volume solver, including rainfall and infiltration terms in the mass conservation equation, and using the Manning formula to compute bed friction. Previous

studies have shown the capacity of the model to adequately represent the spatial distributions of water depth and velocity under overland flow conditions and including rainfall-runoff transformation (Cea *et al.* 2010, Cea and Bladé 2015). The runoff model has also been validated for urban areas in the same laboratory facility described in this work (Fraga *et al.* 2015a, Naves *et al.* 2019a) and also in field applications (Fraga *et al.* 2016). The input factors in the hydrodynamic equations are the rain intensity (R), the bed roughness Manning coefficient (n), and the surface initial losses (IL).

2.1.2 Wash-off model

The original H-R model uses a vertical layer structure where the sediments can be part of three different compartments. The first compartment is the original soil from which sediments can be detached through the effect of raindrop impacts or through the shear generated by overland flow. The eroded sediments become part of the flow's suspended solid concentration, and can remain in the flow or be deposited over the bed, forming a deposited layer from where they can become re-detached. In the application of the formulation to urban drainage, the original soil corresponds with the impervious surface, so the interactions with the flow are only made from the deposited layer, which is where the urban surface sediments build up. In this way, the time and spatial evolution of the suspended sediment concentration is computed from the following depth-averaged equation:

$$\frac{\partial hC}{\partial t} + \frac{\partial q_x C}{\partial x} + \frac{\partial q_y C}{\partial y} = e_r + r_r - d \quad (1)$$

where C (kg/m^3) represents the depth-averaged concentration of sediment in the water column, h (m) is the water depth, q_x and q_y (m^2/s) are the two components of the specific discharge, e_r ($\text{Kg}/\text{m}^2/\text{s}$) and r_r ($\text{Kg}/\text{m}^2/\text{s}$) are, respectively, the rainfall-driven and flow-driven detachment rates from the deposited layer, and d ($\text{Kg}/\text{m}^2/\text{s}$) is the deposition rate.

The rainfall-driven detachment rate e_r is usually assumed to have a linear relation with rain intensity (Sharma *et al.* 1993, 1995, Gao *et al.* 2003) and is computed as:

$$e_r = \alpha R \varepsilon \quad (2)$$

$$\varepsilon = \min \left[\frac{M_s}{M_{s_{cr}}}, 1 \right] \quad (3)$$

$$\alpha = \begin{cases} \alpha_0, & h \leq h_0 \\ \alpha_0 \left(\frac{h_0}{h} \right)^b, & h > h_0 \end{cases} \quad (4)$$

where α_0 ($\text{kg}/\text{m}^2/\text{m}$) is the rainfall detachability coefficient, h_0 (m) is a water depth threshold from where the rainfall detachment rate begins to decrease due to the damping

of the rainfall energy on the water layer, b is a constant exponent, ε is a correction coefficient to account for the availability of sediment over the impervious non-erodable surface, Ms (Kg/m^2) is the mass of deposited sediment per unit surface, and Ms_{cr} (Kg/m^2) is the mass of sediment over the non-erodable layer needed to achieve the potential rain-driven detachment. Some authors do not implement the correction coefficient ε when modelling soil erosion in rural catchments because in such applications the availability of deposited sediment is guaranteed. This is not the case in urban environments, where the small amount of sediment available over the impervious layer, as well as its heterogeneous distribution, makes it necessary to include this parameter in the model. In this way, it is possible to consider the lower detachment rates in areas where the mass of deposited sediments is low, as well as the decrease in the detachment rate produced when the sediment is washed off.

The flow-driven term r_r models the transfer of solids due to the effect of bed friction and is computed using the following equation:

$$r_r = \begin{cases} \frac{\rho_s F(\Omega - \Omega_0) \varepsilon}{(\rho_s - \rho_w) g h}, & \text{if } \Omega > \Omega_0 \\ 0, & \text{otherwise} \end{cases} \quad (5)$$

where ρ_s and ρ_w (kg/m^3) are the density of the solid particles and water, respectively, Ω (W/m^2) is the runoff stream power per unit surface, Ω_0 (W/m^2) is the critical stream power threshold below which the entrainment rate is zero, F is the fraction of stream power excess over Ω_0 that contributes to the entrainment of sediments, g (m/s^2) is the gravity acceleration, and ε is a correction coefficient to account for the availability of deposited sediment, as explained above. This formulation assumes that only a fraction of the total stream power dissipation, given by $F(\Omega - \Omega_0)\varepsilon$, contributes to sediment detachment and the rest is spent in other head losses.

The deposition rate d of solids from the flow to the surface is modelled as:

$$d = \rho_s w_s C \quad (6)$$

where w_s is the settling velocity of sediment particles (m/s), which depends on the density and the mean diameter (D_{50}) of the particles, and is computed using the formulation in Van Rijn (1984).

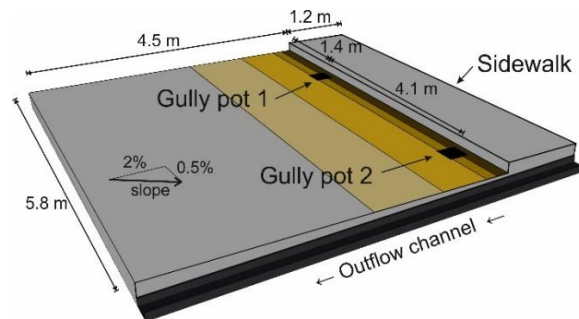
Finally, the evolution of the sediment mass in the surface is computed by solving the following mass balance equation:

$$\frac{\partial Ms}{\partial t} = d - (e_r + r_r) \quad (7)$$

2.2 Laboratory experiments

A series of wash-off experiments performed in an urban drainage physical model have been used as the basis for a SA of the wash-off model. The advantage of using these experiments instead of field data is that the variables involved in the wash-off process can be measured with a high degree of accuracy under controlled laboratory conditions. In our case, the initial sediment conditions and the rest of hydraulic input factors could be fixed to a constant value, and the global SA was focused on the influence of the poorly-known H-R parameters. The experiments were also used to determine the ranges of the local SA, where hydrodynamic variables and parameters, and initial sediment conditions, are considered.

The experimental facility is located in the Hydraulic Laboratory of the CITEEC, at the University of A Coruña, and consists of a 36 m² full-scale street section. A rainfall simulator is located 2.6 m over a concrete street surface, which is divided into a sidewalk and a roadway (Figure 6.1). The detailed surface elevation data of the facility and the details of the rainfall simulator, which is able to generate rain intensities of 30 mm/h, 50 mm/h and 80 mm/h with high spatial uniformity, were described in Naves *et al.* (2019a). The generated rainfall runoff drains into two gully pots located along the curb and into a lateral outflow channel. The surface has an approximate transversal slope of 2% up to the sidewalk and a 0.5% longitudinal slope up to the outflow channel.



Sediment initial distribution




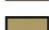
	zone 1 (0-15 cm):	104.0 g/m ² (78%)
	zone 2 (15-30 cm):	13.3 g/m ² (10%)
	zone 3 (30-100 cm):	2.6 g/m ² (9%)
	zone 4 (70-200 cm):	0.6 g/m ² (3%)

Figure 6.1. Physical model scheme and initial distribution of the sediment.

The experiments consist of measuring the hydraulics and the total suspended solids (TSS) at the entrance of the gully pots, given a known initial load of sediment over the roadway

surface. The initial amount and spatial distribution of sediments over the surface have been determined following previous wash-off studies by the authors (Naves *et al.* 2017) and the references included therein. The initial load of sediment was fixed to 20 g per meter of curb. It was distributed realistically over the street section, following the results of Sartor and Boyd (1972), since it is known that roadway sediments tend to accumulate close to curbs (Grottker 1987, Deletic and Orr 2005). As shown in Figure 6.1, most of the sediment (78%) was placed homogeneously within the first 0.15 m from the curb. 10% and 9% of the sediment was then placed over the next 0.15 and 0.70 m, and the remaining 3% over the rest of the surface up to the road median, which in our case was fixed at 2 m from the sidewalk. The sediment deployed was collected from a real road surface, which is described in Fraga *et al.* (2016), and sieved to obtain four different uniform granulometries (sediment classes in Table 5.1) with gradation coefficients ($\sigma_g = \sqrt{D_{84}/D_{16}}$) between 1.3 and 2.2 (Julien 2010). The density of the material, measured by a pycnometer for all the granulometries, was $2557 \pm 16 \text{ kg/m}^3$, this corresponding to a high value within the range obtained in Pitt *et al.* (2004), where different urban build-up studies were reviewed.

Table 6.1. Sediment granulometries considered (D1-D4) and total washed off mass for the twelve laboratory experiments.

Sed. class	Granulometries				Washed off mass (g)		
	D ₅₀ (μm)	D ₁₆ (μm)	D ₈₄ (μm)	σ _g	30 mm/h	50 mm/h	80 mm/h
D1	30.1	11.4	54.6	2.19	31.0	48.3	61.2
D2	68.1	46.3	91.8	1.41	13.2	32.5	53.8
D3	143.9	105.8	186.8	1.33	7.5	17.1	28.6
D4	273.8	204.7	351.8	1.31	6.1	13.6	22.9

Each laboratory experiment involves the combination of a sediment class (D1-D4 in Table 6.1) with steady, homogeneous rainfall of 30, 50 or 80 mm/h intensity, with a duration of 5 minutes. The water discharge through both gully pots was measured by means of a triangular weir and an ultrasonic distance sensor (UB500-18GM75-I-V15, Pepperl and Fuchs), while the TSS were obtained from 200 mL manual grab samples taken at regular time intervals. At the end of the experiment, the solids that remained in the physical model were collected to verify the correct operation of the experiments through a sediment mass balance. The mass balance errors remained below roughly the 5% of the total mass, which is very satisfactory considering the complexity of the physical phenomena. The detailed methodology to perform the mass balance can be found in Naves *et al.* (2017). The plots in Figure 6.2 show the flow and TSS results for rain intensities of 80, 50 and 30 mm/h, plus the

different grain sizes. In addition, a more detailed description of the physical model and those experimental results not included here have been uploaded to the open-access repository Zenodo (Naves *et al.* 2019c). The hydraulics of the experiments has already been calibrated successfully, using the measured hydrographs with the 2D shallow water model in Naves *et al.* (2019a).

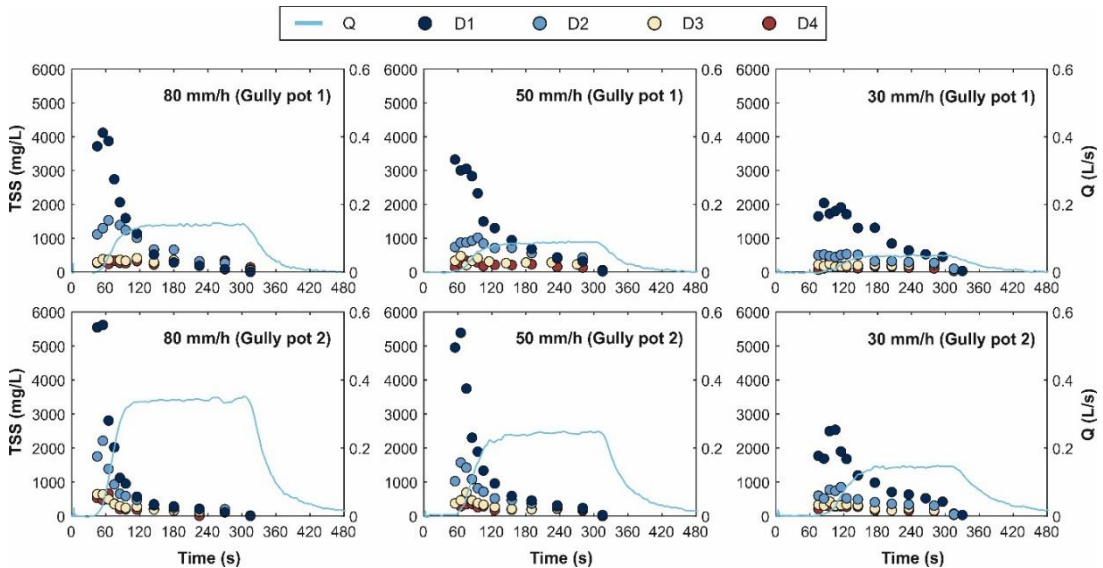


Figure 6.2. Total suspended solids (TSS) and experimental flow results in both gully pots for the four different grain sizes (D1-D4) and rain intensities of 80, 50 and 30 mm/h. It can be seen that the complete pollutographs of the experiments have been a satisfactory measure here, through analyzing the manual grab samples for all the diameters and rain intensities.

2.3 Global sensitivity analysis

A global SA (Saltelli *et al.* 2008) was performed to investigate the variability of the model output under changes in the H-R model parameters. The SA methods and metrics were constrained by the high computational time of the model and the high number of input factors. Thus, to make analysis feasible, the rest of the input factors were not considered, their values being fixed according to the initial conditions of each laboratory experiment. Global SA was evaluated using two techniques: the Standardized Regression Coefficients (SRC), obtained from a multiple linear regression; and the Extended Fourier Amplitude Sensitivity Test (EFAST), which is able to consider the effect of the interactions of factors. These two methods have been applied recently in the field of urban drainage in Gamerith *et al.* (2013) and Donckels *et al.* (2014), respectively. In addition, Vanrolleghem *et al.* (2015) and Mannina *et al.* (2016) used both methods at the same time, showing that robustness of global SA is substantially increased by using multiple methods and multiple objectives.

2.3.1 Standardized Regression Coefficients (SRC)

Standardized Regression Coefficients (Helton, 1993) were used as quantitative measures of the sensitivity of the model outputs to the H-R parameters considered (Saltelli *et al.* 2000, Saltelli *et al.* 2008). The multiple linear regression model takes the following form:

$$y_i = b_0 + \sum_{j=1}^n b_{ij}x_{ij} + \xi \quad (8)$$

where y_i are the different outputs studied, x_i ($x_{i1}, x_{i2}, \dots, x_{in}$) are the n parameters vectors, b_j are the regression coefficients, and ξ is the residual error due to the linear approximation. The SRC (b_stand_{ij}) measure the effect of the input factors (x_j) in the variance of the output (y_i), and are obtained as:

$$b_stand_{ij} = b_{ij} \sqrt{\frac{var(x_{ij})}{var(y_i)}} \quad (9)$$

The absolute value of the regression coefficients represents the influence of each parameter to a certain model output, with negative SRCs indicating inverse relationships. The coefficient of determination (R^2) was used to check the assumption of linearity, so low R^2 indicates unreliable SRCs.

2.3.2 Extended Fourier Amplitude Sensitivity Test (EFAST)

The Fourier Amplitude Sensitivity Test (FAST) is a variance-based method developed by Cukier *et al.* (1973) for sensitivity and uncertainty analysis. The FAST method does not require any assumption of linearity and is based on the exploration of the entire parameter space by an efficient search curve; it is able to obtain the direct influence of each parameter in the total variance (first-order indices, S_i). The EFAST (Saltelli *et al.* 1999), which is an improvement of the FAST method, is used in the current global SA to estimate both the main effect (S_i) as well as the total effect sensitivity indices S_{Ti} , which include all its interactions with other factors at any order. S_i and S_{Ti} are obtained as:

$$S_i = \frac{var_{x_i}[E_{x_{-i}}(Y|x_i)]}{var(Y)} \quad (10)$$

$$S_{Ti} = 1 - \frac{var_{x_{-i}}[E_{x_i}(Y|x_{-i})]}{var(Y)} \quad (11)$$

where var is the variance, E is the expected value, Y the model output, and x_i and x_{-i} indicate, respectively, that the operator is either applied over the i th factor or over all of them except the i th factor. The interaction between factors are therefore represented by the difference between S_{Ti} and S_i .

2.4 Local sensitivity analysis

In a regular field application, it is not possible to measure all the input variables as accurately as in a laboratory facility, especially considering the randomness and variability in the sediment build-up. Therefore, a local SA was carried out including all the model input factors, not only the H-R parameters, to ensure the transferability of the results to real catchments and to analyze the relative importance of hydraulics, initial sediment conditions and H-R parameters in the model outputs. The thirteen input factors considered in the local SA are those described in Section 2.1 plus a uniformity coefficient (UC), which considers the uncertainties in the spatial distribution of the initial sediment load over the street surface. This coefficient varies linearly the distribution of the initial load of sediment among the four predefined zones shown in Figure 6.1, taking a value of zero when all the sediment is placed in the area attached to the curb, and a value of one for a spatially uniform distribution. In our experiments the UC is 0.32.

Performing a variance-based method that considers all the variables was impossible due to the computational expense of the model. Thus, the Elementary Effects (EE) method (Saltelli *et al.* 2008, Campolongo *et al.* 2007, Morris 1991), also known as the Morris screening method, was chosen, following Saltelli and Annoni (2010). This method is based on the evaluation of the model along a determined number of trajectories (r) where the different factors are changed in a one-at-a-time (OAT) experimental design. Considering a model of k independent inputs $X_i, i = 1, \dots, k$, each input is assumed to vary in the k -dimensional unitary hypercube across p selected levels. This means that the input space is discretized into a p -level grid (Ω). The ranges of the factors are assumed to be normalized for sampling, and the actual values are then calculated for simulations. The elementary effect (EE_i) for a given X_i in the output Y is defined as:

$$EE_i = (Y(X_1, \dots, X_i + \Delta, \dots, X_k) - Y(X_1, \dots, X_i, \dots, X_k)) / \Delta \quad (12)$$

where Δ is the distance between two realizations of factor X_i (inside Ω). The starting point and the order and direction in which the inputs are evaluated OAT change randomly between the different trajectories. Therefore, the mean of the absolute values of all the elementary effects obtained in each trajectory (μ^*) and their standard deviation (σ) are the sensitivity measures for each input. μ^* indicates the overall influence of the factors on the output and σ estimates the variability of the EE and thus the dependency with respect to the rest of the factors.

2.5 Variables and parameters ranges

2.5.1 Global sensitivity analysis

Given the lack of work using the H-R model in urban catchments, which is limited to the studies presented in Hong *et al.* (2016a,2016b, 2019), the range of variation of the H-R parameters for the global SA (Table 6.2) was determined by taking into account previous erosion studies (Proffit *et al.* 1991, 1993, Beuselinck *et al.* 2002, Shaw *et al.* 2006, Sander *et al.* 2007, Heng *et al.* 2011 and Cea *et al.* 2016) and thus seeking to cover the complete performance range of the model.

Table 6.2. Parameters and ranges of variation used in the global sensitivity analysis.

Variable	Units	Definition	Range
α_0	Kg/m ² /m	Rainfall detachability coefficient	500 - 3500
h_0	M	Water depth damping threshold	0.0001 - 0.0025
b	-	Positive constant	0.6 - 1.4
$M_{s,cr}$	Kg/m ²	Critical mass to achieve the potential detachment	0 – 2.8
F	-	Effective fraction of excess stream power	0 - 0.03
Ω_0	W/m ²	Critical stream power	0 - 0.02

2.5.2 Local sensitivity analysis

Table 6.3 shows the range of variation of the hydrodynamic variables and parameters and the initial sediment conditions used in the local SA. The ranges were centered according to the experimental layouts and their size was defined following the methodology presented in Brun *et al.* (2002). The input factors were classified on three levels corresponding to the degree of knowledge available in a typical field study. A relative uncertainty of 5 % (accurately known, level 1), 20 % (inaccurate known, level 2) and 50 % (very poorly known, level 3) was assigned to each level, respectively. In this way, as shown in Table 5.3, the hydrodynamic factors were considered as level 1. Due to the randomness and variability in the build-up and wash-off processes, the sediment diameter and the initial deposited mass and distribution of solids were defined as very poorly known variables (level 3). The sediment density was considered as a moderately inaccurate known variable (level 2), given its lower associated uncertainty.

Table 6.3. Input factor ranges for the local sensitivity analysis.

Variable	R	n	IL	D ₅₀	ρ_s	M _{S0}	UC
Units	mm/h	-	mm	μm	Kg/m ³	kg/m _{curb}	-
Uncertainty level	1	1	1	3	2	3	3
Range variation (%)	5	5	5	50	20	50	50
Lab. experiment							
1	29.25-30.75	0.0156-0.0164	0.585-0.615	22.5-37.5	2301-2812	15-25	0.24-0.40
2	48.75-51.25	0.0156-0.0164	0.585-0.615	22.5-37.5	2301-2812	15-25	0.24-0.40
3	78.00-82.00	0.0156-0.0164	0.585-0.615	22.5-37.5	2301-2812	15-25	0.24-0.40
4	29.25-30.75	0.0156-0.0164	0.585-0.615	51.0-85.0	2301-2812	15-25	0.24-0.40
5	48.75-51.25	0.0156-0.0164	0.585-0.615	51.0-85.0	2301-2812	15-25	0.24-0.40
6	78.00-82.00	0.0156-0.0164	0.585-0.615	51.0-85.0	2301-2812	15-25	0.24-0.40
7	29.25-30.75	0.0156-0.0164	0.585-0.615	108.0-180.0	2301-2812	15-25	0.24-0.40
8	48.75-51.25	0.0156-0.0164	0.585-0.615	108.0-180.0	2301-2812	15-25	0.24-0.40
9	7.008-82.00	0.0156-0.0164	0.585-0.615	108.0-180.0	2301-2812	15-25	0.24-0.40
10	29.25-30.75	0.0156-0.0164	0.585-0.615	205.5-342.5	2301-2812	15-25	0.24-0.40
11	48.75-51.25	0.0156-0.0164	0.585-0.615	205.5-342.5	2301-2812	15-25	0.24-0.40
12	78.00-82.00	0.0156-0.0164	0.585-0.615	205.5-342.5	2301-2812	15-25	0.24-0.40

The ranges of the H-R parameters for the local SA (Table 6.4) represent the uncertainty in the correct estimation of these parameters in order to compare the relative importance of their correct determination with respect to the hydraulic and initial sediment conditions inputs. The ranges have been defined from the global SA simulations as the interquartile ranges of the parameter sets whose total washed off mass results differed by less than 5% from the experimental measurement.

Table 6.4. Ranges of Hairsine-Rose parameters for the local sensitivity analysis.

Variable	α_0	h_0	b	$M_{s,cr}$	F	Ω_0
Units	Kg/m ² /m	mm	-	Kg/m ²	-	W/m ²
Lab. experiment						
1	1504-3040	1.05-1.98	0.81-1.17	0.62-1.22	0.009-0.024	0.005-0.016
2	1614-2779	1.02-2.00	0.78-1.19	0.77-1.66	0.010-0.023	0.003-0.013
3	1589-2883	0.95-2.03	0.74-1.14	0.85-1.88	0.008-0.022	0.004-0.014
4	1536-2891	0.91-2.11	0.82-1.22	0.48-1.11	0.011-0.025	0.003-0.015
5	1557-2953	1.03-1.92	0.78-1.20	0.36-0.73	0.009-0.026	0.003-0.013
6	1364-2998	1.08-1.74	0.76-1.12	0.25-0.53	0.009-0.023	0.003-0.014
7	1391-2917	0.66-1.95	0.82-1.18	0.44-0.92	0.011-0.025	0.005-0.014
8	1602-2668	0.45-1.93	0.74-1.21	0.20-0.54	0.011-0.026	0.03-0.012
9	1647-2835	0.95-2.16	0.77-1.16	0.24-0.43	0.010-0.026	0.002-0.012
10	963-2556	0.72-2.11	0.88-1.21	0.25-0.59	0.013-0.026	0.004-0.013
11	1770-2629	0.89-1.96	0.83-1.30	0.14-0.31	0.009-0.025	0.004-0.015
12	1658-2755	1.19-2.07	0.85-1.21	0.12-0.22	0.010-0.025	0.005-0.014

2.6 Implementation

The selected SA methods and metrics have been conditioned by the computationally expensive model. The model is solved using the explicit finite volume solver presented in Cea and Vázquez-Cendón (2012) and compiled for a Windows environment. Each simulation takes about five minutes using an Intel® Core i5-7500 3.4 GHz computer. The methodology implementing the different sensitivity methods and the number of simulations performed for each analysis are included in the following sections.

2.6.1 Standardized regression coefficients

Regarding the SRC, the Latin Hypercube Sampling (LHS) method was used to generate 1000 sets of H-R parameters for each of the twelve laboratory experiments, and considering the ranges of variation established in Table 6.2, using the free Matlab toolbox SAFE (Pianosi *et al.* 2015). Then, the multiple linear regressions were obtained by means of the *regress* function in Matlab. Convergence test considering 100, 500, 1000, 2000 and 5000 simulations showed that convergence was achieved with a sample size of 1000 simulations. Thus, over the twelve laboratory experiments, the total number of simulations was 12000.

2.6.2 Extended Fourier amplitude sensitivity test

The toolbox Eikos, developed by Ekstrom (2005), was used for the calculation of the EFAST indices and for the sampling process, taking into account the ranges defined in Table 6.2. Due to the computational cost of the wash-off model, the number of simulations used for the implementation of the EFAST method was set to 505 per factor (3030 simulations per laboratory experiment and a total of 36360), which remains within the practical recommendations accordingly to Saltelli *et al.* (2005) and Cosenza *et al.* (2013).

2.6.3 Elementary effects

Following Campolongo and Saltelli (1997) Campolongo *et al.* (1999) and Saltelli *et al.* (2000), a number of trajectories $r=10$ and values of $p=4$ ($\{0, 1/3, 2/3, 1\}$) and $\Delta=2/3$ were chosen in the implementation of the EE method. In order to facilitate a better coverage of the input domain, these ten trajectories were selected from a set of twenty-five, which effectively maximizes their spread in the input space (Campolongo *et al.* 2007). The local SA assessed thirteen inputs, so the number of simulations was $10(13+1)=140$ for each laboratory experiment, a total of 1680 simulations.

2.7 Assessment of model predictions

In order to analyze the model performance, we first compared predictions with the results of the laboratory experiments, using the mean of the Nash-Sutcliffe model efficiency coefficient (NSE) in each of the gully pots as an objective function to assess overall prediction performance. Second, we checked the adequacy of the ranges selected for the global SA by visual assessment of the contours of the results of simulations. Although Root-Mean-Squared-Deviation (RMSE) or NSE can be used as objective functions to assess model sensitivity (Hong *et al.* 2016a), in the light of the model performance observed, we chose the TSS concentration peaks and the washed off loads as outputs to analyze. These two outputs are the most significant ones for practitioners, since they are relevant variables for estimating the impacts of the stormwater pollution inflows to sewerage systems or the aquatic media.

3 Results

3.1 Model and ranges performance

To assess the suitability of model predictions, Figure 6.3 shows two examples of the five best TSS with rain intensities of 50 and 80 mm/h and sediment classes D2 and D3, respectively. It can be seen that the flexibility of the model and the established ranges allow for an accurate prediction of the TSS pollutographs in both gully pots at the same time and for both initial conditions. In addition, the parameter sets of the five best-fitted predictions performed for the global SA are also included in Figure 6.3. It can be seen that, as expected, different sets of parameters resulted in very similar pollutographs.

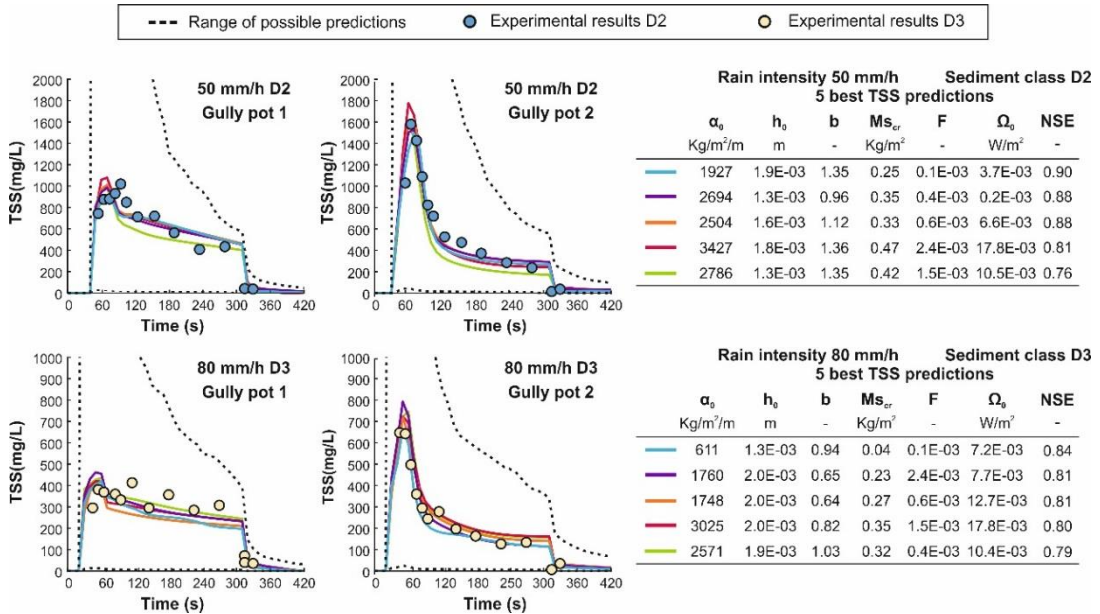


Figure 6.3. TSS experimental results and five best-fitted TSS simulations for the experiments with rain intensities of 50 (up) and 80 mm/h (down) and sediment classes D2 and D3, respectively. It can be seen that predictions agree well with experimental results. The contours of all the simulations performed in the global SA are also included (dashed lines), and illustrate the sensitivity of the model output to the plausible values of H-R parameters.

3.2 Global sensitivity analysis

3.2.1 Standardized Regression Coefficients (SRC)

The SRC of the six H-R parameters regarding the total washed off mass and the TSS peak for each gully pot are shown in Figure 6.4. The plots show the sensitivity indices of each parameter for the twelve laboratory experiments that have been used as layouts for the SA, considering the three different rain intensities and the four sediment grain sizes described above (Section 2.2).

In general, the plots in Figure 6.4 show the critical mass (Ms_{cr}) as the most important H-R parameter, with the highest influence in both outputs and for all the laboratory experiments. The critical mass is the mass required to reach the total rain-driven and flow-driven potential detachment, so its effect on the results is increased in urban catchments due to the scattering of sediment in the low loads presented over the street. In addition, the relative importance of the H-R parameters varies widely with respect to the grain size, and b and Ω_0 remain with a low influence in both outputs and for all the laboratory experiments.

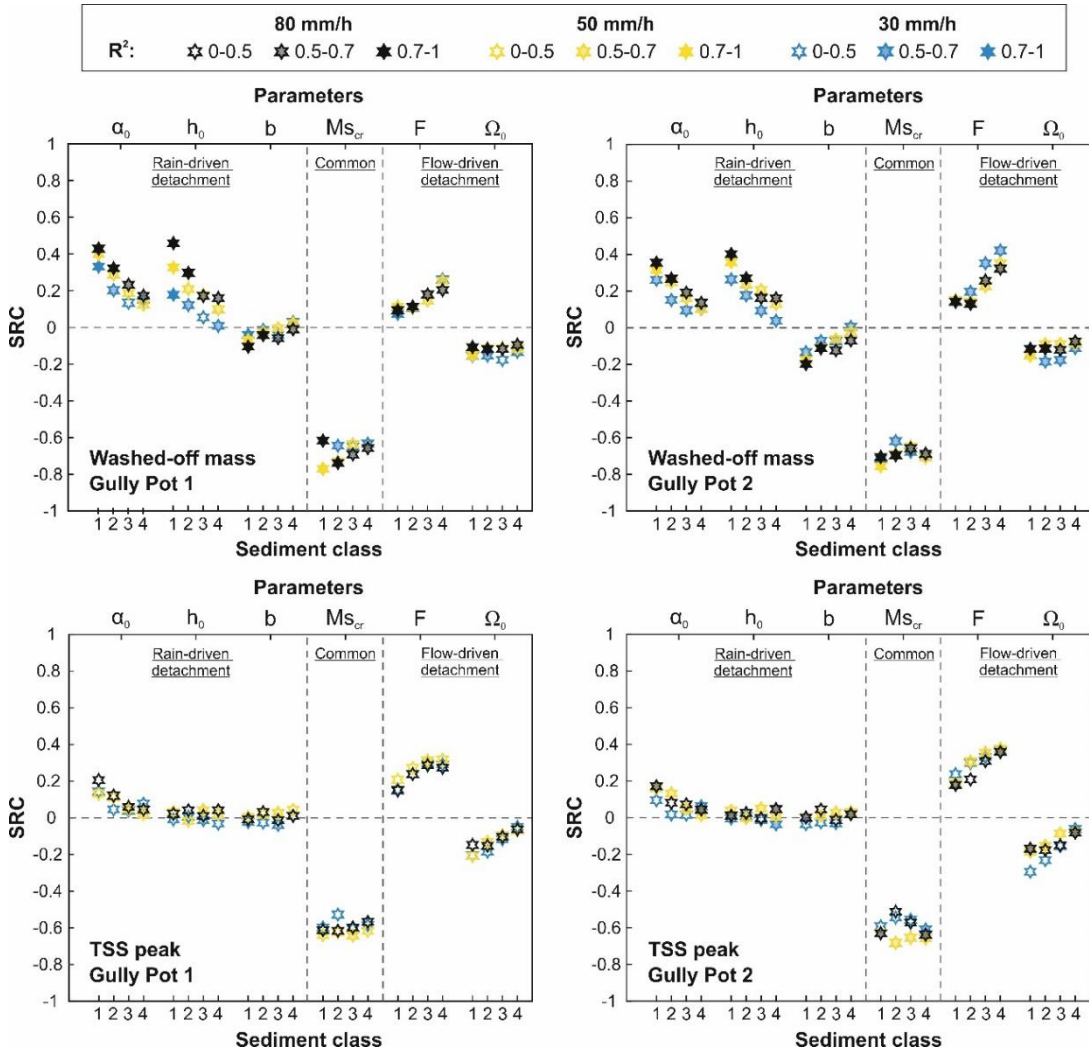


Figure 6.4. Standardized Regression Coefficients (SRC) of the Hairsine-Rose parameters for the total washed off mass (row 1) and the TSS maximum value (row 2) in each gully pot (columns) and for each laboratory experiment (colors for the rain intensities and x-position for the sediment classes). The degree of transparency represents the R^2 value. The plots show that the critical mass is the most important H-R parameter and that there is a strong relation between the grain size of the sediment and the relative importance of rain-driven and flow-driven detachment parameters.

Looking at the total washed off mass sensitivity results in Figure 6.4 (first row plots), it can be seen that as the grain size of the sediment increases, the influence of the rain-driven detachment parameters α_0 and h_0 decrease and F becomes more important. Ms_{cr} , α_0 and h_0 are thus key parameters for modelling wash-off with small grain sizes, but F has to be

taken into account if bigger diameters are involved. An increase in rain intensity also involves a large increase in the sensitivity of the total washed mass results to h_0 , which depends on the water depth. The sensitivity results for the TSS peak (second row plots in Figure 6.4) are very similar in terms of the main parameters and in the different laboratory experiments analyzed. However, h_0 and b become wholly negligible to the results, since h_0 is the water depth threshold from which the rain-driven detachment is dumped, thus the TSS peak, which is produced at the beginning of the rain event, and is not affected.

Another interesting result in Figure 6.4 is the high match between the sensitivity results of both gully-pots. Despite gully pot 2 having a far more important curb flow component, only a slight increase in the sensitivity to F and a small reduction in the sensitivity to α_0 and h_0 were observed for gully pot 2. Finally, it should be noted that the coefficients of determination obtained in the regressions, with values between 0.5 and 0.85 in the total mass and between 0.35 and 0.6 in the TSS peak, indicate that a significant part of the variance is not explained by a linear regression model, which cannot represent the interaction between model parameters. In sum, α_0 , h_0 , MS_{cr} and F appeared to be the important parameters for the washed off mass, and only α_0 , MS_{cr} and F for the TSS concentration peak. In addition, the rain and flow-driven detachment parameters were presented as key for smaller (mean grain sizes of 30 and 68 μm) and larger (144 and 274 μm) sediment particles, respectively

3.2.2 Extended Fourier Amplitude Sensitivity Test (EFAST)

In contrast to SRC, the EFAST method considers the interactions between the different parameters. Figure 6.5 shows the direct or first order effect and the total effect of the H-R parameters in the total washed off mass and the TSS peak, computed with the EFAST methodology. Despite the fact that the coefficients of determination in the SRC analysis indicated in the same cases low reliability, with values below 0.6, the ranking of the most important parameters considering the first order effect results is very similar, as was also found in Cosenza *et al.* (2013). In addition, variations in the first order indices due to the changes of the sediment diameter and rain intensity in the different laboratory experiments show the same trends as in the SRC.

The critical mass (MS_{cr}) is the most important H-R parameter for all the laboratory experiments in the plots presented in Figure 6.5. Regarding the total washed off mass results (first row plots in Figure 6.5), α_0 and h_0 are at a secondary level, with only a low degree of influence, including F in the case of the larger grain sizes (sediment classes 3 and 4). b and Ω_0 appear to be negligible parameters for all the laboratory experiments analysed. In addition, some differences in the EFAST indices between both gully pots should be noted: α_0 and h_0 decrease and F increase their influence in the results for gully pot 2, which has an important curb flow component. Considering the sensitivities of the TSS peak to the

parameters (second row plots in Figure 6.5), the flow-driven detachment parameters F and Ω_0 are low influential parameters, the rest of the rain-driven detachment parameters, α_0 , h_0 and b , being negligible.

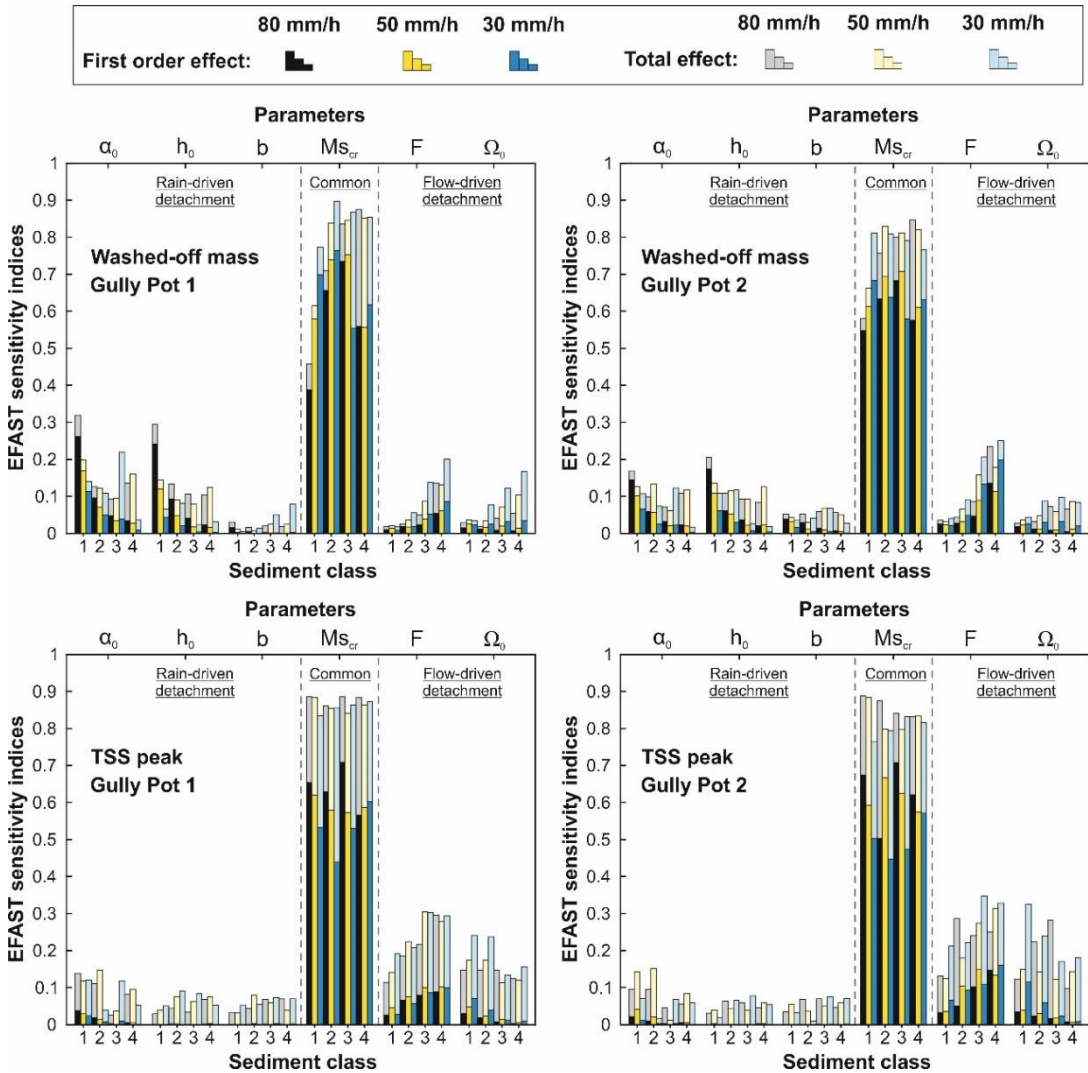


Figure 6.5. EFAST first order and total effect sensitivity indices of the Hairsine-Rose parameters for the total washed off mass (row 1) and the TSS maximum value (row 2) in each gully pot (columns) and for each of the laboratory experiments (colors for rain intensities and x-position for sediment classes). It can be seen that the critical mass is the most important H-R parameter. α_0 , h_0 and F occupy a secondary level of influence with respect to the total washed mass, but only F in the case of the TSS peak results.

The differences between the total (bars with dark colors) and first order effect indices (bars with light colors) in the plots in Figure 6.5 show the variance of the results due to interactions between parameters. It can be seen that the interactions play an important role in the results, especially in the TSS peak concentration and in the larger diameters (sediment classes 3 and 4) for the total washed off mass. Unfortunately, this complicates the separation of the individual effect of each parameter and confirms our expectations that it is indeed challenging to calibrate this model. Summarizing, washed off mass and TSS peak are very sensitivity to $M_{S_{cr}}$ in all the experimental layouts. The same trends as in SRC have been observed between the relative importance of rain-driven and flow-driven detachment parameters and rain intensity and grain size values. In addition, a high level of interaction between parameters was found.

3.3 Local sensitivity analysis

Figure 6.6 shows the absolute mean (μ^*) of the elementary effects of each input factor with respect to the total washed off mass against their standard deviation (σ) for the twelve laboratory experiments. The relation between μ^* and σ is an indicator of the linearity of each variable with respect to the model output, assuming that below 0.1 there are no substantial interactions with other factors. Only the results corresponding to the gully pot 2 are plotted here, but similar results are obtained for the gully pot 1. The initial load of sediment over the surface (M_{S_0}) and its mean diameter (D_{50}), classified as very poorly known variables, are the most influential measurable variables in all cases. The influence of the density is lower than that of the sediment diameter, although both variables affect the settling velocity of the solid particles. This is because its associated uncertainty is lower.

The other input factor that shows a notable influence in the results is critical mass ($M_{S_{cr}}$), which was identified as the most influential H-R parameter in the global SA. Regarding the rest of the H-R parameters, their relative importance is the same in both the SRC and the EFAST analyses. Thus, the influence of α_0 and h_0 is higher for the particles with lower diameters (sediment classes 1 and 2) and decreases as the sediment diameter increases. The influence of the uniformity coefficient (UC) is low in all cases, despite its high level of uncertainty, which allows us to conclude that the differences in sediment distribution considered do not substantially affect the total washed off mass. This confirms the findings of Naves *et al.* (2017). The hydraulic variables and parameters remain with the lowest influence on the results, mainly because of the low uncertainties associated with these.

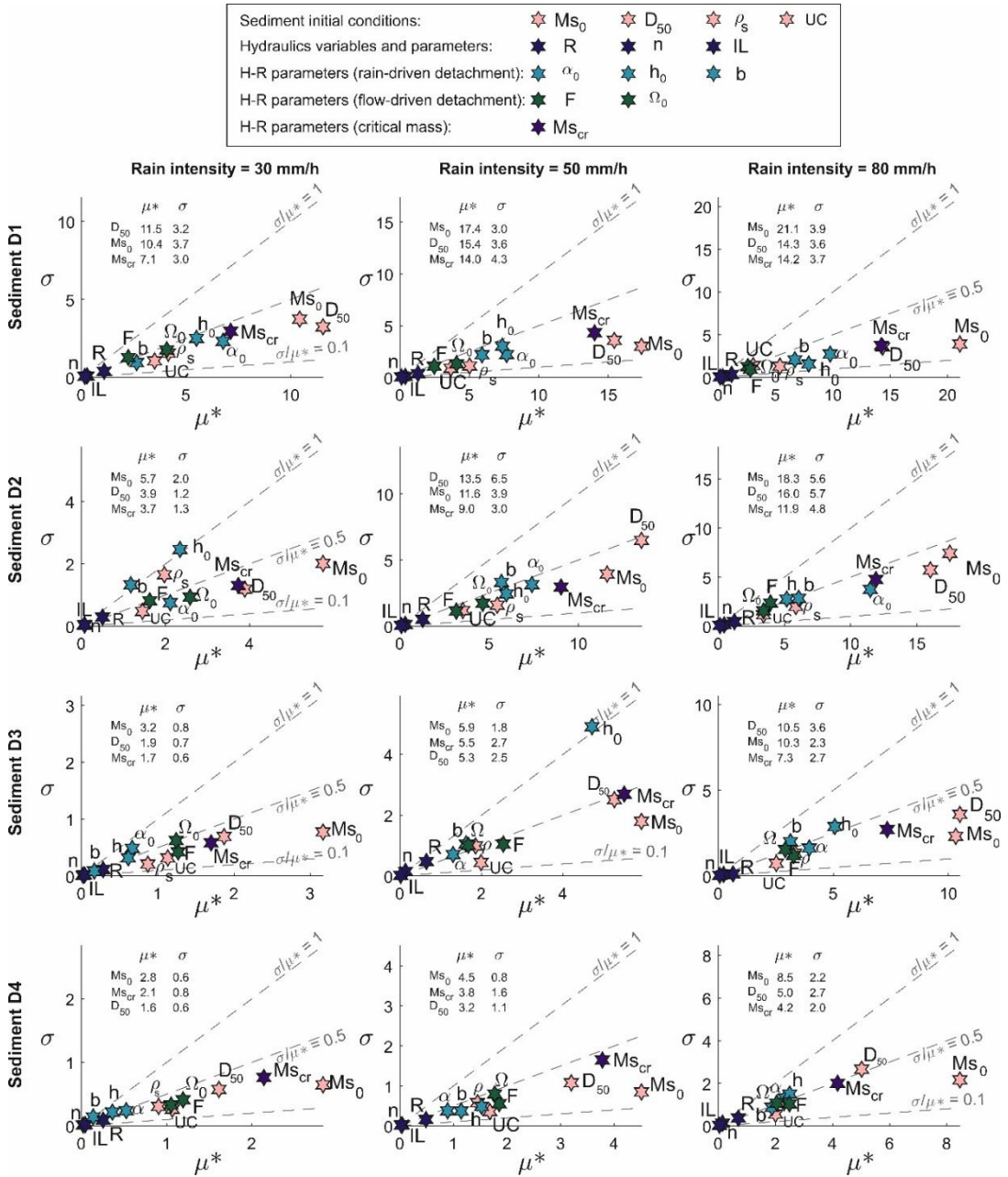


Figure 6.6. Sensitivity results for the Elementary Effects method. Plots show the sensitivity to the total washed off mass through gully pot 2 for each of the three rainfall intensities and four grain sizes considered in the experiments. The ranking of the three most influential input factors is shown in the upper-left corner of each case. In general, Ms_0 , D_{50} and Ms_{cr} are the factors with the most influence on the result for all the laboratory experiments.

The local sensitivity results regarding the TSS peak concentration in gully pot 2 for all the laboratory experiments are included in Figure 6.7. The input factors with most influence in the TSS peak are the same three factors (Ms_0 , D_{50} and Ms_{cr}) as in the case of the total washed off mass. However, the H-R parameters related to the flow-driven detachment, especially F , are at a similar level of importance for the TSS peak. Thus, as seen in the global SA, the flow-driven detachment is key to accurately modelling the maximum TSS concentration. The hydraulic input factors and the rain-driven detachment parameters seem to be almost negligible for this output.

In sum, our findings suggest that the initial load of sediment and the mean grain size were the most important variables. H-R parameters exhibited a high influence in the model outputs, with a similar behavior to that observed in the global SA. Finally, hydraulics input factors variations do not affect the outputs, since their determination has a low degree of uncertainty associated with it.

Sediment initial conditions:	\star Ms_0	\star D_{50}	\star ρ_s	\star UC
Hydraulics variables and parameters:	\star R	\star n	\star IL	
H-R parameters (rain-driven detachment):	\star α_0	\star h_0	\star b	
H-R parameters (flow-driven detachment):	\star F	\star Ω_0		
H-R parameters (critical mass):	\star Ms_{cr}			

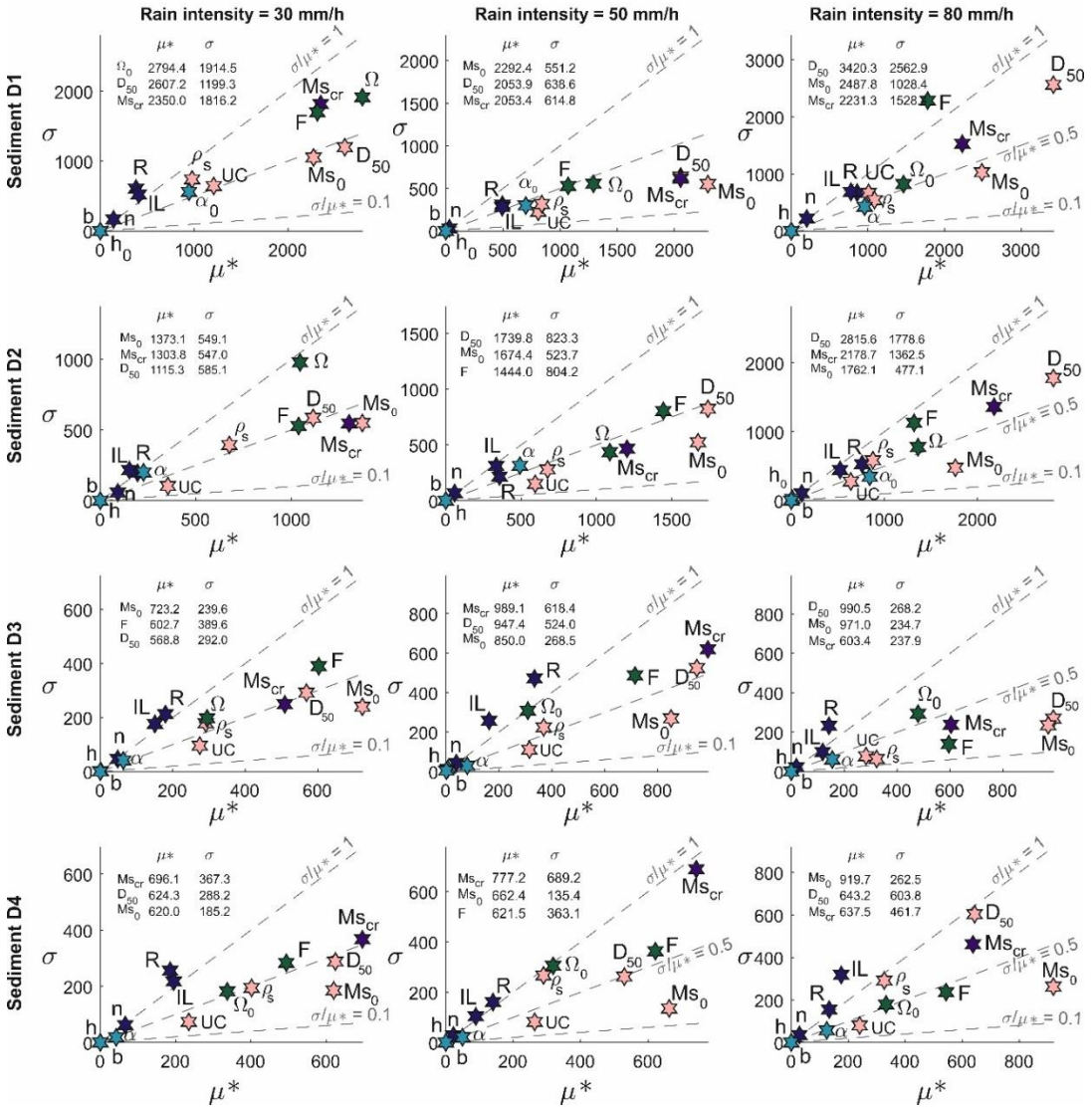


Figure 6.7. Sensitivity results for the Elementary Effects method. Plots show the sensitivity to the TSS maximum value in gully pot 2 in all cases. The ranking of the three most influential input factors is shown in the upper-left corner of each case. In general, Ms_0 , D_{50} , Ms_{cr} and F are the factors with the most influence on results.

4 Discussion

In the previous sections, we have presented a SA of a physically-based urban wash-off model. The study has shown that the flexibility of the model allowed for the replication of the laboratory results from accurately measured initial conditions by tuning the H-R model parameters. However, this flexibility also leads to identifiability problems and makes it difficult to obtain precise predictions in field studies. Therefore, it is important to discuss our findings in terms of: i) a careful interpretation of the SA results, ii) transferability to field studies, and iii) limitations and future steps towards improving urban wash-off predictions.

4.1 Interpretation of the sensitivity analysis results

Uncertainties and interactions between the different processes involved in wash-off modelling such as flow and rain characterization, model parameters, or sediment initial conditions and characteristics, make it difficult to separate their individual contribution to a model's predictions. Therefore, controlled laboratory experiments have been used to eliminate disturbances and to focus the global SA on the H-R model parameters, fixing remaining input variables. However, despite the accurate definition of the initial conditions, Figure 3 shown a wide range of possible model predictions that might alter the H-R parameters. This is a consequence of a lack of knowledge in estimating their possible values in urban catchments. In addition, there is no consensus as to model simplifications in the literature and, to date, it is difficult to define narrower ranges a priori. However, using the obtained global SA results, it is possible to address this lack of knowledge and issues of identifiability, and thus to reduce the number of parameters to calibrate in future research.

While flow-driven detachment is usually negligible in soil erosion (Cea *et al.* 2016), it was seen as an important process for the largest grain sizes (144 and 274 μm) in our urban application. Therefore, rain-driven and flow-driven detachment are the two physical processes that have to be taken into account via the H-R parameters. Regarding flow-driven detachment, exponent b is negligible for all the laboratory experiments that we simulated, so its value could be fixed at 1. The water depth damping threshold, h_0 , is typically set to two third of the mean raindrop size (Heng *et al.* 2011, Hong *et al.* 2016a). However, its high influence in modelling TSS peak concentrations, as well as the current lack of studies accurately measuring rain drop size distributions (DSD), mean that the development of work aimed at adequately fixing this parameter is an interesting line of research. With respect to the flow-driven parameters, Ω_0 showed a low influence in the results and may be fixed to values around 0.01 W/m^2 following previous studies (Proffitt *et al.* 1993, Sander *et al.* 2007, Heng *et al.* 2011).

Among the three remainder parameters α_0 , $M_{s_{cr}}$ and F , which are those with the highest influence in the results, only two parameters are strictly necessary to calibrate, respectively,

the contribution of rain-driven and flow-driven detachment. $M_{S_{cr}}$ affects both processes at the same time, and may be fixed in future applications. However, due to the current lack of knowledge on this parameter, its notable influence in the results, plus its interactions with other parameters, this is not currently recommended. Therefore, given the sensitivity results, we proposed in this section a reduction from 6 to 3 calibration parameters. However, next field and laboratory urban wash-off studies will increase our understanding of the H-R parameters, and may lead to a reduction in parameter ranges and to a consideration of further simplifications.

4.2 Transferability to field studies

When applying the H-R model in real-world catchments, we currently see three main limitations: i) high computational cost, ii) inaccurate input variables, and iii) the consideration of sediment heterogeneity.

The model was already previously calibrated for different rain events in a 2661 m² road urban catchment in Hong *et al.* (2016a, 2016b, 2019). This work is the first and available field application of H-R model in urban environments, and studies in larger field catchments are currently challenging due to the mentioned limitations. However, physical-based wash-off models are at the beginning of their development and can be compared to 2D flood models in the early 2000s, when their applicability to large catchments were limited because computers were still slow and high-resolution terrain models were missing. In the same way as 2D-1D coupling is currently industry standard in urban drainage models, we think that the limitations in the catchment size for urban wash-off physically-based models will be significantly decreased in the near future and this will highlight, also for large catchments, the opportunities raised by physically-based wash-off models. In this regard, the 2D shallow water model Iber has recently been improved, and now takes advantage of the parallelization functionalities of both CPUs (central processing units) and GPUs (graphics processing units), achieving speedups of up to two orders of magnitude in comparison with the version used in the present study (García-Feal *et al.* 2018). In addition, the use of fast emulators has already been applied in hydrodynamic urban drainage models (Carbajal *et al.* 2017, Hong *et al.* 2019), and these might be a very practical solution to reduce the computation time. Meanwhile, the application of physically-based wash-off models to small and medium-size basins is an opportunity to increase understanding of wash-off process and model performance.

Regarding the definition of input variables, as shown by the local SA, the initial load of sediment and mean grain size are the most important input variables in terms of model's predictions, as also found in Hong *et al.* (2016a). Therefore, the uncertainties associated with these variables due to the variability and randomness of sediment build-up can limit the reliability of the results and make the model ineffective. The determination of the initial

conditions, then, is key to the modelling of urban wash-off, and future research should continue to be oriented towards the determination of the initial build-up mass and characteristics, either through field studies analyzing urban dust samples (Wijesiri *et al.* 2015b) or by following the ideas in Sandoval *et al.* (2018) where input variables are estimated from measured pollutographs using virtual state variables.

Spatial heterogeneity is other important issue to consider in terms of the transferability of the model. First, an accurate representation of the surface flow is needed to reduce the propagation of hydraulic uncertainties to the sediment transport equations, since the hydrodynamic model is used as a basis for wash-off equations. Visualization techniques such as large-scale particle image velocimetry (LSPIV) or surface structure image velocimetry (SSIV) can help to achieve the required accuracy here by obtaining useful surface calibration data (Naves 2019a), with the possibility of using surveillance camera footage, as proposed in Leitão *et al.* (2018). The accuracy and resolution of elevation data are also key to attaining a suitable characterization of surface flow. However, current LIDAR techniques are able to provide high-resolution elevations each 0.1 m which, combined with manual measurements to incorporate important elements such as curbs, have demonstrated their effectiveness in representing adequately flow spatial variations (Hong *et al.* 2016a, b). In addition, gully pots and grid performance should be also included at this level of detail. In fact, this is interesting not only for surface flow modelling (Martins *et al.* 2018) but also for water quality interactions and gully pot efficiency (Post *et al.* 2016).

Rainfall input data involves spatial intensity distribution, which allows for obtaining an accurate surface flow, as well as rain energy, which depends on DSD and condition rain-driven detachment. An extensive literature exists on rain distribution and resolution in hydrological processes, but future research in urban wash-off should incorporate DSD measurements more frequently, in order to estimate rain-driven particle detachment from rain kinetic energy. Rainfall simulators, such as the one used in this study, can contribute to an understanding of this process through the use of constant rain intensities and varying DSDs.

Finally, it is necessary to take into account the heterogeneity in the surface sediment mass. In the laboratory experiments described here, there are four different sediment classes with a uniform granulometry, this as a means of achieving greater control of the process. However, available surface sediment presents a high degree of heterogeneity in grain sizes and densities in real catchments, and mean diameter and density are not representative. In addition, representative characteristics of the sediment can change during the event as the lightest particles are washed off first. A multiclass approach, such as the one used in Hong *et al.* (2016b), should therefore be considered as a means of obtaining reliable results with heterogeneous sediment masses. This approach leads to an increase in the complexity of the model, with adequate parameters needed for each class, and hence an assessment of

the benefits and drawbacks that such an approximation might involve would be a useful step. In this regard, the experimental data set used in this study (which is taken from the dataset Naves *et al.* 2019c) also includes experiments where the four sediment classes were mixed to obtain a realistic granulometry and including coulter samples in the inflow to the gully pots, and may be used in future studies.

4.3 General perspectives for modelling urban wash-off

The future aims of wash-off modelling in urban areas should not be seek to implement more and more complex models in which all the physical processes are perfectly defined. Rather, the objective should be to move towards models capable of considering the spatial and temporal heterogeneities of the catchment and able to reproduce the key wash-off process, overcoming the limitations of empirical equations yet maintaining optimal simplicity in the model. For this purpose, more laboratory and field applications of wash-off physical-based models should be conducted to increase our understanding of the parameters and processes here, one very important focus of attention being an effective characterization of catchment, sediment and rain characteristics. The wash-off process is challenging, but in view of the promising results of the first physically-based wash-off studies, it is an important line of research towards better treatment and management techniques for minimizing the impact of urban surface contaminants, such as microplastics, heavy metals and PAH, on the environments of cities and towns.

5 Conclusions

Physically-based models are currently being introduced as novel alternatives to experimental equations in order to consider the spatial and temporal heterogeneities in urban pollutant wash-off studies. These models are able to represent the different processes involved in the wash-off process, but the lack of experience in urban catchments and the need for a large number of input factors lead to a complex calibrations. This study contributes to the understanding of physically-based urban wash-off models by presenting an in-depth SA using a series of specially-tailored laboratory experiments. Thus, the accurate determination of the hydraulics variables and the initial sediment conditions were used to focus a global SA on poorly-known H-R parameters using SRC and EFAST. Then, in order to ensure the transferability of the results to field studies, the relative importance in the model outputs of hydraulics, initial sediment conditions and H-R model parameters was assessed through a local SA, using the EE method and considering uncertainties in their determination in real field studies.

Therefore, this work is novel regarding three specific aspects. First, the 2D shallow water model, which is coupled with the Hairsine-Rose wash-off formulation, was previously calibrated with experimental surface velocities and discharges, so the most realistic description of runoff was used. Second, it is the first sensitivity analysis considering all the model parameters and variables studying urban wash-off. Without this detailed sensitivity analysis, it would be really difficult to condition the model to monitoring data because changes in one parameter can be easily compensated by changes in other parameters. Third, the high-resolution wash-off experiments provide a most accurate reference dataset. This is unique because it is obtained on a realistic and 1:1 scale rainfall simulator of 36 m². The data is available in open access, which makes our research reproducible and enables others to test their own models and hypotheses. Specifically, the following can be concluded based on the results:

- The flexibility of the model allowed us to successfully reproduce the results of the laboratory experiments by tuning the H-R model parameters. However, the predictions obtained suggested a complex calibration process, and thus highlight the usefulness of the SA performed for decision-making in order to simplify the model and to deal with identifiability problems.
- The SRC indicated a strong sensitivity of the results to critical mass in comparison to the other H-R parameters. The parameters related to rain-driven detachment α_0 and h_0 were at a second level of importance, roughly half that of sensitivity, for the total washed off mass with the smallest diameters (mean grain sizes of 30 and 68 μm). When the grain size of the sediment increased (144 and 274 μm), F was included in this second level of influence. In addition, F was also shown to be an important variable with respect to the TSS peak, while b and Ω_0 remained at a low influence for both outputs.
- Although the ranking of the most important parameters obtained from the EFAST analysis was very similar to that for the SRC results, the EFAST total effect indices revealed the high importance of the interaction between parameters in the model outputs, which is also an indicator of the difficulties that can arise when calibrating the model.
- In the local SA, which considered all the input variables and parameters, the initial load of sediment, mean grain size and critical mass were seen to be the most important factors for the total washed off mass and the TSS peak, this is all the laboratory experiments. Therefore, very accurate measurement of the available mass and its characteristics is necessary in order to avoid the variability associated with the build-up process affecting to the reliability of results. H-R parameters were seen to be at a second level of importance, which illustrates the need for accurate

calibration of the model. Finally, variations in hydraulic variables did not affect the outputs since the uncertainty associated with their determination was low.

- In the light of these results, the model may be simplified using the three parameters with the highest influence in the results, α_0 , MS_{cr} and F , as a means of modelling the individual contribution of the rain-driven and flow-driven detachment. Future research should focus on more laboratory and field studies, to increase our knowledge of these parameters and thus to be able to adequately fix them.

Although the problem is complex, these promising results should stimulate efforts towards overcoming the current limitations of physically-based models, such as high computational cost, the need for an accurate definition of the input variables, and the accurate modelling of spatial and sediment heterogeneities.

References

-
- Ackers, J. C., Butler, D., May, R. W. P. (1996). *Design of sewers to control sediment problems* (pp. 1-181). London: Construction Industry Research and Information Association.
- Adrian, R.J., 1991. Particle-imaging techniques for experimental fluid mechanics. *Annual review of fluid mechanics*, 23 (1), 261–304. <https://doi.org/10.1146/annurev.fl.23.010191.001401>
- Akan, A. O. Houghtalen, R. J. (2003). *Urban hydrology, hydraulics, and stormwater quality: engineering applications and computer modelling*. John Wiley & Sons.
- Aksoy, H., Unal, N. E., Cokgor, S., Gedikli, A., Yoon, J., Koca, K., Inci, S.B., Eris, E. (2012). A rainfall simulator for laboratory-scale assessment of rainfall-runoff-sediment transport processes over a two-dimensional flume. *Catena*, 98, 63-72. <https://doi.org/10.1016/j.catena.2012.06.009>
- Al Ali, S., Bonhomme, C., Dubois, P., Chebbo, G. (2017). Investigation of the wash-off process using an innovative portable rainfall simulator allowing continuous monitoring of flow and turbidity at the urban surface outlet. *Science of the Total Environment*, 609, 17-26. <https://doi.org/10.1016/j.scitotenv.2017.07.106>
- Al Mamoon, A., Jahan, S., He, X., Joergensen, N. E., Rahman, A. (2019). First flush analysis using a rainfall simulator on a micro catchment in an arid climate. *Science of The Total Environment*, 693, 133552. <https://doi.org/10.1016/j.scitotenv.2019.07.358>
- Anta, J., Peña, E., Suárez, J., Cagiao, J. (2006). A BMP selection process based on the granulometry of runoff solids in a separate urban catchment. *Water Sa*, 32(3), 419-428. <http://dx.doi.org/10.4314/wsa.v32i3.5268>
- APHA (1995). *Standard methods for the examination of water and wastewater*. American Public Health Association, Washington.
- Armstrong, A., Quinton, J. N. (2009). Pumped rainfall simulators: the impact of rain pulses on sediment concentration and size. *Earth Surface Processes and Landforms*, 34(9), 1310-1314. <https://doi.org/10.1002/esp.1810>
- Arques, S.R., Rubinato, M., Nichols, A., Shucksmith, J.D. (2018). Cost effective measuring technique to simultaneously quantify 2D velocity fields and depth-averaged solute concentrations in shallow water flows. *Flow Measurement and Instrumentation*. 64, 213–223. <https://doi.org/10.1016/j.flowmeasinst.2018.10.022>.
- Ball, J. E., Jenks, R., Aubourg, D. (1998). An assessment of the availability of pollutant constituents on road surfaces. *Science of the Total Environment*, 209(2-3), 243-254. [https://doi.org/10.1016/S0048-9697\(98\)80115-0](https://doi.org/10.1016/S0048-9697(98)80115-0)

- Banasiak, R., Verhoeven, R. (2008). Transport of sand and partly cohesive sediments in a circular pipe run partially full. *Journal of Hydraulic Engineering*, 134(2), 216-224. [https://doi.org/10.1061/\(ASCE\)0733-9429\(2008\)134:2\(216\)](https://doi.org/10.1061/(ASCE)0733-9429(2008)134:2(216))
- Battany, M. C., Grismer, M. E. (2000). Rainfall runoff and erosion in Napa Valley vineyards: effects of slope, cover and surface roughness. *Hydrological processes*, 14(7), 1289-1304. [https://doi.org/10.1002/\(SICI\)1099-1085\(200005\)14:7<1289::AID-HYP43>3.0.CO;2-R](https://doi.org/10.1002/(SICI)1099-1085(200005)14:7<1289::AID-HYP43>3.0.CO;2-R)
- Bertrand-Krajewski, J. L. (2006). *Modelling of sewer solids production and transport*. Cours de DEA "Hydrologie Urbaine".
- Bertrand-Krajewski, J. L., Briat, P., Scrivener, O. (1993). Sewer sediment production and transport modelling: A literature review. *Journal of Hydraulic Research*, 31(4), 435–460. <https://doi.org/10.1080/00221689309498869>
- Beuselinck, L., Govers, G., Hairsine, P. B., Sander, G. C., Breynaert, M. (2002). The influence of rainfall on sediment transport by overland flow over areas of net deposition. *Journal of Hydrology*, 257(1-4), 145-163. [https://doi.org/10.1016/S0022-1694\(01\)00548-0](https://doi.org/10.1016/S0022-1694(01)00548-0)
- Bladé, E., Cea, L., Corestein, G., Escolano, E., Puertas, J., Vázquez-Cendón, E., Dolz, J., Coll, A. (2014). Iber: herramienta de simulación numérica del flujo en ríos. *Revista Internacional de Métodos Numéricos para Cálculo y Diseño en Ingeniería*, 30(1), 1-10. <https://doi.org/10.1016/j.rimni.2012.07.004>
- Boiten, W. (2003). *Hydrometry: IHE Delft Lecture Note Series*. 1st Ed. CRC Press, ISBN 9789054104230.
- Branisavljević, N., Prodanović, D., (2006). Large Scale Particle Image Velocimetry – merenje urbanog oticaja (in Serbian). *Vodoprivreda*. 38 (4–6), 233–238. Available at: <http://www.vodoprivreda.net/wp-content/uploads/2014/08/large.pdf> [Accessed: 16 Sep 2019].
- Brun, R., Kühni, M., Siegrist, H., Gujer, W., Reichert, P. (2002). Practical identifiability of ASM2d parameters—systematic selection and tuning of parameter subsets. *Water research*, 36(16), 4113-4127. [https://doi.org/10.1016/S0043-1354\(02\)00104-5](https://doi.org/10.1016/S0043-1354(02)00104-5)
- Butler, D. Davies, J. (2010). *Urban Drainage*. 3rd Edition. Spon Press, Abingdon, UK.
- Butler, D., Karunaratne, S. H. P. G. (1995). The suspended solids trap efficiency of the roadside gully pot. *Water research*, 29(2), 719-729. [https://doi.org/10.1016/0043-1354\(94\)00149-2](https://doi.org/10.1016/0043-1354(94)00149-2)
- Butler, D., Xiao, Y., Karunaratne, S. H. P. G., Thedchanamoorthy, S. (1995). The gully pot as a physical, chemical and biological reactor. *Water science and technology*, 31(7), 219-228. [https://doi.org/10.1016/0273-1223\(95\)00339-0](https://doi.org/10.1016/0273-1223(95)00339-0)

-
- Butler, D., Memon, F. A. (1999). Dynamic modelling of roadside gully pots during wet weather. *Water research*, 33(15), 3364-3372. [https://doi.org/10.1016/S0043-1354\(99\)00050-0](https://doi.org/10.1016/S0043-1354(99)00050-0)
- Butler, D., May, R., Ackers, J. (2003). Self-cleansing sewer design based on sediment transport principles. *Journal of Hydraulic Engineering*, 129(4), 276-282. [https://doi.org/10.1061/\(ASCE\)0733-9429\(2003\)129:4\(276\)](https://doi.org/10.1061/(ASCE)0733-9429(2003)129:4(276))
- Butler, D., Digman, C. J., Makropoulos, C., Davies, J. W. (2018). *Urban drainage*, 4th edn. Crc Press.
- Campolongo, F., Saltelli, A., (1997). Sensitivity analysis of an environmental model: a worked application of different analysis methods. *Reliability Engineering and System Safety* 52, 49–69. [https://doi.org/10.1016/S0951-8320\(97\)00021-5](https://doi.org/10.1016/S0951-8320(97)00021-5)
- Campolongo, F., Tarantola, S., Saltelli, A. (1999). Tackling quantitatively large dimensionality problems. *Computer Physics Communications* 117, 75–85. [https://doi.org/10.1016/S0010-4655\(98\)00165-9](https://doi.org/10.1016/S0010-4655(98)00165-9)
- Campolongo, F., Cariboni, J., Saltelli, A. (2007). An effective screening design for sensitivity analysis of large models. *Environmental Modelling and Software* 22, 1509–1518. <https://doi.org/10.1016/j.envsoft.2006.10.004>
- Carbajal, J. P., Leitão, J. P., Albert, C., Rieckermann, J. (2017). Appraisal of data-driven and mechanistic emulators of nonlinear simulators: The case of hydrodynamic urban drainage models. *Environmental modelling & software*, 92, 17-27. <https://doi.org/10.1016/j.envsoft.2017.02.006>
- Cea, L., Puertas, J., Pena, L. (2007). Velocity measurements on highly turbulent free surface flow using ADV. *Experiments in Fluids*. 42 (3), 333–348. <https://doi.org/10.1007/s00348-006-0237-3>.
- Cea, L., Garrido, M., Puertas, J. (2010). Experimental validation of two-dimensional depth-averaged models for forecasting rainfall–runoff from precipitation data in urban areas. *Journal of Hydrology* 382 (1), 88–102. <https://doi.org/10.1016/j.jhydrol.2009.12.020>
- Cea, L., Vázquez-Cendón, M. E. (2012). Unstructured finite volume discretisation of bed friction and convective flux in solute transport models linked to the shallow water equations. *Journal of Computational Physics*, 231(8), 3317-3339. <https://doi.org/10.1016/j.jcp.2012.01.007>
- Cea, L., Legout, C., Darboux, F., Esteves, M., Nord, G. (2014). Experimental validation of a 2D overland flow model using high resolution water depth and velocity data. *Journal of hydrology*, 513, 142-153. <https://doi.org/10.1016/j.jhydrol.2014.03.052>
-

- Cea, L., Blade, E. (2015). A simple and efficient unstructured finite volume scheme for solving the shallow water equations in overland flow applications. *Water Resources Research* 51 (7), 5464–5486. <https://doi.org/10.1002/2014WR016547>
- Cea, L., Legout, C., Grangeon, T., Nord, G. (2016). Impact of model simplifications on soil erosion predictions: application of the GLUE methodology to a distributed event-based model at the hillslope scale. *Hydrological Processes*, 30(7), 1096-1113. <https://doi.org/10.1002/hyp.10697>
- Charbeneau, R.J., Barrett, M.E. (1998). Evaluation of methods for estimating stormwater pollutant loads. *Water Environment Research*, 70(7), 1295-1302. <https://doi.org/10.2175/106143098X123679>
- Charters, F.J., Cochrane, T.A., O'Sullivan, A.D. (2015). Particle size distribution variance in untreated urban runoff and its implication on treatment selection. *Water research*, 85, 337-345. <https://doi.org/10.1016/j.watres.2015.08.029>
- Chebbo, G., Gromaire, M.C. (2004). The experimental urban catchment 'Le Marais' in Paris: what lessons can be learned from it? *Journal of Hydrology*, 299(3), 312-323. <https://doi.org/10.1016/j.jhydrol.2004.08.011>
- Chen, J., Hill, A.A., Urbano, L.D. (2009). A GIS-based model for urban flood inundation. *Journal of Hydrology*, 373 (1–2), 184–192. <https://doi.org/10.1016/j.jhydrol.2009.04.021>
- Chow, M.F., Yusop, Z., Abustan, I. (2015). Relationship between sediment build-up characteristics and antecedent dry days on different urban road surfaces in Malaysia. *Urban Water Journal*, 12(3), 240-247. <https://doi.org/10.1080/1573062X.2013.839718>
- Christiansen, J.E. (1942). *Irrigation by sprinkling. Bulletin 670*. Publisher: Agricultural Experiment Station. Berkeley, CAL, USA.
- Ciccarello, A., Bolognesi, A., Maglionico, M., Artina, S. (2012). The role of settling velocity formulation in the determination of gully pot trapping efficiency: comparison between analytical and experimental data. *Water Science and Technology*, 65(1), 15-21. <https://doi.org/10.2166/wst.2011.775>
- Cignoni, P., Callieri, M., Corsini, M., Dellepiane, M., Ganovelli, F., Ranzuglia, G. (2008). Meshlab: an open-source mesh processing tool. In: *Eurographics Italian Chapter Conference* (V. Scarano, R. De Chiara, U. Erra), Pisa, Italy. 129–136.
- Clarke, M. A., Walsh, R. P. (2007). A portable rainfall simulator for field assessment of splash and slopewash in remote locations. *Earth Surface Processes and Landforms: The Journal of the British Geomorphological Research Group*, 32(13), 2052-2069. <https://doi.org/10.1002/esp.1526>

- Cosenza, A., Mannina, G., Vanrolleghem, P.A., Neumann, M.B. (2013). Global sensitivity analysis in wastewater applications: A comprehensive comparison of different methods. *Environmental modelling & software*, 49, 40-52. <https://doi.org/10.1016/j.envsoft.2013.07.009>
- Cukier, R.I., Fortuin, C.M., Shuler, K.E., Petschek, A.G., Schaibly, J. H. (1973). Study of the sensitivity of coupled reaction systems to uncertainties in rate coefficients. I Theory. *The Journal of chemical physics*, 59(8), 3873-3878. <https://doi.org/10.1063/1.1680571>
- De Almeida, G. A., Bates, P., Ozdemir, H. (2018). Modelling urban floods at submetre resolution: challenges or opportunities for flood risk management? *Journal of Flood Risk Management*, 11, S855-S865. <https://doi.org/10.1111/jfr3.12276>
- De Sutter, R., Rushforth, P., Tait, S., Huygens, M., Verhoeven, R., Saul, A. (2003). Validation of existing bed load transport formulas using in-sewer sediment. *Journal of Hydraulic Engineering*, 129(4), 325-333. [https://doi.org/10.1061/\(ASCE\)0733-9429\(2003\)129:4\(325\)](https://doi.org/10.1061/(ASCE)0733-9429(2003)129:4(325))
- Dehghani, S., Moore, F., Akhbarizadeh, R. (2017). Microplastic pollution in deposited urban dust, Tehran metropolis, Iran. *Environmental Science and Pollution Research*, 24(25), 20360-20371. <http://doi.org/10.1007/s11356-017-9674-1>
- Deletic, A., Maksimovic, E., Ivetic, M. (1997). Modelling of storm wash-off of suspended solids from impervious surfaces. *Journal of Hydraulic Research*, 35(1), 99-118. <https://doi.org/10.1080/00221689709498646>
- Deletic, A., Ashley, R., Rest, D. (2000). Modelling input of fine granular sediment into drainage systems via gully-pots. *Water research*, 34(15), 3836-3844. [https://doi.org/10.1016/S0043-1354\(00\)00133-0](https://doi.org/10.1016/S0043-1354(00)00133-0)
- Deletic, A., Orr, D.W. (2005). Pollution buildup on road surfaces. *Journal of Environmental Engineering*, 131(1), 49-59. [https://doi.org/10.1061/\(ASCE\)0733-9372\(2005\)131:1\(49\)](https://doi.org/10.1061/(ASCE)0733-9372(2005)131:1(49))
- Detert, M., Johnson, E.D., Weitbrecht, V., 2017. Proof-of-concept for low-cost and non-contact synoptic airborne river flow measurements. *International Journal of Remote Sensing*. 38 (8–10), 2780–2807. <https://doi.org/10.1080/01431161.2017.1294782>
- Djordjević, S., Saul, A.J., Tabor, G.R., Blanksby, J., Galambos, I., Sabtu, N., Sailor, G. (2013). Experimental and numerical investigation of interactions between above and below ground drainage systems, *Water Science and Technology*, 67(3), 535-542, <https://doi.org/10.2166/wst.2012.570>
- Donckels, B.M.R., Kroll, S., Van Dorpe, M., Weemaes, M. (2014). Global sensitivity analysis of an in-sewer process model for the study of sulfide-induced corrosion of concrete.

- Water Science and Technology*, 69(3), 647-655. <http://doi.org/10.2166/wst.2013.763>
- Dris, R., Gasperi, J., Rocher, V., Saad, M., Renault, N., Tassin, B. (2015). Microplastic contamination in an urban area: a case study in Greater Paris. *Environmental Chemistry*, 12(5), 592-599. <http://doi.org/10.1071/EN14167>
- Egodawatta, P., Thomas, E., Goonetilleke, A., (2007). Mathematical interpretation of pollutant wash-off from urban road surfaces using simulated rainfall. *Water Research*, 41 (13), 3025–3031. <https://doi.org/10.1016/j.watres.2007.03.037>
- Ekstrom, P.A. (2005). *Eikos: a simulation toolbox for sensitivity analysis in matlab*. Uppsala University, Uppsala
- Fletcher I.J., Pratt C. J. (1981) Mathematical simulation of pollution contributions to urban runoff from roadside gully pots. In *Urban Stormwater Quality, Management & Planning* (Edited by Yen B. C.), pp. 116-124. Water Resources, Colo.
- Fraga, I., Cea, L., Puertas, J. (2013). Experimental study of the water depth and rainfall intensity effects on the bed roughness coefficient used in distributed urban drainage models. *Journal of hydrology*, 505, 266-275. <https://doi.org/10.1016/j.jhydrol.2013.10.005>
- Fraga, I. (2015). *Desarrollo de un modelo dual 1D/2D para el cálculo del drenaje urbano: modelo numérico y validación experimental*. Doctoral dissertation. Universidade da Coruña, A Coruña, Spain. <http://hdl.handle.net/2183/14727>
- Fraga, I., Cea, L., Puertas, J. (2015a). Validation of a 1D-2D dual drainage model under unsteady part-full and surcharged sewer conditions. *Urban Water Journal*, 14(1), 74-84. <https://doi.org/10.1080/1573062X.2015.1057180>
- Fraga, I., Cea, L., Puertas, J., Anta, J. (2015b). Nonintrusive method to compute water discharge in pipes with a low depth-to-diameter ratio using ultrasonic Doppler velocimetry. *Journal of Hydraulic Engineering*, 141(3), 06014024. [https://doi.org/10.1061/\(ASCE\)HY.1943-7900.0000982](https://doi.org/10.1061/(ASCE)HY.1943-7900.0000982)
- Fraga, I., Cea, L., Puertas, J., Suárez, J., Jiménez, V., Jácome, A., (2016). Global Sensitivity and GLUE-Based Uncertainty Analysis of a 2D-1D Dual Urban Drainage Model. *Journal of Hydrologic Engineering* 21 (5), 04016004. [https://doi.org/10.1061/\(asce\)he.1943-5584.0001335](https://doi.org/10.1061/(asce)he.1943-5584.0001335)
- Fujita, I., Muste, M., Kruger, A., (1998). Large-scale particle image velocimetry for flow analysis in hydraulic engineering applications. *Journal of Hydraulic Research*, 36 (3), 397–414. <https://doi.org/10.1080/00221689809498626>

- Gamerith, V., Neumann, M.B., Muschalla, D. (2013). Applying global sensitivity analysis to the modelling of flow and water quality in sewers. *Water research*, 47(13), 4600-4611. <http://dx.doi.org/10.1016/j.watres.2013.04.054>
- Gao, B., Walter, M.T., Steenhuis, T.S., Parlange, J.Y., Nakano, K., Hogarth, W.L., Rose, C. (2003) Investigating ponding depth and soil detachability for a mechanistic erosion model using a simple experiment. *Journal of Hydrology*, 277(1–2): 116–124. [https://doi.org/10.1016/S0022-1694\(03\)00085-4](https://doi.org/10.1016/S0022-1694(03)00085-4)
- García-Feal, O., González-Cao, J., Gómez-Gesteira, M., Cea, L., Domínguez, J., Formella, A. (2018). An accelerated tool for flood modelling based on Iber. *Water*, 10(10), 1459. <https://doi.org/10.3390/w10101459>
- Gastaldini, M.D.C., Silva, A.R.V., Cauduro, C., Roberta, A. Silva, V. (2013). Pollutant Distribution on Urban Surfaces: Case Study in Southern Brazil. *Journal of Environmental Engineering-Asce*, 139(2), 269–276. [https://doi.org/10.1061/\(ASCE\)EE.1943-7870.0000617](https://doi.org/10.1061/(ASCE)EE.1943-7870.0000617)
- Gorgoglione, A., Bombardelli, F.A., Pitton, B.J., Oki, L.R., Haver, D.L., Young, T.M. (2019). Uncertainty in the parameterization of sediment build-up and wash-off processes in the simulation of sediment transport in urban areas. *Environmental modelling & software*, 111, 170-181. <https://doi.org/10.1016/j.envsoft.2018.09.022>
- Goring, D.G., Nikora, V.I. (2002) Despiking acoustic Doppler velocimeter data, *Journal of Hydraulic Engineering*, 128 (1), 117–126, [https://doi.org/10.1061/\(ASCE\)0733-9429\(2002\)128:1\(117\)](https://doi.org/10.1061/(ASCE)0733-9429(2002)128:1(117))
- Grismer, M. E. 2011. Rainfall simulation studies—a review of designs, performance and erosion measurement variability. <http://ucanr.org/sites/californiaagriculture/files/145682.pdf>
- Grottker, M. (1987). Runoff quality from a street with medium traffic loading. *Science of the Total Environment*, 59, 457-466. [https://doi.org/10.1016/0048-9697\(87\)90469-4](https://doi.org/10.1016/0048-9697(87)90469-4)
- Grottker, M. (1990). Pollutant removal by gully pots in different catchment areas. *Science of the total environment*, 93, 515-522. [https://doi.org/10.1016/0048-9697\(90\)90142-H](https://doi.org/10.1016/0048-9697(90)90142-H)
- Guillén, N.F., Patalano, A., García, C.M., Bertoni, J.C., (2017). Use of LSPIV in assessing urban flash flood vulnerability. *Natural Hazards*. 87 (1), 383–394. <https://doi.org/10.1007/s11069-017-2768-8>
- Gunn, R., Kinzer, G.D. (1949). The terminal velocity of fall for water droplets in stagnant air. *Journal of Meteorology*, 6(4), 243-248. [https://doi.org/10.1175/1520-0469\(1949\)006<0243:TTVOFF>2.0.CO;2](https://doi.org/10.1175/1520-0469(1949)006<0243:TTVOFF>2.0.CO;2)

- Hairsine, P.B., Rose, C.W., (1992a). Modeling water erosion due to overland flow using physical principles: 1. Sheet flow. *Water Resources Research*, 28, 237–243. <http://doi.org/10.1029/91wr02380>
- Hairsine, P.B., Rose, C.W., (1992b). Modeling water erosion due to overland flow using physical principles: 2. Rill flow. *Water Resources Research*, 28, 245–250. <http://doi.org/10.1029/91wr02381>
- Hannouche, A., Joannis, C., Chebbo, G. (2017) Assessment of total suspended solids (TSS) event load and its uncertainties in combined sewer system from continuous turbidity measurements. *Urban Water Journal*, 14(8), 789-796, <https://doi.org/10.1080/1573062X.2016.1254256>
- Helton, J.C. (1993). Uncertainty and sensitivity analysis techniques for use in performance assessment for radioactive waste disposal. *Reliability Engineering & System Safety*, 42(2-3), 327-367. [https://doi.org/10.1016/0951-8320\(93\)90097-1](https://doi.org/10.1016/0951-8320(93)90097-1)
- Heng, B.C.P., Sander, G.C., Armstrong, A., Quinton, J.N., Chandler, J.H., Scott, C.F. (2011), Modeling the dynamics of soil erosion and size-selective sediment transport over nonuniform topography in flume-scale experiments, *Water Resources Research*, 47, W02513. <https://doi.org/10.1029/2010WR009375>
- Herngren, L. F. (2005a). *Build-up and Wash-off Process Kinetics of PAHs and Heavy Metals on Paved Surfaces Using Simulated Rainfall*. Doctoral dissertation, Queensland University of Technology, Brisbane, Queensland, Australia
- Herngren, L., Goonetilleke, A., Sukpum, R., Silva, D.D. (2005b). Rainfall simulation as a tool for urban water quality research. *Environmental Engineering Science*, 22(3), 378-383. <https://doi.org/10.1089/ees.2005.22.378>
- Hong, M., Bonhomme, C., Le, M.H., Chebbo, G. (2016a). A new approach of monitoring and physically-based modelling to investigate urban wash-off process on a road catchment near Paris. *Water Research*, 102, 96–108, <https://doi.org/10.1016/j.watres.2016.06.027>
- Hong, M., Bonhomme, C., Le, M.H., Chebbo, G. (2016b). New insights into the urban washoff process with detailed physical modelling. *Science of Total Environment*. 573, 924–936. <https://doi.org/10.1016/j.scitotenv.2016.08.193>
- Hong, Y., Liao, Q., Bonhomme, C., Chebbo, G. (2019). Physically-based urban stormwater quality modelling: An efficient approach for calibration and sensitivity analysis. *Journal of environmental management*, 246, 462-471. <https://doi.org/10.1016/j.jenvman.2019.06.003>

- Hudson, N. W. (1963). Raindrop size distribution in high intensity storms. *Rhodesian Journal of Agricultural Research*, 1(1), 6-11.
- Hunter, N.M., Bates, P.D., Neelz, S., Pender, G., Villanueva, I., Wright, N.G., Liang, D., Falconer, R.A., Lin, B., Waller, S., Crossley, A.J., Mason, D.C. (2008). Benchmarking 2D hydraulic models for urban flooding. *Proceedings of the Institution of Civil Engineers Water Management*, 161 (1), 13–30. <https://doi.org/10.1680/wama.2008.161.1.13>
- Isidoro, J. M., de Lima, J. L., Leandro, J. (2012). Influence of wind-driven rain on the rainfall-runoff process for urban areas: Scale model of high-rise buildings. *Urban Water Journal*, 9(3), 199-210. <https://doi.org/10.1080/1573062X.2012.654801>
- Julien, P.Y. (2010). Erosion and sedimentation. Cambridge University Press, Cambridge.
- Júnior, S.S., Siqueira, E.Q. (2011). Development and calibration of a rainfall simulator for urban hydrology research. In *Proceedings of 12th International Conference on Urban Drainage*, Porto Alegre, Brazil (pp. 11-16).
- Kantoush, S.A., De Cesare, G., Boillat, J.L., Schleiss, A.J. (2008). Flow field investigation in a rectangular shallow reservoir using UVP, LSPIV and numerical modelling. *Flow Measurement and Instrumentation*, 19 (3–4), 139–144. <https://doi.org/10.1016/j.flowmeasinst.2007.09.005>
- Kathiravelu, G., Lucke, T., Nichols, P. (2014). Designing the Perfect Rainfall Simulator for Urban Stormwater Studies: An Impossible Dream? In *Proceedings of the 13th International Conference on Urban Drainage* (pp. 1-9). International Water Association.
- Kazhdan, M., Hoppe, H. (2013). Screened poisson surface reconstruction. *ACM Trans. Graph.* 32 (3), 29. <https://doi.org/10.1145/2487228.2487237>.
- Lager, J.A., Smith, W.G., Tchobanoglous, G. (1977). *Catchbasin technology overview and assessment*. Environmental Protection Agency, Office of Research and Development, Municipal Environmental Research Laboratory, Wastewater Research Division, Storm and Combined Sewer Section.
- Laws, J. O. (1941). Measurements of the fall-velocity of water-drops and raindrops. *Eos, Transactions American Geophysical Union*, 22(3), 709-721. <https://doi.org/10.1029/TR022i003p00709>
- Le Coz, J., Hauet, A., Pierrefeu, G., Dramais, G., Camenen, B. (2010). Performance of image-based velocimetry (LSPIV) applied to flash-flood discharge measurements in Mediterranean rivers. *Journal of Hydrology*, 394 (1–2), 42–52. <https://doi.org/10.1016/j.jhydrol.2010.05.049>.

- Leandro, J., Chen, A.S., Djordjević, S., Savić, D.A., (2009). Comparison of 1D/1D and 1D/2D coupled (sewer/surface) hydraulic models for urban flood simulation. *Journal of Hydraulic Engineering* 135 (6), 495–504. [https://doi.org/10.1061/\(asce\)hy.1943-7900.0000037](https://doi.org/10.1061/(asce)hy.1943-7900.0000037).
- Leitão, J.P., Peña-Haro, S., Lüthi, B., Scheidegger, A., de Vitry, M.M. (2018). Urban overland runoff velocity measurement with consumer-grade surveillance cameras and surface structure image velocimetry. *Journal of Hydrology*. 565, 791–804. <https://doi.org/10.1016/j.jhydrol.2018.09.001>.
- Leutnant, D., Muschalla, D., Uhl, M. (2018). Statistical distribution of TSS event loads from small urban environments. *Water*, 10(6), 769. <https://doi.org/10.3390/w10060769>
- Mannina, G., Schellart, A. N. A., Tait, S., and Viviani, G. (2012). Uncertainty in sewer sediment deposit modelling: Detailed vs simplified modelling approaches, *Physics and Chemistry of the Earth, Parts A/B/C*, 42, 11-20, <https://doi.org/10.1016/j.pce.2011.04.003>
- Mannina, G., Cosenza, A., Gori, R., Garrido-Baserbac, M., Sobhani, R., Rosso, D. (2016). Greenhouse gas emissions from wastewater treatment plants on a plantwide scale: sensitivity and uncertainty analysis. *Journal of Environmental Engineering*, 142(6), 04016017. [https://doi.org/10.1061/\(ASCE\)EE.1943-7870.0001082](https://doi.org/10.1061/(ASCE)EE.1943-7870.0001082)
- Martínez-Gomariz, E., Gómez, M., Russo, B., (2016). Experimental study of the stability of pedestrians exposed to urban pluvial flooding. *Natural Hazards*. 82 (2),1–20. <https://doi.org/10.1007/s11069-016-2242-z>
- Martínez Gomariz, E., Gómez, M., Russo, B., Sánchez, P., Montes, J.A. (2017). Metodología para la evaluación de daños a vehículos expuestos a inundaciones en zonas urbanas. *Ingeniería del agua*, 21(4), 247-262. <https://doi.org/10.4995/ia.2017.8772>
- Martínez-Gomariz, E., Gómez, M., Russo B., Sánchez, P., Montes, J.A., (2018). Methodology for the damage assessment of vehicles exposed to flooding in urban areas. *Journal of Flood Risk Management*. e12475. <https://doi.org/10.1111/jfr3.12475>
- Martins, R., Rubinato, M., Kesserwani, G., Leandro, J., Djordjević, S., Shucksmith, J.D. (2018). On the characteristics of velocities fields in the vicinity of manhole inlet grates during flood events. *Water Resources Research*, 54. <https://doi.org/10.1029/2018WR022782>.
- Massoudieh, A., Abrishamchi, A., Kayhanian, M. (2008). Mathematical modeling of first flush in highway storm runoff using genetic algorithm. *Science of the total environment*, 398(1-3), 107-121. <https://doi.org/10.1016/j.scitotenv.2008.02.050>

-
- Memon, F.A., Butler, D. (2002). Identification and modelling of dry weather processes in gully pots. *Water research*, 36(5), 1351-1359. [https://doi.org/10.1016/S0043-1354\(01\)00342-6](https://doi.org/10.1016/S0043-1354(01)00342-6)
- Miguntanna, N.P., Goonetilleke, A., Egodowatta, P., Kokot, S. (2010). Understanding nutrient build-up on urban road surfaces. *Journal of Environmental Sciences*, 22(6), 806-812. [https://doi.org/10.1016/S1001-0742\(09\)60181-9](https://doi.org/10.1016/S1001-0742(09)60181-9)
- Moisy, F., (2017). PIVMat. Available at: <http://www.fast.u-psud.fr/pivmat/> [Accessed: 19 Sep 2019].
- Morgan, D., Johnston, P., Osei, K., Gill, L. (2017). Sediment build-up on roads and footpaths of a residential area. *Urban Water Journal*, 14(4), 378-385. <https://doi.org/10.1080/1573062X.2016.1148182>
- Morris, M.D. (1991). Factorial sampling plans for preliminary computational experiments. *Technometrics* 33, 161–174.
- Moy de Vitry, M., Dicht, S., and Leitão, J.P. (2017). FloodX: urban flash flood experiments monitored with conventional and alternative sensors, *Earth System Science Data*, 9(2), 657-666, <https://doi.org/10.5194/essd-9-657-2017>
- Muste, M., Ho, H.C., Kim, D., (2011). Considerations on direct stream flow measurements using video imagery: outlook and research needs. *Journal of Hydro-environment Research*, 5 (4), 289–300. <https://doi.org/10.1016/j.jher.2010.11.002>
- Muthusamy, M., Tait, S., Schellart, A., Beg, M.N.A., Carvalho, F.R. de Lima, J.L.M.P., (2018). Improving understanding of the underlying physical process of sediment wash-off from urban road surfaces. *Journal of Hydrology* 557, 426–433, <https://doi.org/10.1016/j.jhydrol.2017.11.047>.
- Naves, J (2012) *Montaje y calibración de una instalación experimental a escala real para el análisis de modelos duales de drenaje urbano*. Bachelor thesis. Civil engineering. University of A Coruña. www.geama.org/hidraulica/index.php?o=downloads&i=36.
- Naves, J., Jikia, Z., Anta, J., Puertas, J., Suárez, J., Regueiro-Picallo, M. (2017). Experimental study of pollutant washoff on a full-scale street section physical model. *Water Science and Technology*, 76(10), 2821-2829. <https://doi.org/10.2166/wst.2017.345>
- Naves, J., Anta J., Puertas J., Regueiro-Picallo, M., Suárez, J. (2019a) Using a 2D shallow waters model to assess Large-scale Particle Image Velocimetry (LSPIV) and Structure from Motion (SfM) techniques in a street-scale urban drainage physical model. *Journal of Hydrology* 575, 54-65 <https://doi.org/10.1016/j.jhydrol.2019.05.003>
-

- Naves, J., Rieckermann, J., Cea, L., Puertas, J. Anta, J. (2019b) Using global and local sensitivity analysis to improve the understanding of physically-based urban wash-off models from high-resolution laboratory experiments, *Water Research (in review)*.
- Naves, J., Anta, J., Suárez, J., Puertas, J. (2019c) [dataset] WASHTREET Hydraulic, wash-off and sediment transport experimental data in an urban drainage physical model, *Zenodo*, <http://doi.org/10.5281/zenodo.3233918>
- Naves, J., Puertas, J., Suárez, J., and Anta, J. (2019d) [dataset] WASHTREET Runoff velocity data using different Particle Image Velocimetry (PIV) techniques in a full scale urban drainage physical model, *Zenodo*, <http://doi.org/10.5281/zenodo.3239401>
- Naves, J., Anta, J., Suárez, J., and Puertas, J.: (2019e) [dataset] WASHTREET Application of Structure from Motion (SfM) photogrammetric technique to determine surface elevations in an urban drainage physical model, *Zenodo*, <http://doi.org/10.5281/zenodo.3241337>
- Neal, J.C., Bates, P.D., Fewtrell, T.J., Hunter, N.M., Wilson, M.D., Horritt, M.S. (2009). Distributed whole city water level measurements from the Carlisle 2005 urban flood event and comparison with hydraulic model simulations. *Journal of Hydrology*. 368 (1–4), 42-55. <https://doi.org/10.1016/j.jhydrol.2009.01.026>
- Novak, G., Rak, G., Prešeren, T., Bajcar, T. (2017). Non-intrusive measurements of shallow water discharge. *Flow Measurement and Instrumentation*, 56, 14–17. <https://doi.org/10.1016/j.flowmeasinst.2017.05.007>
- Ota, J. J., and Perrusquia, G. S. (2013) Particle velocity and sediment transport at the limit of deposition in sewers. *Water Science and Technology*, 67(5), 959-967. <https://doi.org/10.2166/wst.2013.646>
- Pedocchi, F., Martin, J.E., García, M.H. (2008). Inexpensive fluorescent particles for large-scale experiments using particle image velocimetry. *Experiments in Fluids*. 45 (1), 183–186. <https://doi.org/10.1007/s00348-008-0516-2>
- Pianosi, F., Sarrazin, F., Wagener, T. (2015). A Matlab toolbox for global sensitivity analysis. *Environmental Modelling & Software*, 70, 80-85. <https://doi.org/10.1016/j.envsoft.2015.04.009>
- Pitt, R., Williamson, D., Voorhees, J., Clark, S. (2004). Review of historical street dust and dirt accumulation and washoff data. *Effective Modeling of Urban Water Systems*, Monograph, 13, 43-54. <https://doi.org/10.14796/JWMM.R223-12>
- Post, J.A.B., Pothof, I.W.M., Dirksen, J., Baars, E.J., Langeveld, J.G., Clemens, F.H.L.R. (2016). Monitoring and statistical modelling of sedimentation in gully pots. *Water research*, 88, 245-256. <https://doi.org/10.1016/j.watres.2015.10.021>

- Proffitt, A.P.B., Rose, C.W., Hairsine, P.B. (1991). Rainfall detachment and deposition: Experiments with low slopes and significant water depths. *Soil Science Society of America Journal*, 55(2), 325-332. <https://doi.org/10.2136/sssaj1991.03615995005500020004x>
- Proffitt, A.P.B., Hairsine, P.B., Rose, C.W. (1993). Modeling soil erosion by overland flow: application over a range of hydraulic conditions. *Transactions of the ASAE*, 36(6), 1743-1753. <https://doi.org/10.13031/2013.28519>
- Raffel, M., Willert, C., Kompenhans, J. (2007). *Particle Image Velocimetry: A Practical Guide*. Springer, Berlin, Germany.
- Regueiro-Picallo, M., Anta, J., Suárez, J., Puertas, J., Jácome, A., Naves, J. (2018). Characterisation of sediments during transport of solids in circular sewer pipes. *Water Science and Technology*, 2017 (1), 8–15. <https://doi.org/10.2166/wst.2018.055>
- Rijn, L.C.V. (1984). Sediment transport, part II: suspended load transport. *Journal of hydraulic engineering*, 110(11), 1613-1641. [https://doi.org/10.1061/\(ASCE\)0733-9429\(1984\)110:11\(1613\)](https://doi.org/10.1061/(ASCE)0733-9429(1984)110:11(1613))
- Rodríguez, J.P., McIntyre, N., Díaz-Granados, M., Maksimović, Č. (2012). A database and model to support proactive management of sediment-related sewer blockages. *Water research*, 46(15), 4571-4586. <https://doi.org/10.1016/j.watres.2012.06.037>
- Roesner, L.A. (1982). Quality of urban runoff. *Urban Stormwater Hydrology, Water Resources Monograph*, 7.
- Rossi, L., Chèvre, N., Fankhauser, R., Krejci, V. (2009). Probabilistic environmental risk assessment of urban wet-weather discharges: an approach developed for Switzerland. *Urban Water Journal*, 6(5), 355-367. <https://doi.org/10.1080/15730620902934801>
- Rossman, L.A., (2015) *Storm Water Management Model, User's Manual*, Version 5.1 No. EPA/600/R-05/040). US Environmental Protection Agency, Cincinnati, OH, USA
- Rubinato, M., Martins, R., Kesserwani, G., Leandro, J., Djordjević, S., Shucksmith, J. (2107). Experimental calibration and validation of sewer/surface flow exchange equations in steady and unsteady flow conditions, *Journal of Hydrology*, 552, 421-432. <https://doi.org/10.1016/j.jhydrol.2017.06.024>
- Rushforth, P.J., Tait, S.J., Saul, A.J. (2003). Modeling the erosion of mixtures of organic and granular in-sewer sediments. *Journal of hydraulic engineering*, 129(4), 308-315.

- Safari, M.J.S., Aksoy, H., Unal, N.E., Mohammadi, M. (2017) Experimental analysis of sediment incipient motion in rigid boundary open channels. *Environmental Fluid Mechanics*, 17(6), 1281-1298. <https://doi.org/10.1007/s10652-017-9550-z>
- Saltelli, A., Tarantola, S., Chan, K. S. (1999). A quantitative model-independent method for global sensitivity analysis of model output. *Technometrics*, 41(1), 39-56. <https://doi.org/10.1080/00401706.1999.10485594>
- Saltelli, A., Chan, K., Scott, E. M. (Eds.). (2000). Sensitivity analysis (Vol. 1). New York: Wiley.
- Saltelli, A., Annoni, P. (2010). How to avoid a perfunctory sensitivity analysis. *Environmental Modelling & Software*, 25(12), 1508-1517. <https://doi.org/10.1016/j.envsoft.2010.04.012>
- Saltelli, A., Ratto, M., Tarantola, S., Campolongo, F. (2005). Sensitivity analysis for chemical models. *Chemical reviews*, 105(7), 2811-2828. <https://doi.org/10.1021/cr040659d>
- Sander, G.C., Parlange, J.Y., Barry, D.A., Parlange, M.B., Hogarth, W.L. (2007). Limitation of the transport capacity approach in sediment transport modeling. *Water Resources Research*, 43(2). <https://doi.org/10.1029/2006WR005177>
- Saltelli, A., Ratto, M., Andres, T., Campolongo, F., Cariboni, J., Gatelli, D., Saisana, M., Tarantola, S. (2008). *Global sensitivity analysis: the primer*. John Wiley & Sons.
- Sandoval, S., Vezzaro, L., Bertrand-Krajewski, J. L. (2018). Revisiting conceptual stormwater quality models by reconstructing virtual state variables. *Water Science and Technology*, 78(3), 655-663. <https://doi.org/10.2166/wst.2018.337>
- Sartor, J.D. Boyd, G.B. (1972). Water pollution aspects of street surface contaminants. United States Environmental Protection Agency, Washington, DC, EPA-R2-72-081
- Schellart, A.N.A., Tait, S.J., Ashley, R.M. (2010). Towards quantification of uncertainty in predicting water quality failures in integrated catchment model studies. *Water research*, 44(13), 3893-3904. <https://doi.org/10.1016/j.watres.2010.05.001>
- Semadeni-Davies, A., Hernebring, C., Svensson, G., Gustafsson, L.G. (2008). The impacts of climate change and urbanisation on drainage in Helsingborg, Sweden: Combined sewer system. *Journal of Hydrology*, 350(1-2), 100-113. <https://doi.org/10.1016/j.jhydrol.2007.05.028>
- Seyoum, S.D., Vojinovic, Z., Price, R.K., Weesakul, S. (2011). Coupled 1D and noninertia 2D flood inundation model for simulation of urban flooding. *Journal of Hydraulic Engineering*. 138 (1), 23–34. [https://doi.org/10.1061/\(ASCE\)HY.1943-7900.0000485](https://doi.org/10.1061/(ASCE)HY.1943-7900.0000485)
- Sharma, P.P., Gupta, S.C., Foster, G.R. (1993). Predicting soil detachment by raindrops. *Soil Science Society of America Journal* 57: 674–680. <https://doi.org/10.2136/sssaj1993.03615995005700030007x>

-
- Sharma, P.P., Gupta, S.C., Foster, G.R. (1995). Raindrop-induced soil detachment and sediment transport from interrill areas. *Soil Science Society of America Journal* 59: 727–734. <https://doi.org/10.2136/sssaj1995.03615995005900030014x>
- Shaw, S. B., Walter, M.T., Steenhuis, T.S. (2006). A physical model of particulate wash-off from rough impervious surfaces. *Journal of Hydrology*, 327(3-4), 618-626. <https://doi.org/10.1016/j.jhydrol.2006.01.024>
- Shaw, S.B., Parlange, J.Y., Lebowitz, M., Walter, M.T. (2009). Accounting for surface roughness in a physically-based urban wash-off model. *Journal of hydrology*, 367(1-2), 79-85. <https://doi.org/10.1016/j.jhydrol.2009.01.004>
- Sikorska, A. E., Del Giudice, D., Banasik, K., Rieckermann, J. (2015). The value of streamflow data in improving TSS predictions—Bayesian multi-objective calibration. *Journal of Hydrology*, 530, 241-254. <https://doi.org/10.1016/j.jhydrol.2015.09.051>
- Skipworth, P.J., Tait, S.J., Saul, A.J. (1999). Erosion of sediment beds in sewers: Model development. *Journal of environmental engineering*, 125(6), 566-573. [https://doi.org/10.1061/\(ASCE\)0733-9372\(1999\)125:6\(566\)](https://doi.org/10.1061/(ASCE)0733-9372(1999)125:6(566))
- Soonthornnonda, P., Christensen, E.R. (2008). A load model based on antecedent dry periods for pollutants in stormwater. *Water Environment Research*, 80(2), 162-171. <https://doi.org/10.2175/106143007X220888>
- Sutherland, R.C., Jelen, S.L., Minton, G. (1998). High efficiency sweeping as an alternative to the use of wet vaults for stormwater treatment. *Advances in Modeling the Management of Stormwater Impacts*, 6, 351-371.
- Tait, S.J., Chebbo, G., Skipworth, P.J., Ahyerre, M., Saul, A.J. (2003). Modeling in-sewer deposit erosion to predict sewer flow quality. *Journal of Hydraulic Engineering*, 129(4), 316-324. [https://doi.org/10.1061/\(ASCE\)0733-9429\(2003\)129:4\(316\)](https://doi.org/10.1061/(ASCE)0733-9429(2003)129:4(316))
- Tang, Y., Zhu, D.Z., Rajaratnam, N., and van Duin, B. (2016). Experimental study of hydraulics and sediment capture efficiency in catchbasins, *Water Science and Technology*, 74(11), 2717-2726. <https://doi.org/10.2166/wst.2016.448>
- Ten Veldhuis, J.A., Clemens, F.H., van Gelder, P.H. (2011). Quantitative fault tree analysis for urban water infrastructure flooding. *Structure and Infrastructure Engineering*, 7(11), 809-821. <https://doi.org/10.1080/15732470902985876>
- Thielicke, W., Stamhuis, E.J. (2014). PIVlab – Towards User-friendly, Affordable and Accurate Digital Particle Image Velocimetry in MATLAB. *Journal of Open Research Software*, 2 (1), e30. <https://doi.org/10.5334/jors.bl>
-

- Tokay, A., Wolff, D.B., Petersen, W.A. (2014). Evaluation of the new version of the laser-optical disdrometer, OTT Parsivel2. *Journal of Atmospheric and Oceanic Technology*, 31(6), 1276-1288. <https://doi.org/10.1175/JTECH-D-13-00174.1>
- Tomanovic, C., Maksimocik, C. (1996). Improved modelling of suspended solids discharge from asphalt surface during storm event. *Water Science and Technology*, 33(45): 365-369.
- Torres, A., Bertrand-Krajewski, J.L. (2008). Partial Least Squares local calibration of a UV-visible spectrometer used for in situ measurements of COD and TSS concentrations in urban drainage systems. *Water Science and Technology*, 57(4), 581-588. <https://doi.org/10.2166/wst.2008.131>
- United Nations, Department of Economic and Social Affairs, Population Division (2018). *The World's Cities in 2018—Data Booklet (ST/ESA/SER.A/417)*
- Vanrolleghem, P.A., Mannina, G., Cosenza, A., Neumann, M.B. (2015). Global sensitivity analysis for urban water quality modelling: Terminology, convergence and comparison of different methods. *Journal of Hydrology*, 522, 339-352. <https://doi.org/10.1016/j.jhydrol.2014.12.056>
- Vaze, J., Chiew, F.H. (2002). Experimental study of pollutant accumulation on an urban road surface. *Urban Water*, 4(4), 379-389. [https://doi.org/10.1016/S1462-0758\(02\)00027-4](https://doi.org/10.1016/S1462-0758(02)00027-4)
- Vogelsang, C., Lusher, A.L., Dadkhah, M.E., Sundvor, I., Umar, M., Ranneklev, S.B., Eidsvoll, D., Meland, S. (2019). *Microplastics in road dust—characteristics, pathways and measures*. Norsk institutt for vannforskning. <http://hdl.handle.net/11250/2493537>
- Wang, L., Wei, J., Huang, Y., Wang, G., Maqsood, I. (2011). Urban nonpoint source pollution buildup and washoff models for simulating storm runoff quality in the Los Angeles County. *Environmental Pollution*, 159(7), 1932–1940. <https://doi.org/10.1016/j.envpol.2011.03.019>
- Wei, T., Wijesiri, B., Jia, Z., Li, Y., Goonetilleke, A. (2019). Re-thinking classical mechanistic model for pollutant build-up on urban impervious surfaces. *Science of The Total Environment*, 651, 114-121. <https://doi.org/10.1016/j.scitotenv.2018.09.013>
- Weitbrecht, V., Kühn, G., Jirka, G.H. (2002). Large scale PIV-measurements at the surface of shallow water flows. *Flow Measurement and Instrumentation*, 13 (5–6), 237–245. [https://doi.org/10.1016/S0955-5986\(02\)00059-6](https://doi.org/10.1016/S0955-5986(02)00059-6)
- Westoby, M.J., Brasington, J., Glasser, N.F., Hambrey, M.J., Reynolds, J.M. (2012). ‘Structure-from-Motion’ photogrammetry: A low-cost, effective tool for geoscience

- applications. *Geomorphology*, 179, 300–314.
<https://doi.org/10.1016/j.geomorph.2012.08.021>
- Wijesiri, B., Egodawatta, P., McGree, J., Goonetilleke, A., (2015a). Incorporating process variability into stormwater quality modelling. *Science of the Total Environment*, 533, 454–461. <https://doi.org/10.1016/j.scitotenv.2015.07.008>.
- Wijesiri, B., Egodawatta, P., McGree, J., Goonetilleke, A. (2015b). Process variability of pollutant build-up on urban road surfaces. *Science of the Total Environment*, 518, 434-440. <https://doi.org/10.1016/j.scitotenv.2015.03.014>
- Wijesiri, B., Egodawatta, P., McGree, J., Goonetilleke, A. (2016). Understanding the uncertainty associated with particle-bound pollutant build-up and wash-off: A critical review. *Water research*, 101, 582-596. <https://doi.org/10.1016/j.watres.2016.06.013>
- Woods-Ballard, B., Kellagher, R., Martin, P., Jefferies, C., Bray, R., Shaffer, P. (2007). *The SuDS Manual* (Vol. 697). London: Ciria
- Wu, C., Agarwal, S., Curless, B., Seitz, S.M. (2011). *Multicore bundle adjustment*. In: *Computer Vision and Pattern Recognition (CVPR)*, Colorado Springs, CO, USA. Institute of Electrical and Electronics Engineers (IEEE). 3057–3064.
- Wu, C. (2013). Towards linear-time incremental structure from motion. In: *2013 International Conference on 3D Vision 3DV*, Seattle, WA, USA. Institute of Electrical and Electronics Engineers (IEEE). <https://doi.org/10.1109/3DV.2013.25>
- Zafra, C. A., Temprano, J., Tejero, I. (2008). Particle Size Distribution of Accumulated Sediments on an Urban Road in Rainy Weather. *Environmental Technology*, 29(5), 571–582. <https://doi.org/10.1080/09593330801983532>
- Zafra, C. A., Temprano, J., Tejero, I. (2011). Distribution of the concentration of heavy metals associated with the sediment particles accumulated on road surfaces. *Environmental technology*, 32(9), 997-1008. <https://doi.org/10.1080/09593330.2010.523436>
- Zafra, C., Temprano, J., Suárez, J. (2017). A simplified method for determining potential heavy metal loads washed off by stormwater runoff from road-deposited sediments. *Science of the Total Environment*, 601, 260-270. <https://doi.org/10.1016/j.scitotenv.2017.05.178>

Appendix A

Resumen extendido de la tesis

Resumen extendido de la tesis

El continuo crecimiento de las ciudades y el consecuente aumento de las superficies impermeables produce un incremento de la escorrentía durante los episodios de lluvia que es necesario gestionar adecuadamente para un desarrollo urbano sostenible. Esta escorrentía moviliza los contaminantes que se depositan en las cuencas urbanas durante el tiempo seco, por lo que pueden suponer una fuente importante de contaminación si no se realiza un tratamiento adecuado. A pesar de esta importancia, la precisión que se obtiene al modelizar los procesos de lavado y transporte de contaminantes en cuencas urbanas es actualmente muy limitada. Además de a la complejidad del fenómeno físico, esto es debido a la alta variabilidad asociada a los procesos de acumulación y lavado de contaminantes en cuencas urbanas, que implica una falta de datos lo suficientemente precisos para el correcto desarrollo de este tipo de modelos. Un ejemplo de este problema es la dificultad para medir en campo variables importantes como la carga de sedimentos depositados o sus características sin afectar a las condiciones iniciales de los eventos.

Esta tesis tiene como objetivo el desarrollo de una extensa campaña experimental en la que se mida con precisión y en condiciones controladas de laboratorio los procesos de lavado y transporte de sedimentos en cuencas urbanas. Para ello se ha utilizado un modelo físico de drenaje urbano a escala real de unos 36 m², formado por una sección de calle que se conecta a través de dos imbornales a una red de tuberías que drenan la escorrentía generada por un simulador de lluvia (Figura A.1). Pretendiendo conseguir la mayor fiabilidad y transferibilidad de los resultados, se plantearon tres objetivos parciales: i) el desarrollo de una metodología experimental adecuada para analizar la movilización de sólidos a través de las distintas partes del modelo, ii) la construcción de un novedoso simulador de lluvia con propiedades similares a la lluvia natural y iii) la caracterización precisa de las variables hidráulicas involucradas, considerando y midiendo los flujos complejos que se dan en las proximidades de cunetas e imbornales. Como último objetivo de la tesis se planteó la utilización de los resultados experimentales para la evaluación y análisis de un modelo de lavado de sedimentos basado en procesos físicos. Este novedoso modelo, que se planteó recientemente como alternativa para representar adecuadamente los complejos fenómenos físicos involucrados, requiere una definición precisa de un mayor número de variables de entrada que los modelos semiempíricos tradicionales. Por ello, los ensayos objeto de la tesis son una inmejorable oportunidad para su análisis, a partir del cual se pretende identificar las variables que gobiernan el proceso para simplificar el modelo de una manera rigurosa y mejorar su aplicabilidad a casos reales.

Como se ha planteado, el primer trabajo abordado por la tesis fue el desarrollo de una metodología experimental que permitiese medir con precisión la movilización de sedimentos, identificando las principales variables a tener en cuenta y asegurando la fiabilidad de los resultados. Para ello, en el Capítulo 2 se presentan una serie de ensayos

preliminares en los que se analizó el lavado de sedimentos para diferentes cargas y distribuciones de sedimentos sobre la superficie del modelo. El simulador de lluvia utilizado fue el desarrollado en el trabajo previo de Fraga (2015), en el cual se validó un modelo dual 2D/1D. El simulador consistía en 4 difusores a presión que generaban una precipitación con una intensidad media de 101 mm/h durante 5 minutos. La Figura A.1 muestra un esquema del modelo físico y el mapa de intensidades de lluvia generado por el simulador de lluvia basado en difusores que se utilizó en estos ensayos preliminares.

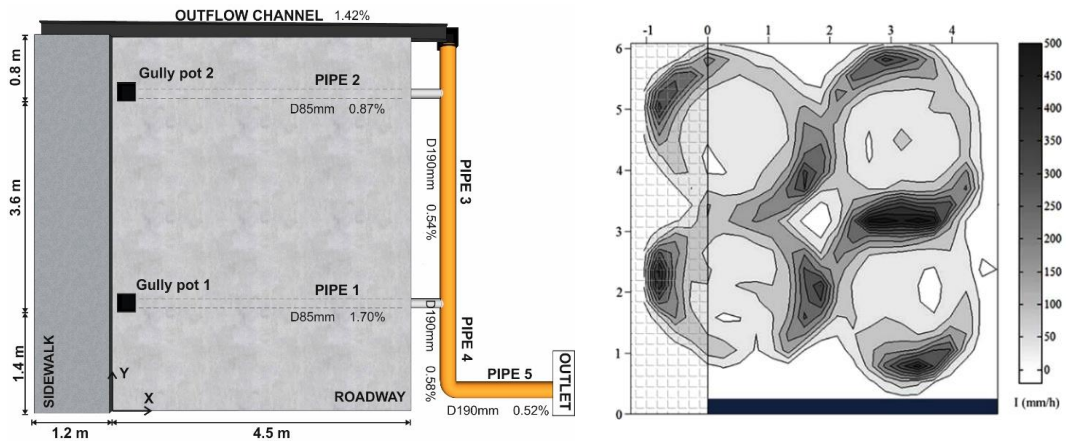


Figura A.1. Esquema general del modelo físico de drenaje urbano y mapa de intensidades de lluvia generado por el simulador de lluvia basado en difusores a presión que se utilizó en los ensayos preliminares.

En los ensayos se registraron caudales mediante un vertedero triangular y se midieron concentraciones de Sólidos en Suspensión Totales (SST) a partir de la toma de muestras manuales y registros de turbidez en continuo a la salida de la red de tuberías. Al final de cada ensayo se realizaron balances de masa entre la carga inicial de sedimento dispuesta sobre la superficie del modelo y la suma de las masas que quedan depositadas en las distintas partes del modelo al final de los ensayos (superficie, arquetas y tuberías) y la masa total lavada del modelo. Este procedimiento permitió comprobar para cada ensayo si se había podido medir con precisión la movilización de SST a través del modelo, indicando la fiabilidad de los resultados obtenidos. Se realizaron un total de once experimentos con esta metodología para evaluar la influencia de la carga inicial de sedimento, del método de distribución, de la posición del sedimento y del área de distribución en el proceso de lavado a partir del análisis de los polutogramas y balances de masas resultantes. En la Figura A.2 se presentan las configuraciones iniciales de sedimento que se ensayaron.

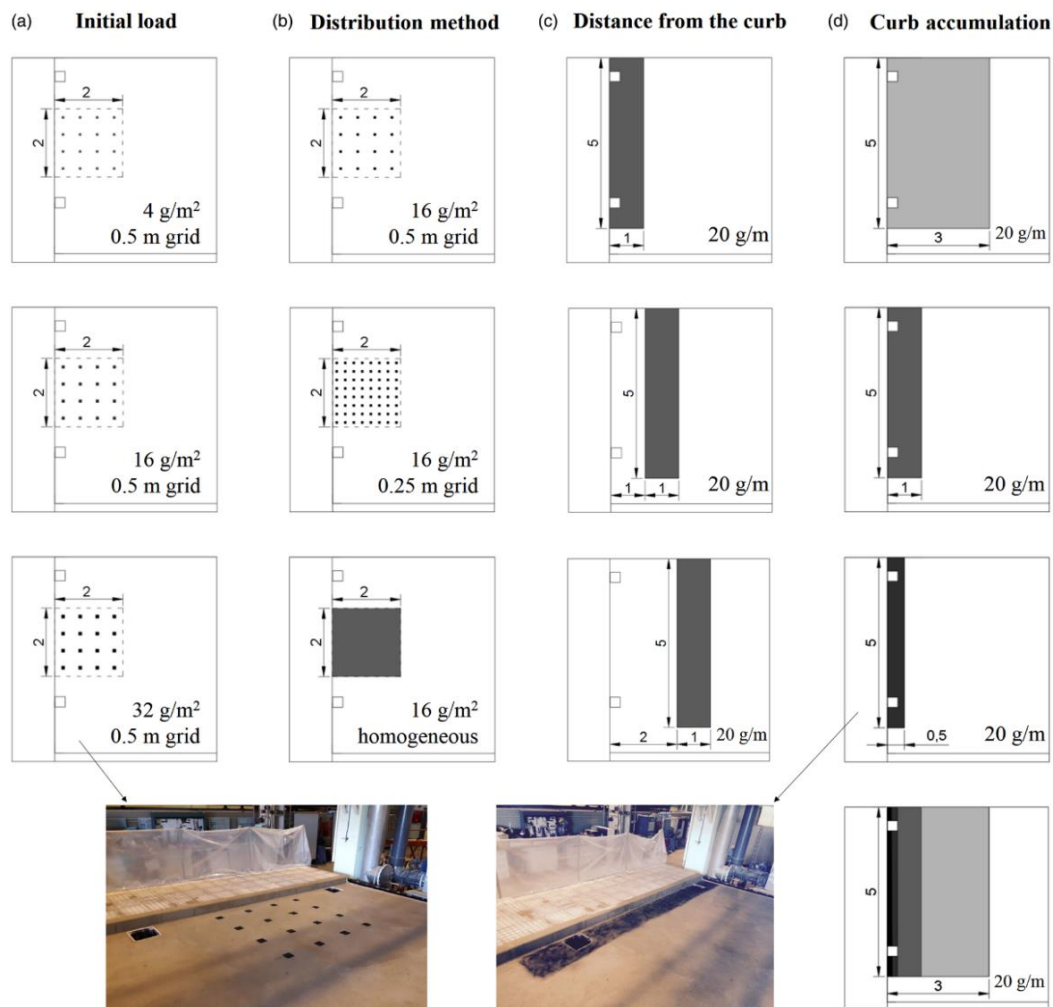


Figura A.2. Cargas iniciales y distribuciones de sedimentos utilizadas en los ensayos preliminares.

Los resultados mostraron que los procesos de lavado y transporte de sedimentos no pueden explicarse únicamente atendiendo a la carga inicial de sedimento y su distribución sobre la superficie de la calle, ya que otros factores como la uniformidad de la lluvia o las características del flujo de escorrentía también afectan a los balances de masas y a los polutogramas en el punto de vertido. Esto se puede comprobar en los resultados obtenidos en los experimentos donde el sedimento fue distribuido a diferentes distancias de la cuneta (Figura A.3). Mientras que la concentración máxima de SST sufrió una esperada y ligera reducción en el caso de alejar el área de distribución del sedimento a 1 metro de la cuneta, la concentración máxima se redujo a más de la mitad en el ensayo con el sedimento a 2 metros. El mismo comportamiento puede observarse en los balances de masas, donde la

cantidad de sedimento que permanece depositado en la superficie del modelo se incrementó drásticamente. Esto se puede explicar por la presencia de un área de altas intensidades situada aproximadamente a 1.5 m de la cuneta (Figura A.1) que condicionaba el flujo de escorrentía y afectaba a la movilización de sedimentos distribuidos a una mayor distancia. En definitiva, los ensayos preliminares realizados permitieron la puesta a punto de una metodología adecuada para la medida precisa del lavado y transporte de sedimentos, pudiendo comprobar la fiabilidad de los resultados obtenidos en cada ensayo, mostrando la gran influencia de las propiedades de la lluvia simulada y revelando la necesidad de una precisa caracterización hidráulica para la comprensión del proceso de lavado y transporte de sedimentos en cuencas urbanas.

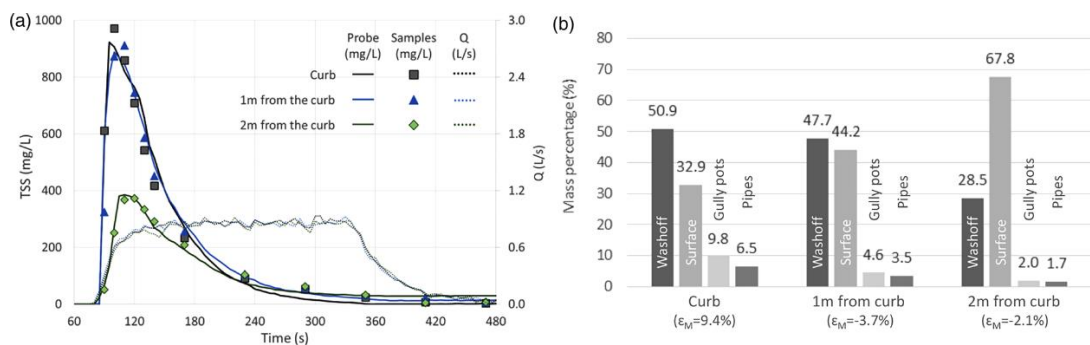


Figura A.3. Concentraciones de SST y caudales (a) y balances de masas al final de los ensayos (b) para una carga de sedimentos de 20 g/m, distribuido uniformemente en un área de 5 m x 1 m, pegada a la cuneta o separada 1 o 2 m de la misma. El error en el cierre de los balances de masas (ϵ_M) se indica para cada caso ensayado.

A continuación, y a la vista de los resultados anteriores, se decidió abordar dos mejoras en la metodología experimental de los ensayos para aumentar la calidad y transferibilidad de los resultados obtenidos: la lluvia simulada y la caracterización hidráulica del flujo superficial de escorrentía. Primero, dada la alta heterogeneidad de la lluvia generada en los ensayos preliminares (Figura A.1) y su gran influencia en los resultados, se construyó un nuevo simulador de lluvia de gran escala cuyo desarrollo y calibración se recoge en el Capítulo 3 de la presente tesis. El nuevo simulador está basado en un total de 1400 goteros autocompensantes en presión instalados en dos circuitos de tuberías que cubren toda la superficie del modelo. Bajo los goteros se instaló una malla que rompe y distribuye las gotas generadas para incrementar la uniformidad de la lluvia y producir distribuciones de tamaños de gotas similares a los de una lluvia real. La posición y la tipología de la malla fueron calibradas utilizando un disdrómetro láser Parsivel 2 y pluviómetros para medir respectivamente las distribuciones de tamaños y velocidades de gotas y la uniformidad e intensidad de la lluvia, comparándolas con medidas de lluvia real. En la Figura A.4 se incluye

una imagen general de la solución final alcanzada y un detalle de los goteros instalados sobre la malla metálica elegida.

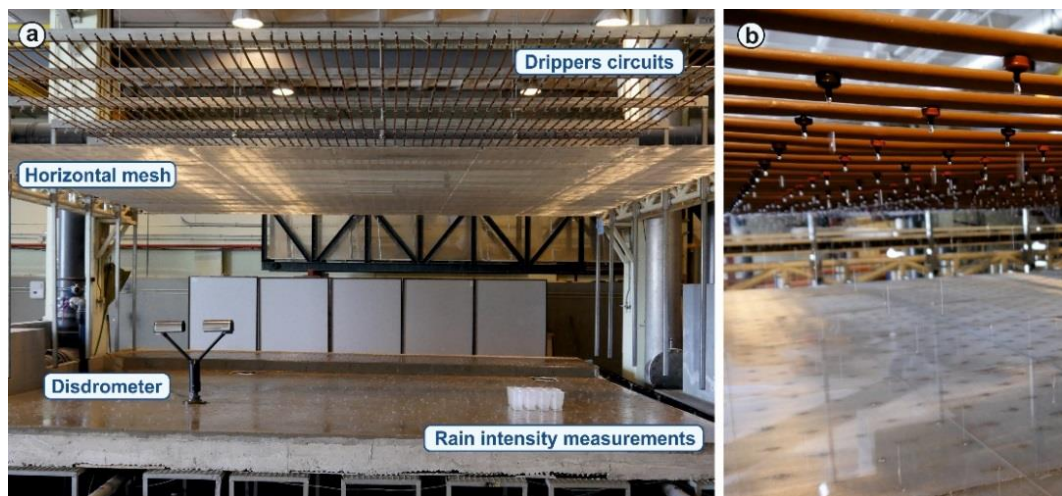


Figura A.4. Imagen general del nuevo simulador de lluvia basado en goteros (a) y detalle de los circuitos de goteros sobre la malla horizontal para romper y distribuir las gotas de lluvia generadas.

Una vez que el simulador fue calibrado se midieron con precisión las propiedades de la nueva lluvia producida. El simulador desarrollado es capaz de generar tres intensidades de lluvia diferentes (intensidades medias de 32.9, 54.9 y 79 mm/h) con Coeficientes de Uniformidad de Christiansen (CU) del 81, 89 y 91% respectivamente, un tamaño medio de gota de 0.95 mm y una velocidad de impacto de entorno al 85% de la velocidad terminal en el caso del tamaño de gota medio. En la Figura A.5 se muestra los mapas de intensidades de lluvia y las distribuciones de tamaños y velocidades de gotas para las tres lluvias que el simulador desarrollado es capaz de generar. La intensidad de lluvia y el tamaño de gota podrían modificarse y adaptarse cambiando los parámetros de diseño del simulador. Esta flexibilidad, sumada a la lluvia casi uniforme conseguida con tamaños de gota similares a los de una lluvia real, presentan a este nuevo generador como una herramienta óptima para el estudio del lavado de sedimentos en laboratorio, asegurando la transferibilidad de los resultados obtenidos a estudios de campo.

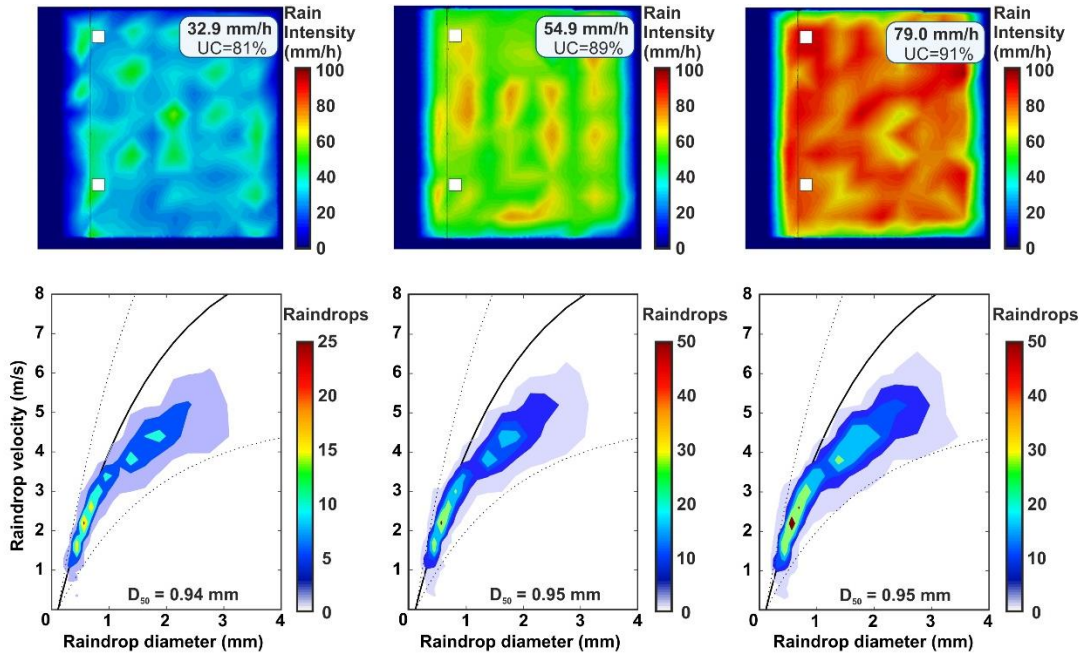


Figura A.5. Mapa de intensidades de lluvia y distribuciones de tamaños y velocidades de gota para las tres lluvias que el simulador es capaz de generar. La curva negra representa la relación experimental entre el diámetro y la velocidad terminal de las gotas.

Después de la mejora del simulador de lluvia, el siguiente objetivo que se planteó fue la definición precisa del flujo superficial de escorrentía, que es clave para entender la movilización de sedimentos en la superficie del modelo. Esta importancia viene dada por el hecho de que el flujo superficial, junto al impacto de gotas de lluvia, contribuye en el proceso de puesta en suspensión de las partículas que se encuentran en la superficie del modelo y, una vez puestas en suspensión, las transporta hasta su deposición. En este contexto, se desarrolló una modificación de la técnica de visualización *Large Scale Particle Image Velocimetry* (LSPIV) en la que se utilizaron partículas fluorescentes como trazadores e iluminación ultravioleta para medir las velocidades superficiales en condiciones de aguas muy someras de pocos milímetros de calado y con la presencia de gotas de lluvia. Los resultados obtenidos mostraron la existencia de canales preferenciales de drenaje perpendiculares a la cuneta debidos a irregulares en la superficie y que condicionan la movilización de partículas sobre la superficie del modelo. La Figura A.6 muestra el montaje experimental utilizado para la grabación de los videos empleados en el análisis LSPIV y las velocidades obtenidas para el caso de la lluvia con menor intensidad.

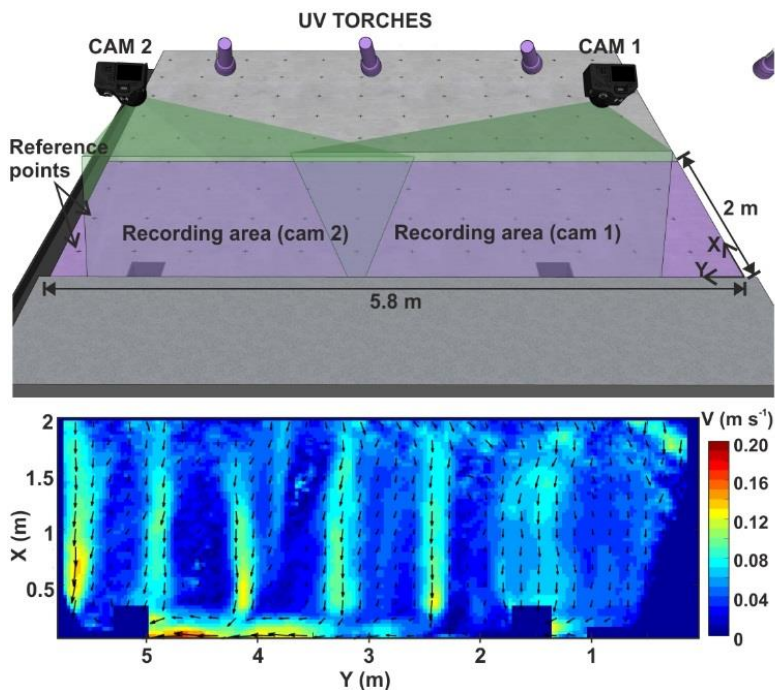


Figura A.6. Configuración experimental para la grabación de los vídeos usados para la medida de velocidades superficiales a través de la técnica PIV. Se incluyen además las velocidades medias obtenidas en régimen permanente para la lluvia con la intensidad más baja.

Los pequeños calados desarrollados hacen necesaria una definición precisa de las elevaciones de la superficie del modelo físico para representar de forma adecuada el flujo superficial. Para ello, se utilizó la técnica fotogramétrica *Structure from Motion* (SfM) para obtener una topografía de alta resolución que permitiese modelizar el flujo superficial usando un modelo 2D de aguas someras. El modelo se calibró mediante los caudales medidos en los dos imbornales existentes, y los resultados se compararon con los obtenidos utilizando una topografía tradicional consistente en medidas manuales de elevaciones, que tienen una resolución de 0.5 m. Los caudales obtenidos en los imbornales fueron muy similares utilizando los mismos valores de los parámetros calibrados. Sin embargo, las distribuciones de velocidades en superficie obtenidas mostraron diferencias significativas, especialmente para las zonas con flujos más someros donde sólo la topografía de alta resolución fue capaz de representar los canales de drenaje preferencial medidos con la técnica LSPIV. La Figura A.7 muestra las elevaciones de la superficie obtenidas con cada una de las técnicas y los campos de velocidad resultantes de utilizar cada topografía en el modelo 2D de aguas someras para la lluvia de 30 mm/h. Este trabajo, en el que se planteó la representación precisa del flujo (Capítulo 4), puso de manifiesto la importancia de una topografía detallada para modelizar el flujo superficial en condiciones de aguas someras, y

la necesidad de datos superficiales adicionales para la correcta calibración de modelos. Además, la técnica LSPIV desarrollada se presenta como una herramienta adecuada para la medida de velocidades en superficie con la presencia de gotas de lluvia. Por último, se evaluó positivamente el uso de técnicas fotogramétricas para la obtención de mapas de elevaciones para modelización hidráulica.

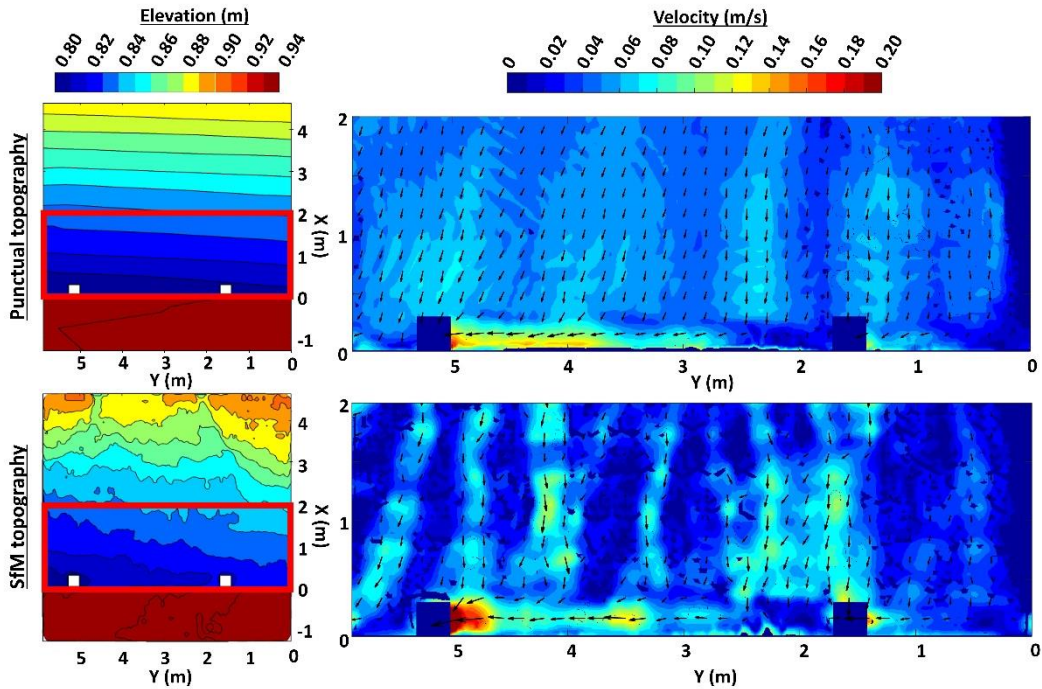


Figura A.7. Mapas de elevaciones obtenidos mediante medidas manuales puntuales (primera fila) y mediante la técnica fotogramétrica SfM (segunda fila). En la segunda columna se muestran las distribuciones de velocidades obtenidas con cada una de las topografías utilizando un modelo 2D de aguas someras y considerando la menor intensidad de lluvia.

A continuación, la detallada caracterización hidráulica de los experimentos fue completada con la medida de calados en superficie y en tubería y con el registro de caudales a la entrada de los imbornales y a la salida de la red de tuberías. Se realizaron un total de seis ensayos teniendo en cuenta los puntos de medida recogidos en la Figura A.8 y las tres intensidades de lluvia que el simulador es capaz de generar. La Figura A.8 también incluye ejemplos de los caudales y calados registrados durante los experimentos para el caso de la intensidad de lluvia más alta. La metodología utilizada y los datos obtenidos están descritos detalladamente en el Capítulo 5. Además, como parte de los ensayos hidráulicos, se incluye el uso de una técnica LSPIV en la que no se utilizan partículas y la medida de velocidades se

basa en el análisis del movimiento de burbujas y reflejos del agua, pudiendo ser una alternativa en aplicaciones de campo donde el uso de partículas fluorescentes e iluminación ultravioleta se hace más complejo.

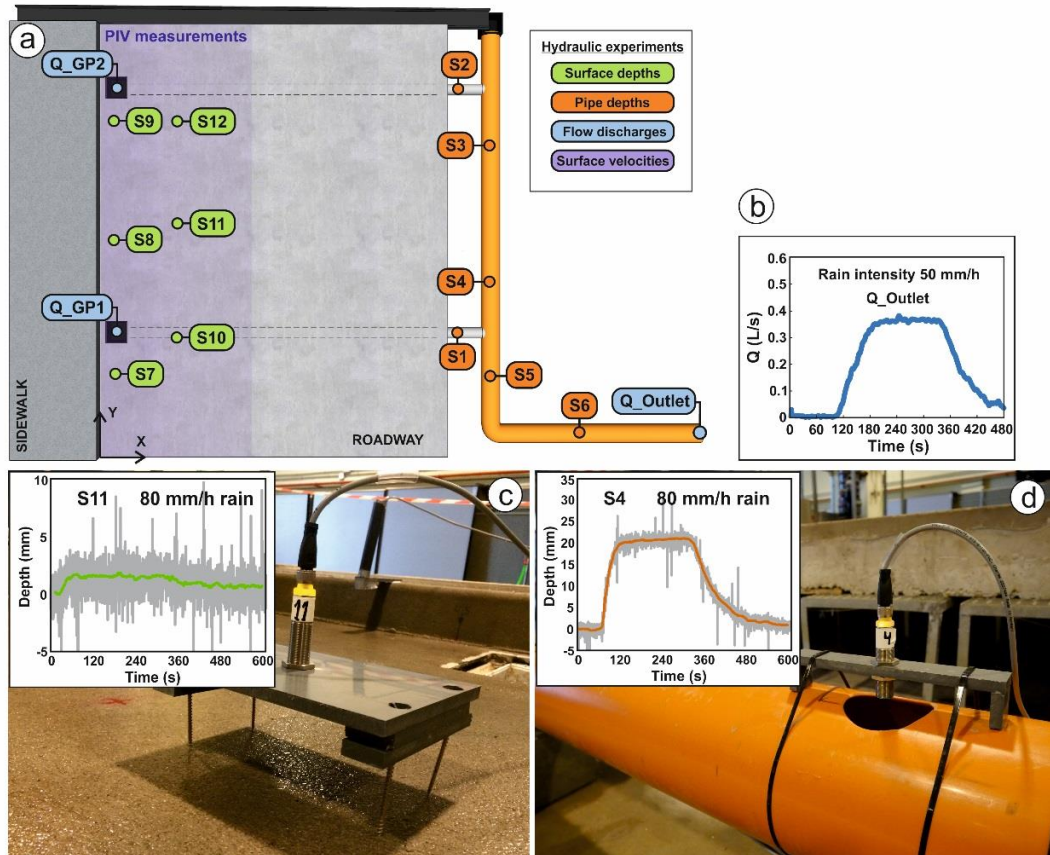


Figura A.8. Puntos de medida de calados superficiales y en tubería, caudales y velocidades en los ensayos hidráulicos realizados (a). También se incluye el caudal registrado a la salida de la red de tuberías (b), y los calados medidos en el punto S11 de la superficie (c) y en el punto S4 de la red de tuberías (d) para la lluvia de mayor intensidad.

Una vez que los experimentos fueron caracterizados hidráulicamente, se realizó una extensa campaña experimental en la que se midió de forma precisa la movilización de sólidos en suspensión a través de las distintas partes del modelo físico. Las tres intensidades de lluvia (30, 50 y 80 mm/h) y cinco clases de sedimentos con diferentes granulometrías (d_{50} entre 30 y 275 μm) fueron utilizadas en 23 ensayos de lavado y transporte de sedimentos (Capítulo 5). La Figura A.9 (izquierda) muestra la granulometría de las distintas clases de sedimento, que se dispusieron sobre la superficie del modelo de una forma realista y con una carga inicial de 20 g por metro de cuneta en cada ensayo (Figura A.9, derecha).

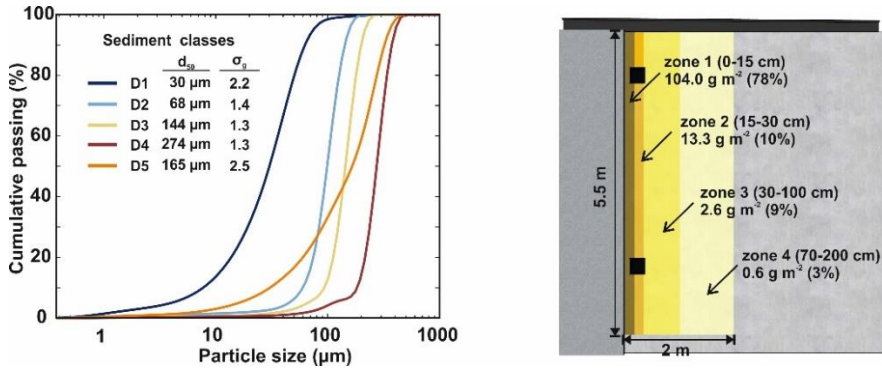


Figura A.9. Granulometrías de las cinco clases de sedimentos utilizadas incluyendo su tamaño medio y su coeficiente de gradación ($\sigma_g = \sqrt{D_{84}/D_{16}}$) (izquierda). Distribución inicial de sedimentos sobre la superficie del modelo (derecha).

Los experimentos consistieron en la generación de una lluvia de 5 minutos de duración y, en cuanto la escorrentía alcanzaba los imbornales y el punto de vertido de la red de tuberías se tomaban muestras manuales de SST y de Distribuciones de Tamaños de Partículas (DTP) para medir la movilización de las diferentes fracciones de partículas a través del modelo. Las muestras para el análisis de DTP son especialmente interesantes en el caso de la granulometría continua (clase de sedimento D5 en la Figura A.9) para analizar en un mismo ensayo el diferente comportamiento de las partículas dependiendo de su tamaño. Además, se realizaron medidas en continuo de los polutogramas en el punto de vertido a partir de registros de turbidez siguiendo la metodología desarrollada durante los ensayos preliminares. Los puntos de medida y las variables analizadas en estos experimentos se muestran en la Figura A.10.

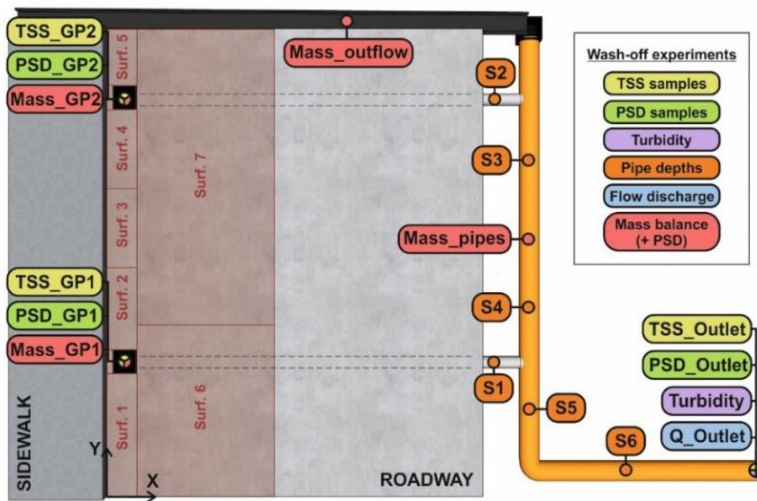


Figura A.10. Puntos de medida y variables consideradas en los ensayos de lavado y transporte de sedimentos.

Los resultados obtenidos midiendo la concentración de SST durante los ensayos para las cinco clases de sedimentos y las tres intensidades de lluvia a la entrada de los imbornales y en el punto de vertido se muestran en la Figura A.11. A la vista de los resultados, se pudo observar cómo el tamaño del sedimento es clave en el proceso de lavado de contaminantes. El sedimento más fino (clase de sedimento D1 con un tamaño medio de $30\ \mu\text{m}$) produjo las mayores concentraciones en la entrada de los imbornales y en el punto de vertido con una diferencia importante respecto al resto de granulometrías ensayadas. Además, las concentraciones de SST medidas para el caso de la granulometría continua D5 ($d_{50}=165\ \mu\text{m}$) se situaron entre los resultados obtenidos para los sedimentos D2 ($d_{50}=68\ \mu\text{m}$) y D3 ($d_{50}=144\ \mu\text{m}$). Por lo tanto, se observó que la consideración del tamaño medio de partícula como representativo para la modelización del lavado y transporte de un sedimento podría llevar a estimaciones erróneas.

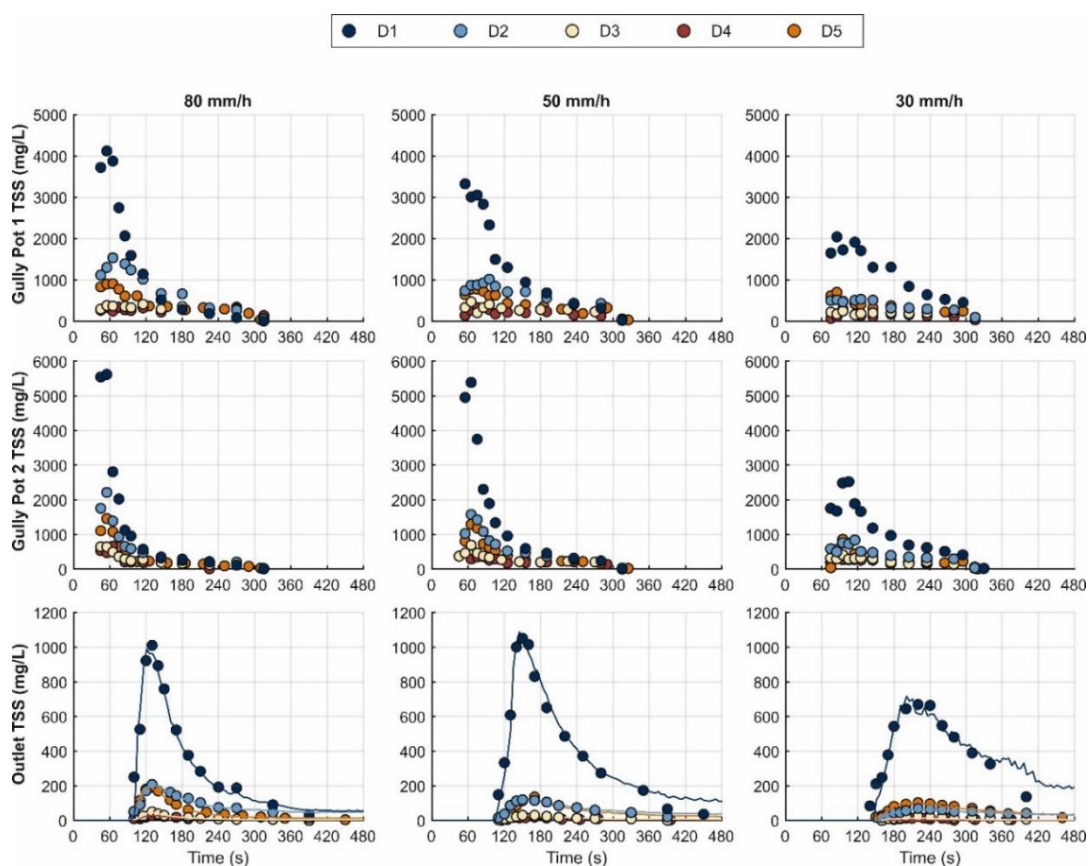


Figura A.11. Sólidos en suspensión totales (SST) en las arquetas y en el punto de vertido para las 5 clases de sedimento diferentes (D1-D5) y las tres intensidades de lluvia.

Siguiendo la metodología desarrollada en los ensayos preliminares, al final de cada ensayo se realizó un balance de masas para evaluar la distribución final de sedimento en las

diferentes partes del modelo físico y asegurar la fiabilidad de los resultados experimentales. En la Figura A.12 se muestran las masas obtenidas para cada uno de los ensayos realizados. Los errores máximos en los balances de masas entre la masa inicial de sedimento distribuida y la suma de la masa recogida al final de los experimentos y la masa total lavada del modelo físico durante los ensayos se situaron alrededor del 5%. Este resultado es muy satisfactorio teniendo en cuenta la complejidad del fenómeno físico y asegura la fiabilidad de los resultados experimentales proporcionados.

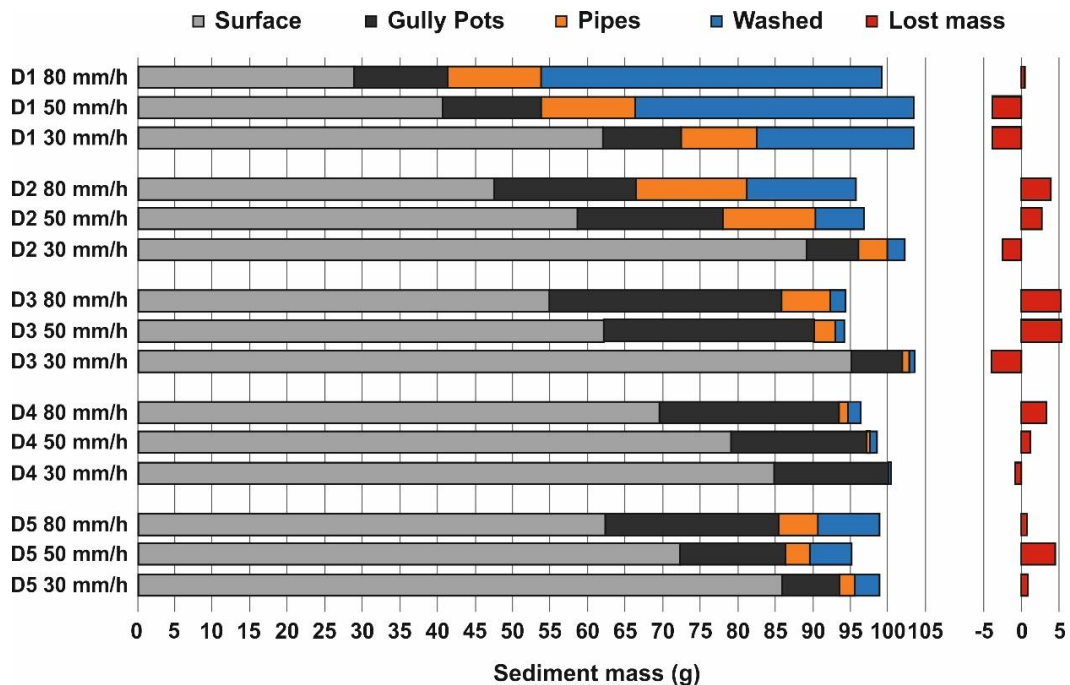


Figura A.12. Balances de masas para las cinco clases de sedimento (D1-D5) e intensidades de lluvia de 80, 50 y 30 mm/h.

Los datos brutos y procesados obtenidos a partir de los diferentes experimentos llevados a cabo en esta tesis están publicados en abierto en el repositorio Zenodo dentro del ámbito del proyecto WASHTREET (<https://zenodo.org/communities/washtreet>) y están disponibles para su uso por parte de otros autores. El paquete de datos principal (Naves *et al.* 2019c) contiene los resultados obtenidos en los ensayos hidráulicos y de lavado y transporte de sedimentos descritos en esta tesis. Los resultados que se proporcionan cubren la necesidad existente de datos precisos para desarrollar, calibrar y validar modelos de drenaje urbano, incluyendo los procesos de lavado y transporte de sedimentos en los diferentes componentes del sistema de drenaje (superficie, imbornales, colectores) y sin tener que considerar las incertidumbres en las variables de entrada. Se incluyeron adicionalmente dos paquetes de datos más (Naves *et al.* 2019d, Naves *et al.* 2019e), en donde se proporciona información detallada relacionada con el análisis LSPIV y la técnica fotogramétrica SfM

respectivamente. Estas bases de datos pueden usarse para evaluar técnicas PIV con y sin partículas y optimizar la novedosa aplicación de técnicas fotogramétricas a la modelización hidráulica.

Por último, la tesis presenta la utilización de las concentraciones de SST medidas a la entrada de los imbornales para evaluar y analizar un modelo de lavado de sedimentos basado en procesos físicos que implementa la formulación de Hairsine-Rose acoplada al modelo 2D de aguas someras *Iber* (Capítulo 6). En la Figura A.13 se muestra las predicciones obtenidas del modelo para los casos con intensidades de lluvia de 50 y 80 mm/h y clases de sedimentos D2 y D3 respectivamente. Los resultados mostraron que la flexibilidad del modelo permite la reproducción de los resultados experimentales ajustando los seis parámetros de la formulación de Hairsine-Rose. Sin embargo, también se observó que esta flexibilidad lleva a problemas de identificabilidad al calibrar el modelo, ya que se obtuvieron resultados similares para diferentes combinaciones de parámetros.

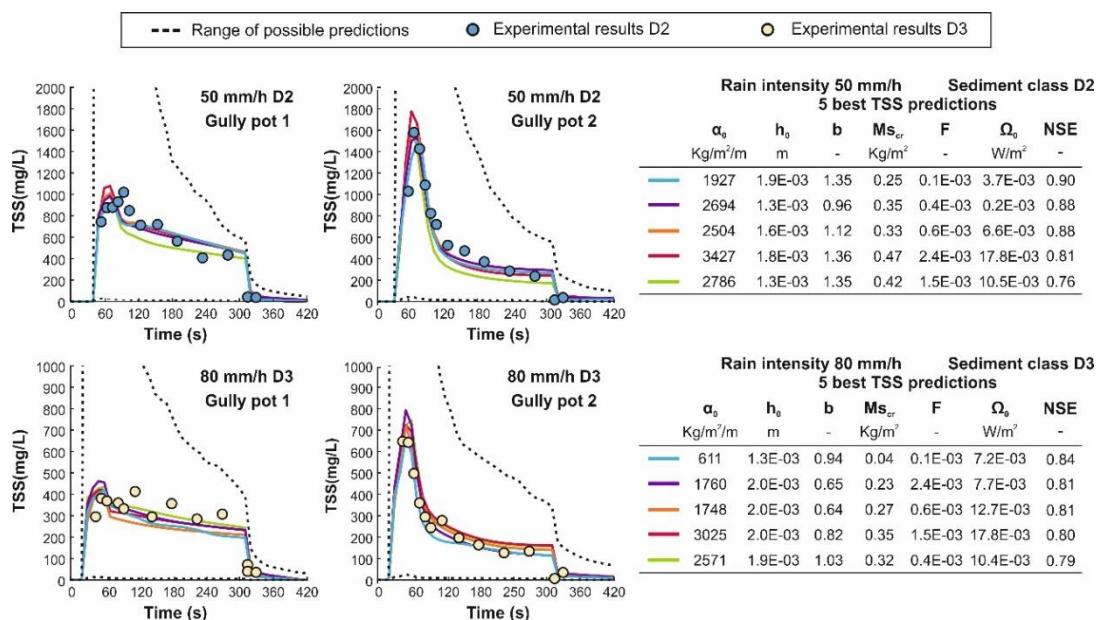


Figura A.13. Resultados experimentales de SST en la entrada de los imbornales y las cinco mejores predicciones para los ensayos con intensidades de lluvia de 50 (arriba) y 80 mm/h (abajo) y clases de sedimento D2 y D3 respectivamente. Se incluye además los valores de los parámetros de la formulación de Hairsine-Rose para los 5 mejores ajustes.

En este contexto, el estudio contribuye al entendimiento de este tipo de modelos de lavado basados en procesos físicos mediante un extenso análisis de sensibilidad con el objetivo de proporcionar la información necesaria para identificar las variables y parámetros más importantes y ser capaz de simplificar el modelo para lidiar con la identificabilidad mostrada.

La medida precisa de las variables de entrada al modelo y la detallada definición de las variables hidráulicas permitieron separar la contribución individual de cada uno de los de los parámetros de la formulación de Hairsine-Rose en la concentración máxima y en la masa total lavada para cada uno de los imbornales. En la Figura A.14 se muestra la sensibilidad global de la masa total lavada a cada uno de los parámetros de la formulación de Hairsine-Rose para los 12 ensayos considerados y utilizando dos métodos diferentes: el método de *Standardized Regression Coefficients* (SRC) y el *Extended Fourier Amplitude Test* (EFAST). El análisis de sensibilidad global realizado mostró que tanto la masa total lavada como la concentración máxima de SST presentan una alta sensibilidad a la masa crítica ($M_{S_{cr}}$), que considera la reducción en la puesta en suspensión de las partículas debido a la disminución del sedimento disponible en la superficie impermeable. Además, los parámetros que condicionan la puesta en suspensión de las partículas debido al impacto de las gotas de lluvia (α_0 , h_0) y al flujo superficial (F) se mostraron como parámetros clave para los menores (tamaños medios entre 30 y 68 μm) y mayores (entre 144 y 274 μm) partículas respectivamente, siendo b y Ω_0 despreciables. Las diferencias entre los índices de primer orden (colores oscuros) y totales (colores claros) en el EFAST representan la variación de los resultados debida a interacciones entre parámetros. Se observó que estas interacciones juegan un papel importante en los resultados, lo que pone de manifiesto la necesidad del análisis realizado para simplificar el modelo antes de realizar una calibración formal del mismo.

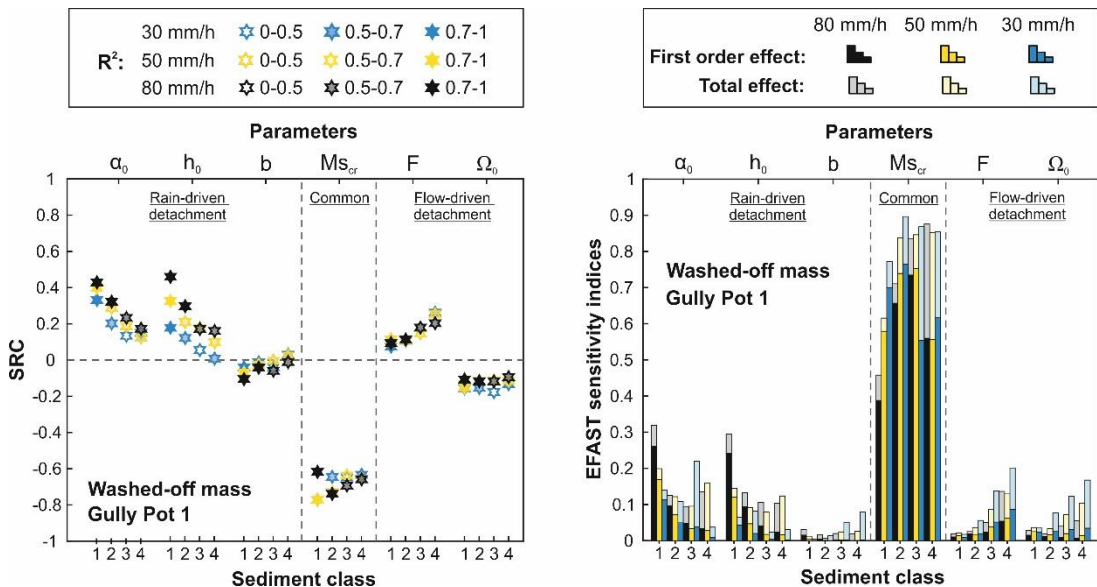


Figura A.14. Coeficientes de sensibilidad global de la masa total lavada por el imbornal 1, obtenidos mediante los métodos SRC y EFAST, respecto a los parámetros de la formulación de Hairsine-Rose y para cada uno de los casos experimentales considerados (colores para las intensidades de lluvia y posición para la clase de sedimentos utilizada).

Por último, se investigó la importancia relativa de los parámetros del modelo analizados con respecto a las condiciones iniciales de sedimento y las variables hidráulicas con el objetivo de asegurar la transferibilidad de los resultados de sensibilidad obtenidos a estudios en campo, donde no es posible definir las entradas al modelo con tanta precisión como en laboratorio. En la Figura A.15 se muestran los resultados del análisis de sensibilidad local que se ha realizado utilizando el método de *Elementary Effects* y considerando todas las variables de entrada para el caso de 30 mm/h y clase de sedimento D1. La carga inicial de sedimento y el tamaño medio de partículas resultaron las variables más importantes, recalcando la necesidad de medidas precisas de las condiciones iniciales para evitar que la variabilidad asociada al proceso de acumulación de contaminantes afecte a la fiabilidad de los resultados obtenidos. Esta necesidad de datos de entrada precisos, junto al alto coste computacional del modelo, limita actualmente su aplicabilidad a estudios de campo. Sin embargo, se están desarrollando mejoras en la velocidad de los modelos que permitirán próximamente su utilización en cuencas cada vez mayores, siendo necesario por lo tanto la realización de más estudios de laboratorio y en campo para incrementar el conocimiento sobre las variables y parámetros del modelo

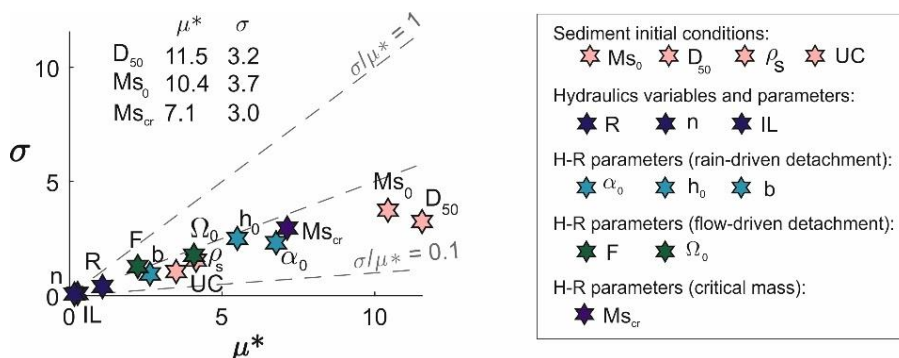


Figura A.15. Resultados del análisis de sensibilidad local para la masa total lavada por el imbornal 2 para el caso de 30 mm/h y clase de sedimento D1, usando el método de Elementary Effects y considerando todas las variables de entrada del modelo.

Como conclusión final, el trabajo realizado en esta tesis pretende incrementar el conocimiento sobre el proceso de lavado y transporte de sedimentos en cuencas urbanas con el objetivo de desarrollar modelos de drenaje urbano más fiables que permitan mejorar la gestión y el diseño de medidas de tratamiento para el crecimiento sostenible de las áreas urbanas. Los resultados obtenidos son un paso adelante hacia este objetivo proporcionando una extensa y precisa base de datos para desarrollar, calibrar o validar formulaciones y modelos más fiables. Además, los prometedores resultados obtenidos presentan a los modelos de lavado basados en procesos físicos como una alternativa para la identificación de las variables que gobiernan el fenómeno de lavado de sedimentos, siendo una importante herramienta hacia modelos más precisos.

Referencias

- Fraga, I. (2015). *Desarrollo de un modelo dual 1D/2D para el cálculo del drenaje urbano: modelo numérico y validación experimental*. Doctoral dissertation. Universidade da Coruña, A Coruña, Spain. <http://hdl.handle.net/2183/14727>
- Naves, J., Anta, J., Suárez, J., Puertas, J. (2019c) [dataset] WASHTREET Hydraulic, wash-off and sediment transport experimental data in an urban drainage physical model, *Zenodo*, <http://doi.org/10.5281/zenodo.3233918>
- Naves, J., Puertas, J., Suárez, J., and Anta, J. (2019d) [dataset] WASHTREET Runoff velocity data using different Particle Image Velocimetry (PIV) techniques in a full scale urban drainage physical model, *Zenodo*, <http://doi.org/10.5281/zenodo.3239401>
- Naves, J., Anta, J., Suárez, J., and Puertas, J.: (2019e) [dataset] WASHTREET Application of Structure from Motion (SfM) photogrammetric technique to determine surface elevations in an urban drainage physical model, *Zenodo*, <http://doi.org/10.5281/zenodo.3241337>

Appendix B

List of publications from thesis outcomes

Title: Experimental study of pollutant wash-off on a full-scale street section physical model

Authors: Juan Naves, Zurab Jikia, Jose Anta, Jerónimo Puertas, Joaquín Suárez, Manuel Regueiro-Picallo

Published: Water Science & Technology

Date: May, 20th 2017

DOI: <https://doi.org/10.2166/wst.2017.345>

Title: Using a 2D shallow water model to assess Large-Scale Particle Image Velocimetry (LSPIV) and Structure from Motion (SfM) techniques in a street-scale urban drainage physical model

Authors: Juan Naves, Jose Anta, Jerónimo Puertas, Manuel Regueiro-Picallo, Joaquín Suárez

Published: Journal of hydrology

Date: May, 6th 2019

DOI: <https://doi.org/10.1016/j.jhydrol.2019.05.003>

Appendix C

List of publication related with thesis topic

Title: Experimental and Numerical Analysis of Egg-Shaped Sewer Pipes Flow Performance

Authors: Manuel Regueiro-Picallo, Juan Naves, Jose Anta, Jerónimo Puertas and Joaquín Suárez

Published: Water

Date: December, 9th 2016

DOI: <https://doi.org/10.3390/w8120587>

Title: Monitoring accumulation sediment characteristics in full scale sewer physical model with urban wastewater

Authors: Manuel Regueiro-Picallo, Juan Naves, Jose Anta, Joaquín Suárez and Jerónimo Puertas

Published: Water Science and Technology

Date: July, 14th 2017

DOI: <https://doi.org/10.2166/wst.2017.118>

Title: Characterisation of sediments during transport of solids in circular sewer pipes

Authors: Manuel Regueiro-Picallo, Jose Anta, Joaquín Suárez, Jerónimo Puertas, Alfredo Jácome and Juan Naves

Published: Water Science and Technology

Date: April, 26th 2018

DOI: <https://doi.org/10.2166/wst.2018.055>